4

Quanta of Spacetime Explain Observations, Dark Energy, Graviton and Nonlocality

Hans-Otto Carmesin

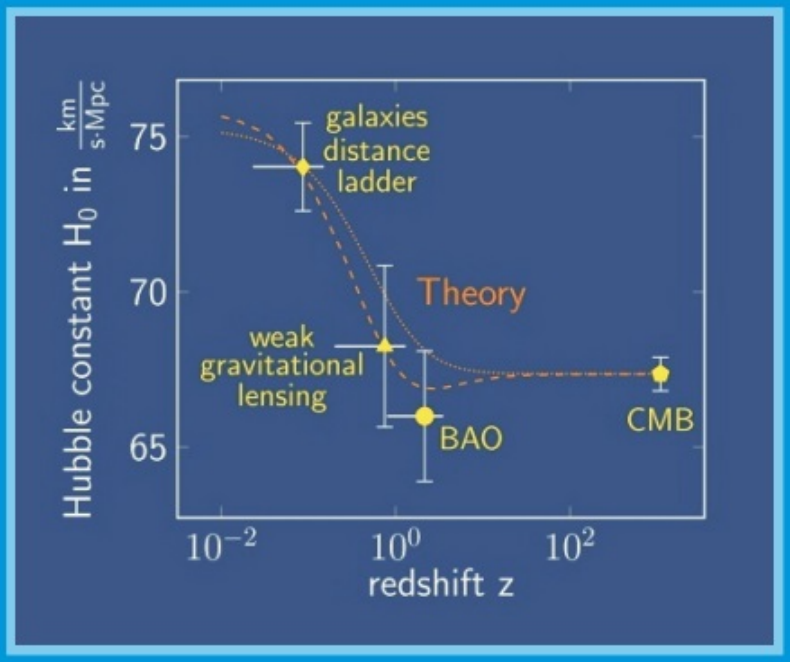

Verlag Dr. Köster
Berlin

Series
Universe: Unified from Microcosm to Macrocosm

H.-O. Carmesin Quanta of Spacetime Explain Observations, Dark Energy, Graviton and Nonlocality 4

Quanta of Spacetime Explain Observations, Dark Energy, Graviton and Nonlocality

Hans-Otto Carmesin

Verlag Dr. Köster
Berlin

Series
Universe: Unified from
Microcosm to Macrocosm

Universe: Unified from Microcosm to Macrocosm -
Die Grundschwingungen des Universums
Bd. 4

ISSN 2629-1525

Bibliografische Information der Deutschen Nationalbibliothek
Die Deutsche Nationalbibliothek verzeichnet diese Publikation in der Deutschen Nationalbibliografie; detaillierte bibliografische Daten sind im Internet über http://dnb.dnb.de abrufbar.

1. Auflage März 2021

Verlag Dr. Köster
IHZ
Friedrichstr. 95
10117 Berlin

Tel. 030 76 40 32 24
info@verlag-koester.de

www.verlag-koester.de

ISBN 978-3-96831-008-4

Modern physics is based on two great concepts: general relativity theory, GRT and quantum theory, QT. However, effects faster than light are called nonlocal, and they seem to be impossible in nature and in GRT, while they occur in QT, this contrast is called EPR paradox.

We solve it as follows: The curved spacetime in GRT corresponds to additionally forming vacuum. We calculate its volume, and we discover:

It explains curvature of space as well as the expansion since the Big Bang.

One half of that volume forms in a nonlocal manner: Thus nature and GRT are nonlocal and so no paradox remains.

The formation of spacetime, however, is local. With it we combine GRT and QT: We derive the field theory, the quadrupole or spin 2 symmetry, the waves and the quanta of spacetime. These provide precise accordance to observation without any fit parameter, of course.

The quanta of spacetime include the propagation and formation of vacuum. So they explain the dark energy and the time evolution of dark energy and structure, which in turn explains the discrepancy inherent to observed values of the Hubble constant H0 and of matter fluctuations ó8.

The quanta of spacetime include the quanta of gravitational interaction. So they explain the graviton by its symmetry, propagation, quantization and mechanism of interaction: Quanta of spacetime form, the resulting heterogeneity generates curvature, and this causes gravitational force. So the graviton is now understood in exceptionally deep detail!

The quanta of spacetime in the visible universe are traced back to one single quantum at the Big Bang. At its space, there immediately formed many quanta of zero-point energies of radiation. Altogether the complete energy and mass of the visible universe is traced back to the Big Bang.

The quanta of spacetime are invariant at Lorentz transformations and at all other linear transformations. These quanta solve many fundamental problems and explain various interesting systems, including black holes.

We derive all results with a smooth progression, and we summarize our findings in 15 propositions and 34 theorems.

ISBN 978 - 3 - 96831 - 008 - 4

4 H.-O. Carmesin Quanta of Spacetime Explain Observations, Dark Energy, Graviton and Nonlocality

Quanta of Spacetime Explain Observations,

Dark Energy, Graviton and Nonlocality

Printed Edition: Verlag Dr. Köster, Berlin, www.verlag-koester.de, permanently available since March 19, 2021

Book Series: Universe: Unified from Microcosm to Macrocosm, Volume 4

Hans-Otto Carmesin

March 25, 2021

Contents

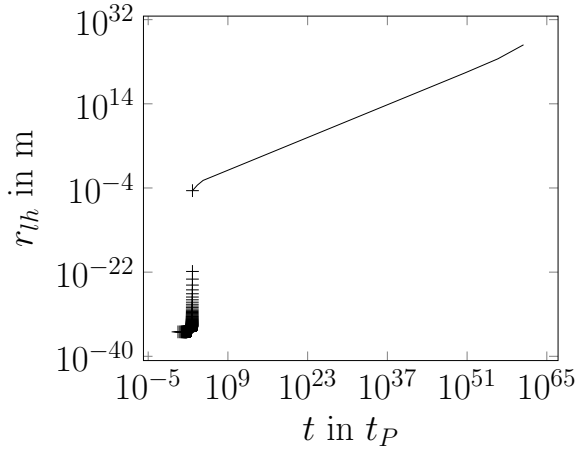

Figure 1: Time evolution of light horizon $r_{lh}(t)$ as a function of the time in Planck times $t_P = 5.391 \cdot 10^{-44}$ s: Discontinuous dimensional phase transitions ranging from the highest possible dimension of the visible space $D_{horizon} = 301$ to $D = 3$ (+) (see Carmesin (2017), Carmesin (2018a),Carmesin (2019b)). Continuous so-called expansion of space in $D = 3$, ranging until today, t_0 (solid line).

0.1 Introduction

Great concepts:

Physical theories are based on two basic concepts: First, Planck (1900) discovered the **quantization of physical objects**, introduced **quantum theory, QT**, including **zero-point oscillations, ZPOs**, and the corresponding **zero-point energy, ZPE** (Planck (1911)). Secondly, Einstein (1905) applied the invariance of the velocity of light c in order to derive the **special relativity theory, SRT**. Moreover, Einstein (1915a) discovered the **curvature of spacetime**, leading to his proposal of the **general relativity theory, GRT**, including a theory for gravity.

Great questions:

Einstein et al. (1935) realized that in QT measurable correlations form at much higher velocities than the velocity of light c,

in this sense **QT is nonlocal**. However, GRT is based on physical objects that propagate at velocities up to c. Consequently Einstein et al. (1935) presumed that GRT would be local and compared to that, QT would be paradoxical. This argument is called the **EPR paradox**.

Another set of questions arises from the expansion of space: Perlmutter et al. (1998) and Riess et al. (2000) discovered a density of the vacuum ρ_v, the so-called **dark energy**. What is its nature?

Based on the GRT, the expansion of space should be characterized by two constants: the Hubble constant H_0 and the amplitude of matter fluctuations σ_8. However, Riess et al. (2019) and Tröster et al. (2020) showed that observers using probes at the early universe obtain a **significant discrepancy of H_0 and σ_8 values** to corresponding values based on probes at the late universe.

Based on the GRT, the space enclosed in the light horizon r_{lh} should expand continuously as shown in the right part of Fig. (1). However, Guth (1981) discovered that there was a **rapid enlargement** in the early universe, see left part in Fig. (1). How does this emerge?

Interesting hypotheses:

Blokhintsev and Galperin (1934) proposed to improve the GRT by an elementary particle that transfers the gravitational interaction, the so-called hypothetical **graviton**. However, that particle has not yet been found.

Nanopoulos et al. (1983) suggested that another elementary particle or field, the so-called hypothetical **'inflaton'**, should cause a very rapid increase of the volume in the early universe. This 'inflaton' has neither been found (Tanabashi et al. (2018)), nor does it obey the law of energy conservation. This causes the so-called reheating problem.

Concerning the energy, Tryon (1973) proposed that the uni-

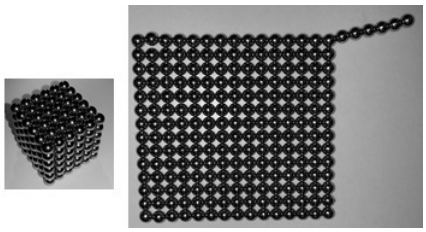

Figure 2: 216 magnetic balls model local objects or observable regions at high density and illustrate the relation between the distance and the dimension D: If the dimension increases from two (right) to three (left), then the largest distance decreases. More generally and conversely, a decrease of the dimension D implies an increase of the largest distance.

verse had zero energy at the beginning, the so-called **zero energy hypothesis**.

Novel results derived in this book:

We analyze the time evolution of the volume or vacuum based on the GRT, and we discover that also **GRT is nonlocal**. This provides a first solution to the EPR paradox: **Nature is nonlocal**.

We derive fields, waves and **quanta of spacetime** in a Lorentz invariant manner. Thereby we analyze quadrupolar symmetry and spin 2 as well as the full dynamics of propagation and formation. As a result we explain the **dark energy in four progressively more advanced theories**. We apply these quanta to the measurement of H_0 and σ_8 based on probes at various times of the evolution of the universe. Hereby we achieve a very **precise accordance with observations**. So we **explain the significant discrepancy of H_0 and σ_8 values**.

Using a combination of GRT and QT, we find the spontaneous formation of shortcuts in space whenever the density is above a **critical density** $\tilde{\rho}_{cr.conn.}$. Using a shortcut, an object can propagate at velocities up to c, but arrive at a distant point as if the velocity were above c. This provides a second solution

to the EPR paradox: **Nature can appear nonlocal but use shortcuts locally**.

The spontaneous formation of many shortcuts can be interpreted by a dimensional phase transition. Note that such dimensions have been found experimentally (Lohse et al. (2018), Zilberberg et al. (2018)). We analyze such phase transitions by using a mean field theory and by using a quantum gas. In all cases we confirm these transitions. These represent a dimensional rearrangement of quanta of vacuum analogously to the magnet balls in Fig. (2). That Fig shows that there occurs a rapid enlargement of distances at such a transition. This fully explains the rapid enlargement occurring in the early universe (Fig. 1). So we are not surprised that the hypothetical 'inflaton' has not been found.

We analyze the time evolution of the energy and discover that visible space can be traced back to the energy of a primordial quantum of spacetime. Thereby the zero energy hypothesis is explained and confirmed by the quanta of spacetime. Moreover, the quanta of spacetime include space, time and gravity in a coherent manner, so the hypothetical graviton is included in these quanta and so the corresponding hypothesis is confirmed.

I emphasize that the derived theory of the quanta of spacetime provides a precise accordance to observations. Thereby the only numerical input are the four universal constants c, G, k_B and h. In particular, I used no fit parameters. This provides a strong additional evidence for the derived results.

In this book we derive the results in a direct and smooth manner. In a glossary you can immediately find contextual information, if desired. We summarize our results concisely in 15 propositions and 34 theorems. So you can easily apply our findings according to your individual interests, activities, questions or purposes.

Chapter 1

Volume and Fields

In this chapter we investigate the dynamics of the volume that can be derived from the well known **general relativity theory, GRT** (Einstein (1905) or Carmesin (1996), Straumann (2013), Moore (2013)).

1.1 Problems of spacetime

Einstein (1905) introduced the concept of spacetime, including **curved spacetime** (Einstein (1915a)). There remain essential questions: For instance, Planck (1900) introduced the concept of **quantization**. Inherent to it is the phenomenon of **non-locality**, which was suggested to be apparently paradoxical to spacetime (Einstein et al. (1935)). In this section we address the following seven questions. Thereby we apply the concept of the volume[1] outlined in the following section.

1. What is a useful **frame for the homogeneous universe**?
2. Can we describe the Schwarzschild solution, SSM, with help of an **energy function**?
3. Can we describe the **curvature** of the SSM by a **locally formed volume or vacuum, LFV**?

[1] The vacuum has a volume and a density (Perlmutter et al. (1998), Riess et al. (2000)), and it propagates with the velocity of light, as it is fully relativistic.

4. Can we describe the **expanding universe**[2] in terms of a **complete formed vacuum, CFV**?
5. How large is the **difference** of the CFV and the LFV, the **nonlocally formed vacuum, NFV**?
6. Is the **GRT nonlocal**?
7. Is the nonlocality of GRT a first solution of the **EPR paradox** (Einstein et al. (1935) or (Ballentine, 1998, p. 585-609))?

1.2 New concept: dynamics of vacuum

We solve the above problems by the application of a new concept: We analyze the full dynamics of the vacuum[3]. Thereby we discover the local and nonlocal formation of vacuum, waves and quanta of vacuum. For it we analyze and extend the concepts of spacetime and quantization. In the next section, we analyze why the concept of the volume is fundamental to concepts such as fields or GRT.

1.3 Principle of linear superposition

In this section we summarize and analyze essential physical quantities that can be added linearly.

1.3.1 Volume

Definition 1 The principle of linear superposition of the volumes: *If a volume ΔV consists of two volumes ΔV_1 and ΔV_2, then ΔV is the sum of ΔV_1 and ΔV_2.*

$$\Delta V = \Delta V_1 + \Delta V_2 \tag{1.1}$$

[2]The corresponding geometry is the **uniform scaling**, and the respective DEQ is the **FLE** (Friedmann (1922), Lemaitre (1927)).

[3]The vacuum has a volume and a density (Perlmutter et al. (1998), Riess et al. (2000)), and it propagates with the velocity of light, as it is fully relativistic.

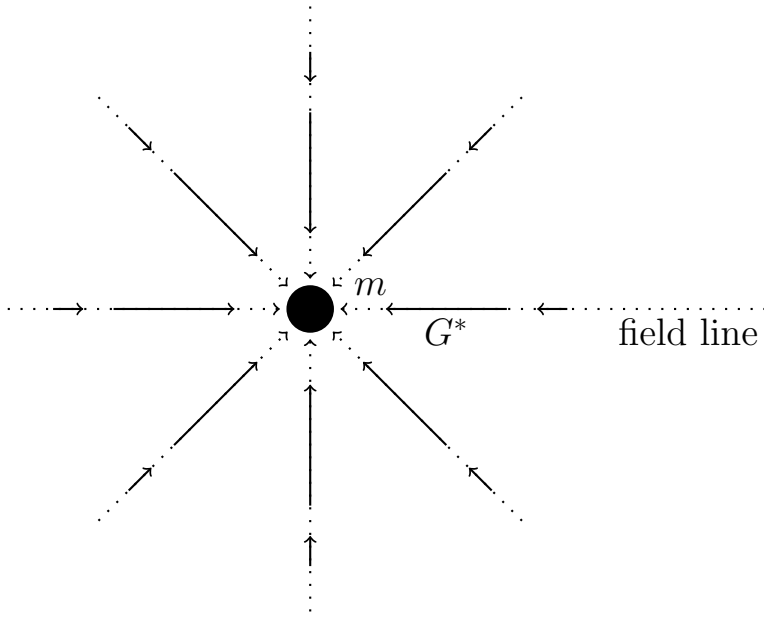

Figure 1.1: Mass m with field lines (dotted) and vectors (solid) of the gravitational field G^*.

Proposition 1 Necessity of linear superposition of volumes: *The principle of linear superposition of volumes in a frame is necessary for the following concepts:*

(1) The density ρ_E of a physical quantity E that can be distributed to two volumes ΔV_1 and ΔV_2.

(2) The theory of general relativity.

Proof: (1) We apply the principle of linear superposition of volumes to a quantity E and its density ρ_E:

$$\Delta E = \rho_E \cdot \Delta V = \rho_E \cdot (\Delta V_1 + \Delta V_2) \tag{1.2}$$

We expand:

$$\Delta E = \rho_E \cdot \Delta V_1 + \rho_E \cdot \Delta V_2 = \Delta E_1 + \Delta E_2 \tag{1.3}$$

If the principle of linear superposition of volumes would not hold, then the concept of the distribution of the quantity ΔE to the two volumes[4] ΔV_1 and ΔV_2 would not be applicable.

[4]For instance, if a room with a volume $\Delta V = 60m^3$ is divided into two rooms with equal volumes, then each of these rooms has the volume $\Delta V_1 = 30m^3$ and $\Delta V_2 = 30m^3$.

(2) The theory of general relativity essentially applies the concept of the energy density. For instance, that density is an element of the energy momentum tensor (Landau and Lifschitz (1981)). Additionally, the cosmological constant Λ characterizes an energy per volume (Einstein (1917)) and it corresponds to the dark energy, an energy per volume that was discovered[5] by Perlmutter et al. (1998) and Riess et al. (2000).

Altogether, the volume is a deep concept underlying also the GRT, for instance. In this book we analyze the formation of volumes that is inherent to the GRT. In particular, we will use that analysis of volumes in order to discover the time evolution, the dynamics, the waves, the quantization and the essential principles of the formation of volumes, vacuum and gravity in nature.

1.3.2 Fields, tensors, waves and quanta

The concept of fields includes the principle of linear superposition (Faraday (1852), Maxwell (1865)).

The concept of the tensor includes linear superposition. For instance strain tensors can be added linearly.

Also the concepts of a wave function in quantum theory and of a relatively small elongation of a wave fulfill linear superposition. Moreover, numbers of quanta are added linearly.

In this book we apply these concepts of linear superposition, as they have been tested empirically many times.

As gravity is essential for spacetime, we analyze properties of the universal law of gravitation in the next section.

1.4 $1/r^2$ law of fundamental fields

Newton (1686) proposed the **universal law of gravitation**: Two masses at a distance r interact by a force F proportional

[5] During the time between the proposal in 1917 and the discovery in 1998, there have been various opinions about Λ, see for instance (Zeldovich (1968)).

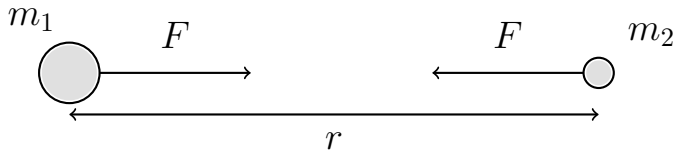

Figure 1.2: Universal law of gravitation.

to $1/r^2$ (1.2):

$$|\vec{F}| = \frac{G \cdot m_1 \cdot m_2}{r^2} \tag{1.4}$$

Similarly, Coulomb (1785) discovered the same $1/r^2$ law for the case of electric forces. However, it remained unclear, how these forces can act at a distance.

As an explanation, Faraday (1852) proposed that **field lines** of a **gravitational field** emerge from each mass m and distribute in the vicinity of that mass as illustrated in Fig. (1.1). Moreover, vectors G^* of the gravitational field emerge in the vicinity of that mass, these are parallel to the field lines. The force acting on a probing mass m is the product of the field G^* and m. So the field of a mass m at a distance r is:

$$|\vec{G^*}| = \frac{G \cdot m}{r^2} \tag{1.5}$$

Hereby G denotes the gravitational constant (Sect. 9.1).

Geometric basis of the $1/r^2$-law: According to the symmetry, the field lines distribute regularly in space. So they propagate radially from m with the direction equal to the inward direction of the force (Fig. 1.1). Hence the number N of lines crossing a sphere around m and with a radius r is invariant, in particular, it does not depend on r (Fig. 1.3). As the surface of the sphere is $A = 4\pi \cdot r^2$, the density N/A exhibits an $1/r^2$ law:

$$\frac{N}{A} = \frac{N}{4\pi \cdot r^2} \tag{1.6}$$

Since the lines emerge from the mass m, it is plausible that N is proportional to m. As the vectors $\vec{G^*}$ are parallel to the field

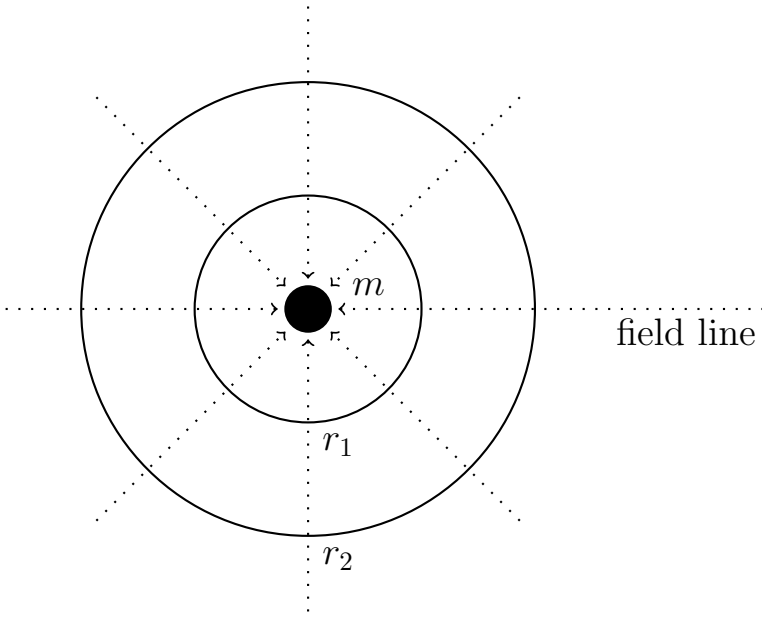

Figure 1.3: Mass m with field lines (dotted) and concentric spheres at radii r_1 and r_2. The number N of field lines crossing a concentric sphere with radius r is invariant.

lines, it makes sense that these are proportional to N/A:

$$\frac{N}{A} \propto |\vec{G}^*| \propto \frac{m}{r^2} \tag{1.7}$$

This establishes a geometric basis for the $1/r^2$ law of gravity and of other fundamental interactions.

The gravitational forces cannot be screened, and they decrease proportional to $\frac{1}{r^2}$, while the volume increases proportional to r^2. Hence the gravitational forces exhibit a **global range of influence** that cannot be screened. As a consequence, for any local investigation we need a universal frame in which that global range of influence is not present. Such a frame is developed in the next section.

1.5 Homogeneous universe frame HUF

While in section (1.4) we investigated the field of a mass without analyzing the surroundings, we consider the surroundings

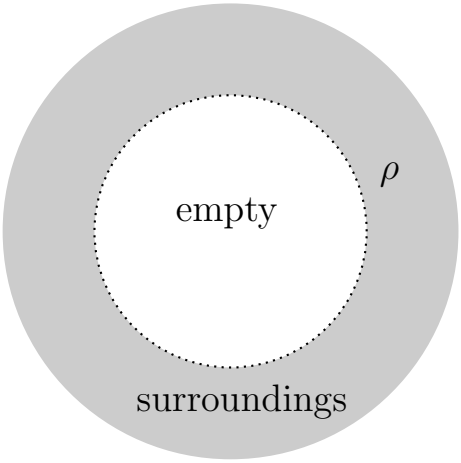

Figure 1.4: Empty ball embedded in a homogeneous surrounding: It establishes the **homogeneous universe frame, HUF**.

in this section. In particular, we analyze the field in an empty ball, embedded in surroundings with a homogeneous density, a **homogeneous fluid** (Fig. 1.4, Carmesin (2020b)). We emphasize that there is not even vacuum in this ball, so it is a purely mathematical model, as physical space is constituted by vacuum. So the empty ball is a tool[6] used for the analysis of the vacuum.

Newton (1686) showed that there is no field in such a sphere. For the case of the GRT, Birkhoff (1921) derived that there is no field in that sphere.

Even if the gravitational interaction propagates at the finite velocity of light, then the fields are limited by the light horizon, and each point of the sphere has its own light horizon. However, all these horizons are equivalent, as a result of translation invariance. So each point experiences the same gravitational field. Since the system is isotropic, that field is zero. Altogether, in the ball of vacuum, the field $\vec{G}^*$ is zero. We introduce a corresponding frame:

[6]In GRT, results are often derived by using an appropriate frame (see for instance Straumann (2013), Stephani (1980), Moore (2013)).

Definition 2 Homogeneous universe frame, HUF:

(1) If an empty ball is embedded in homogeneous surroundings ranging from the ball to the light horizon, and if that ball is not accelerated, then the frame with the origin at the center of the ball is called **homogeneous universe frame** *(Fig. 1.4).*

(2) A **vacuum HUF,** *HUF_v is a HUF for which the surroundings have the following property: The density parameters of radiation Ω_r and of the matter Ω_m (table 9.2) tend to zero. So the surroundings of a HUF_v consist of vacuum, up to an infinitesimal amount of radiation and matter, while $\Omega_K \approx 0$ (table 9.2).*

The field $\vec{G}^*$ is zero in the HUF. More realistically, the density of the surroundings exhibit fluctuations. These are analyzed in quantitative detail in section (8.3). As a result, the average of the field $\langle \vec{G}^* \rangle$ is zero in the HUF, and the variance $(\Delta \vec{G}^*)^2$ is nonzero. However, the variance $(\Delta \vec{G}^*)^2$ is a function of the radius R of the HUF, and that function decreases according to a power law: $(\Delta \vec{G}^*)^2 \propto R^{5-2D}$ for each dimension $D \geq 3$. The field variance $(\Delta \vec{G}^*)^2$ is particularly small for the case of a vacuum HUF. We summarize our findings:

Proposition 2 The HUF has the following properties.

The gravitational field is zero in the empty ball of the HUF.

A single object that might be added in the HUF does not experience any force or acceleration.

If there are fluctuations of the density in the surroundings, then the average of the field $\langle \vec{G}^* \rangle$ is zero in the HUF, and the variance of the field $(\Delta \vec{G}^*)^2$ tends to zero as the radius R of the HUF tends to infinity.

In the vacuum HUF, the variance of the field $(\Delta \vec{G}^*)^2$ is particularly small.

Corollary 1 *(1) The gravitational field in the HUF does not depend on the density of the surroundings. In particular, that density can be zero, corresponding to empty space.*

(2) The **potential of the HUF** *can be nonzero.*

In order to prepare the analysis of systems in the HUF, we summarize essential principles in the next section.

1.6 Equivalence principle and relativity

Above we saw that the field G^* emerges at a mass and spreads in space regularly. However, the field G^* cannot easily be distinguished from acceleration, moreover, space and time are connected to a spacetime as a consequence of the invariance of the velocity of light. We summarize these facts in this section.

Galileo (1638) discovered: If a mass m generates a gravitational field G^* (Eq. 1.5), and if a freely falling probing mass m experiences the corresponding force $F = m \cdot G^*$, then m exhibits an acceleration a that is equal to the field G^*:

$$\vec{G}^* = \vec{a} \rightarrow \quad \text{Galileo's EP} \tag{1.8}$$

This is Galileo's equivalence principle, EP. Einstein confirmed this principle and added, that an observer in a small box cannot distinguish the acceleration a from the gravitational field G^* on the basis of local observations.

$$\vec{G}^* \text{ locally indistinguishable from } \vec{a} \rightarrow \textbf{ Einstein's EP, EEP} \tag{1.9}$$

Michelson and Morley (1887) discovered that the velocity of light c is an invariant. On that basis, Einstein (1905) introduced the **special relativity theory, SRT**, in order to describe objects with high velocity in various **inertial frames**, these are frames that are not accelerated. As a particular consequence, space and time are no longer invariant, instead they form a four dimensional **spacetime**.

For instance, if two events occur within an object resting in its **own inertial frame**, then the time interval Δt beginning at the first event and ending at the second event depends on the inertial frame measuring Δt. The shortest Δt is measured in the own frame of the object, while the corresponding intervals are longer in external frames moving at a velocity v relative to the object:

$$\Delta t_{own} \leq \Delta t_{external} = \Delta t_{own} \cdot \gamma \text{ with } \gamma = \frac{1}{1 - v^2/c^2} \quad (1.10)$$

Thereby γ is called **Lorentz factor**, and v is the corresponding velocity.

Now we are well prepared to investigate the **Schwarzschild metric, SSM** by using the concepts of the HUF and the volume in the next three sections.

1.7 Schwarzschild metric, SSM: curvature

While the SRT describes objects that are not accelerated, Einstein (1915a) developed the **general relativity theory, GRT**, in order to describe accelerated objects and gravity. In the GRT, the spacetime may exhibit a continuous **curvature**. Using the GRT, Einstein (1915b) explained the precession of the perihelion of mercury. Additionally, Dyson et al. (1920) discovered the curvature of spacetime optically.

By applying the GRT, Schwarzschild (1916) derived the curvature of spacetime in the vicinity of a mass. That curvature of spacetime is usually described by the so-called **Schwarzschild metric, SSM**.

1.7.1 Novel results about the SSM

In the next two sections, we do not at all change the SSM, but we derive essential novel results about the SSM: In section (1.8), we apply the HUF or the HUF_v in order to derive an energy

function and a position factor. Hereby the position factor is the analogue of the Lorentz factor of SRT, and so it provides a very useful structure of the SSM that is an important basis of the following chapters.

In section (1.9), we derive the formation of additional volume that is inherent to the SSM. With it we derive in full detail the essential relation between local phenomena and global phenomena that are described by the GRT (see the following chapters).

1.8 SSM: gravitational field

In this section, we derive the SSM on the basis of the gravitational field G^*, the **EEP** and the SRT.

1.8.1 Field in curved spacetime

In this section, we derive the field[7] in the vicinity of a mass M. There is no gravity in the horizontal direction, by definition. Therefore there is no spatial elongation in this direction. Thus a circle with a radius r and with its center at a field-generating mass M at the **radial coordinate** $r = 0$ has the following circumference U:

$$U = 2\pi \cdot r \tag{1.11}$$

Likewise, a sphere with the center at $r = 0$ and with the **radial coordinate** r has the following surface A:

$$A = 4\pi \cdot r^2 \tag{1.12}$$

With it we derive G^* (Sect. 1.4):

$$\boxed{G^*(r) = -\frac{G \cdot M}{r^2}} \tag{1.13}$$

[7]Usually, we emphasize a field generating mass by a large letter M. Of course, all masses are in principle equal in physics. The distinction between a field generating mass and a probing mass is just a method of the analysis. It can easily be avoided by considering both masses as field generating masses and probing masses simultaneously. The above distinction may be appropriate, when one mass is relatively large compared to the other. Whenever a high accuracy is essential, then this distinction is not appropriate, of course.

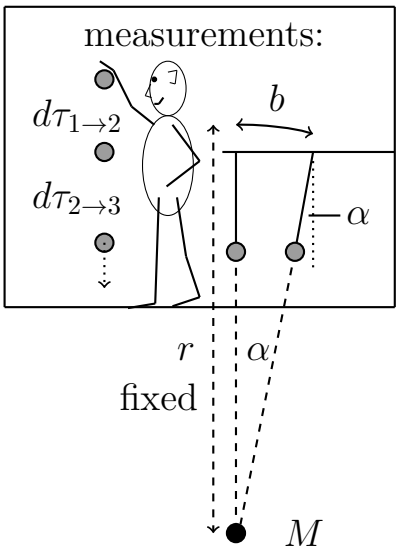

evaluation:

$$r = \frac{b}{\alpha}$$

for $j = 1$ and $j = 2$:

$$dr_{j\to j+1} = r_{j+1} - r_j$$

$$v_{j\to j+1} = \frac{dr_{j\to j+1}}{d\tau_{j\to j+1}}$$

$$dv = v_{2\to3} - v_{1\to2}$$

$$d\tau = \frac{d\tau_{1\to2}}{2} + \frac{d\tau_{2\to3}}{2}$$

$$a = \frac{dv}{d\tau} = G^*$$

$$M = -\frac{G^* \cdot r^2}{G}$$

Figure 1.5: A local observer localized at an object at r measures: Two hand leads provide the angle α and the arc length b. A falling ball yields time intervals in the observer's frame $d\tau_{j\to j+1}$. Therefrom r, v, a, G^* and M are evaluated.

1.8.2 Local measurements in curved spacetime

In this section, we derive physical quantities that can be measured locally in the vicinity of a mass M. An object at a coordinate r can be investigated in the object's own frame: In particular, a local observer localized at the object can measure the **radius** r, the 'object's own time' $d\tau$, the velocity $v = \frac{dr}{d\tau}$ relative to the mass M, the acceleration $a = \frac{dv}{d\tau}$ and the mass M as elaborated in Fig. (1.5). We summarize our results:

$$v = \frac{dr}{d\tau} \text{ and } a = \frac{dv}{d\tau} \text{ can be measured locally in GRT} \quad (1.14)$$

Definition 3 Field generating mass frame, FMF:

If a mass M (Fig. 1.5) is in a HUF, then there is a frame with M at its origin and with a radial coordinate r. We call it the **field generating mass frame, FMF**.

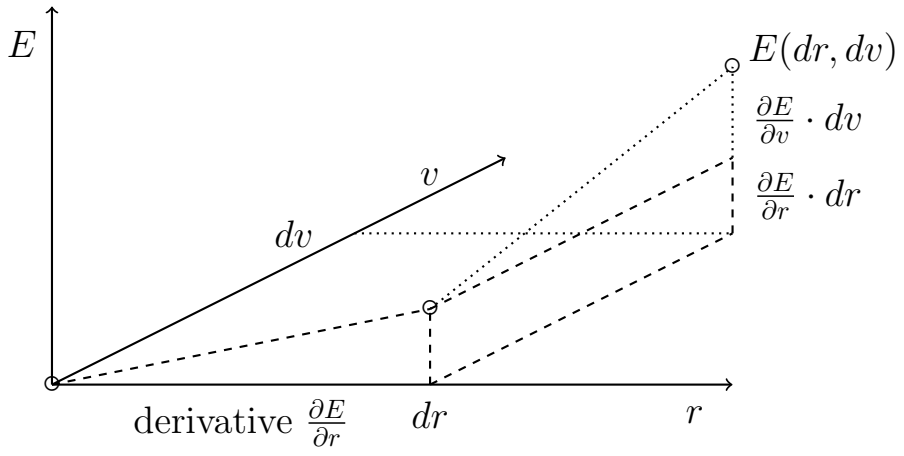

Figure 1.6: Change dE of $E(r, v)$ ($\circ$): The two slope triangles result in the changes $\frac{\partial E}{\partial v} \cdot dv$ and $\frac{\partial E}{\partial r} \cdot dr$. The total change $dE = E(r+dr, v+dv) - E(r, v)$ is the sum $dE = \frac{\partial E}{\partial v} \cdot dv + \frac{\partial E}{\partial r} \cdot dr$.

Proposition 3 Local observer:

If a mass M and a local observer at a fixed distance r relative to M (Fig. 1.5) are in a HUF, then the following holds:

(1) The situation can be analyzed in the FMF.

(2) M generates a radial gravitational **field** *with* $|\vec{G}^*| = \frac{GM}{r^2}$.

(3) The local observer at r (Fig. 1.5) can **locally observe** *the body's radial velocity $v(r) = \frac{\partial r}{\partial \tau}$ and its radial coordinate r of the FMF.*

1.8.3 Freely falling mass m

In this section we derive the **energy function** $E(r, v)$ of a mass m that is falling in the field of a mass M, and that starts at $r \to \infty$ and $v = 0$. Thereby, the velocity v and the radius r are measured relative to the mass M, and the own mass or rest mass is denoted by m_0. Solutions with more general initial conditions are elaborated in (Carmesin (2020b)).

For it we apply the **principle of energy conservation** (Mayer (1842)). In particular, we apply the **relativistic en-**

ergy derived in SRT (Einstein (1905) or Carmesin (2020b)):

$$E(v) = m_0 \cdot c^2 \cdot \gamma(v) \quad \text{in SRT and with} \quad \gamma(v) = \frac{1}{\sqrt{1 - v^2/c^2}} \tag{1.15}$$

As m is falling, the velocity v increases and r decreases. Hence the energy would increase by the factor $\gamma(v)$ according to Eq. (1.15). Correspondingly, the energy decreases by a **position factor** $\epsilon(r) = 1/\gamma(v)$, so that the energy is conserved. So we get:

$$E = m_0 \cdot c^2 \cdot \gamma(v) \cdot \epsilon(r) \quad \text{with} \quad \gamma(v) = 1/\epsilon(r) \tag{1.16}$$

The functional term of $\epsilon(r)$ must be determined. We consider the change dE of the energy, which obviously depends on r and v (Fig. 1.6). Accordingly we get:

$$dE = \frac{\partial E}{\partial r} dr + \frac{\partial E}{\partial v} dv \tag{1.17}$$

From this equation we obtain a differential equation, DEQ, for $\epsilon(r)$. According to the principle of energy conservation, dE is zero. The derivative regarding v is $\frac{\partial E}{\partial v} = E \cdot \gamma^2 \cdot v/c^2$, while the derivative regarding r is $\frac{\partial E}{\partial r} = E \cdot \epsilon'/\epsilon$ with $\epsilon' = \frac{d\epsilon}{dr}$. So we get:

$$0 = E \cdot \frac{\epsilon'}{\epsilon} \cdot dr + E \cdot \gamma^2 \cdot \frac{v}{c^2} \cdot dv \tag{1.18}$$

We divide by E and $d\tau$ and use $v = \frac{dr}{d\tau}$ and $a = \frac{dv}{d\tau}$ (Eq. 1.14 and Fig. (1.5). We also resolve for ϵ'. Therefore we obtain:

$$\epsilon' = -\frac{\epsilon \cdot \gamma^2}{c^2} \cdot a \tag{1.19}$$

We use $\gamma(v) = 1/\epsilon(r)$ (Eq. 1.16). We utilize the equivalence principle of the GRT $a = -G^* = -\frac{G \cdot M}{r^2}$ (Eq. 1.13, here a is directed downwards, see Fig. 1.5), too. So we derive:

$$\epsilon' = \frac{1}{\epsilon \cdot c^2} \cdot \frac{G \cdot M}{r^2} \tag{1.20}$$

We use the well known term $R_S = \frac{2G \cdot M}{c^2}$ for the **Schwarzschild radius**. So we get the following DEQ for $\epsilon(r)$:

$$\boxed{\epsilon' = \frac{1}{\epsilon} \cdot \frac{R_S}{2r^2}} \tag{1.21}$$

Solution of the DEQ for ϵ: For the case of a constant mass M, we solve the DEQ for ϵ with the following Ansatz:

$$\boxed{\epsilon(r) = \sqrt{1 - \frac{R_S}{r}}} \tag{1.22}$$

The derivative corresponds to the DEQ (1.21). So Eq. (1.22) is a solution. We use the two factors $\epsilon(r)$ and $\gamma(v)$ in Eqs. (1.16, 1.22, 1.15)). So we get a term for the **invariant** energy depending on r and v:

$$\boxed{E(r, v) = m_0 \cdot c^2 \cdot \frac{\sqrt{1 - \frac{R_S}{r}}}{\sqrt{1 - v^2/c^2}}} \tag{1.23}$$

This term generally represents the functional dependence of the energy on r and v. Landau and Lifschitz (1981) obtain the same result (page 299), this confirms our derivation. We summarize:

Proposition 4 Energy in the FMF: *If a* **field generating mass** *M is in a HUF, then an* **own mass** *m_0 has the following properties:*

(1) The mass m_0 can be analyzed in the FMF.

(2) In the FMF, M generates a radial gravitational **field** *with the value $G^* = |\vec{G}^*| = \frac{GM}{r^2}$.*

(3) A local observer at r can **locally observe** *the body's radial velocity $v(r) = \frac{\partial r}{\partial \tau}$ and its radial coordinate r of the FMF (see proposition 3 and Fig. 1.5).*

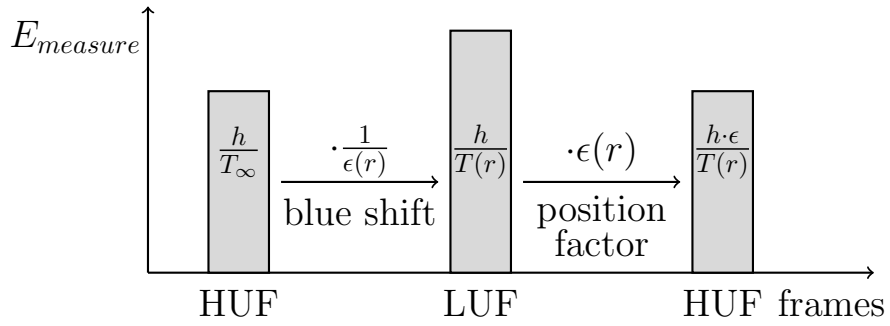

Figure 1.7: Photon propagating down towards a mass M: Measured energy $E_{measure}$ in the HUFand LUF.

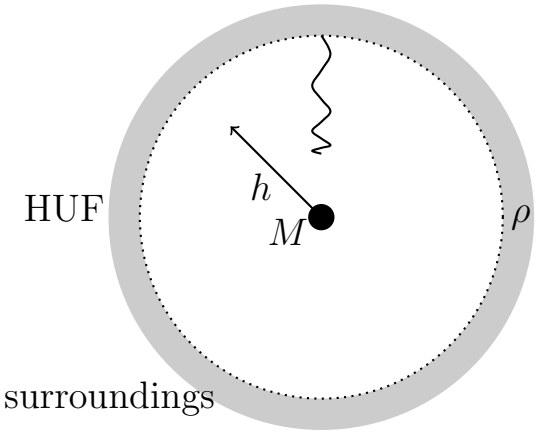

Figure 1.8: A **field generating mass frame, FMF**, is embedded in a HUF. The height h characterizes the field. A photon is falling down, thereby its wavelength decreases.

(4) If the probing mass falls freely in the field of M, and if $v = 0$ at $r \to \infty$, then the **energy function** *$E(r, v)$ of m_0 is described by Eq. (1.23):*

$$E(r, v) = m_0 \cdot c^2 \cdot \frac{\sqrt{1 - \frac{R_S}{r}}}{\sqrt{1 - v^2/c^2}} \tag{1.24}$$

(5) In particular, that energy function $E(r, v)$ of m_0 represents an **invariant** *of the motion in the FMF.*

1.8.4 Metric

In this section we derive the Schwarzschild metric on the basis of the above derived energy function in Eq. (1.23).

Blue shift: For it we consider a photon that is placed in a HUF, and that starts at $r \to \infty$, and that has a corresponding periodic time T_∞ (see left rectangle in Fig. 1.7), and that falls vertically towards a field-generating mass M at $r = 0$. Thus the energy of the photon is:

$$E_{HUF}(r \to \infty) = \frac{h}{T_\infty} \tag{1.25}$$

The field generating mass M generates the field G^*. The energy in the field is described by the position factor $\epsilon(r)$.

For instance, if the position r of the photon decreases, then its energy decreases by that position factor $\epsilon(r)$ and is simultaneously multiplied by the inverse factor $\frac{1}{\epsilon(r)}$, so that the energy remains invariant.

If the photon is observed in a local frame at the radius r, then the observer has the same position factor as the photon, and so the measurement apparatus only takes care of the inverse position factor $\frac{1}{\epsilon(r)}$ by measuring the energy $\frac{h}{T_\infty} \cdot \frac{1}{\epsilon(r)}$ of the photon in the local frame. As a consequence, the photon appears to have the short periodic time:

$$T(r) = T_\infty \cdot \epsilon(r) \tag{1.26}$$

This corresponds to a blue shift (see central rectangle in Fig. 1.7), and the energy of the photon in the local frame is as follows:

$$E_{blue\ shift} = \frac{h}{T(r)} = \frac{h}{T_\infty \cdot \epsilon(r)} = \frac{E_{HUF}(r \to \infty)}{\epsilon(r)} \tag{1.27}$$

Many observations are carried out in such a local frame (see central rectangle in Fig. 1.7).

Definition 4 Local universe frame, LUF: *A frame that is accelerated or that experiences a field or a curvature of space-time or that is falling freely is called* **local universe frame, LUF**.

For instance, a LUF may be embedded in a HUF, and it may contain a field generating mass, or it may be falling freely.

In general, the energy in such a local frame is obtained from the corresponding energy in the HUF by multiplication with the inverse position factor, $\frac{1}{\epsilon(r)}$.

$$\boxed{E_{LUF} = \frac{E_{HUF}(r \to \infty)}{\epsilon(r)} \text{ for description via } \epsilon(r)} \tag{1.28}$$

Alternatively, the local frame can be described by a potential energy $E_{pot}(r)$ instead of a position factor $\epsilon(r)$. In that case, the energy in the LUF is obtained from the corresponding energy in the HUF by subtracting the potential energy $E_{pot}(r)$:

$$E_{LUF} = E_{HUF}(r \to \infty) - E_{pot}(r) \text{ descr. via } E_{pot} \tag{1.29}$$

Conversely, the energy in the HUF is obtained from the energy in the LUF by multiplication with the position factor, see right rectangle in Fig. (1.7) and Eq. (1.28). In the case of a description with a potential energy, the energy in the HUF is obtained from the energy in the LUF by subtracting the potential energy, see Eq. (1.28).

Gravitational time dilation: The periodic time $T(r)$ of photons is used for time measurement, e.g. in atomic clocks (Bundesanstalt (2007), Lombardi et al. (2007)). Accordingly, the periodic time changes the time interval $dt(r)$ by the same factor:

$$dt(r) = dt_\infty \cdot \epsilon(r) \text{ in the LUF} \tag{1.30}$$

Altogether, the time elapses at a decreased rate near M. This effect is called **gravitational time dilation**.

Gravitational radial elongation: An observer in the HUF at $r \to \infty$ measures a radial length L_{LUF} in a LUF at finite r. For it, the observer sends a light signal to a mirror in a LUF, detects the reflected signal, and measures the **t**ime **o**f **f**light $t_{tof,HUF}$ with a clock in the HUF. The observer evaluates the length (as the light propagates the path twice, there is a factor 1/2):

$$L_{HUF} = t_{tof,HUF} \cdot c \cdot \frac{1}{2} \tag{1.31}$$

We apply $t_{tof,HUF} = t_{tof,LUF}/\epsilon(r)$:

$$L_{HUF} = t_{tof,LUF} \cdot c \cdot \frac{1}{2} \cdot \frac{1}{\epsilon(r)} \tag{1.32}$$

We identify $t_{tof,LUF} \cdot c \cdot \frac{1}{2}$ by L_{LUF}:

$$L_{HUF} = L_{LUF} \cdot \frac{1}{\epsilon(r)} > L_{LUF} \tag{1.33}$$

Altogether, the radial length increases near M. We identify this effect as a **gravitational radial elongation**.

Metric tensor: For the purpose of possible comparisons with a tensor formulation of GRT (see for instance Einstein (1915a), Stephani (1980), Carmesin (1996), Moore (2013)), we express the above results in terms of the metric tensor. A line element ds in spacetime is expressed as follows:

$$ds^2 = \Sigma_{i=0,j=0}^{i=3,j=3} \; g_{ij} \; dx_i \cdot dx_j \tag{1.34}$$

For the case of a change $dx_j = c \cdot dt_\infty = dx_i$, we get:

$$dt(r)^2 = |g_{tt}| \cdot dt_\infty^2 \;\; \text{or} \;\; |g_{tt}| = \epsilon(r)^2 = 1 - \frac{R_S}{r} \tag{1.35}$$

For the case of a change $dx_j = dr_\infty = dx_i$, we get:

$$dR(r)^2 = g_{rr} \cdot dR_\infty^2 \;\; \text{or} \;\; g_{rr} = \frac{1}{\epsilon(r)^2} = \frac{1}{1 - \frac{R_S}{r}} \tag{1.36}$$

According to the isotropic field near M, the metric factors for the angular polar coordinates are zero, as there is no gravity in the horizontal direction:

$$g_{\theta\theta} = 1 = g_{\phi\phi} \tag{1.37}$$

For the same reason, all non-diagonal elements are zero.

$$g_{i,j} = 0 \text{ for } i \neq j \tag{1.38}$$

According to a convention, the element g_{tt} is supplemented by a factor -1 (Straumann (2013), Stephani (1980), Carmesin (1996)). We present the derived tensor elements by the vector notation in the following Eq. below. We summarize our derivation:

Theorem 1 Direct derivation of the SSM from the EEP, the gravitational field and the SRT: *The Schwarzschild metric, SSM, can be derived from the SRT as follows:*

(1) The energy function $E(r, v)$ in the **field generating mass frame, FMF** *is derived from the gravitational field, the EEP and the SRT*[8]*:*

$$E(r, v) = m_0 \cdot c^2 \cdot \frac{\sqrt{1 - R_S/r}}{\sqrt{1 - v^2/c^2}} \tag{1.39}$$

(2) The elements of the metric tensor g_{ij} are derived by analyzing a photon in the **local universe frame, LUF***:*

$$g_{i,j} = \begin{pmatrix} 1 - \frac{R_S}{r} & 0 & 0 & 0 \\ 0 & \frac{1}{1-\frac{R_S}{r}} & 0 & 0 \\ 0 & 0 & 1 & 0 \\ 0 & 0 & 0 & 1 \end{pmatrix} \tag{1.40}$$

.

In the case of the SSM, both frames are equal, as the field of the LUF is generated by the mass of the FMF.

[8]It will be derived later that physical states fulfill the relation $R > R_S$.

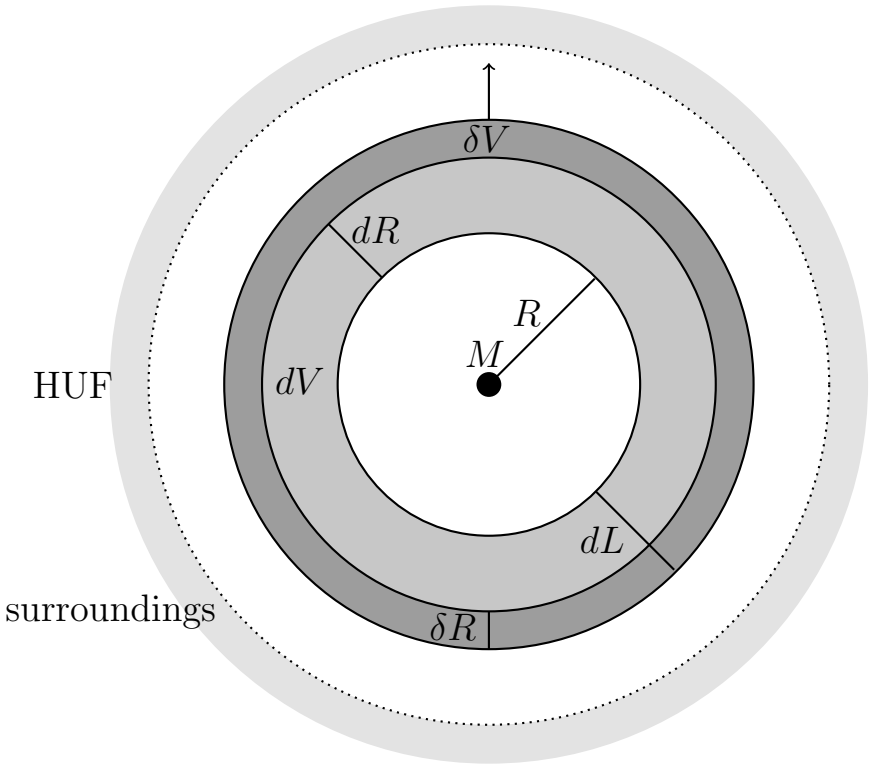

Figure 1.9: In the Schwarzschild metric, a length dR is elongated by an additional length δR, corresponding to an additional volume δV.

1.9 SSM: additional vacuum

The SSM describes the radial elongation of the lengths. As a consequence, there is an **additional volume of radial elongation**, δV_{SSM} see Fig. (1.9). In this section we analyze the amount of that δV_{SSM}.

In the vicinity of a mass M, a radial coordinate distance dR is increased by an additional coordinate distance δR, see Fig. (1.9). Here and in the following, we describe an infinitesimal radius R by dR, and we describe it by δR, for the case of an additional or formed volume. Analogously, we name other infinitesimal quantities. That additional length corresponds to an additional vacuum δV_{SSM}. It is analyzed in this section.

According to the SSM (see Schwarzschild (1916) or Carmesin (2020b)), the coordinate distance dR at a coordinate R in Fig. (1.9) is elongated to the following length dL:

$$dL = \frac{dR}{\sqrt{1 - R_S/R}} \quad \text{with} \quad R_S = \frac{2GM}{c^2} \tag{1.41}$$

Thus the additional coordinate distance in Fig. (1.9) is:

$$\delta R = dL - dR \tag{1.42}$$

Hence the additional volume in Fig. (1.9) is:

$$\delta V = 4\pi \cdot R^2 \cdot \delta R \tag{1.43}$$

Linear approximation: For large distances, $\frac{R_S}{R} << 1$, we expand Eq. (1.41) linearly in $\frac{R_S}{R}$. So we get:

$$dL \doteq dR + dR \cdot \frac{1}{2} \cdot \frac{R_S}{R} \quad \text{or} \tag{1.44}$$

$$\boxed{\delta R_{SSM} \doteq dR \cdot \frac{1}{2} \cdot \frac{R_S}{R}} \tag{1.45}$$

Principle of equivalence of curvature and vacuum: In general, the space in which we live exhibits a curvature and consists of vacuum (with a measurable density ρ_Λ). Hence a possible increase of the volume caused by the curvature should be equivalent to additionally formed vacuum. We express that insight in terms of a principle:

Definition 5 Principle of the equivalence of curvature and vacuum:

If the curvature of spacetime at a point $(t, \vec{R})$ corresponds to an elongation δR of a length $dR = c \cdot dt$ that is orthogonal to an area dA, then the volume $\delta V = \delta R \cdot dA$ is filled with **locally formed vacuum, LFV** *that propagates through that volume δV.*

According to the above principle, the additional volume is:

$$\boxed{\delta V_{SSM} \doteq 2\pi \cdot R \cdot R_S \cdot dR = dV \cdot \frac{1}{2} \cdot \frac{R_S}{R}} \tag{1.46}$$

The additional vacuum is in the vicinity of the mass M. We specify it in a definition:

Definition 6 Locally formed vacuum: *The additional vacuum δV that forms in the vicinity of a local source with a mass or dynamical mass M is called* **locally formed vacuum, LFV**.

(1) Hereby the mass M is characterized by its Schwarzschild radius:

$$R_S = \frac{2GM}{c^2} \tag{1.47}$$

(2) If the mass M is a dynamical mass, then it is characterized by that Schwarzschild radius, to which it would collapse. In particular, if M is characterized by a radius R, then R_S is as follows:

$$R_S = \frac{2GM(R_S)}{c^2} \quad \text{with} \quad M(R) = M(R_S) \cdot \frac{R_S}{R} \tag{1.48}$$

(3) In principle the LFV can flow inward or outward. In the case of a Big Bang, the direction of the flow of the vacuum is outwards. In the case of a conceivable Big Crunch (Goodstein (1997)), the direction of the flow of the vacuum is reversed, while the required volume and the caused elongations remain the same. As our universe expands, we elaborate the outflow of vacuum in this book.

We summarize our novel concept and result:

Theorem 2 Locally formed vacuum of the SSM: *As a consequence of the SSM, a mass M with a Schwarzschild radius R_S at the center of an empty sphere with radius R, generates the* **locally formed vacuum, LFV**, *$\delta V_{SSM,LFV}$, in that sphere during a time δt as follows:*

(1) The locally formed vacuum, LFV has the following amount:

$$\delta V_{SSM}(M,R,dt) \doteq 2\pi \cdot R \cdot R_S \cdot dR = dV \cdot \frac{1}{2} \cdot \frac{R_S}{R} \qquad (1.49)$$

(2) In a shell with radius R and width $dR = c \cdot dt$, the LFV $\delta V_{SSM,LFV}$ that permanently flows outwards, can fill a shell with the following radius:

$$\delta R_{SSM,LFV}(M,R,dt) \doteq dR \cdot \frac{1}{2} \cdot \frac{R_S}{R} \qquad (1.50)$$

While we analyzed the additional volume in the SSM in the previous sections, we apply that concept to the expansion of space according to the FLE in the next three sections. Thereby we compare these volumes, of course.

1.10 Expansion of space

Einstein (1917) analyzed a possible expansion of the space. Slipher (1915) discovered the redshift of distant galaxies, Wirtz (1922) analyzed empirical evidence for the expansion of space,

and Hubble (1929) obtained a convincing empirical basis for that expansion of space.

That expansion of space since the Big Bang is usually described by a **uniform scaling**. In this section we derive the DEQ for the case of a homogeneous ball embedded in a HUF (Fig. 1.10).

1.10.1 DEQ of uniform scaling: derivation

The surroundings do not generate a field $\vec{G}^*$ in the embedded sphere (sect. 1.5). A homogeneous sphere with a mass M generates a field in its vicinity that is equal to the field generated by the mass M in the center of the ball (Gauss (1840)). So the Schwarzschild solution applies (Eq. 1.23), and thus the energy of a probing mass with the condition $(r|v) = (r|\dot{r}) = (\infty|0)$ at some time is as follows (other conditions are analyzed in Carmesin (2020b)):

$$E(r,v) = m_0 \cdot c^2 \cdot \gamma(v) \cdot \epsilon(r) = E_0 \text{ or } E_{ref} \tag{1.51}$$

Thereby the factors are:

$$\gamma(v) = \frac{1}{\sqrt{1 - v^2/c^2}} \; ; \; \epsilon(r) = \sqrt{1 - \frac{R_S}{r}} \text{ and } m_0 \cdot c^2 = E_0 \tag{1.52}$$

The Eq. (1.51) represents a DEQ, as it contains v, which in turn represents a derivative. This DEQ describes the dynamics of the probing mass. Next we transform this DEQ, in order to obtain a transformed DEQ, still describing the dynamics of m and $r(t)$.

1.10.2 Structured energy function

In this section we derive a **structured energy function**. This may be interpreted as a result of a mathematical transformation of the DEQ, or it may be interpreted physically in addition:

The structured energy function might be interpreted as a normalized **excess energy** (Carmesin (2020b)) as follows:

In SRT, the difference of the square E^2 of the energy and of the square of the own energy $m_0^2 \cdot c^4 = E_0^2$ represents the square of the kinetic energy $p^2 \cdot c^2$. By construction, it represents the square of the excess energy that the mass m has compared to its own mass m_0.

In GRT, that excess energy contains the kinetic energy and, additionally, a gravitational energy in the field.

Correspondingly, we derive the excess energy in GRT as follows: We take the square of Eq. (1.51), and we subtract the squared own energy $m_0^2c^4$ (so we obtain the square of the generalized excess energy):

$$E(r,v)^2 - m_0^2c^4 = m_0^2 \cdot c^4 \cdot (\epsilon(r)^2 \cdot \gamma(v)^2 - 1) \tag{1.53}$$

In the model of the uniform scaling, there is no essential velocity of the objects in space. Correspondingly, we divide by γ^2, in order to transform the energy to a **frame in which the velocity is zero** (see Eq. 1.51):

$$\frac{E(r,v)^2 - m_0^2c^4}{\gamma^2} = m_0^2 \cdot c^4 \cdot (\epsilon(r)^2 - \gamma(v)^{-2}) \tag{1.54}$$

In order to simplify, we insert the factors $\epsilon(r)$ and $\gamma(v)$:

$$\boxed{\frac{E(r,v)^2 - m_0^2c^4}{\gamma^2} = m_0^2c^4 \cdot \left(\frac{v^2}{c^2} - \frac{R_S}{r}\right)} \tag{1.55}$$

Conventional form: In this paragraph, we derive a conventional energy function with a conventional kinetic and potential energy term. For it we divide by $2m_0c^2$. So we get:

$$\frac{E(r,v)^2 - m_0^2c^4}{2\gamma^2 m_0c^2} = m_0 \cdot c^2 \cdot \left(\frac{v^2}{c^2} - \frac{R_S}{r}\right) \cdot \frac{1}{2} \tag{1.56}$$

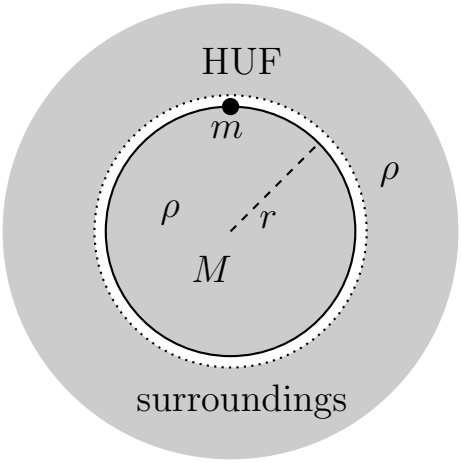

Figure 1.10: Ball with mass M and radius r embedded in a homogeneous surrounding and exhibited to a probing mass m.

We denote that energy function with a bar, $\bar{E}(r, v)$. We apply the Schwarzschild radius $R_S = \frac{2GM}{c^2}$: So the result is a conventional structured energy function:

$$\boxed{\frac{E(r,v)^2 - E_0^2}{2\gamma^2 E_0} =: \bar{E}(r,v) = \frac{m_0 \cdot v^2}{2} - \frac{G \cdot M \cdot m_0}{r}} \tag{1.57}$$

Form with the Hubble parameter: In this part we transform the DEQ (1.55) further so that we obtain a term for the **Hubble parameter**:

$$H = \frac{\dot{r}}{r} \tag{1.58}$$

For it, we multiply with $\frac{1}{m_0^2 \cdot c^4} \cdot \frac{c^2}{r^2}$, and we use the density $\rho = \frac{M}{r^3 \cdot 4\pi/3}$. So we get:

$$\frac{E(r,\dot{r})^2 - m_0^2 c^4}{m_0^2 \cdot c^4 \gamma^2} \cdot \frac{c^2}{r^2} = \frac{\dot{r}^2}{r^2} - \frac{8\pi G \cdot \rho}{3} \tag{1.59}$$

We identify the scaled squared energy $-\frac{E(r,\dot{r})^2 - m_0^2 c^4}{m_0^2 \cdot c^4 \gamma^2}$ or the scaled energy term $-\frac{2\bar{E}(r,\dot{r})}{m_0 \cdot c^2}$ with the so-called **curvature parameter** k (Friedmann (1922), Lemaitre (1927), Stephani (1980)), we

identify $\frac{\dot{r}^2}{r^2}$ by the squared Hubble parameter H^2, and we solve for H^2. So we get the **Friedmann Lemaître equation, FLE** (Friedmann (1922) and Lemaitre (1927)), the DEQ for the homogeneous system:

$$\boxed{H^2 = \frac{8\pi G \cdot \rho}{3} - k \cdot \frac{c^2}{r^2}} \tag{1.60}$$

Observations (Collaboration (2020), Bennett et al. (2013)) and theory (Carmesin (2020b)) show that the curvature parameter k is zero, which means the space is globally flat. We summarize our derivation:

Theorem 3 Direct derivation of the FLE from the SSM: *The expansion of the universe has the following properties:*

(1) In classical GRT, it is described by a **uniform scaling** *with a scale factor $r(t)$ Fig. (1.10).*

(2) In classical GRT, the time evolution of the scale factor $r(t) $ is described by the FLE:

$$H^2 = \left(\frac{\dot{r}}{r}\right)^2 = \frac{8\pi G \cdot \rho}{3} - k \cdot \frac{c^2}{r^2} \tag{1.61}$$

(3) The FLE of that uniform scaling can be derived from the time evolution of a **microscopic probing mass** *m as follows:*

(3a) In the HUF with density ρ, there is a homogeneous ball of the universe with the same density and generating a field $\vec{G}^*$, and m is at the surface of that ball (Fig. 1.10).

(3b) The time evolution of m is derived from the SSM, see the DEQ (1.51) as well as the transformed DEQ (1.57).

(4) Thereby, these above two DEQs use a **structured energy function** *$\bar{E}(r,\dot{r})$ with $\bar{E}(r,\dot{r}) = 0 = k = $ invariant:*

$$\boxed{-k := \frac{2\bar{E}(r,\dot{r})}{m_0 \cdot c^2} \text{ with } \bar{E}(r,\dot{r}) = \frac{m_0 \dot{r}^2}{2} - \frac{GMm_0}{r}} \tag{1.62}$$

(5) That **structured energy function** *is defined as follows and proportional to E_0 and a normalized energy $E_{norm} = \frac{\bar{E}}{E_0}$:*

$$\boxed{\frac{E(r,\dot{r})^2 - E_0^2}{2\gamma^2 E_0} =: \bar{E}(r,\dot{r}) = E_0 \cdot \left(\frac{\dot{r}^2}{2c^2} - \frac{G \cdot M}{r \cdot c^2}\right)} \tag{1.63}$$

After we analyzed the expansion of space by using the concepts of the uniform scaling, the HUF and the law of energy conservation, we analyze the additional vacuum in the following section.

1.11 Homogeneous metric: new vacuum

The expansion of space is usually described by a mathematical transformation: the uniform scaling. In this section we analyze, how that transformation is generated by the permanent and ubiquitous formation of new vacuum. This novel analysis is based on the fundamental concept of linear superposition of volume (see proposition 1).

1.11.1 Rate of formed vacuum

The increase of the radius corresponds to an increase of the volume. Hence additional vacuum is formed. In this section we summarize the rate at which the vacuum forms. This rate is derived from the FLE[9]. The flat, isotropic and homogeneous space expands according to the Hubble parameter:

$$H = \frac{\partial a}{\partial t \cdot a} = \sqrt{8\pi \cdot G/3} \cdot \sqrt{\rho} \tag{1.64}$$

The volume of a ball of the universe with radius a is $V = \frac{4\pi}{3}a^3$. With it we derive the rate of increase of the volume V by applying the chain rule:

$$\frac{\partial V}{\partial t \cdot V} = \frac{1}{V} \cdot \frac{\partial V}{\partial t} = \frac{1}{V} \cdot \frac{\partial V}{\partial a} \cdot \frac{\partial a}{\partial t} = \frac{3}{a} \cdot \frac{\partial a}{\partial t} = 3H \tag{1.65}$$

[9]Carmesin (2018c), Carmesin (2018b), Carmesin (2019b)

So the flat, isotropic and homogeneous space expanding according to the Hubble parameter exhibits the following DEQ for the rate of increase of the volume:

$$\boxed{\left(\frac{\partial V}{\partial t \cdot V}\right)^2 = 24\pi \cdot G \cdot \rho} \tag{1.66}$$

Similarly as in the case of the volume generated in the SSM (see theorem 1), we denote the additional volume by δV. Correspondingly, we denote the time difference by δt. Moreover, we may consider infinitesimal amounts of volume dV rather than V So we derive the following DEQ:

$$\left(\frac{\delta V}{\delta t \cdot dV}\right)^2 = 24\pi \cdot G \cdot \rho \tag{1.67}$$

Furthermore, we denote the **relative volume** by ε:

$$\frac{\delta V}{dV} = \varepsilon \tag{1.68}$$

With it we derive the **rate of the formation of relative volume**:

$$\dot{\varepsilon} = \sqrt{24\pi \cdot G \cdot \rho} \tag{1.69}$$

We summarize our novel concept and our derivation:

Theorem 4 Formed vacuum causes expansion of space: *The uniform scaling that describes the expansion of space is caused by a rate of additionally formed vacuum with the following properties:*

(1) The density ρ in a ball causes the permanent formation of additional vacuum.

(2) For a ball with radius R, the volume of the additional vacuum δV per volume dV and per time δt is described by the following rate:

$$\frac{\delta V}{\delta t \cdot dV} = \dot{\varepsilon} = \sqrt{24\pi \cdot G \cdot \rho} \tag{1.70}$$

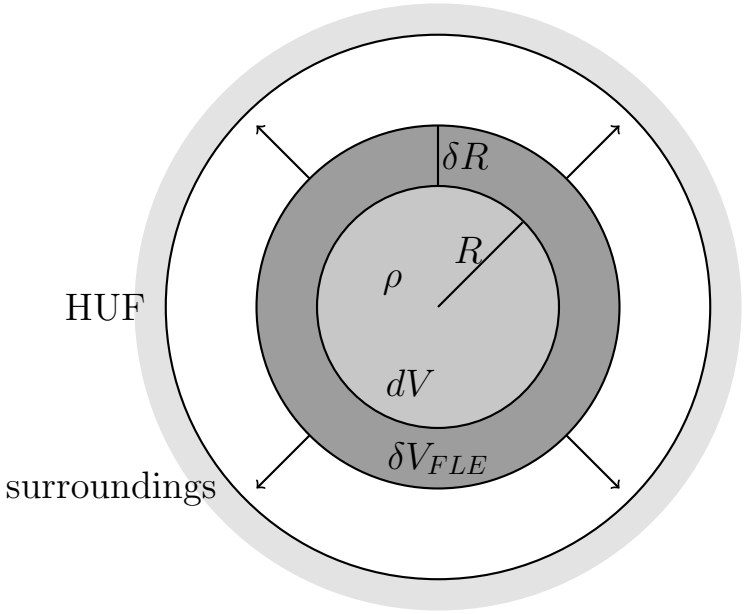

Figure 1.11: A ball with a density ρ and a radius R is placed in a HUF, and it generates a vacuum δV_{FLE} during a time δt. It flows outward, and it requires a shell with a thickness δR.

After we identified and quantified the additional vacuum that forms during the expansion of space, we derive a DEQ describing that formation directly. Moreover we compare the rates of formation of vacuum inherent to the SSM and to the uniform scaling.

1.12 Vacuum formed according to FLE

In this section we analyze the vacuum that is formed by a homogeneous mass M with the radius R_M that is larger than its Schwarzschild radius R_S.

We consider a dynamical mass that exhibits a redshift when it expands from $R = R_S$. So the mass $M(R)$ is a function of its radius R as follows:

$$M(R) = M(R_S) \cdot \frac{R_S}{R} \tag{1.71}$$

So the density is:

$$\rho = \frac{M(R)}{R^3 \cdot 4\pi/3} = \frac{3}{4\pi} M(R_S) \cdot R_S \cdot R^{-4} \tag{1.72}$$

We apply the Schwarzschild radius $R_S = \frac{2GM(R_S)}{c^2}$:

$$\rho = \frac{3}{8\pi \cdot G} \cdot c^2 \cdot R_S^2 \cdot R^{-4} \tag{1.73}$$

We derive the vacuum δV that is formed by this constant density by using the corresponding rate (theorem 4):

$$\delta V = dt \cdot dV \cdot \sqrt{24\pi \cdot G \cdot \rho} \tag{1.74}$$

We insert the above density, and we apply the volume of the ball $dV = \frac{4\pi}{3} R^3$ (Fig. 1.11):

$$\delta V = dt \cdot \frac{4\pi}{3} R^3 \cdot \sqrt{9c^2 \cdot R_S^2 / R^4} \tag{1.75}$$

We evaluate the root, and we simplify. So we derive the vacuum δV_{FLE} that is formed according to the FLE (see theorem 4) during a time dt in a ball with density a ρ and radius R:

$$\boxed{\delta V = 4\pi \cdot R_S \cdot R \cdot dt \cdot c = \delta V_{FLE}(M, R, dt)} \tag{1.76}$$

The vacuum that is formed according to the FLE describes the vacuum that additionally arrives in the expanding universe. So it is the **complete formed vacuum, CFV**. The difference of the CFV and the LFV must be formed nonlocally, so it is **nonlocally formed vacuum, NFV**.

Definition 7 Complete and nonlocal formed vacuum:

The vacuum formed during the expansion of space is called **complete formed vacuum, CFV**.

The CFV minus the LFV is the **nonlocally formed vacuum, NFV**.

1.13 A volume of spacetime

In this section we analyze the following **spacetime volume**:

System: If there is a HUF with a center at a radial coordinate $r = 0$, and if a mass M has its center of mass at $r = 0$, and if a shell in the HUF has its center at $r = 0$, a radius R and a **thickness** $dR = c \cdot dt$, and if $R_S = \frac{2GM}{c^2}$, and if $dV = 4\pi R^2 \cdot c \cdot dt$ is the volume of the shell, then the **spacetime volume** $dV \cdot dt$ can increase as follows: dV can increase by the volume δV that forms in the ball with radius R during the time dt, and dt can increase by δt as a result of a curvature.

SSM: In the SSM we apply the total differential:

$$\delta(dV \cdot dt)_{SSM} = \delta V_{SSM} \cdot \frac{\partial(dV \cdot dt)}{\partial dV} + \delta t_{SSM} \cdot \frac{\partial(dV \cdot dt)}{\partial dt} \quad (1.77)$$

We evaluate the derivatives:

$$\delta(dV \cdot dt)_{SSM} = \delta V_{SSM} \cdot dt + \delta t_{SSM} \cdot dV \quad (1.78)$$

Next we apply the above **thickness relation** $dR = c \cdot dt$:

$$\delta t_{SSM} = \frac{\partial dt}{\partial dR} \delta R_{SSM} = \frac{1}{c} \cdot \delta R_{SSM} \quad (1.79)$$

We insert that result into Eq. (1.78):

$$\delta(dV \cdot dt)_{SSM} = \delta V_{SSM} \cdot dt + \frac{1}{c} \cdot \delta R_{SSM} \cdot dV \quad (1.80)$$

We apply[10] $dL = \frac{dR}{\sqrt{1-\frac{R_S}{R}}}$ in order to derive a term for δR_{SSM}:

$$\delta R_{SSM} = dL - dR = dR \cdot \left(\frac{1}{\sqrt{1 - \frac{R_S}{R}}} - 1 \right) \quad (1.81)$$

[10]It will be derived later that physical states fulfill the relation $R > R_S$.

We multiply with $4\pi \cdot R^2$ and apply $\delta V_{SSM} = 4\pi \cdot R^2 \delta R_{SSM}$ and $dV = 4\pi \cdot R^2 dR$:

$$\boxed{\delta V_{SSM} = dV \cdot \left(\frac{1}{\sqrt{1 - \frac{R_S}{R}}} - 1 \right)} \tag{1.82}$$

We apply these relations to Eq. (1.80). Moreover we factorize the bracket in the above Eq.:

$$\delta(dV \cdot dt)_{SSM} = \left(dV \cdot dt + \frac{dR}{c} \cdot dV \right) \cdot \left(\frac{1}{\sqrt{1 - \frac{R_S}{R}}} - 1 \right) \tag{1.83}$$

We use the **thickness relation** $\frac{dR}{c} = dt$. So we get:

$$\delta(dV \cdot dt)_{SSM} = 2 \cdot dt \cdot dV \cdot \left(\frac{1}{\sqrt{1 - \frac{R_S}{R}}} - 1 \right) \tag{1.84}$$

We identify the product of dV and of the bracket in the above Eq. by δV_{SSM}:

$$\boxed{\delta(dV \cdot dt)_{SSM} = 2 \cdot dt \cdot \delta V_{SSM}} \tag{1.85}$$

FLE: In this part we analyze the same system as above (see part 1.13) with the additional condition that the mass M is distributed uniformly in the ball with radius R (see Fig. 1.11), and we derive the formed vacuum by using the FLE.

First we apply the total differential:

$$\delta(dV \cdot dt)_{FLE} = \delta V \cdot \frac{\partial(dV \cdot dt)}{\partial dV} + \delta t \cdot \frac{\partial(dV \cdot dt)}{\partial dt} \tag{1.86}$$

We evaluate the derivatives:

$$\delta(dV \cdot dt)_{FLE} = \delta V_{FLE} \cdot dt + \delta t_{FLE} \cdot dV \tag{1.87}$$

Next we apply the fact that the time increases at a constant rate in the FLE, so we get $\delta t_{FLE} = 0$. With it we derive:

$$\boxed{\delta(dV \cdot dt)_{FLE} = dt \cdot \delta V_{FLE}} \tag{1.88}$$

Equality of spacetimes: For the case of radiation we derived $\delta V_{FLE} = 2\delta V_{SSM}$ (Eqs. 1.49, 1.76). That relation is also derived (Eq. 1.91) by using the following principle[11] proposed here:

Definition 8 Principle of the equality of spacetimes:

If vacuum with a volume δV forms during a time dt in a compact isotropic volume V with a surface A, then that vacuum crosses the surface layer of V with the thickness $dR = c \cdot dt$ and volume $dV = A \cdot dR$ by propagating outwards, and then dR increases by $\delta R = \delta V/A$, and if dt increases microscopically by $\delta t = \delta R/c$, then the spacetime $dV \cdot dt$ of the layer increases by an amount of spacetime $\delta(dV \cdot dt)$, and then $\delta(dV \cdot dt)$ is the same according to the microscopic and the macroscopic (cosmological) dynamics:

$$\boxed{\delta(dV \cdot dt)_{micro} = \delta(dV \cdot dt)_{macro}} \tag{1.89}$$

Equal amounts of spacetimes cause different amounts of vacuum: We apply the principle of equality of microscopic and macroscopic spacetime (definition 8) to Eqs. (1.85, 1.88):

$$\delta(dV \cdot dt)_{FLE} = dt \cdot \delta V_{FLE} = 2 \cdot dt \cdot \delta V_{SSM} = \delta(dV \cdot dt)_{SSM} \tag{1.90}$$

$$\boxed{\rightarrow \delta V_{FLE} = 2 \cdot \delta V_{SSM}} \tag{1.91}$$

As the macroscopic dynamics describes the complete formed vacuum, CFV, we find $\delta V_{FLE} = \delta V_{CFV}$. As the microscopic dynamics describes the locally formed vacuum, LFV, we find $\delta V_{SSM} = \delta V_{LFV}$. So we get:

$$\boxed{\delta V_{CFV} = 2 \cdot \delta V_{LFV}} \tag{1.92}$$

[11] That principle is also confirmed for the cases of black holes including dark matter (C. 3) and possibly for dark energy (S. 6.6). Def. (8) can be applied to annihilating vacuum with volume δV analogously.

Theorem 5 Nonlocality of general relativity:

(1) If there is a HUF with a center at a radial coordinate $r = 0$, and if a mass M has its center of mass at $r = 0$, and if a shell in the HUF has its center at $r = 0$, a radius R and a thickness $dR = c \cdot dt$, and if $R_S = \frac{2GM}{c^2}$, and if dV is the volume of the shell, then in the shell there flows locally formed vacuum δdV_{SSM} according to the SSM with the following properties:

(1a) The amount of that LFV is as follows:

$$\delta V_{SSM} = dV \cdot \left(\sqrt{1 - R_S/R}^{-1} - 1 \right) \tag{1.93}$$

It will be derived later that physical states fulfill $R > R_S$.

(1b) The amount of the spacetime $\delta(dV \cdot dt)_{SSM}$ according to the dynamics of the SSM is as follows:

$$\delta(dV \cdot dt)_{SSM} = 2 \cdot dt \cdot \delta V_{SSM} \tag{1.94}$$

(1c) The amount in (1b) is the locally formed vacuum, LFV:

$$\delta(dV \cdot dt)_{LFV} = 2 \cdot dt \cdot \delta V_{LFV} \tag{1.95}$$

(2a) If the system in part (1) is analyzed according to the FLE, then the amount of additional spacetime $\delta(dV \cdot dt)_{FLE}$ is as follows:

$$\delta(dV \cdot dt)_{FLE} = dt \cdot \delta V_{FLE} \tag{1.96}$$

(2b) The amount in (2a) is the completely formed vacuum, CFV:

$$\delta(dV \cdot dt)_{CFV} = dt \cdot \delta V_{CFV} \tag{1.97}$$

(2c) The CFV in parts (2a) and (2b) forms in each macroscopic dynamics of the expansion of space, in which the time evolves at a constant rate.

(3a) According to the principle of equality of spacetimes, the LFV is one half of the CFV:

$$\delta V_{CFV} = 2 \cdot \delta V_{LFV} \tag{1.98}$$

(3b) The difference of the CFV minus the LFV is the nonlocally formed vacuum NFV:

$$\delta V_{NFV} = \delta V_{LFV} = \delta V_{CFV}/2 \tag{1.99}$$

(3c) The nonlocality of the GRT is derived directly from Eqs. (1.49) and (1.76).

(3d) Since the vacuum and its volume constitute an essential basis for the concepts of density and of GRT (Prop. 1), and as one half of the vacuum formed according to GRT is nonlocally formed vacuum, the GRT is a nonlocal theory.

Corollary 2 General relativity is nonlocal:

(1) The theory of general relativity is nonlocal, though it was designed on the basis of local rules. In this case, the amount of nonlocality is 50 %.

(2) This nonlocality of the GRT provides a basic solution of the EPR paradox, as the locality of the GRT is a premise of the paradox, However, the above shows that this premise is wrong.

(3) As the SSM and the solutions of the FLE have been empirically confirmed in a precise manner (Will (2006), Collaboration (2020)), the nonlocality of the GRT is a property of nature.

(4) The nonlocality of GRT enables that theory to describe local curvature and universal expansion.

(5) What are the mechanisms of nonlocality? Answers to this interesting question are derived in the next chapters.

1.13.1 Nonlocality of GRT

The above theorem shows that GRT is nonlocal, though the theory was based on local physical principles.

Such things can happen in science. For instance, the theory of rational numbers is based on very rational rules of addition, subtraction, multiplication and division. But a square

with length 1 has a diagonal with the length $\sqrt{2}$, an irrational number.

Another example is Maxwell's theory of electrodynamics. The theory is based on the concept that the time evolves at a constant rate. But an electromagnetic wave, an important solution of Maxwell's theory, exhibits a constant velocity of light, which in turn is the basis of the SRT, in which time evolves at various rates, depending of the frame of reference.

An additional example is Columbus. He started his expedition in order to find a route from Europe to India. But he discovered America.

We will develop explanations for the derived nonlocality in the following chapters.

1.13.2 First solution of the EPR paradox

Einstein et al. (1935) showed that quantum theory includes the nonlocal formation of correlations. That means, correlations form faster than light can propagate. They classify that situation as paradoxical. This indicates that they presume that the GRT is local.

Now the GRT and the quantum theory are both nonlocal. So the basis for the paradox between both theories vanishes. In this sense, the nonlocality if the GRT presents a first solution of the EPR paradox.

Later in this book, we will derive two other solutions of the EPR paradox, and these will provide a deeper insight. For it we analyze the quadrupolar symmetry inherent to the additionally formed vacuum that is underlying the SSM as well as the uniform scaling of the expansion of space. This is elaborated in the next chapter.

Chapter 2

Fields and Quadrupoles

As a result of GRT, gravity is established by a curvature of space and by the expansion of space. In the first chapter, we realized that this curvature and expansion of space are constituted by the formation of vacuum.

In this chapter we analyze the symmetry of that formed vacuum, and thereby we derive the symmetry of gravity. Thereby, we discover the precise quadrupolar and monopolar symmetries of gravity in general, and in particular phenomena such as gravitational waves, curvature near a mass and isotropic expansion of space. For it we derive corresponding tensors, four-vectors, Lorentz scalars and DEQs.

2.1 Energy density of the field

In this section we derive the energy density ρ_f of the field G^* located in a HUF. For it we analyze the energy ΔE_M that is necessary in order to lift a mass M in a shell with a radius R to a shell with a radius $R + \Delta R$, see Fig. (2.1). Thereby, the mass is lifted as follows: Differential parts dM are lifted, while the part M_{rest} is still at R. Moreover, the velocity of M remains zero, in an ideal manner. So a part dM is lifted at the gravitational field of the part M_{rest}:

$$|\vec{G}^*(M_{rest})| = G^*(M_{rest}) = \frac{G \cdot M_{rest}}{R^2} \tag{2.1}$$

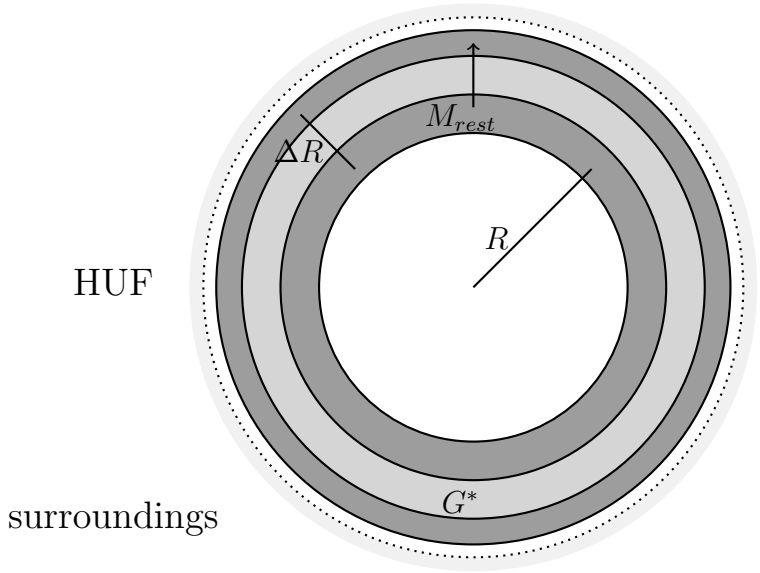

Figure 2.1: In a HUF (light grey), a mass M (dark grey) in a shell at a radius R is lifted to a radius $R + \Delta R$ as follows: Differential parts dM are lifted, while the rest M_{rest} is still at R. Thereby the field G^* (medium grey) in the shell with radius R and thickness ΔR becomes zero (see Fig. 2.2).

So the field G^* is proportional to the part M_{rest} (Fig. 2.2). If a mass dM is lifted, and if the mass M_{rest} is still at R, then dM experiences the force[1] $F = G^*(M_{rest}) \cdot dM$, thus the energy $dE = F \cdot \Delta R$ is required:

$$dE = G^*(M_{rest}) \cdot dM \cdot \Delta R = \frac{G \cdot M_{rest}}{R^2} \cdot dM \cdot \Delta R \qquad (2.2)$$

We derive the full change in gravitational energy ΔE_M by integrating the above Eq.:

$$\Delta E_M = \int_0^E dE = \int_M^0 \frac{G \cdot M_{rest}}{R^2} dM \cdot \Delta R \qquad (2.3)$$

When a mass dM is lifted, then the mass M_{rest} is decreased by dM. So $dM_{rest} = -dM$. Thus we get:

$$\Delta E_M = -\int_M^0 \frac{G \cdot M_{rest}}{R^2} dM_{rest} \cdot \Delta R \qquad (2.4)$$

[1]The force can be used instead of the position factor, as ΔR is infinitesimal.

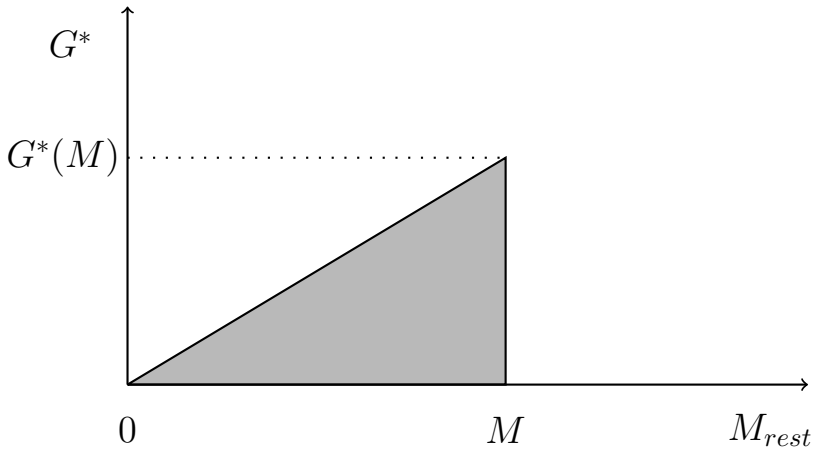

Figure 2.2: The field G^* is shown as a function of the mass M_{rest} that is still at the shell with the radius R.

We evaluate the integral:

$$\Delta E_M = \frac{G \cdot M^2 \cdot \Delta R}{2R^2} \tag{2.5}$$

Location of the energy ΔE_M: While the mass M was lifted in the above process, the energy ΔE_M was added to the system. Where is this energy ΔE_M located in the system?

As the mass M is identical to the probing mass m and to the field-generating mass $M_f = M$, the mass M is not in an external field. So the position factor is 1 at the beginning and at the end of the process. Hence the energy ΔE_M is not located in the mass.

There is a **modification in the shell** between the radii R and $R + \Delta R$. It can be characterized by the additional curvature. That additional curvature can be characterized by additionally formed volume flowing outwards at the velocity c. As we derived the curvature from the EEP to which the field is inherent, that outflow can also be described by the field G^*.

Hence, **in the HUF the energy ΔE_M is located in the modifications in the shell between R and $R + \Delta R$, and it can be characterized by the field**.

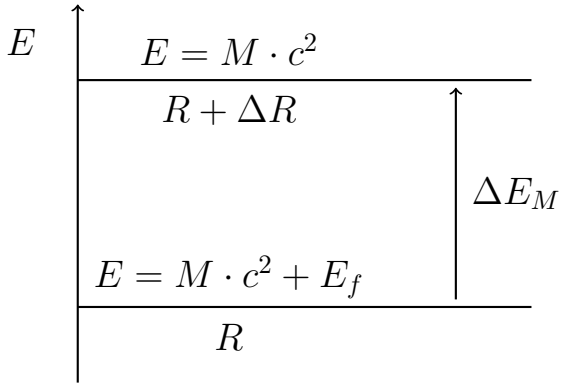

Figure 2.3: The energy of the mass is shown at the initial radius R and at the final radius $R + \Delta R$.

Energy density u_f of the field: The field G^* is in the shell with radius R and thickness ΔR (see Fig. (2.1). The corresponding volume is $\Delta V = 4\pi \cdot R^2 \cdot \Delta R$. So we derive the energy density by the dividing the energy ΔE_M by the volume ΔV. So we get:

$$u_f = \frac{\Delta E_f}{\Delta V} = \frac{G \cdot M^2 \cdot \Delta R}{2R^2 \cdot 4\pi \cdot R^2 \cdot \Delta R} \tag{2.6}$$

We simplify the above term, we expand by G, and we apply the field $G^* = \frac{G \cdot M}{R^2}$. So we get:

$$\boxed{u_f = \frac{\vec{G}^{*2}}{8\pi \cdot G} = \rho_f \cdot c^2} \tag{2.7}$$

Sign of the field energy E_f: The sign of an energy is determined from the law of energy conservation. For instance, in quantum physics, there occur solutions with a negative energy, corresponding to antimatter. However, the mass of such an antiparticle is positive. We know this from the fact that we need energy in order to generate such an antiparticle. So we know it from the law of energy conservation. Before the above process, the system has the energy of the mass $M \cdot c^2$, plus the energy E_f of the field in the HUF (Fig. 2.3):

$$E_{before} = M \cdot c^2 + E_f \tag{2.8}$$

During the process, the energy ΔE_M is added to the system. At the end of the above process, the system has the energy of the mass $E_{after} = M \cdot c^2$ in the HUF. According to the law of energy conservation, the energy E_{after} is equal to E_{before} plus ΔE_M:

$$M \cdot c^2 = E_{after} = \Delta E_M + E_{before} = M \cdot c^2 + E_f + \Delta E_M \quad (2.9)$$

We simplify:

$$0 = E_f + \Delta E_M \quad (2.10)$$

As the sign of ΔE_M is positive, **the sign of the energy of the field E_f is negative**.

The energy density of the field is just a possible description of the modifications of curvature and additional volume in the shell between R and $R + \Delta R$. So an adequate interpretation will be presented in later chapters, on the basis of corresponding results.

Proposition 5 Energy density of the gravitational field:

(1) The gravitational energy is inherent to modifications of space such as curvature or additionally formed volume or a gravitational field.

(2) In a HUF, a gravitational field $\vec{G}^*$ has the energy density u_f as follows:

$$|u_f| = \frac{\vec{G}^{*2}}{8\pi \cdot G} \quad (2.11)$$

2.2 Dynamic mass of the field

In this section we derive the dynamic mass M_f of a field G^*, that is generated by a mass M (Fig. 2.4).

For it we derive the field at a radius R:

$$|\vec{G}^*| = G^* = \frac{G \cdot M}{R^2} \quad (2.12)$$

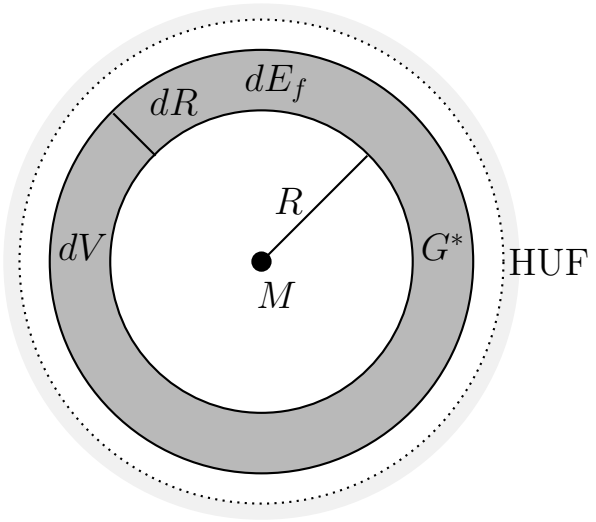

Figure 2.4: A mass M generates a field G^* and a corresponding energy dE_f in a shell with radius R, thickness dR and volume dV.

The energy density of that field is (Eq. 2.7):

$$|u_f| = \frac{G \cdot M^2}{8\pi \cdot R^4} \tag{2.13}$$

The shell has the volume:

$$dV = 4\pi \cdot R^2 \cdot dR \tag{2.14}$$

So the energy dE_f of the field in the shell is:

$$|dE_f| = dV \cdot |u_f| = \frac{G \cdot M^2}{2 \cdot R^2} \cdot dR \tag{2.15}$$

The total energy E_f of the field is obtained by integration from the smallest possible radius R_S to infinity:

$$|E_f| = \int_0^\infty |dE_f| = \frac{GM^2}{2} \cdot \int_{R_S}^\infty \frac{1}{R^2} dR \tag{2.16}$$

We evaluate the integral, and we apply $R_S = \frac{2GM}{c^2}$:

$$|E_f| = \frac{G \cdot M^2}{2} \cdot \frac{1}{R_S} = \frac{M \cdot c^2}{4} \tag{2.17}$$

We divide by c^2 and apply the equivalence of the energy to the dynamical mass $M_f = |E_f| \cdot c^2$:

$$\boxed{M_f = \frac{M}{4}} \tag{2.18}$$

We summarize our derivations:

Proposition 6 Dynamic mass M_f of the gravitational field: *A mass M in a HUF generates a field G^* with the following properties:*

If the radius of the empty ball of the HUF tends to infinity, then the field G^* has the following properties:

(1) If there is only the mass M in the empty ball of the HUF, then the only field in that ball is the field G^* of M.

(2) If the radius of the empty ball of the HUF tends to infinity, then the dynamic mass M_f of the field G^* is one fourth of the field generating mass M, i. e. $M_f = M/4$.

After we analyzed the formation of additional vacuum in the previous chapter and the energy density of a gravitational field in the HUF, we are well prepared in order to analyze the symmetry of the process of the formation of that vacuum. This is elaborated in the next section.

2.3 Quadrupolar symmetry

In this section we analyze and apply the symmetry of the formation of additional volume underlying the curvature of space and the gravitational interaction as a consequence.

2.3.1 Direction vector of the field

The field $\vec{G}^*$ represents a vector. The field propagates together with the generated volume (see theorems 1, 2) and according to

a corresponding momentum $\vec{k}$. The field $\vec{G}^*$ is parallel or anti parallel to its momentum $\vec{k}$. We realize this for the case of a single mass: The field emerges at the field-generating mass and propagates in radial direction and parallel to the field vector $\vec{G}^*$. We characterize that direction by its unit **direction vector** $\vec{s}$:

$$|\vec{s}| = 1 \quad \text{and} \quad \vec{s} \parallel \vec{G}^* \quad \text{and} \quad \vec{s} \parallel \vec{k} \tag{2.19}$$

2.3.2 Quadrupole of the field

As gravity is always attractive, it essentially has a **quadrupolar symmetry**. As a dipolar structure would provide two signs of interaction, corresponding to attractive and repulsive forces. Correspondingly, the hypothetic quanta of gravity have **spin 2** (see for instance Tanabashi et al. (2018)).

In the present case of an isotropic quadrupolar symmetry, the orientation can be represented by an **orientation vector** $\vec{q}$ with norm one, see for instance (Carmesin (1987), Carmesin and Binder (1987)).

$$|\vec{q}| = 1 \tag{2.20}$$

Plan of investigation: The symmetry of quadrupoles or of objects with spin 2 should be described in a mathematical manner, in order to generalize the isotropic formation of vacuum in the expansion of space (see Eq. 1.66) to the case of unidirectional formation of vacuum in the SSM, to the case of gravitational waves and to even more cases[2].

As we aim to describe the symmetry of gravity, we plan to extend the gravitational constant G by a quadrupolar factor. We achieve this in two steps: First we develop and test that **factor** in Sect. (2.3). Secondly, we devise the corresponding **tensors** in Sect. (2.4).

[2]Note for comparison that also in dipolar symmetry there occurs linear polarization as well as circular polarization.

2.3.3 Proposed quadrupolar factor

The gravitational interaction is essential in the formation of vacuum, this is indicated by the constant G and the density ρ in the rate Eq. (1.66):

$$\left(\frac{dV}{dt \cdot V}\right)^2 = 24\pi \cdot G \cdot \rho \tag{2.21}$$

Accordingly, we propose that the gravitational constant G in that rate Eq. is multiplied by a **quadrupolar factor** $Q(\vec{q}, \vec{s})$, which is a quadrupolar function of $\vec{q}$ and $\vec{s}$. As the directions of $\vec{q}$ are randomly distributed, we apply the average according to a uniform distribution of orientations. So we get:

$$\left(\frac{dV}{dt \cdot V}\right)^2 = 24\pi \cdot G \cdot \langle Q(\vec{q}, \vec{s}) \rangle \cdot \rho \tag{2.22}$$

Test of the symmetry: If we multiply the vector $\vec{s}$ by -1, then the direction of propagation of $\vec{G}^*$ is inverted, and this does not modify the rate $\frac{dV}{dt \cdot V}$ of the production of volume, even if we apply the density of the field (Eq. (2.7):

$$u_f = \rho_f \cdot c^2 \tag{2.23}$$

So the factor $Q(\vec{q}, \vec{s})$ has **quadrupolar symmetry**.

Method: We derive the above quadrupolar factor $Q(\vec{q}, \vec{s})$ as follows. Firstly, we realize physical properties. Secondly, we formulate possible multipolar terms. Thirdly, we derive the corresponding coefficients.

2.3.4 Physical properties

In this section we note useful physical conditions of the formation of vacuum.

Formation of vacuum in the Big Bang: In order to determine the coefficients, we analyze the case of the expansion of space according to the FLE and rate Eq. (1.66). Correspondingly, we use the positive square root of that Eq. Hence the generated volume has a positive sign, and the quadrupolar factor is positive:

$$Q \geq 0 \quad \text{or} \quad Q_{min} = 0 \tag{2.24}$$

Additionally, the average $\langle Q \rangle$ is one:

$$\langle Q \rangle = 1 \tag{2.25}$$

In the case of the expansion of space, usually modeled by a uniform scaling, gravity generates vacuum in each of the three directions x, y, z or r, y, z. Accordingly, the maximum value is three, or the dimension D, more generally. However, in the case of a field generating mass, the field has the radial direction, and the corresponding vacuum can be formed in that direction only, accordingly, the maximum value is one. So we obtain:

$$Q_{max} = \begin{cases} 3 & \text{for expansion of space or uniform scaling} \\ 1 & \text{for field generating mass or unidir. formation} \end{cases} \tag{2.26}$$

2.3.5 Multipolar terms

In this section we formulate the multipolar terms that are essential for the cases of vacuum formation studied here: Since there is no additional anisotropy in the system, the quadrupolar factor can be represented with help of the isotropic part of the quadrupolar interaction, see for instance (Carmesin (1987), Carmesin and Binder (1987)):

$$(\vec{q} \cdot \vec{s})^2 - 1/3 \tag{2.27}$$

We denote it by $Q_{2,0}$, as it is proportional to the **spherical harmonic function** $Y_{l=2,m=0} = \frac{3}{2} \cdot \sqrt{\frac{5}{4\pi}} \cdot \left(\cos^2(\theta) - \frac{1}{3}\right)$:

$$Q_{2,0} = (\vec{s} \cdot \vec{q})^2 - 1/3 \tag{2.28}$$

The spherical harmonic functions form an orthonormal system (Ballentine (1998)). For that purpose they require a subtrahend such as 1/3 inherent to $Y_{l=2,m=0}$. That subtrahend might not be essential in each physical application. In order to take care of this possibility, we allow for the monopole spherical harmonic function $Y_{l=0,m=0} = \sqrt{\frac{1}{4\pi}}$, additionally. Accordingly, we include a monopolar term:

$$Q_{0,0} = 1, \tag{2.29}$$

So the quadrupolar factor Q is a linear combination with corresponding coefficients $a_{2,0}$ and $a_{0,0}$:

$$Q = a_{2,0} \cdot Q_{2,0} + a_{0,0} \cdot Q_{0,0} \tag{2.30}$$

2.3.6 Determination of coefficients for expansion

In this section we derive the coefficients for the case of the expansion of space. We apply Eq. (2.24):

$$Q_{min} = 0 = a_{2,0} \cdot Q_{2,0} + a_{0,0} \cdot Q_{0,0} \tag{2.31}$$

We insert Eqs. (2.28) and (2.29):

$$Q_{min} = 0 = a_{2,0} \cdot [(\vec{s} \cdot \vec{q})^2 - 1/3] + a_{0,0} \tag{2.32}$$

For the present case of minimal Q_{min}, the vectors are orthogonal, and we insert zero for the scalar product:

$$Q_{min} = 0 = a_{2,0} \cdot [-1/3] + a_{0,0} \tag{2.33}$$

So we get:

$$a_{0,0} = a_{2,0} \cdot [1/3] \tag{2.34}$$

We apply Eq. (2.26). So we get:

$$\langle Q_{max} \rangle = 3 = a_{2,0} \cdot [(\vec{s} \cdot \vec{q})^2 - 1/3] + a_{0,0} \tag{2.35}$$

For the present case of maximal Q_{max}, the vectors are parallel, and we insert one for the scalar product:

$$Q_{max} = 3 = a_{2,0} \cdot 2/3 + a_{0,0} \tag{2.36}$$

So we get:

$$a_{0,0} = 3 - a_{2,0} \cdot 2/3 \tag{2.37}$$

We subtract Eq. (2.37) from Eq. (2.34):

$$0 = 3 - a_{2,0} \quad \text{or} \quad a_{2,0} = 3 \tag{2.38}$$

We insert that result into Eq. (2.34). So we get:

$$a_{0,0} = 1 \tag{2.39}$$

Altogether, we derive the quadrupolar factor:

$$\boxed{Q = 3 \cdot (\vec{s} \cdot \vec{q})^2 \quad \text{for expansion of space}} \tag{2.40}$$

Test of the quadrupolar factor: We insert the above quadrupolar factor into Eq. (2.25), and we test, whether the result is indeed one.

$$\langle Q \rangle = 3 \cdot \langle (\vec{s} \cdot \vec{q})^2 \rangle \tag{2.41}$$

The above average is equal to the average $\langle x^2 \rangle = 1/3$. Alternatively, it is equal to the average $\langle \cos^2(\theta) \rangle = 1/3$, whereby $\vec{s}$ and $\vec{q}$ enclose the angle θ. So we get:

$$\langle Q \rangle = 3 \cdot 1/3 = 1 \tag{2.42}$$

This confirms the derived interaction term and it is the first positive test of our interaction hypothesis.

Rate equation: We apply this result to the DEQ (2.22)

$$\boxed{\left(\frac{\delta V}{dt \cdot V} \right)^2 = 24\pi \cdot G \cdot \rho \quad \text{for expansion of space}} \tag{2.43}$$

2.3.7 Determination of coefficients for field generating mass

In the case of a field generating mass, the coefficients are derived in the same manner as above. As a result we get:

$$a_{0,0} = 1/3, \quad a_{2,0} = 1 \quad \text{and} \quad \langle Q \rangle = 1/3 \quad \text{for unidir. formation} \tag{2.44}$$

Consequently we derive:

$$\boxed{Q = (\vec{s} \cdot \vec{q})^2 \quad \text{for unidirectional or radial symmetry}} \tag{2.45}$$

So we get the rate equation:

$$\boxed{\left(\frac{\delta V}{dt \cdot V}\right)^2 = 8\pi \cdot G \cdot \rho \quad \text{for unidirectional vacuum formation}} \tag{2.46}$$

We summarize our derivations:

Theorem 6 Quadrupolar symmetry of gravity: *There is a linear quadrupolar symmetry inherent to gravity. That symmetry has the following properties:*

(1) The direction of $\vec{G}^*$ can be represented by a **direction vector** $\vec{s}$.

(2) As the interaction is attractive, it exhibits quadrupolar symmetry, and it can be represented by an **orientation vector** $\vec{q}$.

(3) Altogether, the quadrupolar symmetry can be represented by a **quadrupolar factor** $Q(\vec{q}, \vec{s})$. *It is a function of $\vec{q}$ and $\vec{s}$, and it is multiplied by the universal constant G of gravitation in the rate equation (2.22).*

(4) The **quadrupolar factor** *takes the following form:*

$$Q = (\vec{q} \cdot \vec{s})^2 \cdot \begin{cases} 3 & \textit{for isotropic expansion of space} \\ 1 & \textit{for field generating mass or dynamical mass} \end{cases}$$

(5) $Q(\vec{q},\vec{s})$ represents a linear superposition of monopolar and quadrupolar symmetry, corresponding to the fact that masses present monopoles.

(6) A field generating mass or dynamical mass causes a locally unidirectional (radial) expansion of space.

(7) For the case of isotropic expansion of space, the resulting rate for the formation of new vacuum is as follows:

$$\left(\frac{\delta V}{\delta t \cdot dV}\right)^2 = 24\pi \cdot G \cdot \rho \;\; \textit{for isotropic expansion of space} \tag{2.47}$$

(8) For the case of locally unidirectional expansion of space, including the case of radially expanding space, the resulting rate for the formation of new vacuum is as follows:

$$\left(\frac{\delta V}{\delta t \cdot dV}\right)^2 = 8\pi \cdot G \cdot \rho \;\; \textit{for unidirectional vacuum formation} \tag{2.48}$$

2.3.8 Rate gravity four-vector, RGV

In this section we analyze an essential consequence of the rate generated by a mass or dynamical mass M.

First we abbreviate that rate by $\dot{\varepsilon} = \frac{\delta V}{\delta t \cdot dV}$. So Eq. (2.48) takes the form:

$$\dot{\varepsilon}^2 = 8\pi \cdot G \cdot \rho \tag{2.49}$$

Secondly, we analyze the rate at a location in the vicinity of the mass at which there is the field G^* of the mass M. At such a location, the density ρ in the above Eq. is established by the energy density $u_f = \frac{G^{*2}}{8\pi \cdot G}$ of the field (see proposition 5), $\rho = u_f/c^2$. So we get:

$$\dot{\varepsilon}^2 = 8\pi \cdot G \cdot \frac{G^{*2}}{8\pi \cdot G \cdot c^2} \tag{2.50}$$

We cancel:

$$\dot{\varepsilon}^2 = \frac{G^{*2}}{c^2} \tag{2.51}$$

We subtract the term at the right hand side:

$$\boxed{\dot{\varepsilon}^2 - \frac{G^{*2}}{c^2} = 0} \tag{2.52}$$

We identify the left hand side as a relativistic square of the following **rate gravity four-vector, RGV**:

$$RGV_i = \begin{pmatrix} \dot{\varepsilon} \\ G_x^*/c \\ G_y^*/c \\ G_z^*/c \end{pmatrix} \tag{2.53}$$

.

Sign convention: The relativistic square is evaluated with the following sign convention used in four dimensional spacetime. In the usual index notation, four-vectors are denoted with superscripts (see for instance Moore (2013), Carmesin (1996)), while column labels are denoted as subscripts. Moreover, a sign convention is applied as follows: convention of signs:

$$\eta_{i,j} = \begin{pmatrix} -1 & 0 & 0 & 0 \\ 0 & 1 & 0 & 0 \\ 0 & 0 & 1 & 0 \\ 0 & 0 & 0 & 1 \end{pmatrix} = \eta_i^j \tag{2.54}$$

While this convention is very common (see for instance Moore (2013), Carmesin (1996)), the opposite signs are used in some books (see for instance Landau and Lifschitz (1981), Stephani (1980)).

Rate gravity scalar, RGS: We evaluate the relativistic square of the RGV:

$$RGS = RGV^i \cdot \eta_i^j \cdot RGV_j = \dot{\varepsilon}^2 - (G_x^{*2} + G_y^{*2} + G_z^{*2})/c^2 \tag{2.55}$$

We summarize the coordinates to the absolute value:

$$\boxed{RGS = \dot{\varepsilon}^2 - G^{*2}/c^2 = 0} \tag{2.56}$$

As the RGS is zero, it is invariant with respect to **each linear transformation**, including a **Lorentz transformation**. Hence the RGS is invariant with respect to a transformation from one inertial frame that is embedded in a HUF to another inertial frame that is embedded in the same HUF. In this sense the RGS is a **Lorentz invariant**. Moreover, the *RGS* is a **Lorentz scalar**, as it is a Lorentz invariant scalar. Additionally, there is no acceleration inherent to a HUF, only objects within a HUF might cause a so-called **particular acceleration**. Altogether and more generally, a Lorentz scalar in a HUF that is zero is highly invariant, we call it a **HUF zero Lorentz scalar, HZLS**. Furthermore, if that HZLS is the relativistic square of a four-vector, then we call that four-vector a **HUF zero four-vector, HZFV**. We summarize our results:

Definition 9 Invariants in SRT and GRT:

(1) If a scalar is a Lorentz scalar in a HUF, and if that scalar is zero, then it is called a **HUF zero Lorentz scalar, HZLS**.

(2) If the relativistic square of a four-vector is a HZLS, then we call that four-vector a **HUF zero four-vector, HZFV**.

(3) If objects in a HUF accelerate other objects, then that acceleration is called a **particular acceleration**. *Other accelerations are called* **non particular accelerations**.

Theorem 7 Invariant formation of vacuum:

The DEQ

$$\boxed{RGS = \dot{\varepsilon}^2 - G^{*2}/c^2 = 0} \tag{2.57}$$

for the formed vacuum in the HUF is an invariant for the following reasons:

(1) The only possible accelerations in a HUF are particular accelerations. A field $\vec{G}^*$ of a particular acceleration can be measured by a local observer.

(2) A possible absolute velocity cannot be measured. The DEQ $RGS = 0$ is invariant with respect to a Lorentz transformation LT, as it is HZLS. It is a relativistic square of a HZFV, the rate gravity four-vector:

$$RGV_i = \begin{pmatrix} \dot{\varepsilon} \\ G_x^*/c \\ G_y^*/c \\ G_z^*/c \end{pmatrix} \tag{2.58}$$

(3) If the average of the particular radial accelerations is positive, then additional vacuum must be formed so that the universe expands (Carmesin (2020b), Carmesin (2020a)).

(4) While the RGS shows that the equality of square of the rate $\dot{\varepsilon}^2$ and the square of the field G^{*2}/c^2 is invariant, the rate and the field might be different for different frames.

2.3.9 An invariant energy density function in the HUF

In this section we apply the scalar RGS in order to derive an invariant energy density function in the HUF.

For it we multiply the RGS by $\frac{c^2}{8\pi G}$ in Eq. (2.56):

$$RGS \cdot \frac{c^2}{8\pi G} = \frac{\dot{\varepsilon}^2 \cdot c^2}{8\pi G} - \frac{G^{*2}}{8\pi G} \tag{2.59}$$

We identify the subtrahend in the above Eq. by the energy density of the field. It is negative, so it is a **self attraction of the gravitational field**. Correspondingly, we identify the addend as an energy density. So the rate $\dot{\varepsilon}^2$ of LFV gives rise to a positive energy density.

As the RGS is a relativistic square of the four-vector RGV, it is invariant with respect to a Lorentz transformation, and it

establishes a physical quantity. We call it the **rate gravity energy density, RGED** u_{RG}:

$$u_{RG} = \frac{\dot{\varepsilon}^2 \cdot c^2}{8\pi G} - \frac{G^{*2}}{8\pi G} \tag{2.60}$$

The RGED is an invariant in the HUF, as it is a HZLS. We summarize our result:

Proposition 7 Invariant density RGED in a HUF: *The rate gravity energy density, RGED,*

$$u_{RG} = \frac{\dot{\varepsilon}^2 \cdot c^2}{8\pi G} - \frac{G^{*2}}{8\pi G} \tag{2.61}$$

is an invariant with respect to Lorentz transformations, and it is not influenced by non particular accelerations.

2.4 Quadrupolar model for vacuum

While we derived the quadrupolar symmetry in the previous section, we represent that symmetry in a more systematic and more general manner in the present section.

2.4.1 Rate of formed volume analogous to strain

In this section we derive the analogy between the strain and the formed volume.

The formed volume can be expressed with a tensor, see Fig. (2.5) as follows:

$$\hat{\varepsilon}_{jj} = \frac{\delta V_j}{dV} = \frac{\delta r_j \cdot dA_j}{dr_j \cdot dA_j} = \frac{\delta r_j}{dr_j} \tag{2.62}$$

Here we identify an analogy to the elements $\frac{\delta r_i}{dr_j}$ of the strain tensor ((Sommerfeld, 1978, p. 3,4)):

$$\hat{\varepsilon}_{ij} = \frac{\delta_{r_i}}{dr_j} \quad \text{or} \quad \hat{\varepsilon}_{ij} = \begin{pmatrix} \frac{\delta r_1}{dr_1} & \frac{\delta r_1}{dr_2} & \frac{\delta r_1}{dr_3} \\ \frac{\delta r_2}{dr_1} & \frac{\delta r_2}{dr_2} & \frac{\delta r_2}{dr_3} \\ \frac{\delta r_3}{dr_1} & \frac{\delta r_3}{dr_2} & \frac{\delta r_3}{dr_3} \end{pmatrix} \tag{2.63}$$

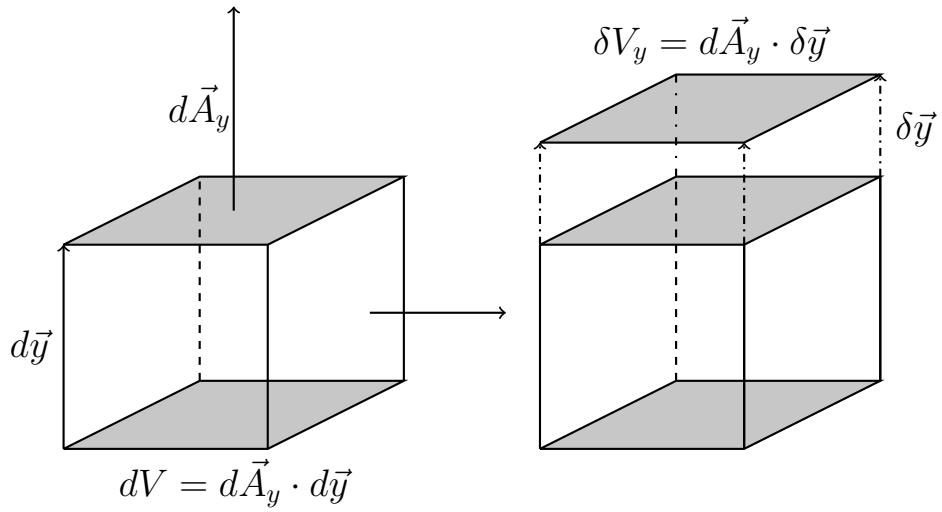

Figure 2.5: Quadrupolar model: A cube with lower and upper surface $d\vec{A}_y$ is modified by shifting the upper surface by an increment δy.

Hence the formed volume is as follows:

$$\boxed{\frac{\delta V}{dV} = \frac{\delta V_x}{dV} + \frac{\delta V_y}{dV} + \frac{\delta V_z}{dV} = \text{Trace}(\hat{\varepsilon}_{ij})} \tag{2.64}$$

Consequently, the rate of formed volume is analogous to the time derivative of the strain tensor as follows:

$$\boxed{\frac{\delta V}{dV \cdot \delta t} = \text{Trace}(\dot{\hat{\varepsilon}}_{ij})} \tag{2.65}$$

According to that analogy, we identify that tensor as the **generalized rate tensor** $\dot{\hat{\varepsilon}}_{ij}$.

The off diagonal elements are analogous to a deformation without formed volume:

$$\delta V = 0 \;\text{ for }\; \hat{\varepsilon}_{ij} \;\text{ with }\; i \neq j \tag{2.66}$$

2.4.2 Generalized field tensor

In this section we use the energy density of the field, in order to develop a generalized relation describing the volume that is

formed by gravity. For it we introduce a generalized gravity tensor as a natural generalization of the gravitational field.

Unidirectional field: A usual field $\vec{G}^*$ constitutes an unidirectional field $\vec{G}^*$, and for the particular case of Cartesian coordinates, we get:

$$\hat{G}_{ij} = G_i^* \cdot G_j^* \tag{2.67}$$

In particular, in the radial direction we get:

$$\hat{G}_{rr} = G_r^* \cdot G_r^* = G_r^{*2} = 8\pi \cdot G \cdot c^2 \cdot \rho_f \tag{2.68}$$

For the case of polar coordinates, the tensor is as follows:

$$\hat{G}_{unidirectional,ij} = \begin{pmatrix} G_r^{*2} & 0 & 0 \\ 0 & 0 & 0 \\ 0 & 0 & 0 \end{pmatrix} = \begin{pmatrix} 1 & 0 & 0 \\ 0 & 0 & 0 \\ 0 & 0 & 0 \end{pmatrix} \cdot 8\pi G c^2 \rho_f \tag{2.69}$$

In both cases, polar coordinates and Cartesian coordinates, we get:

$$\boxed{\text{Trace}(\hat{G}_{ij}) = 8\pi \cdot G \cdot c^2 \cdot \rho_f = G_r^{*2} = \hat{G}_{rr}} \tag{2.70}$$

In order to prepare a generalization, we mark the radial diagonal tensor element $\hat{G}_{rr}$ by an additional index uni, and we neglect the restriction to densities of a field:

$$\boxed{8\pi \cdot G \cdot c^2 \cdot \rho_f = \hat{G}_{uni,rr} = \hat{G}_{rr} \text{ for unidirectional formation}} \tag{2.71}$$

Isotropic expansion: While new vacuum δV is formed in one direction only in the case of a usual unidirectional field,

$$\hat{\varepsilon}_{jj} = \begin{cases} \frac{\delta V_r}{dV} & \text{for radial direction } j = r \\ 0 & \text{for the orthogonal directions } j \neq r \end{cases} \tag{2.72}$$

it is formed in each direction for the case of isotropic expansion:

$$\hat{\varepsilon}_{jj} = \begin{cases} \frac{\delta V_r}{dV} & \text{for any radial direction } j = r \\ \frac{\delta V_j}{dV} = \frac{\delta V_r}{dV} & \text{for the orthogonal directions } j \neq r \end{cases} \tag{2.73}$$

Correspondingly we define the **generalized field tensor** for the case of isotropic expansion as follows

$$\hat{G}_{isotropic,ij} = \begin{pmatrix} 1 & 0 & 0 \\ 0 & 1 & 0 \\ 0 & 0 & 1 \end{pmatrix} \cdot 8\pi G c^2 \rho \tag{2.74}$$

with:

$$\boxed{\hat{G}_{uni,rr} = 8\pi G c^2 \rho = \hat{G}_{xx} = \hat{G}_{yy} = \hat{G}_{zz} \text{ for isotropic expansion}} \tag{2.75}$$

2.4.3 Generalized field tensor and rate tensor:

Using to the above tensors, we express the DEQ of the formation of the vacuum in terms of the generalized field tensor and the rate tensor as follows:

$$\boxed{0 = [\text{Trace}(\dot{\hat{\varepsilon}}_{ij})]^2 - \frac{\text{Trace}(\hat{G}_{ij})}{c^2} = RGS_{tensor}} \tag{2.76}$$

This DEQ represents the tensor form RGS_{tensor} of the Lorentz invariant RGS. Correspondingly, that DEQ and the RGS_{tensor} are Lorentz invariants.

2.4.4 Particular generalized rate tensors

In this section we derive particular generalized rate tensors.

A gravitational wave that propagates in the z-direction is polarized in the x-y-plane, and it forms no volume, an illustration is provided in the chapter (5) about waves, see Fig. (5.1). So there are two possible generalized rate tensors representing two directions of polarization,

$$\hat{\varepsilon}_{pol.\ 1,ij} = \begin{pmatrix} 1 & 0 & 0 \\ 0 & -1 & 0 \\ 0 & 0 & 0 \end{pmatrix} \tag{2.77}$$

and:

$$\hat{\varepsilon}_{pol.\ 2,ij} = \begin{pmatrix} 0 & 1 & 0 \\ -1 & 0 & 0 \\ 0 & 0 & 0 \end{pmatrix} \tag{2.78}$$

We summarize the results of the section:

Theorem 8 DEQ for generalized rate tensor: *The derived quadrupolar symmetry can be applied to densities of fields, masses, dynamical masses or densities as follows:*

(1) The generalized rate tensor is:

$$\hat{\varepsilon}_{ij} = \frac{\delta_{r_i}}{dr_j} \ \ or \ \ \hat{\varepsilon}_{ij} = \begin{pmatrix} \frac{\delta r_1}{dr_1} & \frac{\delta r_1}{dr_2} & \frac{\delta r_1}{dr_3} \\ \frac{\delta r_2}{dr_1} & \frac{\delta r_2}{dr_2} & \frac{\delta r_2}{dr_3} \\ \frac{\delta r_3}{dr_1} & \frac{\delta r_3}{dr_2} & \frac{\delta r_3}{dr_3} \end{pmatrix} \tag{2.79}$$

(2) The generalized field tensor has to be developed for each particular density, density of fields or distribution of possibly dynamical masses.

(2a) For the case of an unidirectional radial expansion of space by a density ρ_f, the generalized field tensor has only one nonzero element, $\hat{G}_{rr}$ as follows:

$$\hat{G}_{unidirectional,ij} = \begin{pmatrix} 1 & 0 & 0 \\ 0 & 0 & 0 \\ 0 & 0 & 0 \end{pmatrix} \cdot 8\pi G c^2 \rho_f \tag{2.80}$$

(2b) For the case of an isotropic expansion by a density ρ, the generalized field tensor in Cartesian coordinates is as follows:

$$\hat{G}_{unidirectional,ij} = \begin{pmatrix} 1 & 0 & 0 \\ 0 & 1 & 0 \\ 0 & 0 & 1 \end{pmatrix} \cdot 8\pi G c^2 \rho \tag{2.81}$$

(3) The formation of vacuum by gravity is described by the following **DEQ***:*

$$[Trace(\dot{\hat{\varepsilon}}_{ij})]^2 = \frac{Trace(\hat{G}_{ij})}{c^2} \tag{2.82}$$

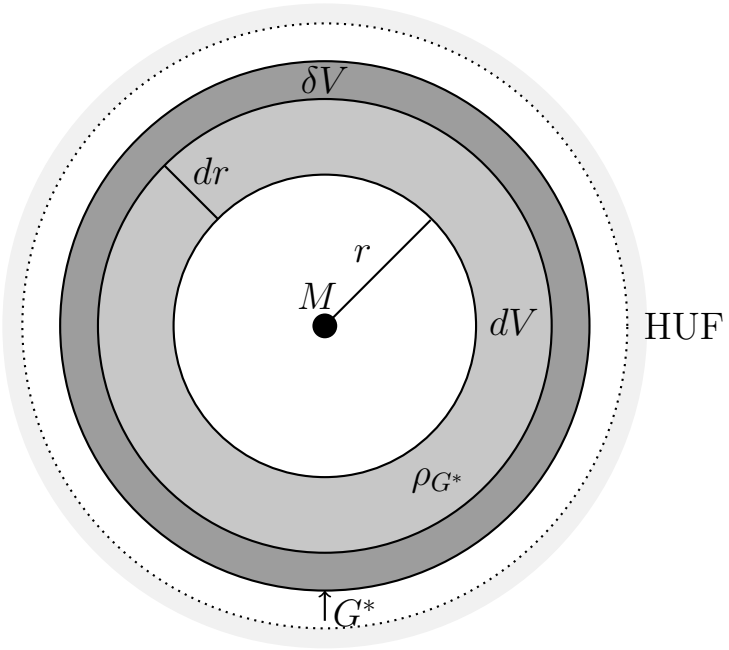

Figure 2.6: A mass M generates a field G^* in a shell (medium grey) around M and with volume dV. The density $\rho_f = u_f/c^2$ of the field forms vacuum with a volume δV.

2.5 Vacuum formed by a mass with $R = R_S$

In this section we derive the locally formed vacuum, LFV, on the basis of the DEQ for the rates $\dot{\varepsilon}$ (see theorems 6, 7, 8). In particular, we derive the LFV that is formed by a mass M with the radius R_M equal to its Schwarzschild radius R_S. We compare our result with the amount of LFV according to the SSM (see theorem 2). This analysis establishes an additional test of our DEQs.

2.5.1 Vacuum formed in a shell

We apply the rate equation (see theorems 6, 7, 8):

$$\frac{\delta V}{\delta t \cdot V} = \sqrt{8\pi \cdot G \cdot \rho} \tag{2.83}$$

We apply this Eq. to the volume dV of the shell with a radius r and thickness dr in Fig. (2.6). So we get:

$$\delta V = \delta t \cdot dV \cdot \sqrt{8\pi \cdot G \cdot \rho} \tag{2.84}$$

We use the density of the gravitational field (2.7):

$$\rho_f = \frac{\vec{G}^{*2}}{8\pi \cdot G \cdot c^2} \tag{2.85}$$

We insert this term for the density in Eq. (2.84):

$$\delta V = \delta t \cdot dV \cdot \frac{G^*}{c} \tag{2.86}$$

We apply $G^* = \frac{GM}{r^2}$ to the above Eq., and we expand with $2c$:

$$\delta V = \delta t \cdot c \cdot dV \cdot \frac{2G \cdot M}{c^2} \cdot \frac{dV}{2r^2} \tag{2.87}$$

We apply $dV = 4\pi \cdot r^2 \cdot dr$, and we identify the Schwarzschild radius $R_S = \frac{2G \cdot M}{c^2}$. So we get the volume δV_{shell} formed in the shell:

$$\boxed{\delta V_{shell} = 2\pi \cdot R_S \cdot dr \cdot \delta t \cdot c} \tag{2.88}$$

Here we realize: In each shell around M and with a thickness dr, the same volume δV_{shell} is generated during a time δt.

2.5.2 Vacuum formed in a ball:

Next we determine the vacuum δV_{ball} that is formed during a time δt in a ball around M and with a radius R (Fig. 2.6). For it we integrate the above Eq. from the smallest possible radius R_S to R:

$$\int_0^{\delta V_{ball}} \delta V_{shell} = 2\pi \cdot R_S \cdot \int_{R_S}^{R} dr \cdot \delta t \cdot c \tag{2.89}$$

We evaluate the integrals. So we get the vacuum δV_{ball} or δV_f that is formed in the ball as a consequence of the field.

$$\boxed{\delta V_{ball} = 2\pi \cdot R_S \cdot (R - R_S) \cdot \delta t \cdot c = \delta V_f} \tag{2.90}$$

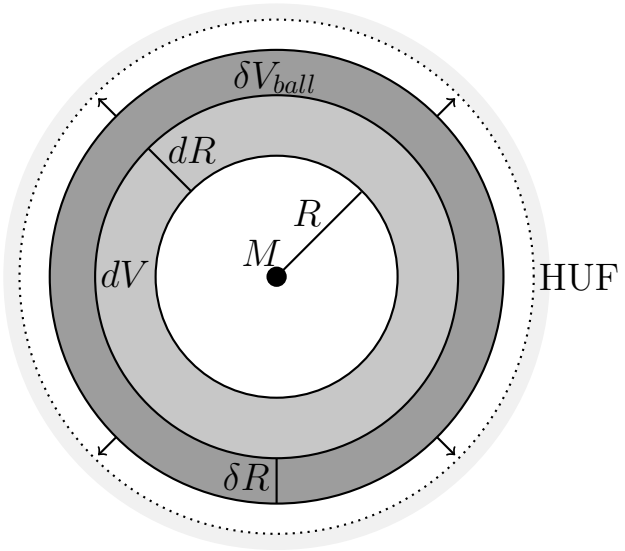

Figure 2.7: A mass M generates a vacuum δV_{ball} in a ball around M and during a time dt. It flows outward, and it requires a shell with thickness δR.

For the case of large $R/R_S >> 1$, and in leading order, we neglect R_S in the above Eq., as an approximation:

$$\delta V_{ball} \doteq 2\pi \cdot R_S \cdot R \cdot \delta t \cdot c = \delta V_f \tag{2.91}$$

This volume δV_{ball} is formed locally in shells, moreover it propagates through space at the velocity c. So it is the locally formed vacuum, LFV.

2.5.3 Elongation caused by new vacuum

In this section we derive the elongation δR of a distance dR that is caused by the formed vacuum δV_{ball}.

Thickness: The vacuum formed in a shell generates a net radial outward flow. Thereby the vacuum of all shells accumulates and establishes the rate of the vacuum δV_{ball} formed in the ball during a time δt (Fig. 2.7, Eq. 2.91). When that vacuum leaves the ball, it forms a shell with a thickness δR and a volume δV_{ball}

around the ball, see Fig. (2.7). So we get:

$$\delta R = \frac{\delta V_{ball}}{4\pi \cdot R^2} \tag{2.92}$$

We insert Eq. (2.91):

$$\delta R \doteq \frac{2\pi \cdot R_S \cdot R \cdot \delta t \cdot c}{4\pi \cdot R^2} = \frac{R_S \cdot \delta t \cdot c}{2 \cdot R} \tag{2.93}$$

Traveled dR: The shell with thickness δR and a volume δV_{ball} causes an elongation of a radial coordinate distance dR. We derive this dR next. The volume δV_{ball} is formed in a time δt. That vacuum propagates at the velocity of light c, as it is fully relativistic (Carmesin (2018c), Carmesin (2018b)). Hence, during the time δt, the vacuum travels the distance $dR = c \cdot \delta t$. Thus that vacuum moves within a shell with the thickness dR during that time δt. Consequently, the volume dV of that shell of thickness dR is increased by δV_{ball}, and the thickness dR is increased by δR. We apply $dR = c \cdot \delta t$ or $dR/c = \delta t$ to Eq. (2.93). So we get the elongation δR_f that is caused by the vacuum formed by the field:

$$\boxed{\delta R \doteq \frac{R_S \cdot dR}{2 \cdot R} = \delta R_f} \tag{2.94}$$

We derive the corresponding volume δV_f by multiplication of δR with $4\pi R^2$. So we get:

$$\boxed{\delta V_f \doteq 2\pi \cdot R_S \cdot R \cdot dR} \tag{2.95}$$

This elongation δR_f corresponds to the elongation δR_{SSM} described by the SSM in Eq. (1.45). We summarize our results derived here:

Theorem 9 Equality of LFV δV_f and $\delta V_{SSM,LFV}$: *For the volume $\delta V_f(R, dR, M)$ in Eq. (2.95) generated by the gravitational field of a mass M holds:*

(1) It is formed locally in shells with radii $r \leq R$, and it propagates at the velocity of light c, so it is a **locally formed vacuum, LFV**.

(2) The LFV $\delta V_f(R, dR, M)$ is generated in the shells that have the center at M, and that have radii $r \leq R$.

(3) The LFV $\delta V_f(R, dR, M)$ has the following amount:

$$\delta V_f \doteq 2\pi \cdot R_S \cdot R \cdot dR \tag{2.96}$$

(4) Inherent to the Schwarzschild metric, SSM, there is a LFV $\delta V_{SSM,LFV}(R, dR, M)$ (see theorem 2) in the shell with the center at M, the radius R and the thickness dR. The comparison shows that this LFV $\delta V_{SSM,LFV}(R, dR, M)$ is equal to the LFV $\delta V_f(R, dR, M)$ formed according to the DEQs of the rates.

Corollary 3 Explanation of the curvature of spacetime of the SSM: *The LFV $\delta V_f(R, dR, M)$ generated by a mass M explains*

(1) the **elongation** *δR of lengths dR in the vicinity of M,*

(2) the additional **volume** *$\delta V_{SSM,LFV}(R, dR, M)$ in the vicinity of M,*

(3) the **SSM** *in the vicinity of M*

(4) the gravitationally **reduced rate of time evolution** *in the vicinity of M, as the same elongations $\delta R_{SSM}(R) = \delta R_f(R)$ cause the same periodic times $T_{SSM}(R) = T_f(R)$, in a time of flight measurement of these elongations.*

2.6 Calculation of fields

In this section we show how the gravitational field of masses or dynamical masses m_j can be calculated in a HUF.

First we calculate the potential (see for instance (Bronstein and Semendjajew, 1980, p. 631-633)) the potential

$$\phi(\vec{r}) = \Sigma_j \frac{G \cdot m_j}{|\vec{r} - \vec{r}_j|} \tag{2.97}$$

Secondly, we apply the gradient $\frac{\partial}{\partial \vec{r}}$:

$$\frac{\partial}{\partial \vec{r}} \phi(\vec{r}) = -\Sigma_j \frac{G \cdot m_j}{|\vec{r} - \vec{r}_j|^2} \cdot \frac{\vec{r} - \vec{r}_j}{|\vec{r} - \vec{r}_j|} \tag{2.98}$$

We identify the term at the left hand side of the above Eq. by $-\vec{G}^*$. So we get:

$$\vec{G}^*(\vec{r}) = \Sigma_j \frac{G \cdot m_j}{|\vec{r} - \vec{r}_j|^2} \cdot \frac{\vec{r} - \vec{r}_j}{|\vec{r} - \vec{r}_j|} \tag{2.99}$$

Moreover, we identify the terms in the sum by the fields $\vec{G}_j^*$ of the masses:

$$\vec{G}^*(\vec{r}) = \Sigma_j \vec{G}_j^*(\vec{r}) \tag{2.100}$$

This Eq. represents the linear superposition of the fields.

Alternatively, we can apply the Gaussian theorem (see for instance (Bronstein and Semendjajew, 1980, p. 631-633)). With it we get:

$$4\pi \cdot G \cdot \int \rho dV = \int \vec{G}^*(\vec{r}) d\vec{A} \tag{2.101}$$

Hereby $d\vec{A}$ represents the oriented surface element of the integration. For the present case of the masses m_j, the integral $\int \rho dV$ is equal to the sum of the masses $\Sigma_j m_j$. So we obtain:

$$4\pi \cdot G \cdot \Sigma_j m_j = \int \vec{G}^*(\vec{r}) d\vec{A} \tag{2.102}$$

We summarize the result:

Proposition 8 Calculation of fields and rates:

(1) In a HUF, the gravitational field $\vec{G}^*$ of masses or dynamical masses m_j can be calculated by using the gravitational potential or by application of the Gaussian divergence theorem:

$$4\pi \cdot G \cdot \Sigma_j m_j = \int \vec{G}^*(\vec{r}) d\vec{A} \tag{2.103}$$

(2) The rate of the LFV can be calculated on the basis of the fields $\vec{G}^*$ by using the DEQ:

$$RGS = \dot{\varepsilon}^2 - G^{*2}/c^2 = 0 \tag{2.104}$$

(3) In particular, if the field $\vec{G}^*(\vec{r})$ cancels at a location $\vec{r}$, then the rate $\dot{\varepsilon}$ of the LFV cancels as well, as a consequence of the Lorentz scalar RGS with the DEQ $RGS = 0$.

2.7 Spacetime: scalar and tensor

In this section we apply the **RGED** u_{RG} and derive an invariant **spacetime scalar** and a corresponding **spacetime tensor**.

For it we apply the fact that u_{RG} is equal to zero. Moreover we multiply the equation $u_{RG} = 0$ by $8\pi \cdot G \cdot (\delta t)^2$ (2.60). So we derive:

$$0 = -G^{*2} \cdot (\delta t)^2 + c^2 \cdot \frac{(\delta V)^2}{(dV)^2} \tag{2.105}$$

As this term is zero, it represents an invariant with respect to all linear transformations, including Lorentz transformations. The positive term represents the time and the negative term represents the space. So that term is the **Lorentz scalar of spacetime, including gravity, the spacetime scalar, STS**.

That STS is represented by a relativistic square of a corresponding **spacetime tensor, STT** as follows:

$$STT_{i,j} = \begin{pmatrix} |G^*| \cdot \delta t & 0 & 0 & 0 \\ 0 & c \cdot \frac{\delta V_x}{dV} & 0 & 0 \\ 0 & 0 & c \cdot \frac{\delta V_y}{dV} & 0 \\ 0 & 0 & 0 & c \cdot \frac{\delta V_z}{dV} \end{pmatrix} \tag{2.106}$$

Hence the STS is the following square:

$$STS = \Sigma_{i,j=0}^{3} STT_{i,j} \cdot \eta_i^j \cdot STT^{i,j} = -G^{*2} \cdot (\delta t)^2 + c^2 \cdot \frac{(\delta V)^2}{(dV)^2} \tag{2.107}$$

We summarize our results:

Definition 10 The RGS can be represented in terms of the Lorentz scalar of spacetime, including gravity, the spacetime scalar, STS:

The STS is as follows

$$STS = -G^{*2} \cdot (\delta t)^2 + c^2 \cdot \frac{(\delta V)^2}{(dV)^2} = 0 \tag{2.108}$$

The STS can be represented in terms of a relativistic square of the following **spacetime tensor, STT***:*

$$STT_{i,j} = \begin{pmatrix} |G^*| \cdot \delta t & 0 & 0 & 0 \\ 0 & c \cdot \frac{\delta V_x}{dV} & 0 & 0 \\ 0 & 0 & c \cdot \frac{\delta V_y}{dV} & 0 \\ 0 & 0 & 0 & c \cdot \frac{\delta V_z}{dV} \end{pmatrix} \tag{2.109}$$

Chapter 3

Shortcut in spacetime

The GRT allows various solutions. Some particular solutions describe connections between very distant points in space. Such connections within the solutions are often called wormholes (see for instance Wheeler (1962), Misner et al. (1973), Morris et al. (1988)).

Such wormholes represent special **shortcuts in space**. In this chapter we analyze the possible formation of shortcuts in space, see Fig. (3.2). For it we use the theory of gravitational fields developed in chapter one as well as the Planck scale, which additionally applies quantum physics (see for instance Planck (1899), Carmesin (2019b)). Thus we analyze shortcuts in space on the basis of quantum gravity. In particular, we ask the following questions.

1. Can the locally formed vacuum LFV form a **shortcut in spacetime**?

2. What energy is sufficient for the formation of a shortcut in spacetime?

3. Can shortcuts in spacetime change the **dimension of the space**?

4. What is a **dimensional phase transition**, what is its **broken symmetry**, and what is its **critical density**?

3.1 Planck scale

In this section we introduce the Planck scale, as we can use it for the analysis of shortcuts.

There are two limits of observation or visibility: the uncertainty Δx and the Schwarzschild radius R_S (Heisenberg (1927), Schwarzschild (1916)). In the following, we combine these two limits.

According to the Schwarzschild radius, the following applies to visible regions:

$$\Delta x \geq R_S = \frac{2G \cdot m}{c^2} = \frac{2G \cdot E}{c^4} \tag{3.1}$$

According to the Heisenberg uncertainty relation, the following applies to a quantum object:

$$\Delta x \geq \frac{\hbar}{2 \cdot \Delta p} \tag{3.2}$$

Thereby we use the standard deviation:

$$\Delta p^2 = \langle p^2 \rangle - \langle p \rangle^2 \tag{3.3}$$

We apply Eq. (3.3) to Eq. (3.2):

$$\Delta x \geq \frac{\hbar}{2 \cdot \sqrt{\langle p^2 \rangle - \langle p \rangle^2}} \geq \frac{\hbar}{2 \cdot \sqrt{\langle p^2 \rangle}} \tag{3.4}$$

Accordingly, the square of the momentum $\langle p^2 \rangle$ must be as large as possible for the smallest possible uncertainty in position Δx. This is the case with high energy of the quantum object. So the object is relativistic and the corresponding energy momentum relation holds, $E^2 \approx \langle p^2 \rangle \cdot c^2$. So we get:

$$\Delta x \geq \frac{\hbar \cdot c}{2 \cdot E} = \frac{\hbar}{2 \cdot \Delta p} \tag{3.5}$$

The limit Δx of the visibility of a spatial structure of a quantum object with an energy E is therefore both proportional to

E (Eq. 3.1) and proportional to the reciprocal energy $1/E$ (Eq. 3.1). Fig. (3.1) shows this relationship: Visible according to Eq. (3.1) is the area to the right of the straight line of origin (light gray), visible according to Eq. (3.5) is the area to the right of the hyperbola (medium gray), the intersection (dark gray) is visible according to both inequalities. The intersection of the border lines represents an absolute limit of visibility. We determine this by equating the terms of the two boundary lines, straight line of origin and hyperbola in Fig. (3.1):

$$\Delta x = \frac{\hbar \cdot c}{2 \cdot E} = \frac{2G \cdot E}{c^4} \tag{3.6}$$

Here we factorize the reciprocal of the left fraction from the right fraction:

$$\Delta x = \frac{\hbar \cdot c}{2 \cdot E} = \frac{2 \cdot E}{\hbar \cdot c} \cdot \frac{\hbar \cdot G}{c^3} = \frac{1}{\Delta x} \cdot \frac{\hbar \cdot G}{c^3} \tag{3.7}$$

We solve for Δx:

$$\Delta x = \sqrt{\frac{\hbar \cdot G}{c^3}} = 1.616 \cdot 10^{-35}\,\mathrm{m} = L_P \tag{3.8}$$

This distance is called **Planck length** L_P. Accordingly, we resolve for the energy of the intersection point:

$$E = \frac{1}{2} E_P \quad \text{with} \quad E_P = \sqrt{\frac{\hbar \cdot c^5}{G}} = 1.956 \cdot 10^9\,\mathrm{J} \tag{3.9}$$

The energy E_P is called **Planck energy** E_P. Further quantities related to that intersection point are shown in table (9.3). These quantities are combinations of the universal constants G, c as well as h and of k_B and ϵ_0 more generally. It is natural to use these five universal constants and the combinations thereof as units, since in that system of units the universal constants have the value 1. Accordingly, these units are called **Planck units or natural units**. Quantities in natural units are marked by serpentine line, e.g. Fig. (3.1). We now analyze in more detail, what physical objects correspond to these two local limits of observation.

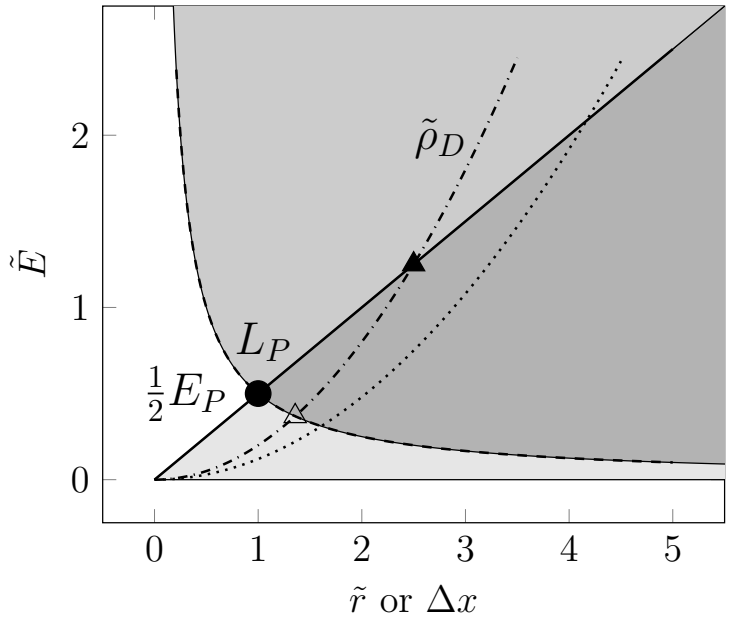

Figure 3.1: Limits of observation: the standard deviation Δx and the Schwarzschild radius $\tilde{r}$ limit the range of observation.

3.1.1 Planck density

Corresponding to the Planck energy, the Planck mass M_P is equal to E_P/c^2:

$$M_P = \frac{E_P}{c^2} = \sqrt{\frac{\hbar \cdot c}{G}} = 2.176 \cdot 10^{-8}\,\mathrm{kg} \tag{3.10}$$

Accordingly, the Planck density is the Planck mass divided by the third power of the Planck length:

$$\rho_P = \frac{M_P}{L_P^3} = \sqrt{\frac{c^5}{G^2 \cdot \hbar}} = 5.155 \cdot 10^{96}\,\frac{\mathrm{kg}}{\mathrm{m}^3} \tag{3.11}$$

The highest possible density is half the Planck density. This can be derived as follows: Among the objects with a radius r, the black hole with radius r has the highest mass or equivalent energy (see Fig. 3.1), and so it has the highest density among these objects too. So the object with the highest density is a black hole.

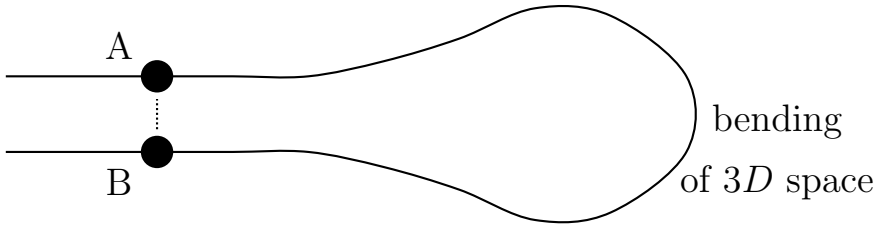

Figure 3.2: Two distant points A and B (black circles) of the three dimensional space (symbolized by a solid line) are connected by locally formed vacuum (dotted). With it, a short way from A to B is formed: a **shortcut**. A **single shortcut** might be considered as part of a topologically complicated $3D$ space or as part of a higher dimensional space.

Next we determine the black hole with the highest density: For it we express the density of a black hole by its radius:

$$\rho = \frac{M}{R_S^3} = \frac{R_S \cdot c^2}{R_S^3 \cdot 2G} = \frac{c^2}{R_S^2 \cdot 2G} \tag{3.12}$$

This term takes its maximum at $R_S = L_P$.

3.2 Energy of a possible shortcut

In this section we derive the energy that is sufficient in order to obtain a shortcut in space, see Fig. (3.2). Three energies might become essential: the energy $E_{conn.}$ for a short connection, the energy $E_{loop(L)}$ for a long connection, the energy E_{bend} for the bending of the space.

3.2.1 Energy for one short connection

For it we analyze the smallest possible additional connection. Its length, width and height have the smallest length L of an object that can be observed at all. It is the Planck length (see Planck (1899), Carmesin (2020b) or appendix):

$$L = L_P = \sqrt{\frac{\hbar \cdot G}{c^3}} = 1.616 \cdot 10^{-35}\text{m} \tag{3.13}$$

At that length, the highest possible density is achieved. It is one half of the Planck density ρ_P. (see Planck (1899), Carmesin (2020b) or appendix):

$$\rho = \frac{1}{2} \cdot \rho_P \quad \text{with} \quad \rho_P = \frac{c^5}{\hbar \cdot G^2} = 5.155 \cdot 10^{96} \frac{\text{kg}}{\text{m}^3} \tag{3.14}$$

So the sufficient energy of the short connection $E_{conn.}$ is as follows (cubes, balls or cylinders are not distinguished at the Planck scale, if details are essential, a harmonic potential is adequate (Carmesin (2018b), Carmesin and Carmesin (2020)):

$$\boxed{E_{conn.} = M \cdot c^2 = \frac{1}{2} \cdot \rho_P \cdot L_P^3 \cdot c^2 = \frac{1}{2} \cdot E_P} \tag{3.15}$$

Hereby E_P is the Planck energy:

$$E_P = \sqrt{\frac{\hbar \cdot c^5}{G}} = 1.956 \cdot 10^9 \text{J} \tag{3.16}$$

3.2.2 Energy for bending

If a short additional connection forms in three dimensional space, then the bending of space becomes necessary as illustrated in Fig. (3.2).

For instance, the additional connection between the points A and B (dotted line in Fig. 3.2) becomes relatively short, as a consequence of the bending of space. How can such a bending be achieved?

We give a rough estimate for a stationary bending of a size L. As such a bending can reverse the direction of the propagation of light, the required energy E_{bend} is of the order of magnitude of a black hole of that size:

$$E_{bend}(L) \approx M \cdot c^2 \quad \text{with} \quad M = \frac{R_S \cdot c^2}{2G} \tag{3.17}$$

We use $L = R_S$ and apply natural units. So we derive:

$$\boxed{E_{bend}(L) \approx \frac{E_P}{2} \cdot \frac{L}{L_P}} \tag{3.18}$$

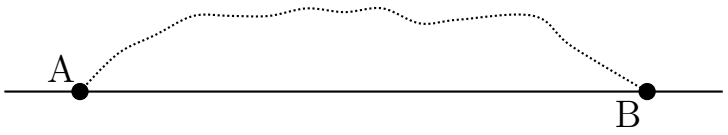

Figure 3.3: Two distant points A and B (black circles) of the three dimensional space (symbolized by a solid line) are connected by **loop way**. While travel times of objects or 'correlations' can decrease, if these use a short shortcut, this is not so in the case of a long connection.

3.2.3 Energy for a long connection

In this section we analyze a possible loop way without bending of space, see Fig. (3.3).

A loop way with a length L can connect the points A and B at a distance $d_{D=3}(A,B) \leq L$. The energy that is sufficient for such a loop way is L/L_P times the sufficient energy of the connection:

$$\boxed{E_{loop}(L) = \frac{L}{L_P} \cdot E_{conn.} = \frac{E_P}{2} \cdot \frac{L}{L_P}} \tag{3.19}$$

As the distance $d_{D=3}(A,B)$ is large compared to the distance of the additional connection $d_{conn.}(A,B) \approx L_P$, the energy of the loop way is large compared to the energy of the connection.

Proposition 9 *The newly formed vacuum can form new connections in space with the following properties:*

(1) The formation of a short connection with the length L_P and the volume L_P^3 requires the energy $E_P/2$.

(2) If the connected points have a distance L in $D = 3$, and if the short connection is enabled by a stationary bending of the space, then an additional energy proportional to L is required:

$$E_{bend}(L) \approx \frac{E_P}{2} \cdot \frac{L}{L_P} \tag{3.20}$$

(3) If the connected points have a distance L in $D = 3$, and if the space is not bent, and if there is no dimensional transition, then

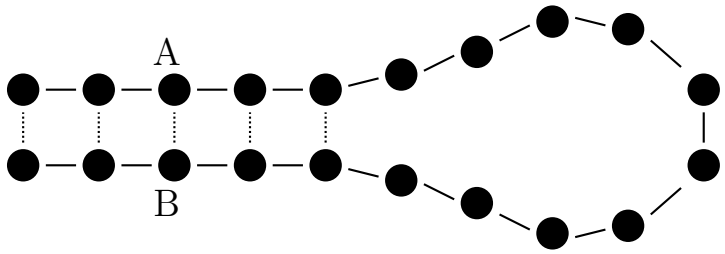

Figure 3.4: At high density at the Planck scale, $\rho \approx \rho_P$, the space exhibits a **grainy structure** (dots) at the scale of the Planck length, $L \approx L_P$. At such a density, a layer of shortcuts (dotted) can **form spontaneously**.

the connection requires a length similar to L, then the energy of such a loop is as follows:

$$E_{loop}(L) = \frac{E_P}{2} \cdot \frac{L}{L_P} \tag{3.21}$$

(4) If there occurs a dimensional phase transition, then short connections can form without bending of space.

3.3 Critical density $\rho_{cr.sc.}$ for shortcuts

In this section we derive the critical density $\rho_{cr.conn.}$, at which connections of length $dL \approx L_P$ and volume $dV \approx L_P^3$ form spontaneously, for an illustration of several formed connections see Fig. (3.4). If the the rate of change of the vacuum inside the connection $\dot{\varepsilon}_{inside} = \frac{\delta V}{\delta t \cdot dV}|_{inside}$ is negative, then the shortcut permanently looses vacuum, so it vanishes. If the the rate of change of the vacuum inside the connection $\dot{\varepsilon}_{inside}$ would be larger than zero, then the shortcut would permanently get new vacuum, so that can happen for a short time only. If the the rate of change of the vacuum inside the connection $\dot{\varepsilon}_{inside}$ is equal to zero, then the shortcut contains a constant amount of vacuum, correspondingly, the shortcut is stable. This shows that the shortcut becomes stable at the condition $\dot{\varepsilon}_{inside} = 0$.

Hence, at the critical density $\rho_{cr.conn.}$, the rate of change of the vacuum inside the connection $\dot{\varepsilon}_{inside} = \frac{\delta V}{\delta t \cdot dV}|_{inside}$ is zero.

Contributions to the rate $\dot{\varepsilon}_{inside}$: Some vacuum flows from the connection to neighboring regions A and B, see Fig. (3.5), at a rate $\dot{\varepsilon}_{out}$. Similarly, some vacuum flows from neighboring regions A and B to the connection at another rate $\dot{\varepsilon}_{in}$. Thirdly, some some vacuum forms in the connection at a rate $\dot{\varepsilon}_{formation}$. Next we analyze these rates in detail.

Rate of outward flow: The vacuum dV of the connection can escape at the velocity of light in two directions, see Fig. (3.5). For that escape it requires the time $dt = L_P/c = t_P$, whereby t_P is the Planck time. Thereby a quantum flows in each of the two directions with the probability 50 %. Thus during the time t_P, the volume dV of the connection leaves that volume. So the rate of outward flow is as follows:

$$\frac{\delta V}{\delta t}|_{out} = -\frac{dV}{t_P} \tag{3.22}$$

We solve for the rate per volume:

$$\dot{\varepsilon}_{out} = \frac{\delta V}{\delta t \cdot dV}|_{out} = -\frac{1}{t_P} \tag{3.23}$$

Rate of inward flow: As the cube of length L_P at a region A has six equal surfaces, one of which is directed to the connection, the sixth part of its rate $\frac{\delta V}{\delta t \cdot dV}|_{from\ A}$ propagates to the connection:

$$\frac{1}{6} \cdot \dot{\varepsilon}|_{from\ A} = -\frac{1}{6 \cdot t_P} \tag{3.24}$$

So the rate propagating from A to the connection is positive and has the absolute value of the above term:

$$\dot{\varepsilon}_{in,from\ A} = +\frac{1}{6 \cdot t_P} \tag{3.25}$$

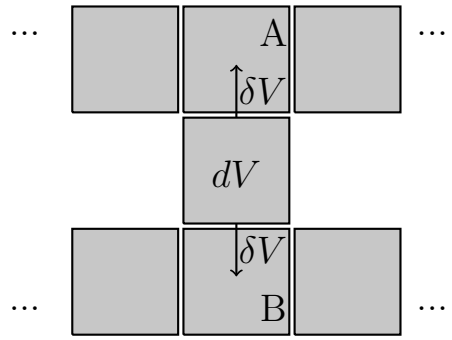

Figure 3.5: Flow of vacuum δV from dV: We assume that the vacuum essentially flows to existing vacuum. In order to get an estimation we analyze cubes with length $L \approx L_P$.

The same rate propagates to the connection coming from B. So we get:

$$\dot{\varepsilon}_{in} = \frac{2}{6 \cdot t_P} \tag{3.26}$$

Rate of formation of vacuum: Additionally, the density ρ of the connection forms vacuum. The exact rate depends on the symmetry. We model and analyze the rate for the unidirectional formation of vacuum, as it may propagate orthogonal to the surface of the cube. So we get:

$$\dot{\varepsilon}_{formation} = \sqrt{8\pi \cdot G \cdot \rho} \tag{3.27}$$

Sum of rates: We add the above three rates. So the total rate is as follows:

$$\dot{\varepsilon}_{inside} = \dot{\varepsilon}_{out} + \dot{\varepsilon}_{in} + \dot{\varepsilon}_{formation} \tag{3.28}$$

We insert the corresponding terms and set the rate to zero:

$$\dot{\varepsilon}_{inside} = \frac{-1}{t_P} + \frac{2}{6 \cdot t_P} + \sqrt{8\pi \cdot G \cdot \rho} = 0 \tag{3.29}$$

We solve for the root in the above Eq.:

$$\sqrt{8\pi \cdot G \cdot \rho} = \frac{2}{3 \cdot t_P} \tag{3.30}$$

We solve for the density:

$$\rho = \frac{1}{18\pi} \cdot \frac{1}{t_P^2 \cdot G} \tag{3.31}$$

The second fraction in the above is equal to the Planck density. So we derive the following for the **critical density of spontaneous connection formation**, $\rho_{cr.conn.}$:

$$\boxed{\rho_{cr.conn.} = \frac{1}{18\pi} \cdot \rho_P = 0.018 \cdot \rho_P} \tag{3.32}$$

In terms of the Planck density for a ball $\bar{\rho}_P = \rho_P \cdot 3/(4\pi)$ (see appendix), we get:

$$\boxed{\rho_{cr.conn.} = \frac{2}{27} \cdot \bar{\rho}_P = 0.074 \cdot \bar{\rho}_P} \tag{3.33}$$

3.3.1 Sequence of critical densities

In this section we derive the critical densities $\tilde{\rho}_{D,cr,conn.}$ for the spontaneous formation of shortcuts at dimensions D ranging from $D = 3$ to $D = 301$. For it we apply the dimensional extension of the FLE, the **EFLE** (chapter 8 and theorem 25). We emphasize that we do not apply the results of this section further in this book, so that any cyclic argument is excluded.

EFLE: We apply the EFLE for the case of negligible curvature parameter k (Eq. 8.32):

$$\frac{\dot{r}^2}{r^2} = -\frac{2[E_{D,j}] \cdot c^2}{[\langle r_j \rangle^2]} \tag{3.34}$$

Hereby we identify the averages over pairs $[\langle r_j \rangle^2]$ and $[E_{D,j}]$ by the corresponding ideal values of cosmology:

$$\frac{\dot{r}^2}{r^2} = -\frac{2E_D \cdot c^2}{r^2} \tag{3.35}$$

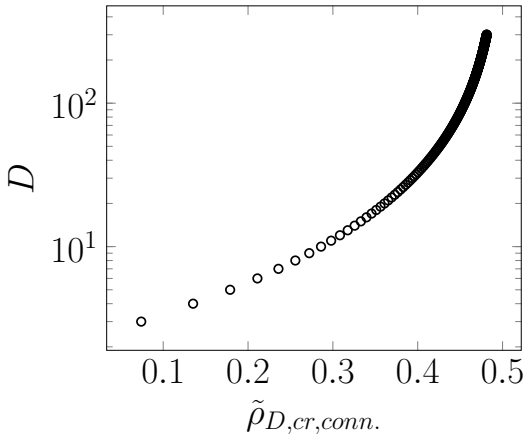

Figure 3.6: Dimension D as a function of the critical densities $\tilde{\rho}_{D,cr,conn.}$.

.

We multiply by r^2, and we apply natural units:

$$\dot{\tilde{r}}^2 = -2E_D \tag{3.36}$$

The reduced normalized energy contains a quantum correction that is numerically not essential here. Accordingly we use the classical part (Eq. 8.54):

$$E_{D,j,cl,G} = -\frac{\tilde{M}_j}{\langle \tilde{r}_j \rangle^{D-2}} \tag{3.37}$$

Again we use the average over the pairs:

$$E_{D,cl,G} = -\frac{\tilde{M}}{\tilde{r}^{D-2}} \tag{3.38}$$

Here we apply $\tilde{M} = \frac{1}{\tilde{a}}$ (Sect. 8.2.3). As an approximation, we use $\tilde{a} \approx \tilde{b}$ and $\tilde{b} = (2\tilde{\rho}_D)^{-1/2}$ (Sect. 8.2.3):

$$E_{D,cl,G} = -\frac{1}{2} \cdot (2\tilde{\rho}_D)^{\frac{D-1}{2}} \tag{3.39}$$

We insert this Eq. into Eq. (3.36):

$$\dot{\tilde{r}}^2 = (2\tilde{\rho}_D)^{\frac{D-1}{2}} \tag{3.40}$$

We apply the root:

$$\dot{\tilde{r}} = (2\tilde{\rho}_D)^{\frac{D-1}{4}} \tag{3.41}$$

We use the chain rule in order to derive the rate of isotropic formation of vacuum:

$$\dot{\tilde{V}} = D \cdot (2\tilde{\rho}_D)^{\frac{D-1}{4}} \tag{3.42}$$

We derive the corresponding rate for the unidirectional formation of vacuum. For it we divide by $\sqrt{D}$:

$$\dot{\tilde{V}}_{uni} = \sqrt{D} \cdot (2\tilde{\rho}_D)^{\frac{D-1}{4}} \tag{3.43}$$

Derivation of $\tilde{\rho}_{D,cr,conn.}$: The outward flow in Eq. (3.22) is expressed in terms of natural units:

$$\dot{\tilde{\varepsilon}}_{out} = -1 \tag{3.44}$$

Similarly, the inward flow in Eq. (3.26) is represented in terms of natural units:

$$\dot{\tilde{\varepsilon}}_{in} = \frac{1}{D} \tag{3.45}$$

The rate of vacuum formation $\dot{\tilde{\varepsilon}}_{formation}$ is equal to the rate for the unidirectional formation of vacuum in Eq. (3.43) divided by $d\tilde{V}$. For the present case of a cube with length L_P, the volume is $d\tilde{V} = 1$. So we get:

$$\dot{\tilde{\varepsilon}}_{formation} = \sqrt{D} \cdot (2\tilde{\rho}_D)^{\frac{D-1}{4}} \tag{3.46}$$

At the critical density, the sum of these three rates is zero (see Eq. 3.28):

$$\dot{\tilde{\varepsilon}}_{inside} = \dot{\tilde{\varepsilon}}_{out} + \dot{\tilde{\varepsilon}}_{in} + \dot{\tilde{\varepsilon}}_{formation} = -1 + \frac{1}{D} + \sqrt{D} \cdot (2\tilde{\rho}_D)^{\frac{D-1}{4}} = 0 \tag{3.47}$$

We solve for the density:

$$\boxed{\tilde{\rho}_D = \tilde{\rho}_{D,cr,conn.} = \frac{1}{2} \cdot \left(\frac{D-1}{D^{3/2}} \right)^{\frac{4}{D-1}}} \tag{3.48}$$

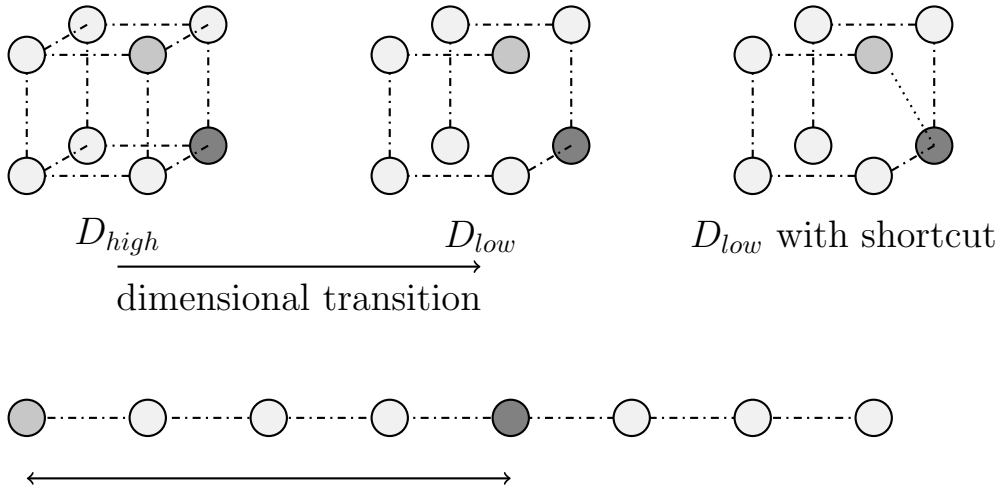

Figure 3.7: Points (circles) and dimensional connections (dash-dotted): **Dimensional transition** from D_{high} (left cube) to D_{low} (middle cube and lower linear representation). At D_{low}, a **shortcut** (dotted) is formed (right cube).

We present the stable dimensions D as a function of the critical densities $\tilde{\rho}_{D,cr,conn.}$, at which shortcuts form spontaneously at D (Fig. 3.6): $\tilde{\rho}_{D,cr,conn.} = \frac{1}{2} \cdot \left(\frac{D-1}{D^{3/2}}\right)^{\frac{4}{D-1}}$

Theorem 10 New vacuum can form new connections.

New connections form spontaneously at densities above the critical density $\tilde{\rho}_{cr.conn.} = \frac{2}{27}$.

At higher dimension, there occurs a sequence of critical densities (Eq. 3.48, Fig. 3.6).

3.4 Geometry in the early universe

In the early universe, there was a **high density** near the Planck density ρ_P, so it was above the critical density $\rho_{sc.conn.}$. Hence the microscopic **connections formed spontaneously** everywhere. Moreover, the smallest observable length was the Planck length L_P, so the space had a **grainy structure**, for an illustration see Fig. (3.4).

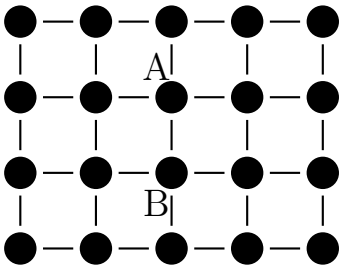

Figure 3.8: Dimensional transition caused by formation of shortcuts in spacetime near the Planck density, $\rho \approx \rho_P$: At low density, space appears continuous (Fig. 3.2). While at high density near ρ_P, space appears grainy (Fig. 3.4) and a high dimensional connectivity may occur, see above. In order to get a single and short shortcut connecting two distant points A and B in $3D$ space, the $3D$ space must bend. In contrast, if many shortcuts form and a dimensional transition takes place, these Points A and B can be connected by the same short shortcut, without bending of space at $D > 3$.

As a result of the spontaneously forming connections, each point had a high connectivity, corresponding to a **high dimension** $D_{high} > 3$ of the space. For an illustration, see the left cube in Fig. (3.7), or see Fig. 3.8). The space within the light horizon had a highest dimension, called the **dimensional horizon,** $D_{horizon}$ (see Carmesin (2018c) or Chap. 8). At that highest dimension $D_{horizon}$, the distances of the locations were roughly equal to the Planck length $d_{D_{hori}}(A, B) \approx L_P$.

During the evolution of the universe, the density ρ decreased, so that the critical density $\rho_{sc.conn.}$ was reached, and the corresponding **dimensional transition** occurred. Note that the objects in space experienced corresponding dimensional transitions at similar critical densities, see for inst. Carmesin (2017), Carmesin (2018a), Carmesin (2019a), Carmesin (2019b).

If D decreases at a dimensional transition, then many dimensional connections are lost, and the distances increase (Fig. 2).

During the so-called era of the hypothetical 'cosmic infla-

tion', the dimension D decreased by phase transitions, correspondingly that era is better called the **era of cosmic unfolding**. Thereby the connectivity of the locations decreased, the remaining connectivity is illustrated by a dashdotted line in Fig. (3.7). So matter and radiation can no longer use the **disconnected paths**.

However, the newly formed vacuum is not restricted to the vacuum present in three dimensional space. Above the critical density $\rho_{cr.\,conn.}$, it can propagate on the disconnected paths. When the disconnected paths are available additionally, then the distance of two points is of the order of the Planck length.

Symmetry breaking: Four dimensional space exhibits four mutually orthogonal directions of translation invariance. In contrast, three dimensional space exhibits only three mutually orthogonal directions of translation invariance. So a transition for four to three dimensions eliminates one of these symmetries. This process is called **spontaneous breaking of symmetry**. Such spontaneous breaking of symmetry characterizes a **phase transition** (Landau and Lifschitz (1979)). Correspondingly, such a change of the dimension of space is a **dimensional phase transition**.

Theorem 11 New vacuum can form new connections that can cause dimensional phase transitions.

(1) New connections can utilize short paths that are **relatively orthogonal to 3D space**, *see Fig. (3.7). If they can use disconnected paths that had been connected in the early universe, then the required energy is* $E \approx \frac{E_P}{2}$.

(2) New connections can use spontaneously forming short paths, so that a **higher dimension is constituted**, *see Figs. (3.6, 3.7, 3.8). Thereby, the space within the light horizon can form dimensions up to the dimensional horizon* D_{hori}.

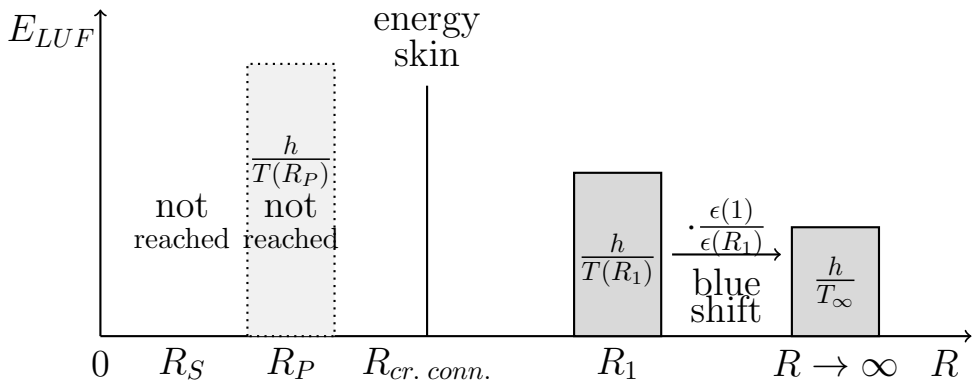

Figure 3.9: **Schematic** evolution of the energy in the LUF of a reference object that experiences a redshift, and that is falling towards a black hole: At a radius $R_{cr.\ conn.} > R_P > R_S$, the energy reaches a critical density $\rho_{cr.\ conn.}$ so that shortcuts form spontaneously.

3.5 Energy skin

In order to analyze regions that can provide densities above $\rho_{sc.conn.}$, we analyze the area in which most energy of a black hole is located, in this section.

For this purpose, we analyze an object falling towards a black hole with a Schwarzschild radius R_S, see Fig. (3.9). Thereby, the object can experience a redshift, and it has a periodic time T_∞ and an energy h/T_∞ at a distance $R \to \infty$. While the object is falling, it experiences a blue shift, and we derive the radius R_{ρ_P}, at which the object reaches the highest possible energy, $E_P/2$ (see for instance Carmesin (2020c), Carmesin (2020b) or the appendix). At a distance R, the periodic time is equal to T_∞ multiplied by the position factor $\epsilon(R) = \sqrt{1 - R_S/R}$. So we obtain:

$$\frac{E_P}{2} = \frac{h}{T_\infty \cdot \sqrt{1 - R_S/R_{\rho_P}}} \tag{3.49}$$

In order to simplify that Eq., we use $E_P = \hbar/t_P$, we solve for

the root, and we apply $\tilde{T}_\infty = T_\infty / t_P$. So we get:

$$\sqrt{1 - R_S/R_{\rho_P}} = \frac{4\pi}{\tilde{T}_\infty} \tag{3.50}$$

Next we solve for R_{ρ_P}:

$$\boxed{R_{\rho_P} = R_S \cdot \frac{\tilde{T}_\infty^2}{\tilde{T}_\infty^2 - 16\pi^2} > R_S} \tag{3.51}$$

Hence the density of the object would tend to the highest possible density $\rho_P/2$ at R_{ρ_P}. However, even before that density is reached, the density $\rho_{cr.\,conn.}$ is achieved at a radius $R_{cr.\,conn.} > R_{\rho_P}$, and shortcuts form spontaneously. We summarize our results:

Theorem 12 Energy skin:

For each object that does not prevent a gravitational collapse, the following holds:

(1) There is a radius $R_{cr.\,conn.} > R_S$ at which the critical density $\rho_{cr.\,conn.}$ for the spontaneous formation of a shortcut is reached.

(2) When the object forms by an infall of energy or matter, then the density $\rho(R)$ increases and when it reaches $\rho_{cr.\,conn.}$, then a shortcut forms spontaneously.

(3) As a consequence of the shortcut, the LFV is equal to the NFV and it is equal to one half of the CFV:

$$LFV = NFV = \frac{1}{2} \cdot CFV \tag{3.52}$$

(4) The shortcut forms by a gravitational instability. Thus the energy and mass of the black hole are located at a small spherical skin with radius $R_{cr.\,conn.}$ in three dimensional space, and that skin additionally is part of the shortcut propagating orthogonal to three dimensional space. That skin is called **energy skin**.

(5) As the shortcut is constituted by vacuum, its building block propagates at the velocity of light.

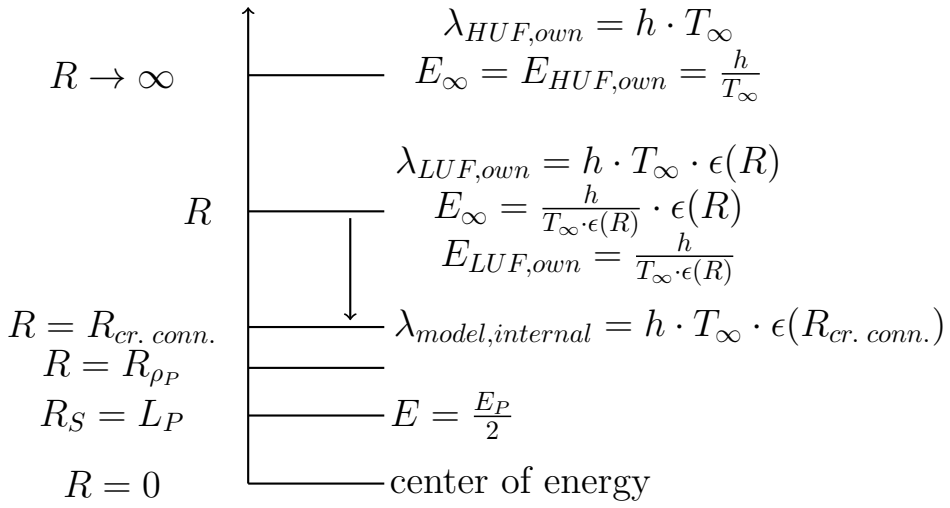

Figure 3.10: A freely falling photon in a HUF, LUF and model. A freely falling atom is similar: $E_{HUF,own} = m_0 \cdot c^2$. $E_{LUF,own} = m_0 \cdot c^2/\epsilon(R)$. Model: E is mainly focused at the nucleus. The scattered atom exhibits $\lambda_{LUF,own}$, though $\lambda_{LUF,nucleus} < \lambda_{LUF,own}$.

3.6 Energy skin of a photon

In this section we apply the fact that the extension R of a photon reaches the Planck length L_P at the energy $E_P/2$, see Fig. (3.1). That relation enables two interpretations:

This is usually interpreted by a photon that falls freely to a body, whereby the photon exhibits a blue shift until its energy is $E_P/2$ and its extension is L_P.

Moreover that relation can be interpreted by a model in which a photon exhibits an internal distribution of energy, and that distribution experiences a gravitational collapse with a corresponding blue shift or contraction. In that case the photon can form an energy skin. We emphasize that this model is not used in the rest of this book.

Internal model of a photon: The model essentially is constituted as follows: A photon might exhibit a gravitational collapse in an

internal model frame, whereby the usual blue shift occurs, and a short wavelength $\lambda_{model,internal}$ forms, see Fig. (3.10). The wavelength is approximately equal to the extension R of the photon, $R \approx \lambda$.

Observer: An **observer in a LUF** measures the wavelength of the photon $\lambda_{LUF,own}$. For instance, that wavelength is observed by a diffraction experiment:

$$\lambda_{LUF,own} = \lambda_{observed} =^{e.g.} \lambda_{\text{diffraction}} \tag{3.53}$$

In a scattering experiment for instance, $\lambda_{LUF,own}$ is measured. With it the own energy of the photon in the LUF can be derived:

$$\boxed{E_{LUF,own} = \frac{h \cdot c}{\lambda_{LUF,own}} = \frac{h}{T_{LUF,own}}} \tag{3.54}$$

At the Planck scale we get:

$$\frac{E_P}{2} = \frac{h \cdot c}{\lambda_P} \tag{3.55}$$

We derive the ratio of the above two Eqs.:

$$\frac{E_P}{2 \cdot E_{LUF,own}} = \frac{\lambda_{LUF,own}}{\lambda_P} \tag{3.56}$$

The ratio of the wavelengths is equal to that of the radii:

$$\frac{E_P}{2 \cdot E_{LUF,own}} = \frac{\lambda_{LUF,own}}{\lambda_P} = \frac{R}{L_P} \tag{3.57}$$

We solve for R:

$$R = L_P \cdot \frac{E_P}{2 \cdot E_{LUF,own}} \tag{3.58}$$

The photon becomes a black hole, when its density reaches the Planck density, and when its radius R reaches L_P, see Fig. (3.1).

So the Schwarzschild radius of the photon is L_P, and its position factor is as follows:

$$\boxed{\epsilon_{photon}(R) = \sqrt{1 - \frac{L_P}{R}} = \sqrt{1 - \frac{\lambda_P}{\lambda_{LUF,own}}} = \sqrt{1 - \frac{\lambda_P}{\lambda_{observed}}}} \tag{3.59}$$

In order to derive a term for λ_P, we use the following relations at the Planck scale:

$$\frac{\hbar c}{L_P} = E_P = \hbar\omega_P = \frac{h}{T(L_P)} = \frac{hc}{\lambda_P} \tag{3.60}$$

We solve for λ_P:

$$\boxed{\lambda_P = 2\pi \cdot L_P} \tag{3.61}$$

L_P represents the limit of observation (Fig. 3.1), Carmesin (2017)), and it corresponds to the energy $\frac{\hbar\omega_P}{2}$ of a ZPO. In contrast, λ_P is a reference wavelength corresponding to the energy $\hbar\omega_P$. We apply Eq. (3.61) to Eq. (3.59) and solve for R:

$$\boxed{R = \frac{\lambda_{LUF,own}}{2\pi} = \frac{\lambda_{observed}}{2\pi}} \tag{3.62}$$

HUF: If the universe expands, then the fraction $\frac{\rho_r}{\rho_\Lambda}$ decreases. In the limit $\frac{\rho_r}{\rho_\Lambda} \to 0$, a HUF or HUF_v is reached. In it the photon exhibits a wavelength $\lambda_{HUF,own} \to \infty$. So its extension tends to infinity as well $R_{HUF,own} \to \infty$, see Fig. (3.10).

Energy: The energy of the photon that can be observed in a LUF is the Planck constant h divided by the periodic time T:

$$E_{LUF,own} = \frac{h \cdot c}{\lambda_{LUF,own}} = \frac{h}{T_{LUF,own}} \tag{3.63}$$

The periodic time $T_{LUF,own}$ in a LUF is equal to the periodic time T_∞ in a HUF, multiplied by the position factor:

$$T_{LUF,own}(R) = \sqrt{1 - \frac{L_P}{R}} \cdot T_\infty \tag{3.64}$$

We solve for T_∞:

$$T_\infty = \frac{T_{LUF,own}(R)}{\sqrt{1-\frac{L_P}{R}}} \tag{3.65}$$

With it we derive the energy in the HUF:

$$E_\infty = \frac{h}{T_\infty} \tag{3.66}$$

This energy is an invariant, and the energy function is characterized by the position factor

$$E_\infty = \frac{h}{T_\infty \cdot \epsilon(R)} \cdot \epsilon(R) = \frac{h}{T(R)} \cdot \epsilon(R) = \text{invariant} \tag{3.67}$$

We summarize our results:

Proposition 10 Energy conservation of a photon:

(1) If a mass or dyn. mass $M = M_P$ is at the center of a HUF, and if a photon falls freely towards M, then the following holds:

(1a) An observer in a LUF can measure the wavelength $\lambda_{LUF,own}$ and periodic time $T_{LUF,own}$ of the photon.

(1b) Based on the measured wavelength $\lambda_{LUF,own}$, the energy $E_{LUF,own}$ and period $T_{LUF,own}$ of the photon can be evaluated:

$$E_{LUF,own} = \frac{h \cdot c}{\lambda_{LUF,own}} = \frac{h}{T_{LUF,own}} \tag{3.68}$$

(1c) Using the measured wavelength $\lambda_{LUF,own}$, the extension R and the position factor $\epsilon(R)$ of the photon can be evaluated:

$$R = \frac{\lambda_{LUF,own}}{2\pi} \text{ and } \epsilon_{photon}(R) = \sqrt{1-\frac{L_P}{R}} \tag{3.69}$$

(1d) Applying the measured wavelength $\lambda_{LUF,own}$, the periodic time T_∞ and the energy E_∞ of the photon in a HUF or HUF_v can be evaluated:

$$T_\infty = \frac{T_{LUF,own}(R)}{\sqrt{1-\frac{L_P}{R}}} = \frac{T(R)}{\sqrt{1-\frac{L_P}{R}}} \text{ and } E_\infty = \frac{h}{T_\infty} \tag{3.70}$$

(1e) The energy of the photon in the vacuum HUF is invariant. The energy function provides a relation between the measured own energy in a LUF $\frac{h}{T(R)}$ and the position factor $\epsilon(R)$:

$$E_\infty = \frac{h}{T_\infty \cdot \epsilon(R)} \cdot \epsilon(R) = \frac{h}{T(R)} \cdot \epsilon(R) = \text{invariant} \qquad (3.71)$$

(2) If the internal model of the photon is applied, then the photon contains an internal energy skin. As a consequence, the photon spontaneously forms a shortcut.

3.7 Explanation of NFV

In this section we develop an explanation of the NFV. For it we summarize objects that do not prevent a gravitational collapse towards the Schwarzschild radius. Using theorem (12) we conclude that these objects form as much NFV as LFV:

3.7.1 NFV of visible particles

As visible particles can form electromagnetic radiation in the process of pair creation (Tanabashi et al. (2018)), such particles have the ability to enclose light. So they presumably form shortcuts in a similar manner. This will be elaborated in full detail in a next volume of the present book series **Universe: Unified from Microcosm to Macrocosm**.

Theorem 13 An explanation of nonlocality of GRT:

(1) Objects that do not prevent a gravitational collapse towards R_S form an energy skin (see theorem 12).

(2) The following objects do not prevent a gravitational collapse towards the Schwarzschild radius: black holes, photons (Prop. (10), elementary particles of dark matter (Carmesin (2019b)), microscopic black holes (Carmesin (2020b)), presumably elementary particles of visible matter (Sect. 3.7.1).

(3) At the energy skin of a black hole, one half of the vacuum CFV flows outwards, while one half of the CFV flows into the shortcut and leaves the shortcut at a location that is uncorrelated to the black hole in three dimensional space. This explains the result that one half of the CFV is NFV (see theorem 5).

(4) Part (2) shows that most objects and presumably all objects form an energy skin. This explains at a local frame the fact that the amounts of LFV and NFV are equal.

(5) Additionally, the vacuum exhibits nonlocality, as it is only a component of the spacetime (Sect. 2.7).

Chapter 4

EPR Paradox

Based on the shortcuts developed in the previous chapter, we derive a second solution of the EPR paradox in this chapter.

4.1 Summary of the EPR paradox

Einstein et al. (1935) proposed a thought experiment as follows.

Prepared state: Two particles move along the x-axis as illustrated in Fig. (4.1). The difference of the locations $\Delta x = x_2 - x_1$ and the sum of the momenta $p = p_1 + p_2 = 0$ can be measured simultaneously, as their commutator vanishes:

$$[x_2 - x_1, p_1 + p_2] = (x_2 - x_1) \cdot (p_1 + p_2) - (p_1 + p_2) \cdot (x_2 - x_1) \quad (4.1)$$

We expand and identify commutators:

$$[x_2 - x_1, p_1 + p_2] = [x_2, p_2] + [x_2, p_1] - [x_1, p_2] - [x_1, p_1] \quad (4.2)$$

The commutators for different particles vanish, while $[x_2, p_2] = i\hbar = [x_1, p_1]$. So we get:

$$[x_2 - x_1, p_1 + p_2] = 0 \quad (4.3)$$

Proposed concept of physical reality: Einstein et al. (1935) proposed: If we can predict precisely the value of a physical quantity, then there is a corresponding **element of physical reality**.

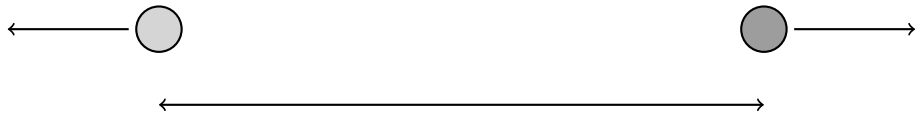

$\Delta x = x_2 - x_1$ can be measured

$p = p_1 + p_2 = 0$ can be measured simultaneously

Figure 4.1: Two quantum objects in a particular state: Two quantum objects (balls) are at a large distance and move apart. Thereby the distance Δx and the momentum p can be measured simultaneously.

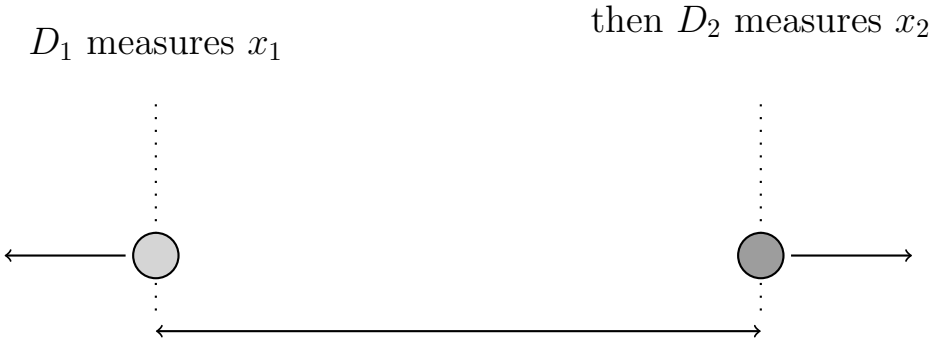

Figure 4.2: Prediction of nonlocally measured value x_2: If x_1 is measured by a detector D_1, and if a detector D_2 measures x_2 later, then we can predict the value $x_2 = x_1 + \Delta x$.

Possible measurement of x_1: First we measure x_1 with a detector D_1 as illustrated in Fig. (4.2). Then we measure x_2 with a detector D_2. For it, we can predict precisely the value $x_2 = x_1 + \Delta x$. So we conclude: x_2 **is an element of physical reality**.

Possible measurement of p_1: First we measure p_1 with a detector D_1 as illustrated in Fig. (4.3). Then we measure p_2 with a detector D_2. For it, we can predict precisely the value $p_2 = p - p_1$. So we conclude: p_2 **is an element of physical reality**.

Apparent paradox: Both, x_2 and p_2 are elements of physical reality, so they can be predicted precisely. However, these two

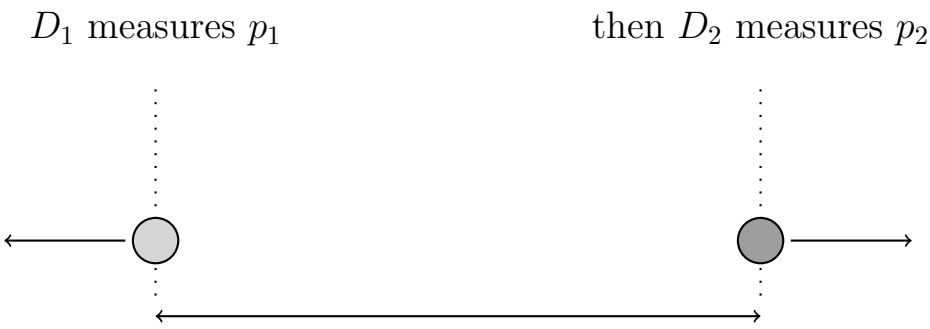

Figure 4.3: Prediction of nonlocally measured value p_2: If p_1 is measured by a detector D_1, and if a detector D_2 measures p_2 later, then we can predict the value $p_2 = p - p_1$.

physical quantities obey the Heisenberg uncertainty relation:

$$\Delta x_2 \cdot \Delta p_2 \geq \frac{\hbar}{2} \tag{4.4}$$

So these two values cannot both be determined precisely. This establishes an apparent paradox, the EPR paradox.

About paradoxes: In general, a paradox is an apparent contradictory situation, the solution of which provides a deeper insight. Accordingly, we should solve that EPR paradox, in order to achieve that deeper insight.

4.2 Consequences of a measurement

If the detector D_1 performs a measurement, then the wave function ψ_{state} prepared according to Fig. (4.1) is modified immediately.

If the detector D_1 measures x_1, then x_2 can be predicted. However, if the detector D_1 measures p_1, then p_2 can be predicted. Altogether, the measurements of the detector D_1 do not enable the predictability of the pair $(x_2|p_2)$.

First insight: As the detector D_1 modifies the wave function ψ_{state} as a consequence of a measurement, D_1 selects which of

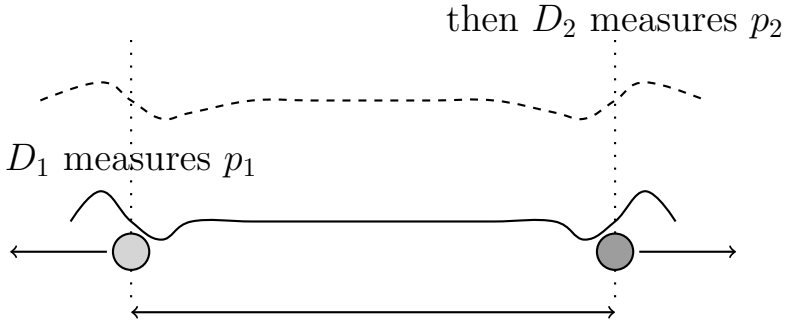

Figure 4.4: Nonlocal change of the wave function: If p_1 is measured by a detector D_1, then the wave function (solid line) changes nonlocally to the new wave function (dashed). This enables the conservation of momentum, thus we can predict the value $p_2 = p - p_1$.

the two values x_2 and p_2 can be predicted. Hence the measurements of D_1 do dot generate any contradiction to the uncertainty relation in Eq. (4.4).

4.3 Nonlocality

The measurements of D_1 do dot generate any contradiction to the uncertainty relation in Eq. (4.4), but the detector changes the wave function ψ_{state} much faster than a signal propagating at the velocity of light could modify that wave function ψ_{state}.

If an event occurs at a pair $(x_1|t_1)$ and causes an effect at a pair $(x_2|t_2)$, and if light is too slow in order to start at $(x_1|t_1)$ and arrive at $(x_2|t_2)$, then the effect is **nonlocal**.

Second insight: The detector D_1 modifies the wave function ψ_{state} in a nonlocal manner as illustrated in Fig. (4.4).

4.4 Necessity of nonlocality

If the measurement of p_1 by detector D_1 would not change the wave function in a nonlocal manner, then the measurement of p_2 by detector D_2 could provide a value different from $p_2 = p - p_1$,

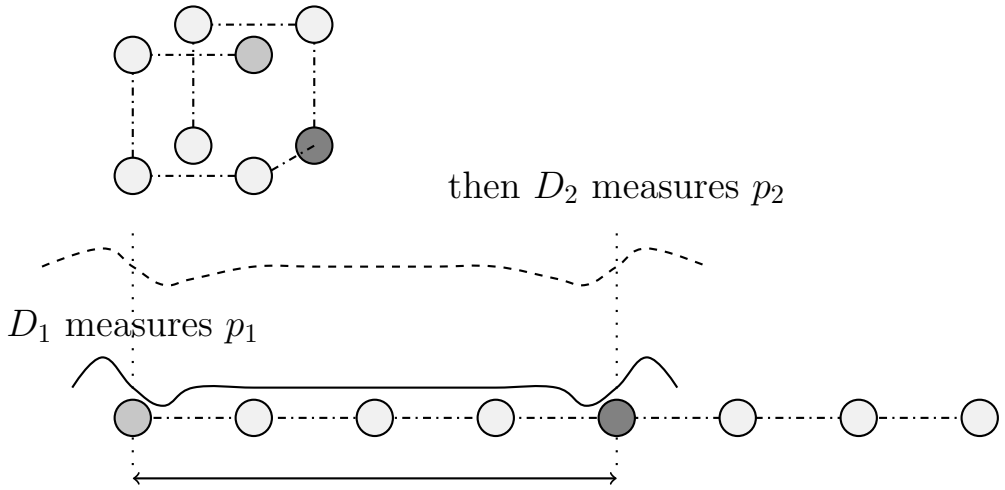

Figure 4.5: Nonlocal change of the wave function: If p_1 is measured by a detector D_1, then the wave function (solid line) changes nonlocally to the new wave function (dashed). This enables the conservation of momentum, thus we can predict the value $p_2 = p - p_1$.

as in quantum physics there is a stochastic element (Fig. 4.4). Then the conservation of momentum could be violated. In this manner the nonlocal change of the wave function provides the **fulfillment of the conservation law** of momentum.

Third insight: The nonlocal modification of a wave function ψ_{state} causes the fulfillment of the conservation laws in spite of the stochastic elements in quantum physics (Fig. 4.4).

4.5 Possible solution of the EPR paradox

In this section we develop a possible second solution of the EPR paradox. The idea is that a particular difference wave function can use the additional shortcuts.

4.5.1 Additional paths

In this section we summarize the additional paths that might be available in order to fulfill the conservation laws (Sect. 4.4).

In the early universe, the locations were connected in a high dimensional space. For an illustration, eight locations are arranged in three dimensions, $D = 3$, as illustrated in Fig. (4.5). The distances of the locations were roughly equal to the Planck length $r \approx L_P$. During the so-called era of the hypothetical 'cosmic inflation', the dimension D decreased by phase transitions, correspondingly that era is better called the **era of cosmic unfolding**. Thereby the connectivity of the locations decreased, the remaining connectivity is illustrated by a dashdotted line in Fig. (4.5). So matter and radiation can no longer use the **disconnected paths**.

4.5.2 Use of additional paths

However, an uncollapsed wave function ψ_{state} can react with some physical object such as a detector, an atom, a molecule or an elementary particle, for instance. Thereby, changes of the wave function ψ_{state} can in principle propagate at or below the velocity of light by using these disconnected paths. So such changes can propagate to any other location during roughly one Planck time. Hereby, the wave function ψ_{state} fulfills all laws of relativity as the modifications propagate at velocities at or below c. Hence the apparent contradiction between quantum physics and relativity is resolved, and the apparent EPR paradox is solved.

4.5.3 Wave functions and additional paths

The wave function must fulfill the principle of linear superposition. So a part of ψ_{state} reaches D_1:

$$\psi_{state,1} = \psi_{state} - \psi_{state,2} \tag{4.5}$$

During the measurement, the probability is one for the measured state:

$$1 = |\psi_{state,1,m}|^2 \tag{4.6}$$

In general, this wave function $\psi_{state,1,m}$ is not equal to $\psi_{state,1}$. So the measurement leaves a deficit:

$$\psi_{state,1,deficit} = -\psi_{state,1,m} + \psi_{state,1} \tag{4.7}$$

This deficit immediately propagates via the shortcuts to D_2: So at D_2 we have:

$$\psi_{state,2,m} = \psi_{state,2} + \psi_{state,1,deficit} \tag{4.8}$$

Next we test the principle of linear superposition. For it we insert $\psi_{state,2} = \psi_{state} - \psi_{state,1}$ and $\psi_{state,1,deficit} = -\psi_{state,1,m} + \psi_{state,1}$:

$$\psi_{state,2,m} = \psi_{state} - \psi_{state,1} - \psi_{state,1,m} + \psi_{state,1} \tag{4.9}$$

We solve for ψ_{state}:

$$\psi_{state,2,m} + \psi_{state,1,m} = \psi_{state} \tag{4.10}$$

So the principle of linear superposition also holds at the moment of the measurement. For it the deficit wave function uses the shortcuts.

In particular, in the case of the example with the momenta, the wave function $\psi_{state,1,m}$ is representing the measured momentum, so it has little uncertainty in momentum. That deficit wave function transfers this little uncertainty of the momentum to the detector D_2. So that detector measures the correct momentum.

Fourth insight: The nonlocal modification of a wave function ψ_{state} is provided by the propagation of the deficit wave function $\psi_{state,1,deficit}$ along paths of the early universe that are disconnected for matter and radiation, but that are available for $\psi_{state,1,deficit}$. (Fig. 4.5).

We summarize our results:

Theorem 14 Second solution of the EPR paradox*:*

The NFV and each nonlocal object can use the omnipresent spontaneously emerging **shortcuts in space** *(see theorem (12). So these objects can reach any place in the universe at a time that is of the order of the Planck time.*

In particular, the **deficit wave function**

$$\psi_{state,1,deficit} = -\psi_{state,1,m} + \psi_{state,1} \tag{4.11}$$

can use these paths. Thereby they can provide the conservation laws at a microscopic level.

This solution solves the nonlocality as follows: Paths that are nonlocal in three dimensional space are **local in high dimensional space***. Moreover such paths have a length of the order of L_P, as shortcuts are used. Furthermore, these shortcuts are short in higher dimensional space. Thereby these shortcuts are energetically available, as they do not require any bending of three dimensional space in higher dimensional space. So the NFV becomes* **locally formed vacuum using shortcuts, LFVUS***.*

Chapter 5

Waves of Spacetime

In this section we derive DEQs for the formation of spacetime that have waves as solutions.

5.1 Problems of spacetime: waves

Einstein (1905) introduced the concept of spacetime, including **curved spacetime** (Einstein (1915a)). There remain essential questions: For instance, Planck (1900) introduced the concept of **quantization**, inherent to which is the phenomenon of **non-locality**, which is apparently paradoxical to spacetime (Einstein et al. (1935)). We solved some of the problems by using fields (Sect. 1.1). Some of the problems can be addressed by using waves:

1. What is the **DEQ for waves of spacetime**?
2. Is that DEQ a **HUF zero Lorentz scalar, HZLS**?
3. Why are the waves described by that DEQ **rate gravity waves, RGWs**?
4. Do the RGWs describe the **physically correct amount of LVF**?
5. What is the **energy of RGWs** in the HUF?

6. How does **gravity propagate** through space?

7. What are the **modes of RGWs**?

5.2 DEQs for waves in vacuum

In this section we derive the DEQ that describes the formation of vacuum at a mass or at a dynamical mass and the propagation of waves.

For it we analyze the DEQ (2.76):

$$[\text{Trace}(\dot{\hat{\varepsilon}}_{ij})]^2 = \frac{\text{Trace}(G_{ij})}{c^2} \tag{5.1}$$

For the case of **vacuum**, the gravitational tensor is established by a **gravitational field** in a direction j, corresponding to an unidirectional symmetry.

$$\frac{\text{Trace}(G_{ij})}{c^2} = \frac{G_j^{*2}}{c^2} \tag{5.2}$$

In that case the rate has unidirectional symmetry as well:

$$\text{Trace}(\dot{\hat{\varepsilon}}_{ij}) = \dot{\hat{\varepsilon}}_j \tag{5.3}$$

With it we get the DEQ:

$$\boxed{\dot{\hat{\varepsilon}}_j^2 - \frac{G_j^{*2}}{c^2} = 0} \tag{5.4}$$

Hence we find a **homogeneous DEQ for the case of vacuum**. Later we analyze the case with additional objects in the space by analyzing corresponding inhomogeneous DEQs and their solutions additionally. Moreover, we form linear combinations of the unidirectional solutions, these include other symmetries such as the isotropic symmetry of the expansion of space.

Potential: We analyze fields without a rotational part. So we can express the field in terms of a potential:

$$G_j^* = -\frac{\partial}{\partial j}\phi = -\partial_j \phi \tag{5.5}$$

Thereby we denote the derivative by the operator ∂_j. So we get the following **homogeneous DEQ**:

$$\boxed{\dot{\varepsilon}_j^2 - \frac{(\partial_j \phi)^2}{c^2} = 0} \tag{5.6}$$

Alternative derivation: This DEQ can also be obtained from the DEQ (2.57)

$$RGS = \dot{\varepsilon}^2 - G^{*2}/c^2 = 0 \tag{5.7}$$

by application of Eq. (5.5).

5.2.1 DEQ in $4D$ spacetime

The above DEQ represents a DEQ in four dimensional spacetime. In this section we elaborate that formulation. For it we apply Eq. (5.5) to the rate gravity four-vector in theorem (7)

$$RGV_i = \begin{pmatrix} \dot{\varepsilon} \\ G_x^*/c \\ G_y^*/c \\ G_z^*/c \end{pmatrix} \tag{5.8}$$

and derive a **slope four-vector** as follows:

$$\bar{\Gamma}^i = \begin{pmatrix} c \cdot \partial_t \varepsilon \\ \partial_x \phi \\ \partial_y \phi \\ \partial_z \phi \end{pmatrix} \tag{5.9}$$

With it we represent the DEQ (5.6) in terms of the **slope four-vector,** $\bar{\Gamma}$.

$$\boxed{\bar{\Gamma}_i \, \eta_j^i \, \bar{\Gamma}^j = c^2 \cdot (\partial_t \varepsilon_r)^2 - (\partial_{\bar{r}} \phi)^2 = 0} \tag{5.10}$$

Hereby, $\partial_{\vec{r}}$ denotes the derivative in the direction of propagation $\vec{r}$, and $\partial_t \varepsilon_r$ represents the unidirectional rate of formation of vacuum. It appears quite obvious that this DEQ has solutions that are periodic in time and space, these are waves. So the DEQs (5.10) and (5.6) are DEQs of waves. We summarize:

Theorem 15 Four-vector and DEQ of vacuum.

(1) Formation of vacuum is described by the slope four-vector:

$$\bar{\Gamma}^i = \begin{pmatrix} c \cdot \partial_t \varepsilon \\ \partial_x \phi \\ \partial_y \phi \\ \partial_z \phi \end{pmatrix} \tag{5.11}$$

(2) The relativistic square of $\bar{\Gamma}^i$ represents a Lorentz scalar and a DEQ for the formation of vacuum:

$$\bar{\Gamma}_i \, \eta^i_j \, \bar{\Gamma}^j = c^2 \cdot (\partial_t \varepsilon_r)^2 - (\partial_{\vec{r}} \phi)^2 = 0 \tag{5.12}$$

(3) So that DEQ for waves is a **HUF zero Lorentz scalar, HZLS**. *So it is highly invariant.*

5.3 Wave in vacuum

In this section we derive solutions of the above **homogeneous DEQ** (5.6). For it we make an Ansatz for plane waves propagating in the direction j

$$\boxed{\varepsilon_j = \hat{\varepsilon}_{j,\omega} \cdot \exp(i \cdot \omega \cdot t - i \cdot k_j \cdot r_j) + \hat{\varepsilon}_{j,const.}} \text{ and} \tag{5.13}$$

$$\boxed{\phi_j = \hat{\phi}_{j,\omega} \cdot \exp(i \cdot \omega \cdot t - i \cdot k_j \cdot r_j) + \hat{\phi}_{j,const.}} \tag{5.14}$$

Hereby, $\hat{\varepsilon}_{j,const.}$ and $\hat{\phi}_{j,const.}$ are constants of integration. Moreover, the amplitudes $\hat{\varepsilon}_{j,\omega}$ include the polarization, this is elaborated in section (5.3.2). Furthermore, the amplitudes $\hat{\phi}_{j,\omega}$ are derived in Eq. (5.18).

We insert into the DEQ (5.6):

$$\hat{\varepsilon}_{j,\omega}^2 \cdot \omega^2 = \frac{k_j^2}{c^2} \cdot \hat{\phi}_{j,\omega}^2 \tag{5.15}$$

The velocity of propagation is:

$$v_{prop} = \frac{\lambda}{T} = \frac{\omega}{k_j} \tag{5.16}$$

As no velocity relative to the vacuum can be measured (see Michelson and Morley (1887)), the vacuum is fully relativistic. Hence it propagates at the **velocity of light** in the vacuum c. So we get:

$$v_{prop} = c = \frac{\omega}{k_j} \tag{5.17}$$

We apply this result to (Eq. 5.15):

$$\boxed{\hat{\phi}_{j,\omega} = \hat{\varepsilon}_{j,\omega} \cdot c^2} \tag{5.18}$$

5.3.1 Elongations of these waves

According to the DEQ (5.4), the elongations of the waves represent the rates of the formation of vacuum and gravitational fields. Accordingly, we call such a wave a **rate gravity wave, RGW**. As these waves include the formation of vacuum (Eq. 5.13) and the formation of a potential (Eq. 5.14), they include the usual gravitational waves as special cases.

5.3.2 Polarization of waves

The wave oscillates in particular directions. These are described by the tensors $\hat{\varepsilon}_{\alpha\beta}$.

In order to provide relatively short formulas, we include these tensors in the amplitude. Accordingly, our index j, ω that summarizes the index ω of the circular frequency, the index j of the

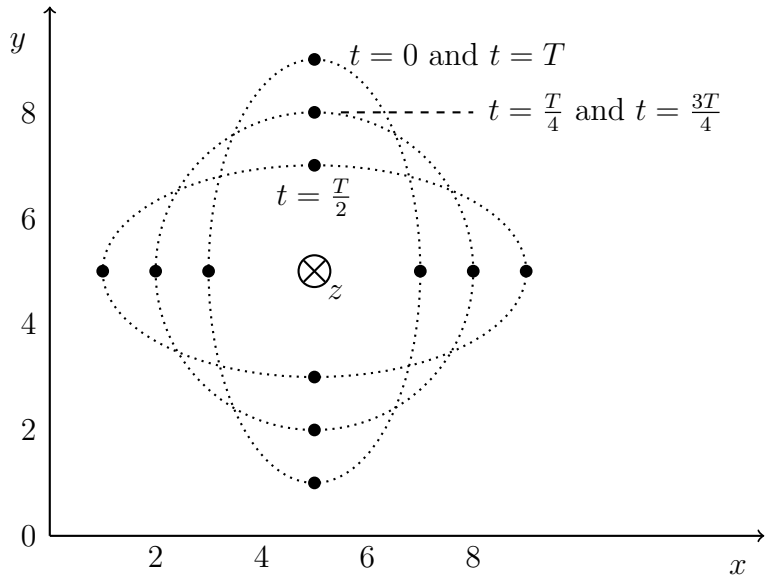

Figure 5.1: Single mode with periodic time T of a gravitational wave propagating to the z direction: Locations in space are indicated by small dots visually combined by dotted lines. The deviations from the metric tensor g_{ij} of flat space are as follows: $g_{yy} - 1 = h_{yy} = \cos\left(\frac{2\pi}{T} \cdot t\right) = -h_{xx} = -(g_{xx} - 1)$.

direction of propagation, the indices of the tensor elements α and $\alpha\beta$, and a possible index q denoting the tensor. So we get:

$$\hat{\varepsilon}_{j,\omega} \hat{=} \hat{\varepsilon}_{j,\omega,q,\alpha\beta} \tag{5.19}$$

In general, these tensors can provide the formation of vacuum, This case will be worked out in the following sections (5.4) and (5.5).

In a particular case, these tensors provide no formation of vacuum. In this case, the waves represent the usual gravitational waves, and the corresponding tensors are presented in Eqs. (2.77) and (2.78).

5.3.3 Gravitational waves

On the basis of the GRT, Einstein (1916) derived fully relativistic waves of spacetime, the so-called **gravitational waves** (Fig.

5.1). Abbott (2016) discovered these waves by using Michelson interferometers. These waves can be described as plane waves with transverse polarization.

So the waves described here in Eq. (5.13) include the observed gravitational waves mathematically. However, the observed gravitational waves have been generated by a binary star, whereas we consider RGWs in general. So the physical circumstances at which the RGWs form may be quite different.

5.3.4 Linear combinations

As the principle of linear superposition is applicable to the rate gravity waves, RGWs, all discrete and continuous linear combinations of the above plane waves are solutions of the homogeneous DEQ as well. This includes waves with other symmetries such as rotational symmetry, for instance. Moreover this includes aperiodic elongations.

5.3.5 Real RGWs

In this section we derive real RGWs. For it we form linear combinations of the RGWs in Eq. (5.13):

$$\varepsilon_{j,\omega} = \hat{\varepsilon}_{j,\omega} \cdot \exp(i \cdot \omega \cdot t - i \cdot k_j \cdot r_j) + \hat{\varepsilon}_{j,const.} \tag{5.20}$$

The first linear combination uses the functions with circular frequencies ω and $-\omega$ and with the same amplitude $\hat{\varepsilon}_{j,\omega}$:

$$\varepsilon_{j,\omega,c} = \frac{\varepsilon_{j,\omega} + \varepsilon_{j,-\omega}}{2} = \frac{\hat{\varepsilon}_{j,\omega}}{2} \cdot \left(e^{i(\omega t - k_j r_j)} + e^{-i(\omega t - k_j r_j)} \right) + \hat{\varepsilon}_{j,const.} \tag{5.21}$$

In the above Eq. we identify the cosine:

$$\boxed{\varepsilon_{j,\omega,c} = \hat{\varepsilon}_{j,\omega} \cdot \cos(\omega t - k_j r_j) + \hat{\varepsilon}_{j,const.}} \tag{5.22}$$

The second linear combination analogously provides a sine function:

$$\varepsilon_{j,\omega,s} = \frac{\varepsilon_{j,\omega} - i\varepsilon_{j,-\omega}}{2i} = \frac{\hat{\varepsilon}_{j,\omega}}{2i} \cdot \left(e^{i(\omega t - k_j r_j)} - ie^{-i(\omega t - k_j r_j)} \right) + \hat{\varepsilon}_{j,const.} \tag{5.23}$$

Here we identify the sine:

$$\boxed{\varepsilon_{j,\omega,s} = \hat{\varepsilon}_{j,\omega} \cdot \sin(\omega t - k_j r_j) + \hat{\varepsilon}_{j,const.}} \tag{5.24}$$

We summarize our results as follows:

Theorem 16 Properties of RGWs:

The RGWs (Eqs. 5.13 and 5.14)

$$\varepsilon_j = \hat{\varepsilon}_{j,\omega} \cdot \exp(i \cdot \omega \cdot t - i \cdot k_j \cdot r_j) + \hat{\varepsilon}_{j,const.} \text{ and} \tag{5.25}$$

$$\phi_j = \hat{\phi}_{j,\omega} \cdot \exp(i \cdot \omega \cdot t - i \cdot k_j \cdot r_j) + \hat{\phi}_{j,const.} \tag{5.26}$$

have the following **properties***:*

(1) Some RGWs are **plane waves or** *discrete or continuous* **linear combinations** *of these. These include real waves and waves with various symmetries, as the plane waves establish a* **complete orthonormal basis** *((Ballentine, 1998, p. 17-22)).*

(2) RGWs **propagate** *at the velocity of light c.*

(3) RGWs represent the rates $\dot{\varepsilon}$ of the **formation of vacuum***.*

(4) RGWs can have transverse tensors with trace zero, corresponding to constant volume and to **gravitational waves***.*

(5) RGWs include a relative formed vacuum $\varepsilon = \frac{\delta V}{dV}$ as a time integral of the rates $\dot{\varepsilon}$. So ε represents some **accumulated new vacuum***. As all vacuum was new vacuum at some time, the vacuum is part of the RGWs. In this manner, the vacuum propagates at the velocity of light.*

(6) In particular, that accumulated formed vacuum represented by ε is essential for the SSM. In particular, it explains the gravitational time dilation, including the **formation of spacetime**

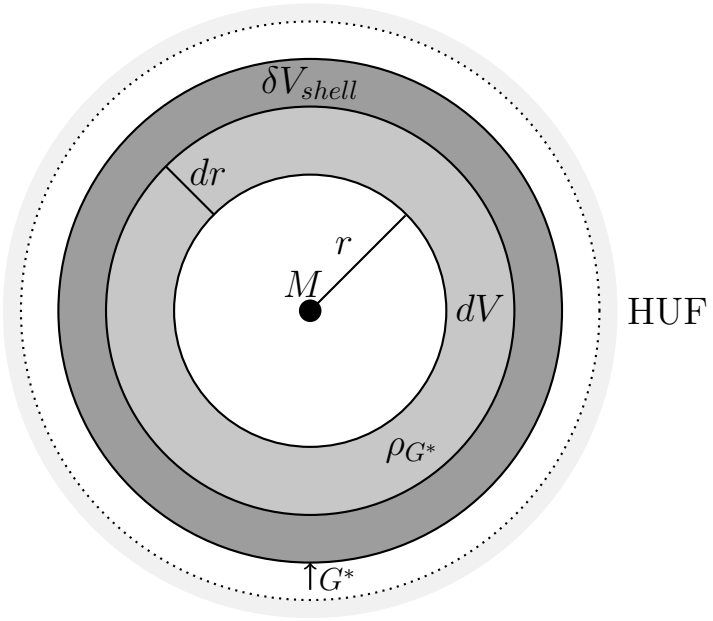

Figure 5.2: A mass M generates a field G^* in a shell (medium grey) around M and with volume dV. The density ρ_{G^*} of the field forms vacuum with a volume δV_{shell}.

(Eqs. 5.13 and 5.14) for the following reason: The LFV δV gives rise to the elongation δR of the SSM. In a time of flight measurement using light, the elongation δR corresponds to an additional time $\delta t = \delta R/c$. Altogether, the **time dilation of the SSM is a consequence of the LFV**.

(7) RGWs represent the **gravitational fields** $\vec{G}^* = -\partial_{\vec{x}}\phi$. *So the* **fields and the gravitational interaction propagate with the velocity of light**.

(8) RGWs include a **gravitational potential** ϕ *as an integral of the fields. So the potential represents some* **accumulated fields**. *As all potential was accumulated at some time (see Carmesin (2020b)), the potential is part of the RGWs.*

5.4 Inhomogeneous DEQ

In this section we derive the DEQ for the case in which there are additional objects in the vacuum.

For it we start with the homogeneous solutions. These are the RGWs $\dot{\varepsilon}_j$, see Eqs. (5.13) and (5.14). In order to emphasize the homogeneity of the DEQ, we add the index hom: $\dot{\varepsilon}_{j,hom}$.

Each additional object in the vacuum can be described by a mass or a dynamical mass or by a density. In all these cases, an additional rate $\dot{\varepsilon}_{inhom}$ of formation of vacuum is caused (see chapter 1).

As the principle of linear superposition can be applied to the vacuum (see section 1.3), this rate can be added to the rate of the homogeneous solution:

$$\dot{\varepsilon}_j = \dot{\varepsilon}_{j,hom} + \dot{\varepsilon}_{j,inhom} \tag{5.27}$$

For instance, for the case of an unidirectional inhomogeneity, the DEQ is as follows:

$$\dot{\varepsilon}_{j,inhom} = \sqrt{8\pi G \cdot \rho} \tag{5.28}$$

For that case, we add the above DEQ to the homogeneous DEQ. So we get the DEQ describing the formation and propagation of RGWs:

$$\boxed{\dot{\varepsilon}_{j,hom} + \dot{\varepsilon}_{j,inhom} - G^*/c = \sqrt{8\pi G \cdot \rho}} \tag{5.29}$$

5.5 Inhomogeneous solution at a mass

In this section we derive the propagating rate generated by a mass M. In a shell with radius r and thickness dr, the mass generates the volume δV_{shell} during a time δt as follows (see Eq. 2.88 and Fig. 5.2):

$$\delta V_{shell} = 2\pi \cdot R_S \cdot dr \cdot \delta t \cdot c \tag{5.30}$$

We use the elongation generated in the shell $d\varepsilon(r) = \frac{\delta V_{shell}}{dV}$, and we utilize $dV = 4\pi \cdot r^2 \cdot dr$:

$$d\varepsilon(r) = \frac{R_S \cdot \delta t \cdot c}{2r^2} \tag{5.31}$$

Next we divide by δt, and we use $R_S = 2GM/c^2$. Moreover we use the notation $\frac{\delta\varepsilon(r)}{\delta t} = \dot{\varepsilon}(r)$. Hence a mass M generates the following **stationary rate of formation of vacuum**:

$$\boxed{\dot{\varepsilon}(r) = \frac{1}{c} \cdot \frac{G \cdot M}{r^2}} \tag{5.32}$$

Next we identify the absolute value $G^*(r) = \frac{G \cdot M}{r^2}$ of the gravitational field in the above Eq.:

$$\frac{G^*(r)}{c} = \dot{\varepsilon}(r) \text{ at a distance r from a mass} \tag{5.33}$$

As both signs are possible (in a Big Crunch for instance), we apply the square:

$$\boxed{\frac{G^{*2}(r)}{c^2} = \dot{\varepsilon}^2(r) \text{ at a distance r from a mass}} \tag{5.34}$$

In order to derive a DEQ of a wave, we express $\vec{G}^*$ by the derivative of a potential $\partial_{\vec{r}}\phi(\vec{r})$. So we get:

$$\boxed{\frac{(\partial_{\vec{r}}\phi(\vec{r}))^2}{c^2} = \dot{\varepsilon}^2(r)} \tag{5.35}$$

This DEQ is a DEQ of a wave. It shows that the inhomogeneous solution obeys a DEQ of a wave. As the energy of a RGW is zero in the HUF or HUF_v, the field and rate of the inhomogeneous solution can always propagate by a wave that forms in addition to the stationary rate in Eq. (5.32).

In order to derive the density of the solution $\rho_{stationary}$, we multiply Eq. (5.34) with $\frac{1}{8\pi \cdot G}$. So we get:

$$\frac{G^{*2}}{8\pi \cdot G \cdot c^2} = \frac{\dot{\varepsilon}^2(r)}{8\pi \cdot G} \text{ at a distance r from a mass} \tag{5.36}$$

At the left hand side of that Eq., we identify the density of the field $\rho_{f,stationary}$. It represents the whole density of that solution $\rho_{stationary}$, as that solution is stationary:

$$\boxed{\rho_{stationary} = \frac{G^{*2}}{8\pi \cdot G \cdot c^2}} \tag{5.37}$$

It is equal to the right hand side of Eq. (5.36). So we can express that density by the rate $\varepsilon(r)$:

$$\boxed{\rho_{stationary}(\dot{\varepsilon}) = \frac{\dot{\varepsilon}^2}{8\pi \cdot G}} \tag{5.38}$$

This relation shows the density as a function of the rate $\dot{\varepsilon}$ of the formation of vacuum, irrespective of the mass or the field. We summarize our results:

Theorem 17 The LVF formed according to the DEQ of the RGW is equal to the LFV according to the SSM.

The rate $\dot{\varepsilon}(r)$ of the local formation of vacuum, LFV, has the following properties:

(1) According to the DEQ of the wave, a mass M generates the volume

$$\delta V_{shell} = 2\pi \cdot R_S \cdot dr \cdot \delta t \cdot c \tag{5.39}$$

It is equal to the volume generated according to the SSM (see theorem 2).

(2) The corresponding stationary rate can be expressed as a function of the mass or dynamic mass, irrespective of the field:

$$\dot{\varepsilon}(r) = \frac{1}{c} \cdot \frac{G \cdot M}{r^2} \tag{5.40}$$

(3) The stationary field G^* and the stationary rate $\dot{\varepsilon}$ obey the DEQ of the wave, and the RGW does not require energy in the HUF. Correspondingly, the field propagates at the velocity of light in the form of a RGW.

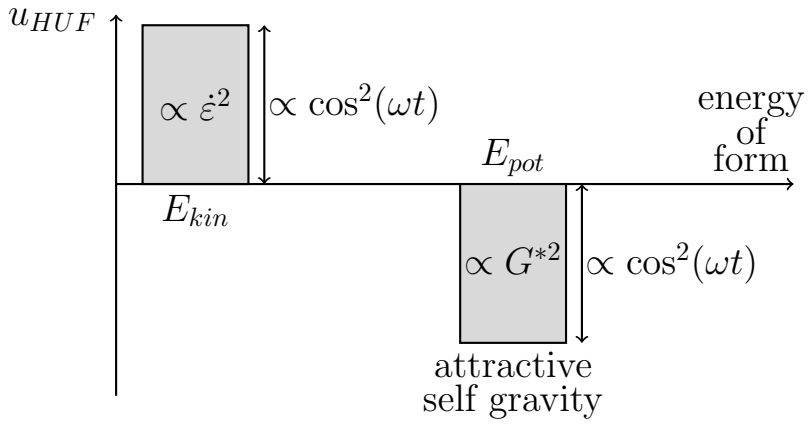

Figure 5.3: Energy density of a RGW in the HUF. The signs are essentially different from those of an electromagnetic wave, so that the usual representation by harmonic oscillators (Ballentine (1998)) is excluded here.

(4) So RGWs can permanently form vacuum.

(5) As another consequence, the constant relative volume $\varepsilon = \frac{\delta V}{dV}$ *of a RGW is a time integral mathematically, and accordingly it represents the accumulated formed vacuum, physically.*

(6) The energy density of that RGW can be expressed as a function of the field or as a function of the rate $\dot{\varepsilon}$*, see Eq. (5.38):*

$$\rho_{stationary}(\dot{\varepsilon}) = \frac{\dot{\varepsilon}^2}{8\pi \cdot G} \tag{5.41}$$

5.6 Energy of RGWs

In this section we analyze the energy of the waves (Eq. 5.13). They are solutions of the DEQ (5.6). In order to obtain the energy density, we replace the potential by the field in that DEQ, and we multiply by $\frac{c^2}{8\pi \cdot G}$. So we get:

$$\boxed{\frac{c^2}{8\pi \cdot G} \cdot \dot{\varepsilon}_j^2 - \frac{G_j^{*2}}{8\pi \cdot G} = 0} \tag{5.42}$$

Alternative derivation: This Eq. can also by derived by multiplying the RGS and its Eq. $RGS = 0$ by $\frac{c^2}{8\pi \cdot G}$.

Here we realize that the subtrahend in the above Eq. is similar to the energy density of the field. Accordingly, the above term represents the energy density of the wave. We derived the above energy term of the wave on the basis of the HUF. We denote that density by $u_{RGW,HUF}$:

$$\boxed{u_{RGW,HUF}(\varepsilon_j, G_j^*) = \frac{c^2}{8\pi \cdot G} \cdot \dot{\varepsilon}_j^2 - \frac{G_j^{*2}}{8\pi \cdot G} = 0} \tag{5.43}$$

We summarize our first derived result:

Proposition 11 Energy of RGWs:

In the HUF, the energy density of the RGW $u_{RGW,HUF}$ is a function of the rate and of the field with the following properties, see Eq. (5.43) and Fig. (5.3):

$$\frac{c^2}{8\pi \cdot G} \cdot \dot{\varepsilon}_j^2 - \frac{G_j^{*2}}{8\pi \cdot G} = 0 \tag{5.44}$$

(1) That energy density is proportional to the RGS. So it is a HZLS, thus it is highly invariant. Moreover that energy density of a wave is a rate gravity energy density, RGED.

(2) That energy density is **zero**. *So in the HUF, the formation of RGWs without any input of energy or mass* **fulfills the law of conservation of energy**.

In order to understand the properties of the RGW in more detail, we analyze the above energy density term in the following subsections.

5.6.1 Field energy of the RGW

By comparison with the energy density of the gravitational field, we identify the energy density of the field of the RGW:

$$\boxed{|u_{RGW,field}(G_j^*)| = \frac{G_j^{*2}}{8\pi \cdot G}} \tag{5.45}$$

5.6.2 Self gravity energy density SGE of the RGW

In the HUF, the energy density contains a subtrahend. It describes the energy density of the gravitation of the RGW with itself, we denote by the **self gravity energy density, SGE**. Its absolute value is equal to $|u_{RGW,field}(G_j^*)|$. In the HUF, the RGW interacts with itself only, and the interaction is attractive, correspondingly the sign of that energy is negative. Accordingly, we denote that energy density by $u_{RGW,SGE}(G_j^*)$:

$$\boxed{u_{RGW,SGE}(G_j^*) = -\frac{G_j^{*2}}{8\pi \cdot G}} \tag{5.46}$$

In the HUF, this is equal to the potential energy density. Accordingly, we denote it by $u_{RGW,HUF,pot}(G_j^*)$:

$$\boxed{u_{RGW,HUF,pot}(G_j^*) = u_{RGW,SGE}(G_j^*) = -\frac{G_j^{*2}}{8\pi \cdot G}} \tag{5.47}$$

We summarize our third derived result:

Proposition 12 Self gravitation:

The RGW exhibits a **gravitational self interaction** *with the following properties:*

(1) The self interaction is **attractive**, *so its energy is negative.*

(2) The self interaction is **constituted by the gravitational field**, *so its energy density $u_{RGW,SGE}$ is equal to $-|u_{RGW,field}|$, see Eq. (5.46).*

(3) In a HUF, the RGW interacts with itself only, hence the density of its **potential energy** *is equal to its energy density of self interaction (Eq. 5.47).*

5.6.3 Kinetic energy of the RGW

As the energy of the RGW is zero in the HUF, and as the energy of the RGW is the sum of its kinetic and its potential energy, and its kinetic energy density $u_{RGW,HUF,kin}$ is equal to $-u_{RGW,HUF,pot}$. Moreover, the kinetic energy is a function of a time derivative. Hence, by comparison with Eq. (5.43) we get:

$$\boxed{u_{RGW,HUF,kin}(\varepsilon_j) = \frac{c^2}{8\pi \cdot G} \cdot \dot{\varepsilon}_j^2} \tag{5.48}$$

We summarize our result:

Proposition 13 Kinetic energy of the RGW:

The RGW includes a permanent periodic variation of the rate $\dot{\varepsilon}_j$. The corresponding kinetic energy density $u_{RGW,HUF,kin}$ is presented in Eq. (5.48).

Corollary 4 Transport of energies by the RGWs:

A propagating wave describes the transport of its energy density. Hence the propagation of the RGWs explains the propagation

(1) of the energy density of the **gravitational field** $|u_{RGW,field}|$,

(2) of the **gravitational field** *(as a consequence),*

(3) of the rate $\dot{\varepsilon}_j$ of formed vacuum,

(4) of the formed vacuum,

(5) of the energy density of the formed vacuum, which is the dark energy.

5.6.4 Polychromatic RGWs

The wave functions in Eqs. (5.13, 5.18) represent monochromatic waves. More generally, a RGW is a linear superposition of such waves with circular frequencies ω_μ and wave number k_μ.

Orthonormal basis: It is convenient to apply a normalization factors ν. With these we use functions, representing plane waves propagating in the direction $\vec{k}$

$$b_\mu = \nu_b \cdot \exp(i \cdot \omega_\mu \cdot t) \text{ and} \tag{5.49}$$

$$f_\mu = \nu_f \cdot \exp(-i \cdot \vec{k}_\mu \cdot \vec{x}) \tag{5.50}$$

So we obtain a set of orthonormal basis functions. Hereby we denote the complex conjugate by a star (for instance, f^*_μ is the complex conjugate of f_μ):

$$\int f_\mu \cdot f^*_{\mu'} \, d^3x = \delta_{\mu,\mu'} \tag{5.51}$$

Representation by orthonormal basis: In that basis, an RGW has amplitudes $\hat{\varepsilon}_\mu$ of the monochromatic waves. So we get:

$$\varepsilon(\vec{x}, t) = \Sigma_\mu \hat{\varepsilon}_\mu \cdot b_\mu(t) \cdot f_\mu(\vec{x}) + \varepsilon_{\mu,const.} \tag{5.52}$$

Similarly, the potentials can be expressed with amplitudes $\hat{\phi}_\mu$:

$$\phi(\vec{x}, t) = \Sigma_\mu \hat{\phi}_\mu \cdot b_\mu(t) \cdot f_\mu(\vec{x}) + \phi_{\mu,const.} \tag{5.53}$$

We apply this representation to the energy density in the HUF in Eq. (5.43). Thereby the squares represent absolute values:

$$u_{RGW,HUF}(\varepsilon, \phi) = \frac{c^2}{8\pi \cdot G} \cdot |\dot{\varepsilon}^2| - \frac{|(\partial_{\vec{x}}\phi)^2|}{8\pi \cdot G} \tag{5.54}$$

Polarization: The RGW can oscillate in various directions represented by the tensors developed in section (2.4) In order to provide relatively short formulas, we include these tensors in

the amplitude. So the index μ summarizes the indices of the basis function f_μ, of the polarization q, and of the tensor i and j. So we get:

$$\hat{\varepsilon}_\mu = \hat{\varepsilon}_{\mu,\text{amplitude of } f_\mu} \cdot \hat{\varepsilon}_{q,ij} \tag{5.55}$$

Correspondingly, the indices inherent to μ must be explicated, whenever they become essential.

Separation of modes μ: Next we separate the modes μ inherent to $|\dot{\varepsilon}^2|$. For it we evaluate $|\dot{\varepsilon}^2|$ by using Eq. (5.52). Moreover, we replace the absolute values of a square z^2 of a complex number z by the product $z \cdot z^*$:

$$|\dot{\varepsilon}^2| = \Sigma_{\mu,\mu'} \hat{\varepsilon}_\mu \hat{\varepsilon}_{\mu'} \cdot \partial_t b_\mu \partial_t b^*_{\mu'} \cdot f_\mu f^*_{\mu'} = \Sigma_{\mu,\mu'} \omega_\mu \omega_{\mu'} \hat{\varepsilon}_\mu \hat{\varepsilon}_{\mu'} \cdot b_\mu b^*_{\mu'} \cdot f_\mu f^*_{\mu'} \tag{5.56}$$

Analogously we evaluate $|(\partial_{\vec{x}}\phi)^2|$:

$$|(\partial_{\vec{x}}\phi)^2| = \Sigma_{\mu,\mu'} \hat{\phi}_\mu \hat{\phi}_{\mu'} \cdot b_\mu b^*_{\mu'} \cdot \partial_{\vec{x}} f_\mu \partial_{\vec{x}} f^*_{\mu'} \tag{5.57}$$

We evaluate the derivative, and we apply $\hat{\phi}_\mu = \hat{\varepsilon}_\mu \cdot c^2$ (Eq. 5.18):

$$|(\partial_{\vec{x}}\phi)^2| = \Sigma_{\mu,\mu'} \vec{k}_\mu \vec{k}_{\mu'} \hat{\varepsilon}_\mu \hat{\varepsilon}_{\mu'} \cdot c^4 \cdot b_\mu b^*_{\mu'} \cdot f_\mu f^*_{\mu'} \tag{5.58}$$

Next we insert Eqs. (5.57) and (5.58) into Eq. (5.54):

$$u_{RGW,HUF}(\varepsilon,\phi) = \Sigma_{\mu,\mu'} \hat{\varepsilon}_\mu \hat{\varepsilon}_{\mu'} \cdot b_\mu b^*_{\mu'} \cdot f_\mu f^*_{\mu'} \cdot \left(\frac{c^2 \omega_\mu \omega_{\mu'}}{8\pi G} - \frac{c^4 \vec{k}_\mu \vec{k}_{\mu'}}{8\pi G} \right) \tag{5.59}$$

In order to derive the energy, we integrate over the space:

$$E_{RGW,HUF} = \int u_{RGW,HUF}\, d^3x \tag{5.60}$$

5.6.5 Modes ranging up to R_{lh}

In this part we integrate the modes ranging from zero up to the light horizon. We call the corresponding energy $E_{RGW,HUF,LH}$.

Thereby the light horizon is a function of time during the expansion since the Big Bang, and the essential light horizon has been elaborated in (Carmesin (2018c), Carmesin (2018b), Carmesin (2019b), Carmesin (2019a)). We apply that range to Eq. (5.60):

$$E_{RGW,HUF,LH} = 4\pi \cdot \int_0^{R_{lh}} r^2 \cdot u_{RGW,HUF}\, dr \tag{5.61}$$

We insert Eq. (5.59), and we evaluate the integral (see Eq. 5.51) as well as the $\delta_{\mu,\mu'}$. So we get:

$$E_{RGW,HUF,LH} = \frac{1}{2} \cdot \Sigma_\mu \hat{\varepsilon}_\mu \hat{\varepsilon}_\mu \cdot b_\mu b_\mu^* \cdot \frac{c^2}{G} \cdot \left(\omega_\mu^2 - c^2 \vec{k}_\mu^2\right) \tag{5.62}$$

Generalized coordinates of RGWs $Q_\mu(t)$: We introduce a **coordinate** Q_μ and its **momentum** P_μ with:

$$\boxed{Q_\mu = \hat{\varepsilon}_\mu \cdot b_\mu \cdot \frac{c}{\sqrt{G}} \text{ and } P_\mu = i\frac{dQ_\mu}{dt} \text{ and } P_\mu^* = i\frac{dQ_\mu^*}{dt}} \tag{5.63}$$

We determine derivatives as follows:

$$P_\mu P_\mu^* = -\frac{dQ_\mu}{dt}\frac{dQ_\mu^*}{dt} = -\omega_\mu^2 Q_\mu Q_\mu^* \tag{5.64}$$

Moreover we utilize $\vec{k}_\mu^2 \cdot c^2 = \omega_\mu^2$:

$$P_\mu P_\mu^* = -\vec{k}_\mu^2 \cdot c^2 Q_\mu Q_\mu^* \tag{5.65}$$

We apply Eqs. (5.64) and (5.65) to Eq. (5.62):

$$\boxed{E_{RGW,HUF,LH} = \frac{1}{2} \cdot \Sigma_\mu \left(Q_\mu Q_\mu^* \cdot \omega_\mu^2 - P_\mu P_\mu^*\right)} \tag{5.66}$$

This energy density is expressed in terms of a momentum four-vector with $P_\mu P_\mu^* = \Sigma_{j=1}^3 P_{\mu,j} P_{\mu,j}^*$:

$$p_\mu^i = \begin{pmatrix} Q_\mu \cdot \omega_\mu \\ P_{\mu,1} \\ P_{\mu,2} \\ P_{\mu,3} \end{pmatrix} \text{ With it we get:} \tag{5.67}$$

$$\boxed{E_{RGW,HUF,LH} = \frac{1}{2} \cdot \Sigma_{\mu,i=0}^{i=3} \left(p_{\mu,i}^{*} \eta_{j}^{i} p_{\mu}^{j} \right)} \tag{5.68}$$

Theorem 18 Four-momentum and modes of RGWs:

In a HUF, the energy of RGWs $E_{RGW,HUF,LH}$ is as follows:

(1) The $E_{RGW,HUF,LH}$ is a sum of energies of modes:

$$E_{RGW,HUF,LH} = \frac{1}{2} \cdot \Sigma_{\mu} \hat{\varepsilon}_{\mu} \hat{\varepsilon}_{\mu} \cdot b_{\mu} b_{\mu}^{*} \cdot \frac{c^2}{G} \cdot \left(\omega_{\mu}^{2} - c^2 \vec{k}_{\mu}^{2} \right) \tag{5.69}$$

That energy function is a HZLS, so it is highly invariant. It is a relativistic square of the following four-vector:

$$\begin{pmatrix} \omega_{\mu} \\ k_{\mu,1} \cdot c \\ k_{\mu,2} \cdot c \\ k_{\mu,3} \cdot c \end{pmatrix} \tag{5.70}$$

(2) The $E_{RGW,HUF,LH}$ is a sum of energies of generalized coordinates and momenta, see Eqs. (5.63) to (5.66):

$$Q_{\mu} = \hat{\varepsilon}_{\mu} \cdot b_{\mu} \cdot \frac{c}{\sqrt{G}} \quad and \quad P_{\mu} = i \frac{dQ_{\mu}}{dt} \quad and \quad P_{\mu}^{*} = i \frac{dQ_{\mu}^{*}}{dt} \tag{5.71}$$

$$E_{RGW,HUF,LH} = \frac{1}{2} \cdot \Sigma_{\mu} \left(Q_{\mu} Q_{\mu}^{*} \cdot \omega_{\mu}^{2} - P_{\mu} P_{\mu}^{*} \right) \tag{5.72}$$

That energy function is a HZLS, so it is highly invariant.

(3) That energy function is a sum of squares of a HZFV, the four-momentum p_{μ}^{j}, see Eqs. (5.67) and (5.68):

$$p_{\mu}^{i} = \begin{pmatrix} Q_{\mu} \cdot \omega_{\mu} \\ P_{\mu,1} \\ P_{\mu,2} \\ P_{\mu,3} \end{pmatrix} \tag{5.73}$$

$$E_{RGW,HUF,LH} = \frac{1}{2} \cdot \Sigma_{\mu,i=0}^{i=3} \left(p_{\mu,i}^{*} \eta_{j}^{i} p_{\mu}^{j} \right) \tag{5.74}$$

(4) An RGW can also be expressed in terms of a spacetime scalar, STS or as a spacetime tensor, STT (see definition 10).

Chapter 6

Quantization of Spacetime

In this chapter we quantize the RGWs in the form of the modes that are expressed by the four-momentum of modes:

$$p_{\mu}^{i} = \begin{pmatrix} Q_{\mu} \cdot \omega_{\mu} \\ P_{\mu,1} \\ P_{\mu,2} \\ P_{\mu,3} \end{pmatrix} \tag{6.1}$$

6.1 Problems of spacetime: quanta

1. How are the RGWs **quantized in an invariant manner**?
2. What are the **quanta of the RGWs**?
3. Is the **GRT complete with respect to the expansion of space**?
4. How can we **derive the density of dark energy in a precise manner**?
5. What **universal constants are inherent to the density of the dark energy**?

6.2 Quantization

In this section we elaborate the quantization of the RGWs. For it we start with the Hamiltonian as a function of the generalized

coordinates and momenta (Eq. 5.66):

$$E_{RGW,HUF,LH} = \frac{1}{2} \cdot \Sigma_\mu Q_\mu Q^*_\mu \cdot \omega^2_\mu - P^*_\mu P_\mu \tag{6.2}$$

For it we introduce operators for the coordinate $\hat{Q}_\mu$ and momentum $\hat{P}_\mu$. So we get:

$$\hat{H}_\mu = \frac{1}{2} \cdot \hat{Q}_\mu \hat{Q^*}_\mu \cdot \omega^2_\mu - \hat{P}_\mu \hat{P^*}_\mu \tag{6.3}$$

Hereby the quantization is given by the commutator (Heisenberg (1927) or (Ballentine, 1998, p.151) or (Grawert, 1977, p. 37)):

$$[\hat{Q}_\mu, \hat{P}_{\mu'}] = i \cdot \hbar \cdot \delta_{\mu,\mu'} \tag{6.4}$$

Linear transformation: In order to derive the so-called ladder operators (for instance (Ballentine, 1998, p. 152)), we apply a linear transformation to operators $\hat{a}^+_\mu$ and $\hat{a}_\mu$ as follows:

$$\hat{Q}_\mu \cdot \omega_\mu = \alpha_\mu \left(\hat{a}^+_\mu + \hat{a}_\mu\right) \tag{6.5}$$

$$\hat{P}_\mu = i \cdot \alpha_\mu \left(\hat{a}^+_\mu - \hat{a}_\mu\right) \tag{6.6}$$

Hereby the parameter α_μ will be determined by the commutation relation in Eq. (6.4). Thereby the ladder operators should obey the following commutation relation:

$$[\hat{a}_{\mu'}, \hat{a}^+_\mu] = \delta_{\mu,\mu'} \tag{6.7}$$

In order to test the Ansatz and to determine α_μ, we insert Eqs. (6.5, 6.6) into Eq. (6.4):

$$[\hat{Q}_\mu, \hat{P}_{\mu'}] = \frac{2i\alpha^2_\mu}{\omega_\mu} \cdot [\hat{a}_\mu, \hat{a}^+_{\mu'}] = \frac{2i\alpha^2_\mu}{\omega_\mu} \cdot \delta_{\mu,\mu'} \tag{6.8}$$

We compare this term with Eq. (6.4). So we get:

$$\frac{2i\alpha^2_\mu}{\omega_\mu} = i \cdot \hbar \;\text{ or }\; \alpha_\mu = \sqrt{\hbar\omega_\mu/2} \tag{6.9}$$

Altogether, the transformation is as follows:

$$\hat{Q}_\mu \cdot \omega_\mu = \sqrt{\hbar\omega_\mu/2}\left(\hat{a}_\mu^+ + \hat{a}_\mu\right) \tag{6.10}$$

$$-i\hat{P}_\mu = \sqrt{\hbar\omega_\mu/2}\left(\hat{a}_\mu^+ - \hat{a}_\mu\right) \tag{6.11}$$

Inverse transformation: From the above Eqs., the inverse transformation is derived by solving for $\hat{a}_\mu$ and $\hat{a}_\mu^+$. As a result we get:

$$\hat{a}_\mu^+ = (\hat{Q}_\mu \cdot \omega_\mu - i\hat{P}_\mu)/\sqrt{2\hbar\omega_\mu} \tag{6.12}$$

$$\hat{a}_\mu = (\hat{Q}_\mu \cdot \omega_\mu + i\hat{P}_\mu)/\sqrt{2\hbar\omega_\mu} \tag{6.13}$$

Energy operator: We insert the coordinate $\hat{Q}_\mu$ and momentum $\hat{P}_\mu$ operators (Eqs. 6.10, 6.11) into Eq. (6.3). For it we derive the products

$$\hat{Q}_\mu \hat{Q^*}_\mu \cdot \omega_\mu^2 = \frac{\hbar\omega_\mu}{2} \cdot \left(\hat{a}_\mu^+\hat{a}_\mu^+ + \hat{a}_\mu\hat{a}_\mu^+ + \hat{a}_\mu^+\hat{a}_\mu + \hat{a}_\mu\hat{a}_\mu\right) \tag{6.14}$$

and:

$$\hat{P}_\mu \hat{P^*}_\mu = \frac{\hbar\omega_\mu}{2} \cdot \left(\hat{a}_\mu^+\hat{a}_\mu^+ - \hat{a}_\mu\hat{a}_\mu^+ - \hat{a}_\mu^+\hat{a}_\mu + \hat{a}_\mu\hat{a}_\mu\right) \tag{6.15}$$

The energy operator is the difference of these products:

$$\hat{H}_\mu = \frac{1}{2} \cdot \hbar\omega_\mu \cdot \left(\hat{a}_\mu \cdot \hat{a}_\mu^+ + \hat{a}_\mu^+ \cdot \hat{a}_\mu\right) \tag{6.16}$$

We apply the commutator. So we get:

$$\boxed{\hat{H}_\mu = \hbar\omega_\mu \cdot \left(\hat{a}_\mu^+ \cdot \hat{a}_\mu + 1/2\right)} \tag{6.17}$$

6.3 RGW number states

In this section we analyze the spectrum of the Hamiltonian $\hat{H}_\mu$. For it we name the operator $\hat{a}_\mu^+\hat{a}_\mu$ by **number operator**:

$$\hat{N}_\mu = \hat{a}_\mu^+\hat{a}_\mu \tag{6.18}$$

Moreover we call its normalized Eigenstates $|n_\mu\rangle$ and the Eigenvalues $|n_\mu\rangle$:

$$\hat{N}_\mu \cdot |n_\mu\rangle = n_\mu \cdot |n_\mu\rangle \tag{6.19}$$

Eigenstates of the number operator: We apply $\hat{N}_\mu$ to $\hat{a}_\mu \cdot |n_\mu\rangle$, and we use the commutator. So we get:

$$\hat{N}_\mu \cdot \hat{a}_\mu \cdot |n_\mu\rangle = \hat{a}_\mu \cdot (n_\mu - 1) \cdot |n_\mu\rangle = (n_\mu - 1) \cdot \hat{a}_\mu \cdot |n_\mu\rangle \tag{6.20}$$

This Eq. shows that $\hat{a}_\mu \cdot |n_\mu\rangle$ is an Eigenstate to the Eigenvalue $n_\mu - 1$, this confirms the name lowering operator.

Similarly we apply $\hat{N}_\mu$ to $\hat{a}^+_\mu \cdot |n_\mu\rangle$, and we utilize the commutator. So we obtain:

$$\hat{N}_\mu \cdot \hat{a}^+_\mu \cdot |n_\mu\rangle = \hat{a}^+_\mu \cdot (n_\mu + 1) \cdot |n_\mu\rangle = (n_\mu + 1) \cdot \hat{a}^+_\mu \cdot |n_\mu\rangle \tag{6.21}$$

This Eq. shows that $\hat{a}^+_\mu \cdot |n_\mu\rangle$ is an Eigenstate to the Eigenvalue $n_\mu + 1$, this confirms the name raising operator.

Matrix elements of the ladder operators: In order to derive the matrix elements of $\hat{a}^+_\mu$, we analyze the square of $\hat{a}^+_\mu \cdot |n_\mu\rangle$:

$$(\hat{a}^+_\mu |n_\mu\rangle)^2 = \langle n_\mu | \hat{a}_\mu \hat{a}^+_\mu | n_\mu \rangle \tag{6.22}$$

Here we identify the number operator:

$$(\hat{a}^+_\mu |n_\mu\rangle)^2 = \langle n_\mu | \hat{N}_\mu + 1 | n_\mu \rangle = (n_\mu + 1)\langle n_\mu | n_\mu \rangle = n_\mu + 1 \tag{6.23}$$

So the corresponding matrix element is $\sqrt{n_\mu + 1}$.

Similarly the matrix element $\sqrt{n_\mu}$ of $\hat{a}_\mu$ can be derived. We summarize the matrix elements of $\hat{a}^+_\mu$ as follows:

$$\boxed{\langle n'_\mu | \hat{a}^+_\mu | n_\mu \rangle = \sqrt{n_\mu + 1} \cdot \delta_{n'_\mu, n_\mu + 1}} \tag{6.24}$$

Accordingly, the matrix elements of $\hat{a}_\mu$ are presented as follows:

$$\boxed{\langle n'_\mu | \hat{a}_\mu | n_\mu \rangle = \sqrt{n_\mu} \cdot \delta_{n'_\mu, n_\mu - 1} \quad \text{for} \quad n_\mu > 0} \tag{6.25}$$

Spectrum: In order to derive the full spectrum of the number operator, we show that the lowering of states ends at the state $|n_\mu\rangle = 0$:

$$\hat{a}_\mu|1\rangle = \sqrt{1}|0\rangle \text{ and } \hat{a}_\mu|0\rangle = \sqrt{0}|-1\rangle = 0 \tag{6.26}$$

Starting at this state, the raising operator can successively create the states with all positive natural numbers:

$$\boxed{n_\mu \in \{0, 1, 2, 3, ...\}} \tag{6.27}$$

ZPE of a mode μ: The spectrum of the number operator has the smallest value zero at the state $|0\rangle$. However, the eigenvalue of the energy of the state $|0\rangle$ is $\hbar\omega_\mu/2$, it can be derived as follows:

$$\langle 0|\hat{H}_\mu|0\rangle = \hbar\omega_\mu \cdot (\langle 0|\hat{N}_\mu|0\rangle + \langle 0|1/2|0\rangle) = \hbar\omega_\mu \cdot (0 + 1/2) \tag{6.28}$$

This energy $\hbar\omega_\mu/2$ is the **zero - point energy, ZPE** of the RGW at the mode μ:

$$\boxed{ZPE_\mu = \hbar\omega_\mu \cdot 1/2} \tag{6.29}$$

Theorem 19 Quantization of RGWs:

The RGWs are quantized in terms of the modes in theorem (18) as follows:

(1) The generalized coordinates are quantized by application of the usual commutation rule:

$$[\hat{Q}_\mu, \hat{P}_{\mu'}] = i \cdot \hbar \cdot \delta_{\mu,\mu'} \tag{6.30}$$

This establishes a quantization of a HUF zero four-vector $HZFV$, so the corresponding HUF zero Lorentz scalar $HZLS$ represents a Lorentz invariant quantization of the RGWs.

(2) The generalized coordinates are transformed to ladder operators as follows:

$$\hat{a}^+_\mu = (\hat{Q}_\mu \cdot \omega_\mu - i\hat{P}_\mu)/\sqrt{2\hbar\omega_\mu} \tag{6.31}$$

$$\hat{a}_\mu = (\hat{Q}_\mu \cdot \omega_\mu + i\hat{P}_\mu)/\sqrt{2\hbar\omega_\mu} \tag{6.32}$$

(3) As a consequence, the ladder operators obey the following commutation rule of bosons:

$$[\hat{a}_{\mu'}, \hat{a}^+_\mu] = \delta_{\mu,\mu'} \tag{6.33}$$

(4) Hence there is the following number operator

$$\hat{N}_\mu = \hat{a}^+_\mu \hat{a}_\mu \tag{6.34}$$

and its eigenstates are the number states $|n_\mu\rangle$ with the following eigenvalues:

$$n_\mu \in \{0, 1, 2, 3, ...\} \tag{6.35}$$

(5) So the energy operator is expressed by the number operator:

$$\hat{H}_\mu = \hbar\omega_\mu \cdot \left(\hat{a}^+_\mu \cdot \hat{a}_\mu + 1/2\right) = \hbar\omega_\mu \cdot \left(\hat{N}_\mu + 1/2\right) \tag{6.36}$$

(6) Thus the ladder operators raise or lower the numbers:

$$\langle n'_\mu | \hat{a}^+_\mu | n_\mu \rangle = \sqrt{n_\mu + 1} \cdot \delta_{n'_\mu, n_\mu + 1} \tag{6.37}$$

Accordingly, the matrix elements of $\hat{a}_\mu$ are presented as follows:

$$\langle n'_\mu | \hat{a}_\mu | n_\mu \rangle = \sqrt{n_\mu} \cdot \delta_{n'_\mu, n_\mu - 1} \;\; for \;\; n_\mu > 0 \tag{6.38}$$

(7) As a particularly interesting consequence, the zero-point energy, ZPE, is as follows:

$$ZPE_\mu = \hbar\omega_\mu \cdot 1/2 \tag{6.39}$$

(8) Inherent to the quantized RGWs, there is only one restriction of the wavelengths: the light horizon inherent to the modes of the RGWs. So the quantized RGWs can exhibit a continuous spectrum.

(9) A quantized RGW can also be expressed in terms of a **quantized spacetime scalar, STS** *or as a* **quantized spacetime tensor, STT** *(Def. 10). This may be denoted as a* **quantum of spacetime** *or as a* **quantum of vacuum**.

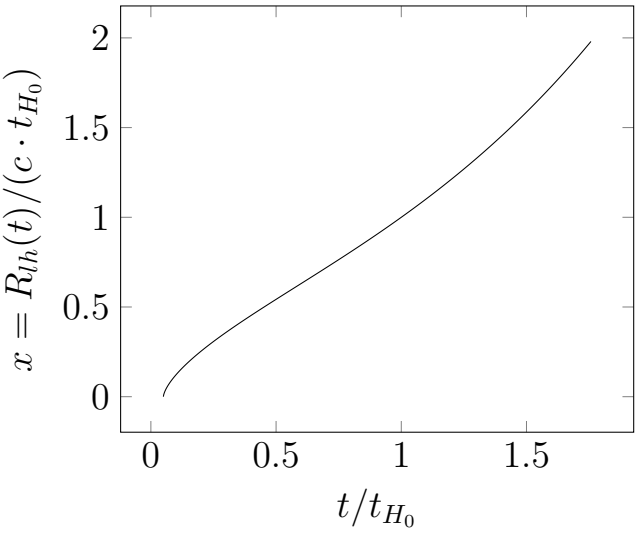

Figure 6.1: Scaled radius $x(t)$ (Eq. 6.41).

6.4 Density limit ρ_{limit} of expansion of space

In physics, there is an upper limit of the density ρ_{limit}. It is one half of the Planck density $\rho_{limit} = \bar{\rho}_P/2$ (Sect. 3.1). As a consequence, the expansion of space discovered by Hubble (Hubble (1929)) and described by the FLE (Friedmann (1922), Lemaitre (1927)) has a limitation in the early universe. In this section we derive that limitation.

6.4.1 Light horizon $R_{lh}(t)$ according to FLE

Our current light horizon R_{lh} describes a ball enclosing a volume. The corresponding radius $R_{lh}(t)$ at former times can be calculated according to the GRT. For it we may apply the FLE:

$$H^2 = \frac{\dot{R}_{lh}^2(t)}{R_{lh}^2(t)} = \frac{8\pi G}{3} \cdot \rho \tag{6.40}$$

Using the Hubble time $t_{H_0} = 1/H_0$, we derive the solution of the above DEQ (see Carmesin (2019b) or Gott et al. (2005)):

$$\int_{x_1}^{x_2} \frac{x \cdot dx}{\sqrt{\Omega_r + \Omega_m \cdot x + \Omega_\Lambda \cdot x^4}} = \frac{t_2 - t_1}{t_{H_0}} \quad \text{with} \quad x = \frac{R_{lh}}{c \cdot t_{H_0}} \tag{6.41}$$

The density parameters in the above Eq. are shown in Sect (9.2). The resulting time evolution is shown in Fig. (6.1).

6.4.2 Density of radiation $\rho_r(t)$

In this section we derive the time evolution of the density of radiation $\rho_r(t)$. For it we express that density as a function of the light horizon $R_{lh}(t)$: The volume of the ball enclosed by $R_{lh}(t)$ is proportional to $R_{lh}^3(t)$. The dynamic mass of the radiation is proportional to $1/R_{lh}(t)$. The density of radiation in the ball limited by $R_{lh}(t)$ is equal to the dynamic mass of radiation divided by the volume, hence it is proportional to $1/R_{lh}^4(t)$. We use the actual values $R_{lh}(t_0)$ and $\rho_r(t_0)$ as a particular reference. So we derive:

$$\frac{\rho_r(t)}{\rho_r(t_0)} = \frac{R_{lh}^4(t_0)}{R_{lh}^4(t)} \tag{6.42}$$

We solve for $\rho_r(t)$:

$$\rho_r(t) = \rho_r(t_0) \cdot \frac{R_{lh}^4(t_0)}{R_{lh}^4(t)} \tag{6.43}$$

6.4.3 Radius $R_{lh,limit}$ corresponding to ρ_{limit}

In this section we derive the radius $R_{lh,limit}$ at which the density of radiation $\rho_r(t)$ would take the upper limit ρ_{limit}. For it we apply the following fact: In the early universe, the density was essentially equal to the density of radiation. Hence the density of radiation is equal to ρ_{limit} at the density ρ_{limit}. Thus we

insert the pair $(R_{lh,limit}, \rho_{limit})$ into Eq. (6.43). So we get:

$$\bar{\rho}_P/2 = \rho_{limit} = \rho_r(t_0) \cdot \frac{R_{lh}^4(t_0)}{R_{lh,limit}^4} \tag{6.44}$$

We solve for $R_{lh,limit}$:

$$R_{lh,limit} = R_{lh}(t_0) \cdot \left(\frac{\rho_r(t_0)}{\bar{\rho}_P/2} \right)^{1/4} \tag{6.45}$$

We insert the observed values (Sect. 9.2):

$$R_{lh,limit} = 4.14 \cdot 10^{26}\,\mathrm{m} \cdot \left(\frac{8.023 \cdot 10^{-31}\ \frac{\mathrm{kg}}{\mathrm{m}^3}}{6.1535 \cdot 10^{95}\ \frac{\mathrm{kg}}{\mathrm{m}^3}} \right)^{1/4} \tag{6.46}$$

We evaluate the above term:

$$R_{lh,limit} = 0.014\,\mathrm{mm} \tag{6.47}$$

6.4.4 Physically observable lengths

The physically observable lengths range from the Planck length towards the light horizon:

$$R_{observable} \in [L_P, R_{lh}(t_0)] = I_{observable} \tag{6.48}$$

The physically observable lengths are elements of the above interval $I_{observable}$. That interval $I_{observable}$ corresponds to a single measurement of a length, whereas a multiple measurement of the same length might provide a more precise result than L_P as a consequence of averaging, if the objects constituting that length do not exhibit a time evolution. However, if a length exhibits a time evolution, then multiple measurements combined with averaging does not improve the precision of the result, in general (Carmesin (2021)). Correspondingly, the lengths in the interval $I_{observable}$ are **physically well defined lengths**, as they can be observed even in a single measurement. We insert the observed values (Sect. 9.2):

$$R_{observable} \in [1.616 \cdot 10^{-35}\,\mathrm{m}, 4.14 \cdot 10^{26}\,\mathrm{m}] = I_{observable} \tag{6.49}$$

Thus the expansion of space described by the FLE or by the GRT is very incomplete, as it describes the time evolution of the light horizon ranging from $R_{lh}(t_0)$ towards $R_{lh,limit}$ only. Hence the enlargement of the light horizon by a factor $Z_{L_P \to R_{lh,limit}}$ is neither described by the FLE nor by the GRT. That factor is equal to the fraction of $R_{lh,limit}$ and L_P:

$$Z_{L_P \to R_{lh,limit}} = \frac{R_{lh,limit}}{L_P} = \frac{1.4 \cdot 10^{-5}\,\mathrm{m}}{1.616 \cdot 10^{-35}\,\mathrm{m}} = 8.66 \cdot 10^{29} \quad (6.50)$$

We summarize our results:

Definition 11 Physically defined lengths:

A length L is physically well defined, if it can be measured by a single measurement, whereby the length L is larger than its standard deviation ΔL of that measurement.

Theorem 20 Incompleteness of the GRT:

The GRT is incomplete with respect of the expansion of the universe since the Big Bang for the following reasons:

(1) The physically defined lengths range from $L_P = 1.616 \cdot 10^{-35}\,\mathrm{m}$ towards $R_{lh}(t_0)$.

(2) The lengths described by the expansion of space according to the FLE or to the GRT range from $R_{lh,limit} = 1.4 \cdot 10^{-5}\,\mathrm{m}$ towards $R_{lh}(t_0)$.

(3) So the expansion of space according to the FLE or to the GRT does not describe the range from $R_{lh,limit} = 1.4 \cdot 10^{-5}\,\mathrm{m}$ towards $L_P = 1.616 \cdot 10^{-35}\,\mathrm{m}$, corresponding to the enlargement factor $Z_{L_P \to R_{lh,limit}} = 8.66 \cdot 10^{29}$. As this factor is essential, the GRT is essentially incomplete with respect to the description of the expansion of the universe since the Big Bang.

6.5 Dark energy: observed values

In this section we summarize results of observations of the dark energy. Einstein (1917) introduced the concept of a constant entity in space and named it **cosmological constant** Λ. Zeldovich (1968) related that constant to a density inherent to the vacuum ρ_Λ. Perlmutter et al. (1998) and Riess et al. (2000) discovered such a density, it is called the dark energy.

6.5.1 Density $\rho_{\Lambda,CMB}$

The density ρ_Λ is the product of the density parameter of the dark energy, Ω_Λ, and the critical density at the actual time t_0, ρ_{cr,t_0} (see for instance Tanabashi et al. (2018)):

$$\rho_\Lambda = \rho_{cr,t_0} \cdot \Omega_\Lambda \tag{6.51}$$

The actual critical density can be derived from the Hubble constant H_0:

$$\rho_{cr,t_0} = \frac{3 \cdot H_0^2}{8\pi \cdot G} \tag{6.52}$$

The CMB has been observed very accurately by the Planck satellite, and the raw data have been evaluated by an elaborated procedure. In particular, results have been presented for various modes of the measured radiation and for averages including data obtained by using gravitational lensing (or BAO spectra) additionally (Collaboration (2020)). Here we use two such evaluations: The most direct evaluation utilizes only the **temperature power spectra, TT**. Collaboration (2020) emphasized a so-called **baseline** evaluation including TT-, TE-, and EE-spectra of the CMB as well as gravitational lensing. The observations of the Hubble constant are as follows:

$$H_{0,CMB} = \begin{cases} 66.88 \pm 0.92 \, \frac{\text{km}}{\text{Mpc·s}} & \text{TT} \\ 67.39 \pm 0.54 \, \frac{\text{km}}{\text{Mpc·s}} & \text{baseline} \end{cases} \tag{6.53}$$

The density parameter observations are as follows:

$$\Omega_{\Lambda,CMB} = \begin{cases} 0.679 \pm 0.013 & \text{TT} \\ 0.6858 \pm 0.0074 & \text{baseline} \end{cases} \tag{6.54}$$

Using these values and the observed gravitational constant G (Newell et al. (2018)),

$$G = 6.67430(15) \cdot 10^{-11} \, \frac{\mathrm{m}^3}{\mathrm{kg} \cdot \mathrm{s}^2} \tag{6.55}$$

we calculate the observed value of the density of the dark energy by using Eqs. (6.52) and (6.51):

$$\boxed{\rho_{\Lambda,CMB} = \begin{cases} (5.690 \pm 0.284) \cdot 10^{-27} \, \frac{\mathrm{kg}}{\mathrm{m}^3} \; (\pm 5\%) & \text{TT} \\ (5.834 \pm 0.156) \cdot 10^{-27} \, \frac{\mathrm{kg}}{\mathrm{m}^3} \; (\pm 2.7\%) & \text{baseline} \end{cases}} \tag{6.56}$$

6.5.2 Density $\rho_{\Lambda,local\ probes}$

Riess et al. (2019) observed distant galaxies that are relatively local, compared with the emission of the CMB. Utilizing these probes, they obtained a significantly higher value of the Hubble constant H_0, compared with the results obtained by using the CMB:

$$H_{0,local\ probes} = 74.03 \pm 1.42 \, \frac{\mathrm{km}}{\mathrm{Mpc} \cdot \mathrm{s}} = 2.399 \pm 0.046 \, \frac{1}{\mathrm{s}} \tag{6.57}$$

Using this value $H_{0,local\ probes}$ and the observed gravitational constant G (6.55), we calculate the observed value of the density of the dark energy by using Eqs. (6.52) and (6.51):

$$\boxed{\rho_{\Lambda,local\ probes} = \begin{cases} (7.047 \pm 0.351) \cdot 10^{-27} \, \frac{\mathrm{kg}}{\mathrm{m}^3} \; (5\%) & \text{TT} \\ (6.988 \pm 0.410) \cdot 10^{-27} \, \frac{\mathrm{kg}}{\mathrm{m}^3} \; (5.9\%) & \text{baseline} \end{cases}} \tag{6.58}$$

6.5.3 Time evolution of density ρ_Λ

The density ρ_Λ has been measured by using many different probes such as the CMB (Collaboration (2020)), relatively near galaxies (Riess et al. (2019)), baryonic acoustic oscillations, BAO (Zhao et al. (2019), Yeche et al. (2019)), weak gravitational lensing (Lu and Haiman (2020)) and gravitational lensing (Wong et al. (2019)).

The essential differences can be elaborated by analyzing two probes: the CMB (Collaboration (2020)) and relatively near galaxies (Riess et al. (2019)). These two probes exhibit a significant difference between the densities $\rho_{\Lambda,local\ probes}$ and $\rho_{\Lambda,CMB}$. The difference is at least $\frac{6.988-0.410-5.834-0.156}{6.988-0.410} = 9\%$, while the average of the baseline difference is

$$\boxed{\Delta\rho_\Lambda = \frac{\rho_{\Lambda,local\ probes} - \rho_{\Lambda,CMB}}{\rho_{\Lambda,local\ probes}} = \frac{6.988 - 5.834}{6.988} = 16.5\%} \tag{6.59}$$

That difference is interpreted as follows: In all probes the measured quantity is electromagnetic radiation. It travels at the velocity of light. So the relatively local probes have been emitted in the relatively late universe (compared to the Big Bang), whereas the relatively distant probes of the CMB have been emitted in the relatively early universe. Hence $\Delta\rho_\Lambda$ represents a difference between observations of $\rho_\Lambda(t)$ at two different times t_{early} and t_{late}. Thus $\Delta\rho_\Lambda$ represents two points of the **time evolution of the density** $\rho_\Lambda(t)$.

In the following we elaborate two theories for the dark energy: First we develop the theory of the dark energy that is based on the RGWs, and that uses the approximation of a constant density $\rho_{\Lambda,const}$. Secondly, we derive the theory of the dark energy that is based on the RGWs, including the time development $\rho_\Lambda(t)$. Thereby we emphasize: In both theories, we do not use any fit parameter.

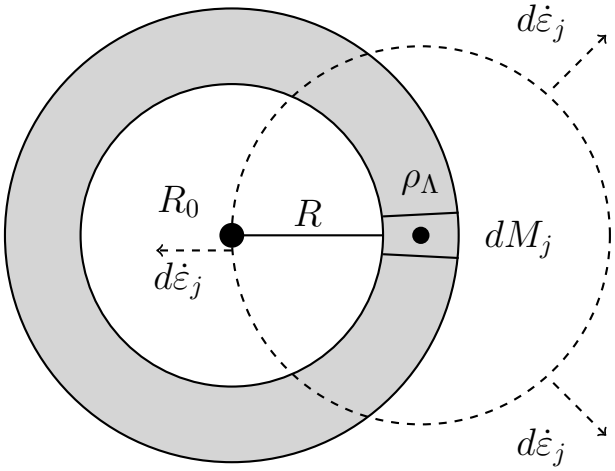

Figure 6.2: The density ρ_Λ in an area at a distance R from R_0 has a dynamic mass M_j. It generates rates $d\dot{\varepsilon}_j$ propagating to all directions.

6.6 Dark energy: theory I

In this section we derive a **semiclassical theory** of the dark energy based on the field theory including the rates $\dot{\varepsilon}$ of formed vacuum and on the result that the LFV is one half of the CFV.

Additional approximation: This semiclassical theory can also be applied to derive the time evolution of the dark energy (Sect. 7.5). In this section, we analyze the simple case of a constant vacuum, the approximation of a constant density $\rho_\Lambda = \rho_{\Lambda,const.}$. Thereby we use the fact that the vacuum is present in the form of quantized RGWs that emit additional quantized RGWs with unidirectional quadrupolar symmetry.

6.6.1 Universe with vacuum only

At a first step, we develop the semiclassical theory for the case of negligible densities of matter and radiation, $\frac{\rho_m}{\rho} \to 0$ and $\frac{\rho_r}{\rho} \to 0$.

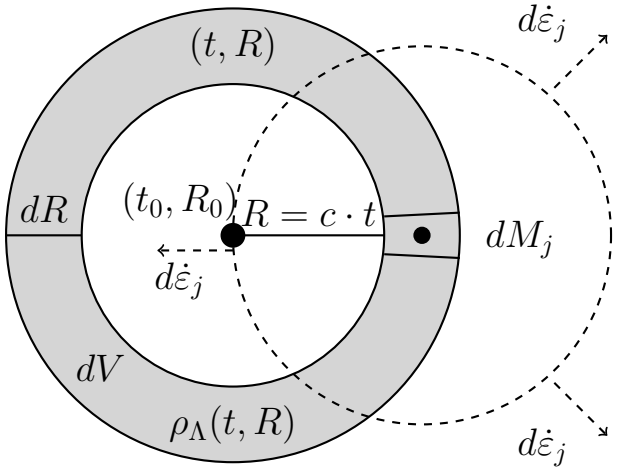

Figure 6.3: More details included to Fig. (6.2): In a shell with a radius R, a thickness dR and a center R_0, there is a density The density $\rho_\Lambda(t)$. That mass generates the rates $d\dot{\varepsilon}_j$ propagating in space towards R_0. These rates are integrated.

6.6.2 RGWs originating at vacuum

A quantized RGW of vacuum with a dynamical mass M_j emits LFV (6.2). This process is **not disturbed**, as the space is filled with vacuum only. That vacuum arrives at an observer at a place R_0. We describe that process in terms of the stationary rate $\dot{\varepsilon}_{\text{LFV, from j}}$ (see theorem 17).

As our universe exhibits a Big Bang (not a Big Crunch), the sign of that rate is always positive, and so these rates do not cancel. In the following, we analyze the presence of these rates at a location R_0, see Fig. (6.3).

6.6.3 Plan of the derivation

We derive the density as follows: We integrate the rates coming from all dynamical masses M_j in the light horizon and propagating to R_0, $\dot{\varepsilon}_{\text{LFV, to } R_0}$ (sections 6.6.4, 6.6.5, 6.6.6, 6.6.7) We derive the rate emitted by the vacuum at R_0, $\dot{\varepsilon}_{\text{LFV, from } R_0}$ Fig. 6.4) (section 6.6.8). In a stationary state, these rates are equal, and from that equality we derive $\rho_{\Lambda,const.}$ (section 6.6.9).

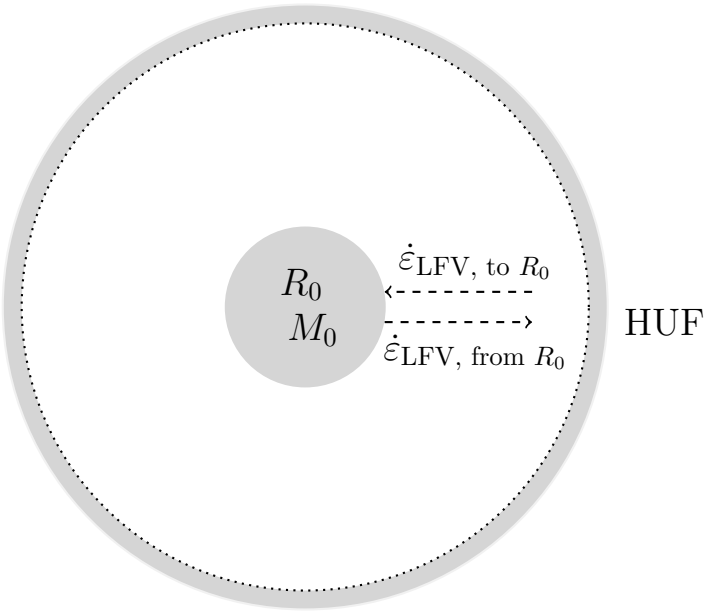

Figure 6.4: RGWs propagating to and from R_0 with dynamical mass M_0.

6.6.4 Propagation of RGWs

The vacuum propagates with the velocity c, as it is fully relativistic. Thereby it propagates in the form of the RGWs (see Sect. 5). Thus the vacuum propagates by the rates $\dot{\varepsilon}$.

First we analyze the rate $\dot{\varepsilon}_{\text{LFV, to } R_0}$ of RGWs propagating to R_0. That rate $\dot{\varepsilon}_{\text{LFV, to } R_0}$ can only originate from other places R_j with a dynamic mass dM_j, hereby M_j generates a rate $d\dot{\varepsilon}_j$ at R_0, see Fig. (6.2).

Hereby these places R_j are within the light horizon $R_j \leq R_{lh}$ of R_0. Hence the rate $\dot{\varepsilon}_{\text{LFV, to } R_0}$ arriving at R_0 and t_0 is the sum of all partial rates $d\dot{\varepsilon}_j$ that originate from a shell with R_0 at the center, see Fig. (6.3):

$$\dot{\varepsilon}_{\text{LFV, to } R_0} = \Sigma_j d\dot{\varepsilon}_j \quad \text{with} \quad R_j \leq R_{lh} \tag{6.60}$$

6.6.5 Rate $d\dot{\varepsilon}_j$ originating at M_j

A mass dM_j at a distance R from R_0 generates the following rate $d\dot{\varepsilon}_j$ of unidirectional LFV, see theorem (17) and Fig. (6.2):

$$d\dot{\varepsilon}_j = \frac{1}{c} \cdot \frac{G \cdot dM_j}{R^2} \tag{6.61}$$

6.6.6 Integration of $d\dot{\varepsilon}_j$ originating in a shell

In this section we integrate the rates $d\dot{\varepsilon}_j$ that arrive at R_0, and that originate in a shell that has its center at R_0, and that has a radius R and a thickness dR, see Fig. (6.3).

Each mass dM_j in that shell generates a rate $d\dot{\varepsilon}_j$ that is proportional to that mass, and these rates are scalars. Hence the sum of the rates $d\dot{\varepsilon}(R) = \Sigma_{j,\, R_j \in \text{shell}}\, d\dot{\varepsilon}_j$ is equal to the rate of the sum of the masses $dM(R) = \Sigma_{j,\, R_j \in \text{shell}}\, dM_j$. So we get:

$$d\dot{\varepsilon}(R) = \frac{1}{c} \cdot \frac{G \cdot dM(R)}{R^2} \tag{6.62}$$

That mass $dM(R)$ is equal to the product of the density $\rho_\Lambda(t, R)$ and the volume $dV = 4\pi \cdot R^2 \cdot dR$ of the shell:

$$dM(R) = \rho_\Lambda(t, R) \cdot 4\pi \cdot R^2 \cdot dR \tag{6.63}$$

According to the homogeneity of space, the densities $\rho_\Lambda(t, R)$ are the same at the same time t. Note that the notion *same time* may be complicated in the context of a local frame in spacetime (see for instance Einstein (1905), Carmesin (2020b), Carmesin et al. (2022)), but it is well defined at a global frame (Carmesin (2018b), Carmesin (2020b)). We call it the **time dependent density of the vacuum** $\rho_\Lambda(t)$:

$$\boxed{\rho_\Lambda(t, R) = \rho_\Lambda(t, R_0) = \rho_\Lambda(t)} \tag{6.64}$$

We insert the mass in Eq. (6.63) into Eq. (6.62):

$$d\dot{\varepsilon}(R) = \frac{1}{c} \cdot \frac{G \cdot \rho_\Lambda(t) \cdot 4\pi \cdot R^2 \cdot dR}{R^2} \tag{6.65}$$

We cancel R^2. So we get:

$$\boxed{d\dot{\varepsilon}(R) = \frac{G \cdot \rho_\Lambda(t) \cdot 4\pi \cdot dR}{c}} \tag{6.66}$$

6.6.7 Integration of rates $d\dot{\varepsilon}(R)$

In this section we integrate the rates of the shells.

The rates $d\dot{\varepsilon}(R)$ arriving at R_0 originate at times of emission $t_{em.}$ after the Hubble time t_H. Thereby the Hubble time is the inverse Hubble constant:

$$t_{em.} \leq t_H = \frac{1}{H_0} \tag{6.67}$$

The corresponding **light travel distance** is the Hubble radius:

$$R_H = c \cdot t_H = \frac{c}{H_0} \tag{6.68}$$

This propagation of vacuum by the RGWs is well defined since the density became smaller than the highest value possible value at $R_{lh,limit}$ (Sect. 6.4 or theorem 20). Accordingly we integrate Eq. (6.66) with these boundaries. So we derive:

$$\int_0^{\dot{\varepsilon}_{\text{LFV, to } R_0}} d\dot{\varepsilon} = \frac{4\pi \cdot G}{c} \cdot \int_{R_{lh,limit}}^{R_H} \rho_\Lambda(t) dR \tag{6.69}$$

We evaluate the left integral:

$$\dot{\varepsilon}_{\text{LFV, to } R_0} = \frac{4\pi \cdot G}{c} \cdot \int_{R_{lh,limit}}^{R_H} \rho_\Lambda(t) dR \tag{6.70}$$

We apply the approximation of a constant density:

$$\text{approximation: } \rho_\Lambda(t) = \rho_{\Lambda,const.} = \rho_\Lambda(t_0, R_0) \tag{6.71}$$

Furthermore we apply the approximation $\frac{R_{lh,limit}}{R_{lh}(t_0)} \approx 0$. With it we get the rates propagating to R_0:

$$\boxed{\dot{\varepsilon}_{\text{LFV, to } R_0} = \frac{4\pi \cdot G \cdot R_H}{c} \cdot \rho_{\Lambda,const.}} \tag{6.72}$$

6.6.8 Density of RGWs propagating from R_0

In this section we analyze the RGWs that propagate from a small region at R_0 that is placed in a small HUF, and that has a dynamical mass M_0 constituted by the density of vacuum ρ_Λ (see Fig. 6.4).

The density of the field generated by M_0 is related to the rate according to theorem (17):

$$\rho_f = \frac{\dot{\varepsilon}^2_{\text{LFV, from } R_0}}{8\pi \cdot G} \tag{6.73}$$

That density must be equal to the density of the LFV of the vacuum, $\rho_f = \rho_{\Lambda,LFV}$. That density of the LFV is one half of the density of the CFV, $\rho_{\Lambda,LFV} = \rho_{\Lambda,CFV}/2$ (see theorems 5, 9, 17, 12, 13).

Altogether we obtain:

$$\rho_f = \rho_{\Lambda,LFV} = \frac{1}{2} \cdot \rho_{\Lambda,CFV} = \frac{\dot{\varepsilon}^2_{\text{LFV, from } R_0}}{8\pi \cdot G} \tag{6.74}$$

6.6.9 Equality of rates

As we model a completely homogeneous system (Sect. 6.6.1), the RGWs propagating to M_0 have the same rate as the RGWs propagating from M_0:

$$\dot{\varepsilon}_{\text{LFV, from } R_0} = \dot{\varepsilon}_{\text{LFV, to } R_0} \tag{6.75}$$

We apply that equality to our result in Eq. (6.74):

$$\frac{1}{2} \cdot \rho_{\Lambda,CFV} = \frac{\dot{\varepsilon}^2_{\text{LFV, to } R_0}}{8\pi \cdot G} \tag{6.76}$$

We insert Eq. (6.72):

$$\frac{1}{2} \cdot \rho_{\Lambda,CFV} = \frac{8\pi G \cdot 2\pi G \cdot R_H^2}{8\pi G \cdot c^2} \cdot \rho^2_{\Lambda,const.} \tag{6.77}$$

We cancel, and we apply the approximation of a constant density of the vacuum (Eq. 6.71), $\rho_{\Lambda,CFV} = \rho_{\Lambda,const.}$. So we derive:

$$\frac{1}{2} \cdot \rho_{\Lambda,const.} = \frac{2\pi G \cdot R_H^2}{c^2} \cdot \rho_{\Lambda,const.}^2 \tag{6.78}$$

We solve for $\rho_{\Lambda,const.}$:

$$\boxed{\rho_{\Lambda,const.} = \frac{c^2}{4\pi \cdot G \cdot R_H^2}} \tag{6.79}$$

Evaluation: We calculate R_H by using Eqs. (6.53, 6.68):

$$R_H = 1.374 \pm 0.01 \cdot 10^{26}\,\mathrm{m} \tag{6.80}$$

With it we calculate the density $\rho_{\Lambda,const}$ by using Eq. (6.79):

$$\boxed{\rho_{\Lambda,const.} = 5.681 \pm 0.091 \cdot 10^{-27}\,\frac{\mathrm{kg}}{\mathrm{m}^3}\ (\pm 1.6\%)} \tag{6.81}$$

The difference $\Delta\rho_\Lambda = \rho_{\Lambda,CMB} - \rho_{\Lambda,const.}$ of the result and the observed value $\rho_{\Lambda,CMB}$ (Eq. 6.56) is as follows:

$$\boxed{\Delta\rho_\Lambda = \begin{cases} 0.009 \cdot 10^{-27}\,\frac{\mathrm{kg}}{\mathrm{m}^3}\ (0.16\%) & \mathrm{TT} \\ 0.153 \cdot 10^{-27}\,\frac{\mathrm{kg}}{\mathrm{m}^3}\ (2.6\%) & \mathrm{baseline} \end{cases}} \tag{6.82}$$

So our derived value in Eq. (6.81) is compatible with the observed values of $\rho_{\Lambda,CMB}$ in Eq. (6.56), as the error of measurement is at least 2.7%, while the difference between observation and theory amounts to 0.16 % for the case of the temperature power spectra, TT, and 2.6% for the case of the baseline.

According to the applied approximation of constant density of the vacuum, the obtained result is not compatible to the density of the vacuum of the late universe.

Density parameter Ω_Λ: We derive the density parameter Ω_Λ, for the case of the approximation of constant $\rho_{\Lambda,const.}$. For it we use Eq. (6.79), $\rho_{cr,t_0} = \frac{3H_0^2}{8\pi G}$ and $H_0 = c/R_H$. So we get:

$$\Omega_\Lambda = \frac{\rho_{\Lambda,const.}}{\rho_{cr,t_0}} = \frac{2}{3} \tag{6.83}$$

6.6.10 Amount of formed vacuum

In this section we analyze the amount of vacuum δV_{CFV} that forms in a volume ΔV around a location R_0.

Propagating volume: Hereby we realize that at each instant of time, the amount of vacuum propagating to ΔV is equal to the amount of vacuum propagating from ΔV (Fig. 6.5). Thus the additional vacuum in ΔV is formed vacuum. So we analyze the rates $\dot{\varepsilon}$.

Propagating rates of LFV: In order to analyze the rates of the LFV, we apply the rate of the RGWs that propagate to R_0 (Eq. 6.72):

$$\dot{\varepsilon}_{\text{LFV, to } R_0} = \frac{4\pi \cdot G \cdot R_H}{c} \cdot \rho_{\Lambda,const.} \tag{6.84}$$

Here we use the constant density of the vacuum $\rho_{\Lambda,const.}$ derived in Eq. (6.79):

$$\dot{\varepsilon}_{\text{LFV, to } R_0} = \frac{4\pi \cdot G \cdot R_H}{c} \cdot \frac{c^2}{4\pi \cdot G \cdot R_H^2} = \frac{c}{R_H} = \frac{1}{t_H} \tag{6.85}$$

We identify that rate $\dot{\varepsilon}_{\text{LFV, to } R_0}$ by the new vacuum δV_{LFV} that is generated per volume of the already present vacuum dV and per time δt. Hereby the time δt is the time t_H of the formation of that new vacuum, as we integrated from R_H to R_0. So we obtain:

$$\frac{\delta V_{\text{LFV}}}{dV \cdot \delta t} = \frac{\delta V_{\text{LFV}}}{dV \cdot t_H} = \dot{\varepsilon}_{\text{LFV, to } R_0} = \frac{1}{t_H} \tag{6.86}$$

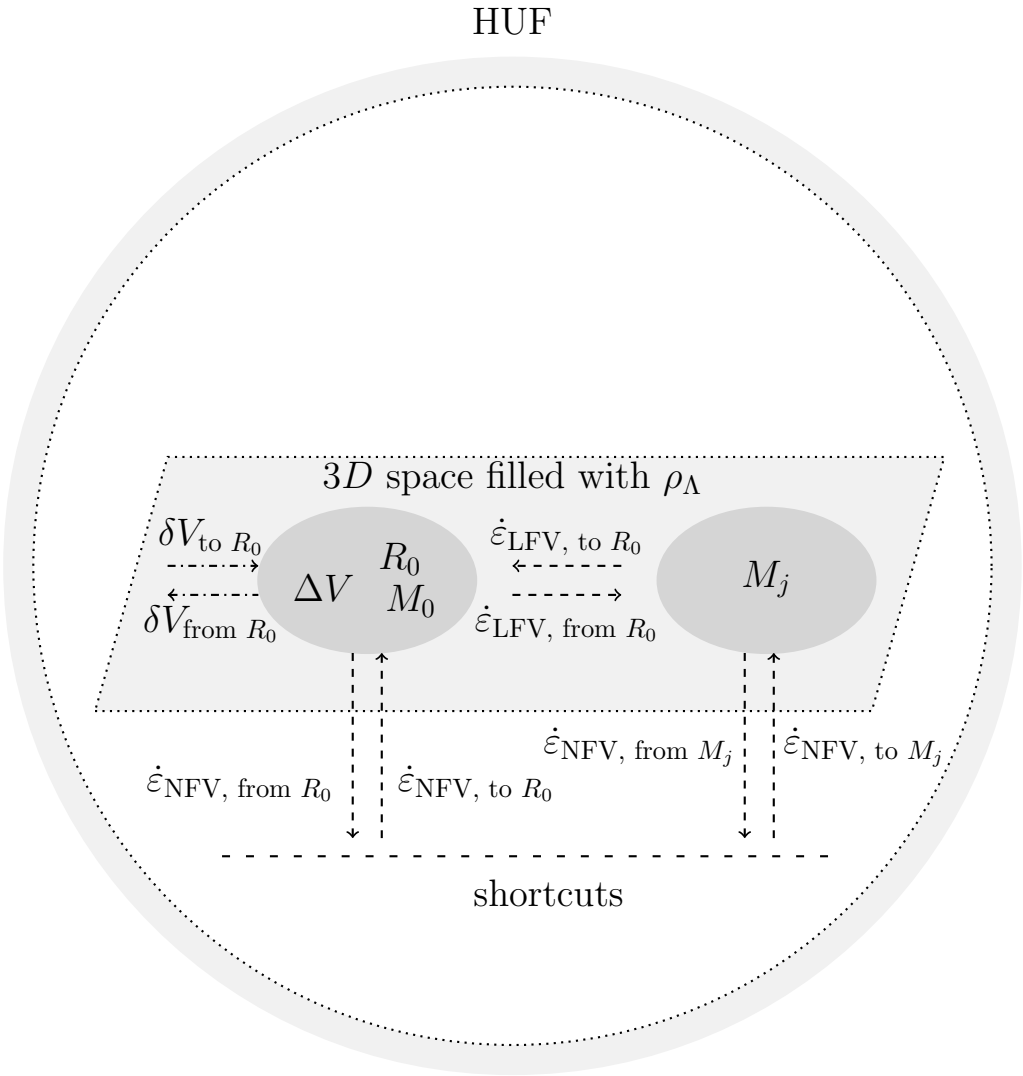

Figure 6.5: Overview of propagation of rates in $3D$ space and in shortcuts corresponding to space in other dimensions. Thereby quanta of vacuum such as M_j emit quantized RGWs of vacuum with unidirectional quadrupolar symmetry.

We solve for $\delta V_{\rm LFV}$ that is $\delta V_{\rm LFV,\ via\ \dot{\varepsilon}\ to\ R_0}$:

$$\delta V_{\rm LFV} \hat{=} \delta V_{\rm LFV,\ via\ \dot{\varepsilon}\ to\ R_0} = dV \ \text{ at each instant of time} \quad (6.87)$$

We divide the above Eq. by $\delta V_{\rm CFV}$, and we abbreviate ratios:

$$q_{\rm LFV} := \frac{\delta V_{\rm LFV}}{dV_{\rm CFV}} = \frac{dV}{dV_{\rm CFV}} =: q \quad (6.88)$$

That ratio is determined by integration (Fig. 6.6) $q_{\rm LFV} = 1/2$. We solve Eq. (6.88) for $\delta V_{\rm LFV}$, and we insert the above Eq.:

$$\boxed{2\delta V_{\rm LFV} \hat{=} 2\delta V_{\rm LFV,\ via\ \dot{\varepsilon}\ to\ R_0} = dV_{\rm CFV}} \quad (6.89)$$

Thus, one half of $dV_{\rm CFV}$ is constituted by $\delta V_{\rm LFV,\ via\ \dot{\varepsilon}\ to\ R_0}$.

6.6.10.1 Interpretation

The formed vacuum $dV_{\rm CFV}$ consists of two equal parts, the vacuum formed by the rate $\dot{\varepsilon}_{\rm LFV,\ to\ R_0}$ plus the vacuum formed by the rate $\dot{\varepsilon}_{\rm LFV,\ from\ R_0}$, see Fig. (6.5). Moreover, the formed time dt is derived, $\delta t_{LFV} dV = \delta V_{LFV} dt$ (Eqs. 1.78, 1.85), using $dV = \delta V_{CFV}$ we get:

$$\boxed{\delta t_{LFV} = \frac{dt}{2} \ \text{ and } \ \delta t_{\rm LFV,\ via\ \dot{\varepsilon}\ to\ R_0} + \delta t_{\rm LFV,\ via\ \dot{\varepsilon}\ from\ R_0} = dt} \quad (6.90)$$

So the symmetry of these two parts provides a **constant and homogeneous rate of formed time**. An additional interpretation in terms of NFV is possible, see Fig. (6.5).

Theorem 21 Derivation of $\rho_{\Lambda,const.}$:

If the semiclassical theory is applied without the densities of radiation and matter, and if the approximation of constant $\rho_{\Lambda,const.}$ is used, then the dark energy shows the following properties:

(1) Its density $\rho_{\Lambda,const.}$ is formed by rates of RGWs coming from the whole space within the Hubble radius R_H and coming from

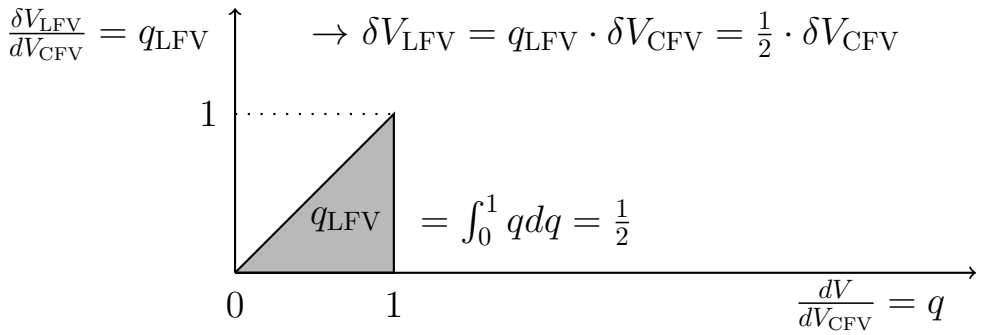

Figure 6.6: Ratio q_{LFV} of LFV as a function of the ratio q of already formed vacuum: The graph as well as the integration show that the LFV is one half of the CFV.

all times since the Big Bang: $\delta V_{LFV,\ via\ \dot{\varepsilon}\ to\ R_0}$. *Additionally, there forms* $\delta V_{LFV,\ via\ \dot{\varepsilon}\ from\ R_0}$.

(2a) That density is (Eq. 6.79):

$$\rho_{\Lambda,const.} = \frac{c^2}{4\pi \cdot G \cdot R_H^2}$$

That density is in precise accordance with the density observed on the basis of the temperature power spectra, TT, of the CMB (Collaboration (2020)), showing a discrepancy of 0.16 %, clearly below the errors of measurement.

(2b) Inherent to the above equation of the density are **only two universal constants:** G **and** c.

(3) The density parameter Ω_Λ *is equal to 2/3. It is in precise accordance with the density observed on the basis of the temperature power spectra, TT, of the CMB (Collaboration (2020)).*

(4) The complete formation of the vacuum in a **volume** dV_{CFV} *at a location* R_0 *is explained (Eq. 6.89). The* **constant and homogeneous rate of the formed time** *is explained (Eq. 6.90). This confirms that the present theory describes the formation of* **spacetime**.

(5) An interpretation using NFV is possible (Sect. 6.6.10.1).

Chapter 7

Structure Formation

Kant (1755), Press and Schechter (1974), Abell et al. (1989), Errani and Penarrubia (2019) and many others investigated the formation of structures with high density in the universe, including their time evolution.

7.1 Description of matter fluctuations

In this section we introduce the concept of overdensities.

Overdensity at a place $\vec{x}$ and at a time t: At an average density or at a homogeneous part of the density $\rho_h(t)$ and at a local density $\rho(\vec{x}, t)$, the fluctuation is

$$\rho_1(\vec{x}, t) = \rho(\vec{x}, t) - \rho_h(t) \tag{7.1}$$

and the relative density

$$\delta(\vec{x}, t) = \frac{\rho(\vec{x}, t) - \rho_h(t)}{\rho_h(t)} \tag{7.2}$$

is called **overdensity** (Kravtsov and Borgani (2012)). As there is an overdensity at each $\vec{x}$, the overdensity establishes a field.

Window function: It is convenient to analyze a signal or physical data according to a **window function** that is non-zero in a particular area in which the data should be analyzed (Kravtsov

and Borgani (2012)). In particular, in this context the spherical top-hat window function is used (Norman (2010) or Stoica and Moses (2005)):

$$W_R(\vec{x}) = \begin{cases} \frac{3}{4\pi R^3} & \text{if } |\vec{x}| < R \\ 0 & \text{otherwise} \end{cases} \tag{7.3}$$

Overdensity in a sphere with radius R: We analyze an **overdensity in a sphere with radius** R by using the following integral (Kravtsov and Borgani (2012)):

$$\delta_R(\vec{x}, t) = \int \delta(\vec{x} - \vec{r}, t) \cdot W_R(\vec{r}) d^3r \tag{7.4}$$

Variance of matter fluctuations in a sphere with radius R: We analyze the **matter fluctuations in a sphere with radius** R by using the variance. It is the empirical averaged value or the corresponding theoretical expectation value of the square of the overdensity in that sphere. We mark that average or expectation value by angle brackets:

$$\langle \delta_R^2(\vec{x}, t) \rangle = \langle \delta_R^2(t) \rangle \tag{7.5}$$

According to the homogeneity of space that variance is the same at all points, usually marked by $\vec{x}$ in this context. As the variance is the square of the standard deviation, the variance $\langle \delta_R^2(t) \rangle$ of matter fluctuations is also called $\sigma_R^2(t)$ (Kravtsov and Borgani (2012)):

$$\langle \delta_R^2(t) \rangle = \sigma_R^2(t) \tag{7.6}$$

Dimensionless Hubble parameter: The continuous expansion of space can be described by a scale radius a (Gott et al. (2005), Carmesin (2019b)). The relative time derivative is called **Hubble parameter** (Eq. 1.58). Its value at the present time t_0 is called **Hubble constant** H_0, with $H_0 = 67.36 \, \frac{\text{km}}{\text{s·Mpc}}$ (Tab.

9.2). Sometimes, a corresponding dimensionless parameter is used (Collaboration (2020)):

$$h_0 = \frac{H_0/100}{\frac{\text{km}}{\text{s·Mpc}}} = 0.6736 \tag{7.7}$$

Amplitude of matter fluctuations: Usually the variance $\sigma_R^2(t)$ is analyzed for the case of a sphere with the radius $R = 8\,\text{Mpc}/h_0$:

$$R_8 = 8\,\text{Mpc}/h_0 \tag{7.8}$$

Thereby that variance $\sigma_R^2(t)$ is investigated for the case of the actual time t_0, and it is denoted by σ_8^2:

$$\sigma_{R_8}^2(t = t_0) = \sigma_8^2 \tag{7.9}$$

That standard deviation σ_8 is also called **amplitude of mass fluctuations** (Fan et al. (1997)) or **amplitude of matter fluctuations** (see (Lu and Haiman, 2020, p. 1)). Any observation of σ_8 probes fluctuations that existed at times $t \neq t_0$, and the corresponding fluctuations at $t = t_0$ **are evaluated in linear theory** (see for instance (Collaboration, 2014, p. 8)).

7.2 Fourier transformation of overdensities

The observations are often evaluated in terms of a spectrum of the overdensities. For it the Fourier transform is applied (Fourier (1822) or Stoica and Moses (2005)):

$$\tilde{f}(k) = \int_{-\infty}^{\infty} f(x) \exp(-ikx) dx = (\mathcal{F}f)(k) \tag{7.10}$$

The corresponding inverse transform is:

$$f(x) = \frac{1}{2\pi} \int_{-\infty}^{\infty} \tilde{f}(k) \exp(ikx) dk = (\mathcal{F}\tilde{f})(x) \tag{7.11}$$

Of course, this transformation can be applied in a space at any integer dimension $D \geq 1$:

$$\tilde{f}(\vec{k}) = \int_{-\infty}^{\infty} f(\vec{x}) \exp(-i\vec{x} \cdot \vec{k}) dx^D = (\mathcal{F}f)(\vec{k}) \tag{7.12}$$

The corresponding inverse transform is:

$$f(\vec{x}) = \frac{1}{(2\pi)^D} \int_{-\infty}^{\infty} \tilde{f}(\vec{k}) \exp(i\vec{k} \cdot \vec{x}) dk^D = (\mathcal{F}\tilde{f})(\vec{x}) \tag{7.13}$$

7.2.1 Spectral power density

In quantum physics, the probability density of a photon with a wave number k is proportional to the square $|\tilde{\Psi}(k)|^2$ of the corresponding wave function $\tilde{\Psi}(k)$. The energy $E = p \cdot c$ of the photon is proportional to $\hbar k \cdot c$. So the energy density is proportional to $|\tilde{\Psi}(k) \cdot \sqrt{k}|^2$. Moreover, the energy density times c is the power density, and so the power density is proportional to $|\tilde{\Psi}(k) \cdot \sqrt{k}|^2$. This motivates to denote the square $\tilde{f}(k)$ of the Fourier transform by **power density** (Hansen (2002)) or **energy density** ((Stoica and Moses, 2005, p. 3)) or **power spectrum** ((Collaboration, 2014, p. 8)):

$$|\tilde{f}(k)|^2 = P(k) \tag{7.14}$$

The integral I of that density is the same as a function of k or x,

$$I = \frac{1}{2\pi} \int_{-\infty}^{\infty} |\tilde{f}(k)|^2 dk \tag{7.15}$$

We confirm this:

$$I = \frac{1}{2\pi} \int_{-\infty}^{\infty} dk \int_{-\infty}^{\infty} dx \int_{-\infty}^{\infty} dy f(x) f^*(y) e^{-ik(x-y)} \tag{7.16}$$

Here the star denotes the complex conjugate.

$$I = \int_{-\infty}^{\infty} dx \int_{-\infty}^{\infty} dy f(x) f^*(y) \left(\frac{1}{2\pi} \int_{-\infty}^{\infty} dk e^{-ik(x-y)} \right) \tag{7.17}$$

The bracket in the above Eq. is equal to the delta-distribution of $x - y$. With it we evaluate the integral over dy, so we get (qed):

$$I = \int_{-\infty}^{\infty} dx |f(x)|^2 \tag{7.18}$$

7.2.2 Window function

The average of the matter fluctuation $\delta(x,t)$ over an interval $[x-R, x+R]$ can be expressed with a rectangular window function (see (Stoica and Moses, 2005, p. 54)), the one dimensional, $1D$, analogue of the top-hat window:

$$\delta_R(x,t) = \int_{-\infty}^{\infty} dy \delta(y,t) \cdot W_R(x-y) \tag{7.19}$$

Thereby the normalized window function is:

$$W_R(x) = \begin{cases} \frac{1}{2R} & \text{if } |x| < R \\ 0 & \text{otherwise} \end{cases} \tag{7.20}$$

The integral in Eq. (7.19) is a convolution. So its Fourier transform is the following product of Fourier transforms:

$$(\mathcal{F}\delta_R)(k) = (\mathcal{F}\delta)(k) \cdot (\mathcal{F}W_R)(k) \tag{7.21}$$

We prove this relation: For it we apply the Fourier transform to Eq. (7.19):

$$\delta_R(x) = \int_{-\infty}^{\infty} dy \delta(y) \cdot \frac{1}{2\pi} \int_{-\infty}^{\infty} dk e^{ik(x-y)} (\mathcal{F}W_R)(k) \tag{7.22}$$

We factorize the exponential function:

$$\delta_R(x) = \frac{1}{2\pi} \int_{-\infty}^{\infty} dk e^{ikx} (\mathcal{F}W_R)(k) \cdot \int_{-\infty}^{\infty} dy \delta(y) e^{-iky} \tag{7.23}$$

We identify the second integral with the Fourier transform of $\delta(y)$:

$$\delta_R(x) = \frac{1}{2\pi} \int_{-\infty}^{\infty} dk e^{ikx} (\mathcal{F}W_R)(k) \cdot (\mathcal{F}\delta)(k) \tag{7.24}$$

We identify the integrand with the Fourier transform of $\delta_R(x)$. So we derive Eq. (7.21) (qed).

7.2.3 Autocorrelation function

In this section we introduce the autocorrelation function $\xi(\vec{r})$, and we show how $\xi(\vec{r})$ can be used in order to obtain the standard deviation of fluctuations σ_R.

Autocorrelation function: We analyze the correlation of overdensites at different places $\vec{x}$ and $\vec{x} + \vec{r}$ by using the autocorrelation function (Broersen (2006), Hansen (2002)):

$$\xi(\vec{r}) = \langle \delta(\vec{x}) \cdot \delta(\vec{x} - \vec{r}) \rangle \tag{7.25}$$

Average: Hereby the average can be expressed as an average taken according to the window function:

$$\xi(\vec{r}) = \int_{-\infty}^{\infty} d^3x \delta_R(\vec{x}) \cdot \delta_R(\vec{x} - \vec{r}) \tag{7.26}$$

This is a convolution. So the Fourier transform is the product of Fourier transforms:

$$(\mathcal{F}\xi)(\vec{k}) = [(\mathcal{F}\delta_R)(\vec{k})]^2 \tag{7.27}$$

We apply Eq. (7.21):

$$(\mathcal{F}\xi)(\vec{k}) = [(\mathcal{F}\delta)(\vec{k})]^2 \cdot [(\mathcal{F}W_R)(\vec{k})]^2 \tag{7.28}$$

We identify the first factor with the power density (Eq. 7.14):

$$(\mathcal{F}\xi)(\vec{k}) = P(\vec{k}) \cdot [(\mathcal{F}W_R)(\vec{k})]^2 \tag{7.29}$$

We apply the Fourier transform:

$$\xi(\vec{r}) = \frac{1}{(2\pi)^3} \int_{-\infty}^{\infty} d^3k e^{i\vec{k}\vec{r}} P(\vec{k}) \cdot [(\mathcal{F}W_R)(\vec{k})]^2 \tag{7.30}$$

According to the isotropy, we apply polar coordinates:

$$\xi(r) = \frac{1}{2\pi^2} \int_0^{\infty} dk k^2 e^{ikr} P(k) \cdot [(\mathcal{F}W_R)(k)]^2 \tag{7.31}$$

Standard deviation: We analyze the autocorrelation function $\xi(\vec{r})$ in Eq. (7.26) at $\vec{r} = 0$:

$$\xi(\vec{r} = 0) = \int_{-\infty}^{\infty} d^3x \delta_R(\vec{x})^2 \tag{7.32}$$

Since the window function is normalized, the above integral is equal to the corresponding average:

$$\xi(\vec{r} = 0) = \int_{-\infty}^{\infty} d^3x \delta_R(\vec{x})^2 = \langle \delta_R(\vec{x})^2 \rangle = \sigma_R^2 \tag{7.33}$$

We evaluate the same average by using Eq. (7.31):

$$\xi(\vec{r} = 0) = \frac{1}{2\pi^2} \int_0^{\infty} dk k^2 P(k) \cdot [(\mathcal{F}W_R)(k)]^2 = \sigma_R^2 \tag{7.34}$$

This result is commonly used in the analysis of matter fluctuations (see for instance (Kravtsov and Borgani, 2012, p. 11), (Hansen, 2002, p. 27), Fan et al. (1997)). In the above derivations, we did not use any restriction for the time t, thus this relation holds for each time t:

$$\xi(\vec{r} = 0, t) = \frac{1}{2\pi^2} \int_0^{\infty} dk k^2 P(k, t) \cdot [(\mathcal{F}W_R)(k)]^2 = \sigma_R^2(t) \tag{7.35}$$

7.3 Time evolution of small overdensities

In this section we develop the **linear theory of the overdensities**.

Euler's equations of motion in space: Based on Newton's laws of motion, Euler (1757) derived the equations of motion for a classical fluid. In particular, he derived the dynamics of the density field $\rho = \rho(\vec{r}, t)$, that exhibits a velocity field $\vec{v} = \vec{v}(\vec{r}, t)$, and that has a pressure field $P = P(\vec{r}, t)$, and that evolves in a potential field $\Phi = \phi(\vec{r})$:

$$\partial_t \rho + \partial_{\vec{r}}(\rho \vec{v}) = 0 \tag{7.36}$$

$$\partial_t \vec{v} + (\vec{v} \cdot \partial_{\vec{r}})\vec{v} + \frac{1}{\rho}\partial_{\vec{r}} P + \partial_{\vec{r}}\Phi = 0 \tag{7.37}$$

$$\partial_{\vec{r}}^2 \Phi = 4\pi G \cdot \rho \tag{7.38}$$

The fields ρ, $\vec{v}$, P, and Φ are described by the homogeneous part marked by an index h plus a fluctuating part marked by the index 1. In the particular case of the velocity, we use a local description with $\vec{v}_h = 0$:

$$\rho = \rho_h + \rho_1, \;\; P = P_h + P_1, \;\; \Phi = \Phi_h + \Phi_1, \;\; \vec{v} = \vec{v}_1 \tag{7.39}$$

As a consequence we obtain Euler's equations in linear order of the fluctuations:

$$\partial_t \rho_1 + \rho_h \partial_{\vec{r}} \vec{v}_1 = 0 \tag{7.40}$$

In order to derive the linear version of Eq. (7.37), we multiply with ρ, and we neglect all terms that are quadratic in the overdensities, including $(\vec{v}_1 \cdot \partial_{\vec{r}})\vec{v}_1$:

$$\rho_h \partial_t \vec{v}_1 + \partial_{\vec{r}} P + \rho_h \partial_{\vec{r}} \Phi_1 + \rho_1 \partial_{\vec{r}} \Phi_h = 0 \tag{7.41}$$

As the derivative $\partial_{\vec{r}}$ applied to Φ_h is zero, we get:

$$\rho_h \partial_t \vec{v}_1 + \partial_{\vec{r}} P + \rho_h \partial_{\vec{r}} \Phi_1 = 0 \tag{7.42}$$

We apply the chain rule to the pressure term:

$$\partial_{\vec{r}} P = \frac{\partial P}{\partial \vec{r}} = \frac{\partial P}{\partial \rho} \cdot \frac{\partial \rho}{\partial \vec{r}} \tag{7.43}$$

Next we apply $\frac{\partial \rho}{\partial \vec{r}} = \frac{\partial \rho_h}{\partial \vec{r}} + \frac{\partial \rho_1}{\partial \vec{r}}$, whereby $\frac{\partial \rho_h}{\partial \vec{r}} = 0$. So we get:

$$\partial_{\vec{r}} P = \frac{\partial P}{\partial \vec{r}} = \frac{\partial P}{\partial \rho} \cdot \frac{\partial \rho_1}{\partial \vec{r}} \tag{7.44}$$

The first factor is equal to the square of the isentropic velocity of sound v_s^2 (see for instance (Piatella et al., 2014, p. 2), (Hansen, 2002, p. 22)). So we get:

$$\rho_h \partial_t \vec{v}_1 + v_s^2 \cdot \partial_{\vec{r}} \rho_1 + \rho_h \partial_{\vec{r}} \Phi_1 = 0 \tag{7.45}$$

Euler's equations of motion in expanding space: We add a homogeneous potential that describes the formation of vacuum according to the expansion of space, we mark that potential by the subindex H: Φ_H. So we get:

$$\partial_{\vec{r}}^2 \Phi_H = 4\pi G \cdot \rho_h \tag{7.46}$$

In this description, the potential is the sum of Φ_H and the potential of the overdensities $\Phi = \Phi_H + \Phi_1$. Hereby we have:

$$\partial_{\vec{r}}^2 \Phi_1 = 4\pi G \cdot \rho_1 \tag{7.47}$$

Wave equation: We apply the derivative $\partial_{\vec{r}}$ to Eq. (7.45):

$$\partial_t(\rho_h \partial_{\vec{r}} \vec{v}_1) + v_s^2 \cdot \partial_{\vec{r}}^2 \rho_1 + \rho_h \partial_{\vec{r}}^2 \Phi_1 = 0 \tag{7.48}$$

We apply Eqs. (7.40) and (7.47):

$$0 - \partial_t^2 \rho_1 + v_s^2 \cdot \partial_{\vec{r}}^2 \rho_1 + 4\pi G \cdot \rho_h \cdot \rho_1 = 0 \tag{7.49}$$

We solve for the inhomogeneity of the above DEQ:

$$\partial_t^2 \rho_1 - v_s^2 \cdot \partial_{\vec{r}}^2 \rho_1 = 4\pi G \cdot \rho_h \cdot \rho_1 \tag{7.50}$$

Harmonic solution: The solution of the above wave equation is a linear combination of harmonic solutions:

$$\rho_1(\vec{r}, t) = e^{i\vec{k}\cdot\vec{r} + i\omega t} \tag{7.51}$$

We insert into Eq. (7.50):

$$\omega^2 = v_s^2 \cdot k^2 - 4\pi G \cdot \rho_h \tag{7.52}$$

For the case of negative ω^2, we obtain imaginary values of ω. These correspond to exponentially growing or decaying modes. Here we analyze the growing modes. These occur, if the wave number k is smaller then the so-called **Jeans wave number** k_J:

$$\text{growth for } \; k < k_J = \sqrt{\frac{4\pi G \rho_h}{v_s^2}} \tag{7.53}$$

In the following, we consider wave numbers that grow fast:

$$\text{fast growth for } \; k << k_J \tag{7.54}$$

So the term proportional to the pressure or proportional to v_s^2 can be neglected.

Application of the Hubble parameter: The density is proportional to the scaling radius to the power -3:

$$\rho_h(t) = \rho_h(t_0) \cdot (a(t_0)/a(t))^3 \tag{7.55}$$

In the uniform scaling, each observer can measure an increase of a location vector $\vec{r}$ of an object according to the Hubble parameter H:

$$\dot{\vec{r}}(t) = H \cdot \vec{r} \tag{7.56}$$

The homogeneous part of the potential is determined so that Eq. (7.46) is obeyed. So we get:

$$\partial_{\vec{r}} \Phi_H = \frac{4\pi G}{3} \rho_h \vec{r} \tag{7.57}$$

We confirm the latter Eq. by applying the derivative $\partial_{\vec{r}}$, thereby we use the relation $\partial_{\vec{r}} \vec{r} = \partial x \cdot x + \partial y \cdot y + \partial z \cdot z = 3$, and so we recover Eq. (7.46). Next we derive Euler's equation for the case of an expanding space.

Euler's equation for a particle: For a particle of mass m, we apply Newton's second law of motion:

$$m \cdot \frac{d\vec{v}}{dt} = -\partial_{\vec{r}} \Phi \cdot m \tag{7.58}$$

We consider a moving object of mass m, volume V and density ρ. We derive the DEQ, for it we divide Eq. (7.58) by V:

$$\rho \cdot \frac{d\vec{v}}{dt} = -\partial_{\vec{r}} \Phi \cdot \rho \tag{7.59}$$

Next we introduce a velocity field $v(\vec{r},t) = v_1(\vec{r},t) + \dot{\vec{r}}(t)$. For it we apply the chain rule to the above Eq., and we divide by ρ:

$$\frac{d\vec{v}}{dt} = \frac{\partial \vec{v}}{\partial t} + \frac{\partial \vec{v}}{\partial \vec{r}} \cdot \frac{\partial \vec{r}}{\partial t} = -\partial_{\vec{r}}\Phi \tag{7.60}$$

DEQ for overdensities: We insert the velocity (see Eq. 7.56)

$$\vec{v} = \vec{v}_1 + H \cdot \vec{r} \tag{7.61}$$

into Eq. (7.60). Thereby we use that the term $\frac{\partial \vec{v}}{\partial \vec{r}}$ is dominated by the expansion $\frac{\partial H\vec{r}}{\partial \vec{r}}$:

$$\frac{\partial \vec{v}_1}{\partial t} + \frac{\partial H\vec{r}}{\partial t} + \frac{\partial H\vec{r}}{\partial \vec{r}} \cdot \frac{\partial \vec{r}}{\partial t} = -\partial_{\vec{r}}\Phi \tag{7.62}$$

The Hubble parameter varies very slowly as a function of time, compared to other changes in the system. So we get:

$$\frac{\partial H\vec{r}}{\partial t} = H \cdot \frac{\partial \vec{r}}{\partial t} = H \cdot \vec{v} \tag{7.63}$$

Moreover the Hubble parameter is homogeneous, so we obtain:

$$\frac{\partial H\vec{r}}{\partial \vec{r}} = H \cdot \frac{\partial \vec{r}}{\partial \vec{r}} \tag{7.64}$$

We separate the vector in the homogeneous part describing the expansion of space $\vec{r}_H$ and the part describing the location of an observed overdensity $\vec{r}_1$. So we get:

$$\frac{\partial H\vec{r}}{\partial \vec{r}} = H \cdot \frac{\partial (\vec{r}_H + \vec{r}_1)}{\partial \vec{r}} \tag{7.65}$$

Hereby the part $\vec{r}_1$ is negligible compared to the homogeneous part $\vec{r}_H$. Moreover, the homogeneous part is constituted by a radial component only, $\vec{r}_H = \vec{r}_{H,radial}$. The derivative $\frac{\partial \vec{r}_{H,radial}}{\partial \vec{r}}$ is equal to one, as the component orthogonal to the radial direction $\vec{r}_\perp$ is zero, and so we derive $\frac{\partial \vec{r}_{H,radial}}{\partial \vec{r}} = \partial_r \cdot r + \partial_\perp \vec{r}_\perp = 1 + 0 = 1$. Hence we get:

$$\frac{\partial H\vec{r}}{\partial \vec{r}} = H \cdot \frac{\partial \vec{r}_H}{\partial \vec{r}} = H \tag{7.66}$$

We insert the particular results in Eqs. (7.63, 7.66) into Eq. (7.62):

$$\frac{\partial \vec{v}_1}{\partial t} + H \cdot \vec{v} + H \cdot \frac{\partial \vec{r}}{\partial t} = -\partial_{\vec{r}} \Phi \tag{7.67}$$

Additionally we utilize $\frac{\partial \vec{r}}{\partial t} = \vec{v}$. So we get:

$$\frac{\partial \vec{v}_1}{\partial t} + 2H\vec{v} = -\partial_{\vec{r}} \Phi \tag{7.68}$$

Here we apply the derivative $\frac{\partial}{\partial \vec{r}}$:

$$\frac{\partial}{\partial t}\frac{\partial \vec{v}_1}{\partial \vec{r}} + 2H\frac{\partial \vec{v}_1}{\partial \vec{r}} = -\partial^2_{\vec{r}} \Phi \tag{7.69}$$

Here we apply the linear version of Euler's first Eq. (7.40):

$$\frac{\partial}{\partial t}\frac{-\dot{\rho}_1}{\rho_h} + 2H\frac{-\dot{\rho}_1}{\rho_h} = -\partial^2_{\vec{r}} \Phi \tag{7.70}$$

Next we apply $\frac{\dot{\rho}_1}{\rho_h} = \dot{\delta}$:

$$\ddot{\delta} + 2H\dot{\delta} = \partial^2_{\vec{r}} \Phi \tag{7.71}$$

As we describe the formation of structure in space, we apply the fluctuating part of the potential only:

$$\ddot{\delta} + 2H\dot{\delta} = \partial^2_{\vec{r}} \Phi_1 \tag{7.72}$$

Here we apply Eq. (7.47) as well as $\rho_1 = \rho_h \cdot \delta$. So we get:

$$\boxed{\ddot{\delta} + 2H\dot{\delta} = 4\pi G \cdot \rho_h \cdot \delta} \tag{7.73}$$

Linear growth factor $D(t)$ or $D_z(z)$: In general, the **overdensity** $\delta(\vec{x}, t)$ is a function of the position vector $\vec{x}$ and the time t. In the linear theory, that twofold dependence is factorized into a **linear growth factor** $D(t)$ and a spatial factor $\Delta(\vec{x})$ (see for instance (Reblinsky, 2000, p. 15), Fan et al. (1997), Kravtsov and Borgani (2012)). Accordingly an **overdensity at a time**

t is the overdensity at the actual time t_0 multiplied by the linear growth factor $D(t)$:

$$\boxed{\delta(\vec{x},t) = \frac{D(t)\cdot\delta(\vec{x},t_0)}{D(t_0)} \text{ with } D(t_0)=1} \tag{7.74}$$

Hereby we normalize the actual linear growth factor to one. We insert the above Eq. into Eq. (7.73):

$$\ddot{D} + 2H\dot{D} = 4\pi G\cdot\rho_h\cdot D(t) \tag{7.75}$$

7.3.1 Dynamics of $D(t)$

In this section we derive a general solution for the linear growth factor: The square of the Hubble parameter is the following function of the density:

$$H^2(a) = \frac{8\pi G}{3}\cdot\rho \tag{7.76}$$

We apply the FLE

$$H^2 = \frac{8\pi G}{3}\cdot\rho_0\cdot\left(\Omega_r\left(\frac{a_0}{a}\right)^4 + \Omega_m\left(\frac{a_0}{a}\right)^3 + \Omega_K\left(\frac{a_0}{a}\right)^2 + \Omega_v\right) \tag{7.77}$$

Hereby the density parameter Ω_K represents the curvature parameter k, observation shows $\Omega_K = 0.0027 \pm 0.0039$ ((Bennett et al., 2013, p. 1)), and we derive $\langle\Omega_K\rangle = 0$ (Carmesin (2020b)). Without loss of generality, we choose $a_0 = 1$, we apply $H_0^2 = \frac{8\pi G}{3}\cdot\rho_0$, and we calculate the derivative of H^2:

$$2H\dot{H} = H_0^2\cdot\frac{\dot{a}}{a}\cdot\left(-4\frac{\Omega_r}{a^4} - 3\frac{\Omega_m}{a^3} - 2\frac{\Omega_K}{a^2}\right) \tag{7.78}$$

We divide by $2H = 2\frac{\dot{a}}{a}$:

$$\dot{H} = H_0^2/2\cdot\left(-4\frac{\Omega_r}{a^4} - 3\frac{\Omega_m}{a^3} - 2\frac{\Omega_K}{a^2}\right) \tag{7.79}$$

We take the derivative:

$$\ddot{H} = H_0^2 H \cdot \left(8\frac{\Omega_r}{a^4} + \frac{9}{2}\frac{\Omega_m}{a^3} + 2\frac{\Omega_K}{a^2} \right) \tag{7.80}$$

We add Eqs. (7.78) and (7.80):

$$\ddot{H} + 2H\dot{H} = H_0^2 H \cdot \left(4\frac{\Omega_r}{a^4} + \frac{3}{2}\frac{\Omega_m}{a^3} \right) \tag{7.81}$$

We analyze the time after the formation of the CMB at $z \approx 1090$. This is much later than the time of matter radiation equality at $z = z_{eq} \approx 3400$. Accordingly, we may neglect the density of radiation:

$$\ddot{H} + 2H\dot{H} = H_0^2 H \cdot \frac{3}{2}\frac{\Omega_m}{a^3} \tag{7.82}$$

We apply $H_0^2 = \frac{8\pi G}{3} \cdot \rho_0$ and $\frac{\Omega_m \cdot \rho_0}{a^3} = \rho_m$:

$$\ddot{H} + 2H\dot{H} = 4\pi G \cdot H\rho_m \tag{7.83}$$

In the matter era considered here, we apply $\rho_h = \rho_m$ to Eq. (7.75). Moreover, we multiply by H:

$$H\ddot{D} + 2H^2\dot{D} = 4\pi G \cdot \rho_m \cdot DH \tag{7.84}$$

We subtract the above Eq. from D times Eq. (7.83):

$$D\ddot{H} - H\ddot{D} + 2H(\dot{H}D - H\dot{D}) = 0 \tag{7.85}$$

We multiply a^2:

$$a^2\frac{d}{dt}(D\dot{H} - H\dot{D}) + \frac{da^2}{dt}(\dot{H}D - H\dot{D}) = 0 \tag{7.86}$$

The above DEQ is equivalent to:

$$\frac{d}{dt}\left(a^2 H^2 \frac{d}{dt}\frac{D}{H} \right) = 0 \tag{7.87}$$

This can be verified by evaluating the derivatives. The solution is:

$$\boxed{D(t) = H(t) \cdot \int \frac{dt}{a^2 H^2}} \tag{7.88}$$

This can be verified by inserting into the DEQ and by evaluating the derivatives.

Alternative $D(a)$: We express the above quantities as a function of the scaling radius a. For it we solve $H = \frac{da}{dt}\frac{1}{a}$ for dt, $dt = da \cdot \frac{1}{H \cdot a}$, and we apply this term to the above Eq.:

$$\boxed{D(a) = H(a) \cdot \int \frac{da}{a^3 H^3}} \tag{7.89}$$

Alternative $D(z)$: Next we express the above quantities as a function of the redshift z.

$$\frac{1}{x} = \frac{a_0}{a} = \frac{\lambda_0}{\lambda} = \frac{\lambda_0 - \lambda}{\lambda} + 1 = z + 1, \tag{7.90}$$

With it we analyze:

$$H(x) \cdot x = \frac{d}{dt}x = \frac{dz}{dt}\frac{d}{dz}a = \frac{dz}{dt}\frac{d}{dz}\frac{1}{z+1} = \frac{dz}{dt}\frac{-1}{(z+1)^2} \tag{7.91}$$

Here we apply $H(x) \cdot x = H(z)/(z+1)$, and we solve for dt:

$$dt = dz \cdot \frac{-1}{(1+z) \cdot H(z)} \tag{7.92}$$

We apply this Eq. to Eq. (7.88):

$$D(z) = -H(z) \cdot \int d\zeta \, \frac{1+\zeta}{H^3(\zeta)} \tag{7.93}$$

Here the integral starts at $z(a)$ and ends at $z(a_0) = 0$. We exchange these boundaries and multiply by -1:

$$\boxed{D(z) = H(z) \int_0^z d\zeta \, \frac{1+\zeta}{H^3(\zeta)}} \tag{7.94}$$

7.3.2 Linear dynamics of σ_R

In this section we apply the linear growth factor (Eq. 7.94) to the standard deviation of matter fluctuations $\sigma_R^2(t)$ (Eqs. 7.5, 7.6) and to the amplitude of matter fluctuations σ_8.

For it, we apply Eq. (7.94) to Eq. (7.74):

$$\delta(\vec{x}, z) = D(z) \cdot \delta(\vec{x}, z = 0) \tag{7.95}$$

We divide by $D(z)$:

$$\delta(\vec{x}, z)/D(z) = \delta(\vec{x}, z = 0) \tag{7.96}$$

Next we apply the window function Eq. (7.4):

$$\delta_R(\vec{x}, z)/D(z) = \int \delta(\vec{x} - \vec{r}, z = 0) \cdot W_R(\vec{r}) d^3r = \delta_R(\vec{x}, z = 0) \tag{7.97}$$

Using this Eq., we derive the variance (Eq. 7.5) by squaring and averaging:

$$\langle \delta_R^2(\vec{x}, z = 0) \rangle = \langle \delta_R^2(z = 0) \rangle = \langle \delta_R^2(z) \rangle / D(z)^2 \tag{7.98}$$

We identify the above term with the squared standard deviation of matter fluctuations (Eq. 7.6):

$$\langle \delta_R^2(z) \rangle / D(z)^2 = \sigma_R^2(z = 0) \tag{7.99}$$

We apply this result to $R = R_8$. So we obtain the square of the amplitude of matter fluctuations:

$$\langle \delta_{R_8}^2(z) \rangle / D(z)^2 = \sigma_8^2 \tag{7.100}$$

Thus the amplitude of matter fluctuations is proportional to the inverse of the linear growth factor (see for instance Fan et al. (1997), Reblinsky (2000)):

$$\boxed{\frac{1}{D(z)} \cdot \sqrt{\langle \delta_{R_8}^2(z) \rangle} = \sigma_8} \tag{7.101}$$

7.3.3 Fluctuations at the CMB

Smoot et al. (1992) estimated the temperature fluctuation of the CMB:

$$\frac{\Delta T}{T} = 11 \cdot 10^{-6} \tag{7.102}$$

According to the Planck distribution, the density ρ is proportional to T^4, so we derive:

$$\Delta\rho = \frac{\partial\rho}{\partial T}\Delta T = 4 \cdot \frac{\Delta T}{T} \cdot \rho \tag{7.103}$$

Thus we get the overdensity:

$$\delta(z = 1090) = \frac{\Delta\rho}{\rho} = 4 \cdot \frac{\Delta T}{T} = 0.44 \cdot 10^{-4} \tag{7.104}$$

7.3.4 Estimates for a linear growth factor

In this section we derive an estimate for the linear growth factor $D(z = 1090)$ describing the growth of the overdensity $\delta(Z = 1090)$ of the CMB (Eq. 7.104) until its actual value σ_8.

Nonlinear effects: The linear growth factor that we introduced to small overdensities has been generalized to small and large overdensities (see for instance Navarro et al. (1997)). Thereby a local collapse occurs at overdensities $\delta(\vec{x}) = \delta_c \approx 1.688$ (for instance (Reblinsky, 2000, p. 19)).

In order to obtain a realistic value, we apply the measurement of $\sigma_8 = 0.8111$ obtained by Collaboration (2020). We derive an estimate by using Eq. (7.101):

$$\frac{1}{D(z)} \cdot \sqrt{\langle \delta^2_{R_8}(z) \rangle} = \sigma_8 \tag{7.105}$$

We solve for $\frac{1}{D(z)}$:

$$\frac{1}{D(z)} = \frac{\sigma_8}{\delta_{R_8}(z)} \tag{7.106}$$

Hereby we use $\delta_{R_8}(z = 1090) = 0.44 \cdot 10^{-4}$ (Eq. 7.104). So we get:

$$\frac{1}{D(z = 1090)} = \frac{0.8111}{0.44 \cdot 10^{-4}} = 18434 \tag{7.107}$$

We summarize:

Based on the observations $\sigma_8 = 0.8111$ (Collaboration (2020)) and $\delta_{R_8}(z = 1090) = 0.44 \cdot 10^{-4}$ (Eq. 7.104 and Smoot et al. (1992)), we derive an increase of the overdensities of the CMB until today by the factor 18434.

7.3.5 Relation of H_0 and $D(z)$

In this section we derive a relation between H_0 and $D(z)$. Later we will use that relation in the following context: Firstly, we improve our model of the dark energy by deriving an equation for vacuum density $\rho_\Lambda(z)$ as a function of the redshift. Secondly, we apply that density $\rho_\Lambda(z)$ in order to derive an equation for Hubble constant $H_0(z)$ as a function of the redshift. Thirdly, we apply that function $H_0(z)$ in order to derive a correction factor $D_{corr}(z)$ for the linear growth factor. Fourthly, with it we derive a term for the amplitude of matter fluctuations $\sigma_8(z)$ as a function of the redshift.

Relation: In order to derive a term for the Hubble parameter, we apply Eq. (2.28 in Carmesin (2019b)), thereby we use the convention $a_0 = 1$ and $x = a/a_0 = 1/(z+1)$:

$$H(z) = H_0 \cdot (z+1)^2 \cdot \sqrt{\Omega_r + \frac{\Omega_m}{z+1} + \frac{\Omega_v}{(z+1)^4}} \tag{7.108}$$

We apply this Eq. to the DEQ (7.94):

$$D(z) = \frac{(z+1)^2 \cdot \sqrt{\Omega_r + \frac{\Omega_m}{z+1} + \frac{\Omega_v}{(z+1)^4}}}{H_0^2} \cdot I(z) \tag{7.109}$$

Hereby $I(z)$ represents the following integral:

$$I(z) = \int_0^z \frac{d\zeta}{(\zeta+1)^5 \cdot \sqrt{\Omega_r + \frac{\Omega_m}{\zeta+1} + \frac{\Omega_v}{(\zeta+1)^4}}^3} \tag{7.110}$$

Correction factor $D_{corr}(z)$: If the Hubble constant H_0 is replaced by a function $H_0(z)$, whereas all other factors in the term for $D(z)$ in Eq. (7.109) remain unchanged, then $D(z)$ is multiplied by the following correction factor:

$$\boxed{D_{corr}(z) = \frac{H_0^2}{H_0^2(z)}} \tag{7.111}$$

7.3.6 Linear dynamics for small fluctuations

As the CMB formed in the matter era, we analyze the case $\Omega_m = 1$, the ideal matter era: In that case the scale radius a exhibits the following power law:

$$x = a/a_0 = (t/t_0)^{\frac{2}{3}} \tag{7.112}$$

With it we derive:

$$\dot{x} = \frac{2}{3}(t/t_0)^{-\frac{1}{3}} = \frac{2}{3}x^{-\frac{1}{2}}, \quad H = \frac{2}{3}(t/t_0)^{-1} = \frac{2}{3}x^{-\frac{3}{2}} = \frac{2}{3}(1+z)^{\frac{3}{2}} \tag{7.113}$$

We apply this term to the DEQ (7.94):

$$D(z) = \frac{9}{4}(1+z)^{\frac{3}{2}} \cdot \int_0^z d\zeta\,(1+\zeta)^{-\frac{7}{2}} = \frac{9}{10}(1+z)^{-1} \tag{7.114}$$

7.4 Probes

In this part we present essential probes at corresponding redshifts z that can be used in order to measure H_0 and σ_8. These measurement probes have been taken by various groups or huge collaborations of astronomers all over the world. With an enormous effort, they achieved very accurate recordings at very different redshifts. We describe typical results of such measurements.

7.4.1 Probes providing values of H_0

In this section we summarize probes that form at a redshift z_{probe} and that are particularly appropriate in order to measure a corresponding value of the Hubble constant $H_0(z_{probe})$.

Distance ladder and observed galaxies: Riess et al. (2019) measured H_0 from the redshift z and distance of observed galaxies. Thereby the distance has been obtained by using the so-called distance ladder (Howard (2011)). The used sample of galaxies has redshifts in the range $z \in [0.023, 0.15]$ (Riess et al. (2016), (Riess et al., 2019, p. 16)).

Observed baryonic acoustic oscillations: Alam et al. (2017) and Blomquist et al. (2019) as well as Gil-Marin et al. (2016) and many others observed baryonic acoustic oscillations and derived a value of H_0 therefrom. Alam et al. (2017) used probes in an interval $z \in [0.2, 0.75]$ of small redshifts, and they obtained $H_0 = 67.6 \frac{\text{km}}{\text{s·Mpc}} \pm 0.5$. Blomquist et al. (2019) used probes in the interval $z \in [1.77, 3.5]$, and they measured $H_0 = 68.7 \frac{\text{km}}{\text{s·Mpc}} \pm 1.45$. Similarly, Gil-Marin et al. (2016) probed an interval with high redshifts, $z \in [0.8, 2.2]$. They obtained $H_0 = 63.3 \frac{\text{km}}{\text{s·Mpc}} \pm 2.8$. We combine the last two observations, and so we get $z \in [0.8, 3.5]$ and $H_0 = 66 \frac{\text{km}}{\text{s·Mpc}} \pm 2.1$.

7.4.2 Probes providing values of σ_8

In this section we summarize probes that form at a redshift z_{probe} and that are particularly appropriate in order to measure a corresponding value of the amplitude of matter fluctuations $\sigma_8(z_{probe})$.

CMB: The CMB represents a probe emitted $z = 1090$ and provides very precise information about the fluctuations in the early universe ((Collaboration, 2020, p. 16)).

Weak gravitational lenses: The weak gravitational lenses represent a probe that corresponds to quite typical masses ((Lu and Haiman, 2020, p. 1, 2)), in contrast to strong gravitational lenses. Thereby, (Lu and Haiman, 2020, p. 1, 2) achieved low statistical errors by observing and using approximately 4.2 million galaxies.

Galaxy clustering: The clustering of galaxies has been evaluated by applying three different correlation functions to 26 million galaxies ((Abbott et al., 2019, p. 6, 15)). So the combined result provides a σ_8 value based on relatively extensive observations.

Baryon acoustic oscillations: (Tröster et al., 2020, p. 1, 2) analyzed 1.2 million galaxies of the data release 12 of the 'baryon oscillation spectroscopic survey' (Alam et al. (2017)) in the framework of the power spectrum $P(k)$. So an estimation of σ_8 at a relatively low redshift $z = z_{probe} = 0.475$ has been obtained.

7.4.3 Further probes

In this section we summarize further probes.

Observed strong gravitational lenses: Wong et al. (2019) summarized measurements of H_0 that are based on six quasars, each observed through a corresponding gravitational lens (Fig. 7.1). These probes have an exceptionally high mass, as they are gravitational lenses. So the local vacuum exhibits an unusually high density. The data are systematically above the theoretical dotted curve in Fig. (7.1). Moreover, the data show the typical increase of H_0 for the case of decreasing z, see dashdotted curve in Fig. (7.1), showing a regression that is linear at the logarithmic scale, and that has a correlation coefficient of 0.925. Altogether, these data provide additional evidence for the theoretical curve (dotted, representing the average over the

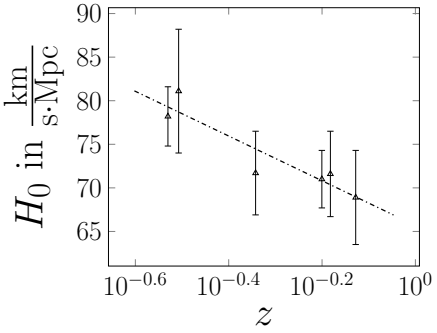

Figure 7.1: H_0 as a function of the redshift z of the probe. Probes: Six strong gravitational lenses (exceptionally high mass, local vacuum and H_0) ($\triangle$, Wong et al. (2019)). Regression for lenses (dashdotted). As strong gravitational lenses exhibit untypical overdensities, they are not included in the present analysis of typical overdensities.

typical vacuum) as well as for the increase of the late and local H_0 value for probes with exceptionally high mass.

7.5 Dark energy: theory II: time evolution

In this section we start with the semiclassical theory I of dark energy in Sect. (6.6). In that theory the space is filled with the densities ρ_Λ of the vacuum. As a result of that theory I, the density of the vacuum does not vary with the time.

In this section, we supplement that theory I with the homogeneous densities of matter $\rho_{m,h}$ and of radiation $\rho_{r,h}$, as well as with the overdensities of matter, $\rho_{m,h} \cdot \delta(\vec{r})$, see Fig. (7.2). We do not model the overdensities of radiation, as these are too small in order to show an essential effect.

As results we will derive the time evolution of the density $\rho_\lambda(t)$ or $\rho_\lambda(z)$. As a consequence, we will derive the time evolution of the Hubble constant $H_0(t)$ or $H_0(z)$, as well as the time evolution of the amplitude of matter fluctuations $\sigma_8(t)$ or $\sigma_8(z)$. With it we will find a precise accordance with observations.

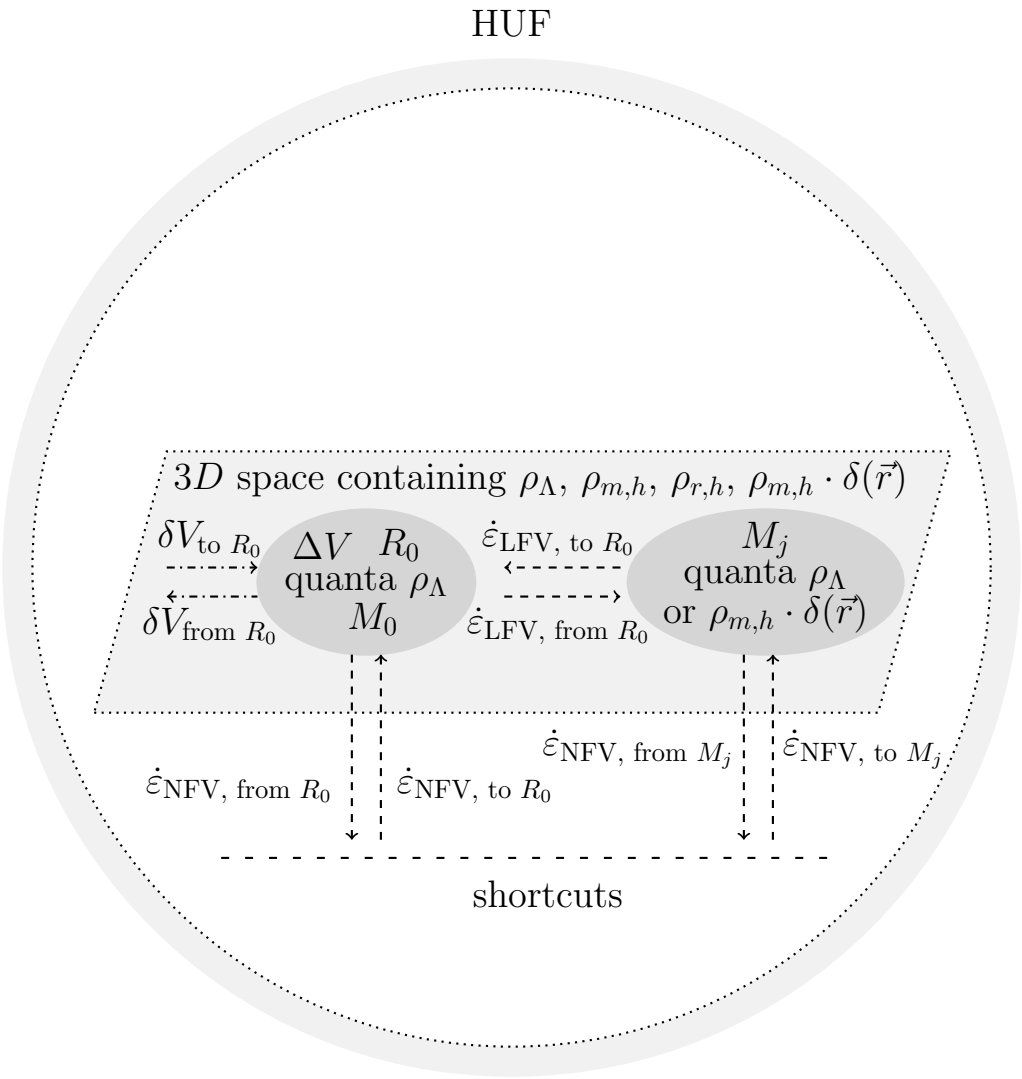

Figure 7.2: Overview of propagation of semiclassical rates in $3D$ space and in shortcuts corresponding to space in other dimensions. Thereby overdensities $\rho_{m,h} \cdot \delta(\vec{r})$ or quanta of vacuum such as M_j emit quantized RGWs of vacuum with unidirectional quadrupolar symmetry. In contrast, the homogeneous vacuum of matter $\rho_{m,h}$ and radiation $\rho_{m,h}$ is characterized by an isotropic formation of vacuum with zero localized field $\vec{G}^*$ and rate $\dot{\varepsilon}$.

7.5.1 Rates of RGWs in the heterogeneous universe

In this section we derive the rates $\dot{\varepsilon}_{\text{propagating to } R_0}$ of the vacuum ρ_Λ for the case of a heterogeneous universe.

For it we analyze the RGWs that propagate to a location R_0, see Eq. (6.70). Hereby we analyze the density ρ as a function of the distance R to R_0. So we obtain:

$$\dot{\varepsilon}_{\text{propagating to } R_0} = \frac{4\pi \cdot G}{c} \cdot \int_{R_{lh,limit}}^{R_H} \rho(R) dR \tag{7.115}$$

The heterogeneity became essential in the matter era. So we need not analyze the density of radiation. Hence the densities of the vacuum and of matter are essential. For the case of the heterogeneous universe we get:

$$\rho(R) = \rho_{\Lambda,const.} + \rho_m(R) \tag{7.116}$$

Overdensity: We express the density of matter by using the homogeneous part of the density $\rho_{m,h}$, the overdensity $\rho_{m,1}(R)$ and the relative overdensity $\delta\rho_m(R)$ as follows (see Eqs. 7.1, 7.2):

Hereby, the overdensity of matter $\delta\rho_m(R)$ is presumably large compared to a possible overdensity of ρ_Λ. Thus the density is characterized as follows:

$$\rho_m(R) = \rho_{m,h} + \rho_{m,h} \cdot \frac{\rho_m(R) - \rho_{m,h}}{\rho_{m,h}} = \rho_{m,h} + \rho_{m,h} \cdot \delta(R) \tag{7.117}$$

Window function and standard deviation: We apply the usual statistical tools: a window function with the radius R_8 and the standard deviation (see Sect. 7.1). So we obtain:

$$[\delta(R)]^2 \hat{=} \langle \delta_{R_8}^2 \rangle = \sigma_{R_8}^2 \tag{7.118}$$

The corresponding value at the actual time $t = t_0$ or at the redshift $z = 0$ is the amplitude of matter fluctuations σ_8 (see Sect. 7.1):

$$\sigma_8 = \sigma_{R_8,t=t_0} = \sigma_{R_8,z=0} \tag{7.119}$$

Evolution of $\sigma_{R_8,z}$: In the linear theory, the evolution of $\sigma_{R_8,z}$ as a function of the redshift is expressed with help of the linear growth factor $D(z)$ as follows: (Eq. 7.101):

$$\sqrt{\langle \delta^2_{R_8}(z) \rangle} = \sigma_8 \cdot D(z) \tag{7.120}$$

With it the density of matter corresponds to the following statistical term (Eq. 7.117):

$$\rho_m(R) \hat{=} \rho_{m,h} + \rho_{m,h} \cdot \sigma_8 \cdot D(z) \tag{7.121}$$

Evolution of $D(z)$ or $D(x)$: We use the evolution of the **linear growth factor** as a function of the redshift z (Eq. 7.114):

$$D(z) = \frac{9}{10} \cdot (1+z)^{-1} \tag{7.122}$$

Moreover we use the **linear growth factor** as a function of the scaled radius:

$$D(x) = \frac{9}{10} \cdot x \quad \text{with} \quad x = \frac{R}{R_H} = \frac{1}{1+z} \tag{7.123}$$

Two separate rates: We apply the above density (Eq. 7.121) and the **linear growth factor** (Eq. 7.123) to Eq. (7.116):

$$\rho(R) = \rho_{\Lambda,const.} + \rho_{m,h} + \rho_{m,h} \cdot \sigma_8 \cdot D(x) \tag{7.124}$$

The homogeneous density of matter exhibits an isotropic formation of vacuum, a corresponding isotropic quadrupolar factor and fields as well as rates of the RGWs that are zero. So the propagating rates of the RGWs are as follows:

$$\dot{\varepsilon}_{\text{LFV, to } R_0 \text{ from } \rho_\Lambda} = \frac{4\pi \cdot G}{c} \cdot \int_{R_{lh,limit}}^{R_H} \rho_{\Lambda,const.} dR \tag{7.125}$$

The rate originating from the homogeneous part vanishes. The rate originating from the heterogeneous part is formed similarly:

$$\dot{\varepsilon}_{\text{LFV, to } R_0 \text{ from } \delta_{R_8}} = \frac{4\pi \cdot G}{c} \cdot \int_{R_{lh,limit}}^{R_H} \rho_{m,h} \cdot \sigma_8 \cdot D(x) dR \tag{7.126}$$

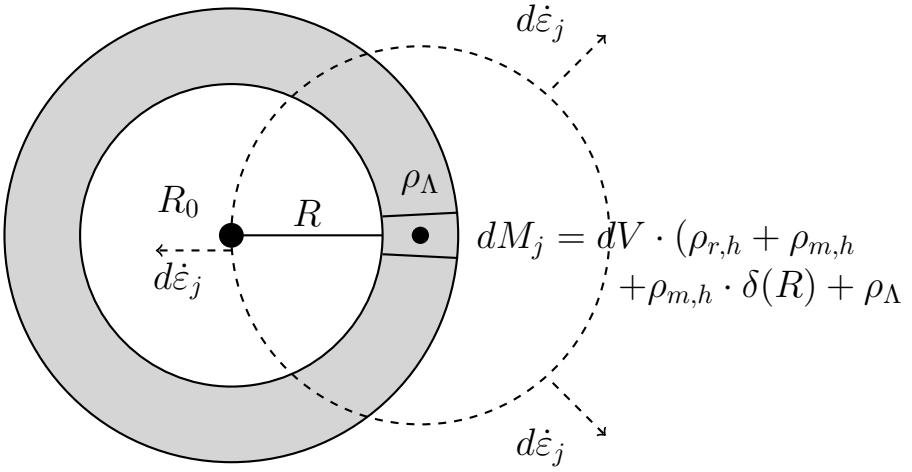

Figure 7.3: The density ρ in an area at a distance R from R_0 has a dynamic mass M_j. It generates rates $d\dot{\varepsilon}_j$ propagating to all directions.

Averages of rates: We derive the average of the rates originating from the matter fluctuations. For it we substitute $x = R/R_H$. Moreover we analyze the integral of the rates from $x = 0$ to a maximum x:

$$\dot{\varepsilon}_{q,\text{LFV, to } R_0 \text{ from } \delta_{R_8}}(x) = \frac{4\pi G \rho_{m,h} \sigma_8 R_H}{c} \cdot \int_0^x D(\xi) d\xi \quad (7.127)$$

We insert $D = 9/10 \cdot \xi$:

$$\dot{\varepsilon}_{q,\text{LFV, to } R_0 \text{ from } \delta_{R_8}}(x) = \frac{4\pi G \rho_{m,h} \sigma_8 R_H}{c} \cdot \frac{9}{20} x^2 \quad (7.128)$$

We apply $\rho_{m,h} = \rho_{\Lambda,const.} \frac{\Omega_m}{\Omega_\Lambda}$. So we get:

$$\dot{\varepsilon}_{q,\text{LFV, to } R_0 \text{ from } \delta_{R_8}}(x) = \frac{4\pi G \rho_{\Lambda,const.} R_H}{c} \cdot \frac{\Omega_m}{\Omega_\Lambda} \sigma_8 \frac{9}{20} x^2 \quad (7.129)$$

We identify the first fraction with the rate originating from the vacuum, see Eq. (7.125):

$$\dot{\varepsilon}_{q,\text{LVF, to } R_0 \text{ from } \rho_\Lambda} = \frac{4\pi G \cdot R_H \cdot \rho_{\Lambda,const.}}{c} \quad (7.130)$$

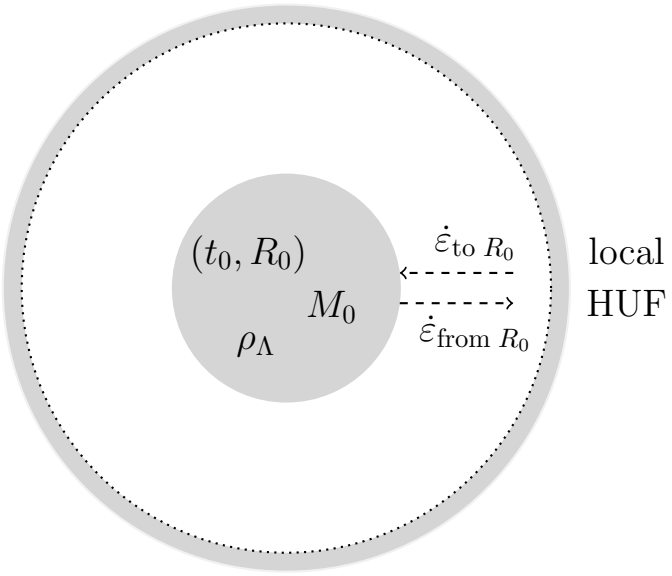

Figure 7.4: RGWs propagating to and from R_0 with dynamical mass M_0 constituted by ρ_Λ.

We abbreviate the remaining factor by κ and express it as a function of x or $z+1=1/x$:

$$\boxed{\kappa = \frac{\Omega_m}{\Omega_\Lambda} \cdot \sigma_8 \cdot \frac{9}{20} \cdot x^2 = \frac{\Omega_m}{\Omega_\Lambda} \cdot \sigma_8 \cdot \frac{9}{20} \cdot \frac{1}{(1+z)^2}} \tag{7.131}$$

So we get:

$$\dot{\varepsilon}_{q,\text{LFV, to } R_0 \text{ from } \delta_{R_8}}(x) = \dot{\varepsilon}_{q,\text{LFV, to } R_0 \text{ from } \rho_\Lambda} \cdot \kappa \tag{7.132}$$

Altogether we derive the sum of both RGWs:

$$\boxed{\dot{\varepsilon}_{q,\text{LFV, to } R_0} = \dot{\varepsilon}_{q,\text{LFV, to } R_0 \text{ from } \rho_\Lambda} \cdot (1+\kappa)} \tag{7.133}$$

7.5.2 Density of RGWs propagating from R_0

In this section we analyze the RGWs that propagate from a small region at R_0 that is placed in a small HUF, and that has a dynamical mass M_0 constituted by the density of vacuum ρ_Λ (see Fig. 7.4).

The density of the field generated by M_0 is related to the rate according to theorem (17):

$$\rho_f = \frac{\dot{\varepsilon}^2_{\text{LFV, from } R_0}}{8\pi \cdot G} \tag{7.134}$$

That density must be equal to the density of the LFV of the vacuum, $\rho_f = \rho_{\Lambda,LFV}$. That density of the LFV is one half of the density of the CFV, $\rho_{\Lambda,LFV} = \rho_{\Lambda,CFV}/2$. Altogether we obtain:

$$\rho_f = \rho_{\Lambda,LFV} = \frac{1}{2} \cdot \rho_{\Lambda,CFV} = \frac{\dot{\varepsilon}^2_{\text{LFV, from } R_0}}{8\pi \cdot G} \tag{7.135}$$

7.5.3 Equality of rates

In a stationary state, the rate of the RGWs propagating to M_0 is equal to the rate of the RGWs propagating from M_0:

$$\dot{\varepsilon}_{\text{LFV, from } R_0} = \dot{\varepsilon}_{\text{LFV, to } R_0} \tag{7.136}$$

We apply that equality to our result in Eq. (7.135):

$$\frac{1}{2} \cdot \rho_{\Lambda,CFV} = \frac{\dot{\varepsilon}^2_{\text{LFV, to } R_0}}{8\pi \cdot G} \tag{7.137}$$

We insert Eqs. (7.133 and 6.72):

$$\frac{1}{2} \cdot \rho_{\Lambda,CFV} = \frac{8\pi G \cdot 2\pi G \cdot R_H^2}{8\pi G \cdot c^2} \cdot \rho^2_{\Lambda,const.} \cdot (1+\kappa)^2 \tag{7.138}$$

We cancel, and we apply the approximation of a homogeneous density $\rho_{\Lambda,h}$ of the vacuum, $\rho_{\Lambda,CFV} = \rho_{\Lambda,h}$. So we derive:

$$\frac{1}{2} \cdot \rho_{\Lambda,h} = \frac{2\pi G \cdot R_H^2}{c^2} \cdot \rho^2_{\Lambda,h} \cdot (1+\kappa)^2 \tag{7.139}$$

We solve for $\rho_{\Lambda,h}$:

$$\boxed{\rho_{\Lambda,h} = \frac{c^2}{4\pi \cdot G \cdot R_H^2} \cdot (1+\kappa)^2} \tag{7.140}$$

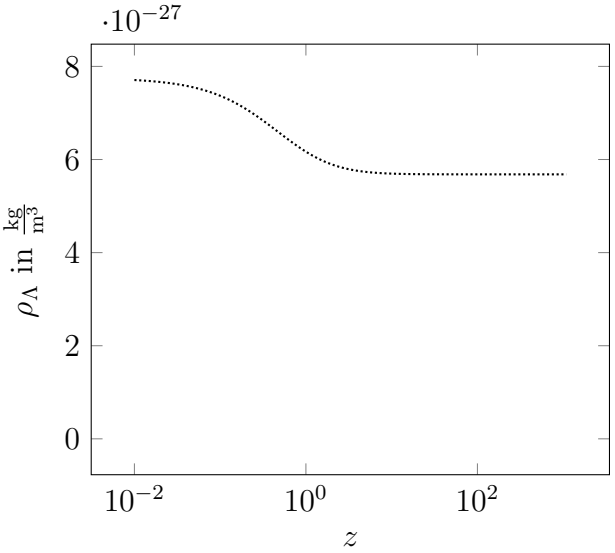

Figure 7.5: $\rho_\Lambda(z)$ as a function of the redshift of the probe.

We identify the fraction in the above Eq. by $\rho_{\Lambda,const.}$ (Eq. 6.79). So we obtain:

$$\boxed{\rho_{\Lambda,h} = \rho_{\Lambda,const.} \cdot (1+\kappa)^2} \tag{7.141}$$

That density is shown as a function of the redshift in Fig. (7.5).

7.5.4 Time evolution of $H_0(t)$

In this section we derive the Hubble constant $H_0(t)$ that is observed on the basis of probes of radiation emitted at a scaled radius x or at a corresponding redshift $z = 1/x - 1$. Thereby the density of radiation can be neglected in the matter era, $\rho_r/(\rho_m + \rho_\Lambda) << 1$. The Hubble constant is a function of the density:

$$H_0^2(t_0, R_0) = \frac{8\pi G}{3} \cdot (\rho_m + \rho_\Lambda(t_0, R_0)) \tag{7.142}$$

We insert the density of the vacuum (Eq. 7.141):

$$H_0^2(t_0, R_0, x) = \frac{8\pi G}{3} \cdot [\rho_m + \rho_{\Lambda,const.} \cdot (1+\kappa(x))^2] \tag{7.143}$$

As $\kappa(x)$ is proportional to x^2, a measurement based on probes emitted at $x \approx 0$ yield the following Hubble constant:

$$H_0^2(t_0, R_0, x = 0) = \frac{8\pi G}{3} \cdot [\rho_m + \rho_{\Lambda,const.}] \tag{7.144}$$

Fraction of measured H_0 values: In order to obtain a comparison, we derive the fraction of the squares of observed H_0 values.

$$\frac{H_0^2(t_0, R_0, x)}{H_0^2(t_0, R_0, x = 0)} = \frac{\rho_m + \rho_{\Lambda,const.} \cdot (1 + \kappa(x))^2}{\rho_m + \rho_{\Lambda,const.}} \tag{7.145}$$

Here we use the density parameters $\Omega_m = \frac{\rho_m}{\rho_m + \rho_{\Lambda,const.}}$ and $\Omega_\Lambda = \frac{\rho_{\Lambda,const.}}{\rho_m + \rho_{\Lambda,const.}}$:

$$\frac{H_0^2(t_0, R_0, x)}{H_0^2(t_0, R_0, x = 0)} = \Omega_m + \Omega_\Lambda \cdot (1 + \kappa(z))^2 \tag{7.146}$$

We use the following approximation that is very close to exactness:

$$H_0^2(t_0, R_0, x = 0) \hat{=} H_0^2(t_0, R_0, z = 1090) \tag{7.147}$$

So we derive:

$$\frac{H_0^2(t_0, R_0, z)}{H_0^2(t_0, R_0, z = 1090)} = \Omega_m + \Omega_\Lambda \cdot (1 + \kappa(z))^2 \tag{7.148}$$

We solve for $H_0(t_0, R_0, z)$:

$$\boxed{H_0(t_0, R_0, z) = H_0(t_0, R_0, z = 1090) \cdot \sqrt{\Omega_m + \Omega_\Lambda \cdot (1 + \kappa)^2}} \tag{7.149}$$

The resulting evolution is shown in Fig. (7.6).

7.5.5 Explanation of discrepancy between H_0-values

In this section, we compare the H_0-value based on the distance ladder and probing at $z = 0.0865$ with the H_0-value based on the CMB and probing at $z = 1090$. These values exhibit a highly significant difference, and we show that our theory explains that difference.

Probe at $z = 0.0865$: The value at $z = 0.0865$ is as follows (Riess et al. (2019)): $H_{0,\text{ distance ladder}} = 74.03 \pm 1.42 \frac{\text{km}}{\text{Mpc·s}}$

Probe at $z = 1090$: At $z = 1090$ the following values have been obtained (Collaboration (2020)): The most direct evaluation utilizes only the **temperature power spectra, TT**. Collaboration (2020) emphasized a so-called **baseline** evaluation including TT-, TE-, and EE-spectra of the CMB as well as gravitational lensing. The observations of the Hubble constant are as follows:

$$H_{0,CMB}(z = 1090) = \begin{cases} 66.88 \pm 0.92 \, \frac{\text{km}}{\text{Mpc·s}} & \text{TT} \\ 67.39 \pm 0.54 \, \frac{\text{km}}{\text{Mpc·s}} & \text{baseline} \end{cases} \tag{7.150}$$

The density parameter observations are as follows:

$$\Omega_{\Lambda,CMB}(z = 1090) = \begin{cases} 0.679 \pm 0.013 & \text{TT} \\ 0.6858 \pm 0.0074 & \text{baseline} \end{cases} \tag{7.151}$$

The amplitudes of matter fluctuations σ_8 are as follows:

$$\sigma_{8,CMB}(z = 1090) = \begin{cases} 0.811 \pm 0.0089 & \text{TT} \\ 0.8091 \pm 0.006 & \text{baseline} \end{cases} \tag{7.152}$$

Results of the *dark energy theory II*: Using the results of one probe at one redshift z, our theory can predict the value of $H_0(z)$ that should be measured by another probe at another redshift z. Using the above results measured at $z = 1090$ (that redshift corresponds to the CMB probe), the theory predicts the values at all redshifts z, see the densely dotted line in Fig. (7.6).

Using the above errors of measurement at $z = 1090$, the theory predicts the corresponding values at all redshifts z, see the loosely dotted line in Fig. (7.6). That Fig. (7.6) shows a precise accordance between the measurements at very different redshifts and the *dark energy theory II*. Hence the theory explains the highly significant difference:

$$\Delta H_0 = H_{0,CMB}(z = 1090) - H_{0,\text{ distance ladder}}(z = 0.0865) \tag{7.153}$$

$$\Delta H_0 = \begin{cases} -7.15 \pm 2.34 \, \frac{\text{km}}{\text{Mpc·s}} & \text{TT} \\ -6.64 \pm 1.96 \, \frac{\text{km}}{\text{Mpc·s}} & \text{baseline} \end{cases} \tag{7.154}$$

Moreover, we realize an especially accurate accordance at $z = 0.0865$. That interesting accordance is investigated numerically: Using our *dark energy theory II*, one derives the following value for $z = 0.0865$:

$$H_{0,\text{ theory}}(t_0, R_0, z = 0.0865) = \begin{cases} 73.77 \pm 1.39 \frac{\text{km}}{\text{Mpc·s}} & \text{TT} \\ 74.053 \pm 1.09 \frac{\text{km}}{\text{Mpc·s}} & \text{baseline} \end{cases} \tag{7.155}$$

Obviously these results of the *dark energy theory II* are very close to the observed value $74.03 \frac{\text{km}}{\text{Mpc·s}}$. That is made explicit in terms of the percentage:

$$\frac{H_{0,\text{ theory}}(t_0, R_0, z) - H_{0,\text{ distance ladder}}}{H_{0,\text{ distance ladder}}} \begin{cases} -0.353\% & \text{TT} \\ 0.03\% & \text{baseline} \end{cases} \tag{7.156}$$

Indeed, the *dark energy theory II* provides a very precise accordance with measurements, achieving even 0.03% in one case. Altogether, the *dark energy theory II* explains the highly significant difference (Eq. 7.154) between H_0-values taken at the early universe and at the late universe. This explanation and the precise accordance provide a clear evidence for the *dark energy theory II*.

7.5.6 Evolution of $\sigma_8(t)$

In this section we derive the evolution of the matter fluctuations σ_8 as a function of the redshift z or of the time t. We express it by $\sigma_{8,corrected}(z)$.

For it we apply the linear growth factor (see Eq. (7.106):

$$\sigma_8 = \frac{\delta_{R_8}(z)}{D(z)} \tag{7.157}$$

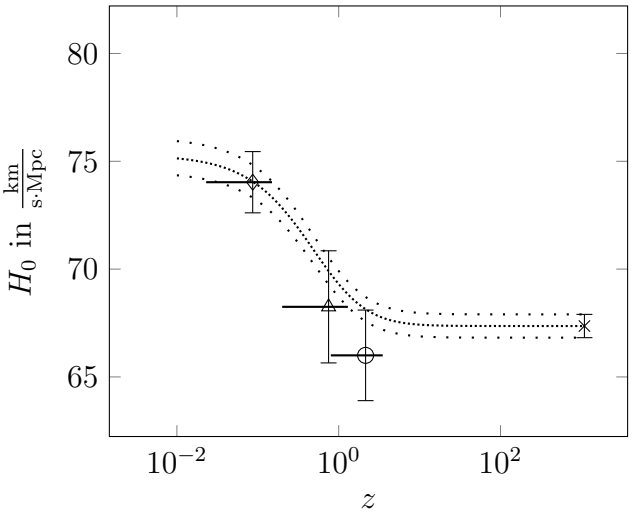

Figure 7.6: H_0 as a function of the redshift z of the probe: distance ladder ($\diamond$, Riess et al. (2019)), BAO (o, Blomquist et al. (2019)), weak gravitational lensing (Δ, Lu and Haiman (2020)), CMB ($\times$, Collaboration (2020)). Theory of the vacuum (dotted) and by using the parameters Ω_Λ, σ_8 and H_0 plus or minus the 68 % limits (Collaboration (2020)) (loosely dotted).

We improve that term by the correction factor in Eq. (7.111):

$$\sigma_{8,corrected}(z) = \frac{\delta_{R_8}(z)}{D(z) \cdot D_{corr}(z)} = \frac{\sigma_8}{D_{corr}(z)} \tag{7.158}$$

Here we insert the correction factor in Eq. (7.111):

$$\sigma_{8,corrected}(z) = \sigma_8 \cdot \left(\frac{H_0}{H_0(z)} \right)^2 \tag{7.159}$$

We use the reference values of the CMB at $z = 1090$, and we insert Eq. (7.148). So we get:

$$\boxed{\sigma_{8,corrected}(z) = \frac{\sigma_8(z = 1090)}{\Omega_m + \Omega_\Lambda \cdot (1 + \kappa(z))^2}} \tag{7.160}$$

The resulting function $\sigma_{8,corrected}(z)$ is shown in Fig. (7.7).

In summary, the *dark energy theory II* explains the highly significant difference between σ_8-values taken at the early universe and at the late universe, see Fig. (7.7). Moreover the

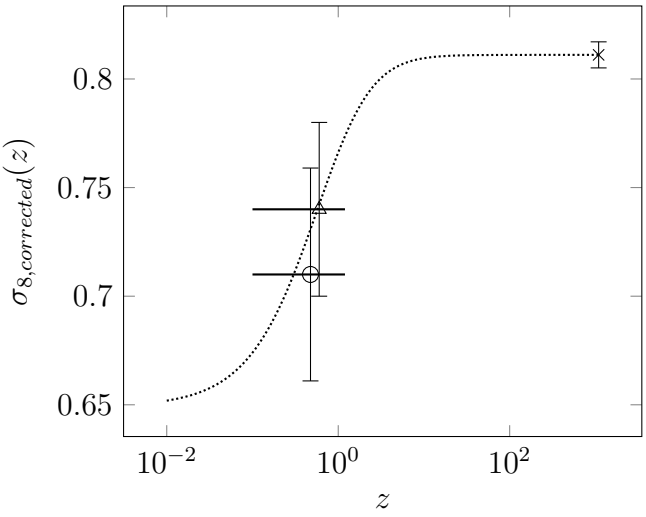

Figure 7.7: Matter fluctuation amplitude σ_8 as a function of the redshift z of the probe. Probes: weak gravitational lenses (Δ (Joachimi et al., 2020, p. 26)), baryonic acoustic oscillations ($\circ$ (Tröster et al., 2020, p. 1, 2)), CMB ($\times$, (Collaboration, 2020, p. 16)). Theory without fit parameter (dotted).

dark energy theory II provides an accurate accordance with the measured values of $\sigma_8(z)$ that are based on very different redshifts z. That explanation and the precise accordance provide another clear evidence for the *dark energy theory II*, as shown in Fig. (7.7).

Theorem 22 Time evolution of the density of the vacuum $\rho_{\Lambda,h}(z)$:

According to the approximation of a homogeneous density $\rho_{\Lambda,h}$, the dark energy has the following properties:

(1) Its density $\rho_{\Lambda,h}$ is formed by the following RGWs:

(1a) The first part of $\rho_{\Lambda,h}$ is represented by the RGWs that are emitted by vacuum (with the density $\rho_{\Lambda,h}$). These RGWs propagate from the whole space within the Hubble radius R_H, and these RGWs are emitted at all times since the Big Bang, and these RGWs represent LFV.

(1b) The second part of $\rho_{\Lambda,h}$ is represented by the NFV[1] *corresponding to the RGWs described in (1a).*

(1c) The third part of $\rho_{\Lambda,h}$ is represented by the RGWs that are emitted by overdensities $\rho_{m,h} \cdot \delta(\vec{R})$. These RGWs propagate from the whole space within the Hubble radius R_H, and these RGWs are emitted at all times since the Big Bang, and these RGWs represent LFV.

(1d) The fourth part of $\rho_{\Lambda,h}$ is represented by the NFV corresponding to the RGWs described in (1c).

(2a) The sum of the parts described in (1c) and (1d) is characterized by a correction factor as a function of the redshift z or of the scaled radius x:

$$\kappa = \frac{\Omega_m}{\Omega_\Lambda} \cdot \sigma_8 \cdot \frac{9}{20} \cdot x^2 = \frac{\Omega_m}{\Omega_\Lambda} \cdot \sigma_8 \cdot \frac{9}{20} \cdot \frac{1}{(1+z)^2}$$

(2b) The sum of the four parts described in (1a), (1b), (1c) and (1d) is as follows:

$$\rho_{\Lambda,h} = \frac{c^2}{4\pi \cdot G \cdot R_H^2} \cdot (1+\kappa)^2$$

That sum is alternatively described as follows:

$$\rho_{\Lambda,h} = \rho_{\Lambda,const.} \cdot (1+\kappa)^2$$

(3) For the case of the CMB, $z \approx 1090$, the following holds:

(3a) $\rho_{\Lambda,h}$ is in precise accordance with the density observed on the basis of the temperature power spectra, TT, of the CMB (Collaboration (2020)), showing a discrepancy of 0.16 %, clearly below the errors of measurement.

(3b) The density parameter Ω_Λ is equal to 2/3.

(3c) The vacuum dV at a location R_0 that is filled with vacuum only is equal to the vacuum δV that is formed within the Hubble radius R_H of R_0, and that propagates to R_0 (Sect. 6.6.10).

[1]The interpretation used in theorem (21) can be applied here alternatively.

(4) The density $\rho_{\Lambda,h}$ is increased in the late universe or at small redshift z as shown in Fig. (7.5).

(5) The Hubble constant H_0 is a function of the redshift as follows:

$$H_0(t_0, R_0, z) = H_0(t_0, R_0, z = 1090) \cdot \sqrt{\Omega_m + \Omega_\Lambda \cdot (1 + \kappa(z))^2}$$

That function $H_0(z)$ is shown in Fig. (7.6). Our result is in precise accordance with observations, and so the model **solves the discrepancy of observed Hubble constants** H_0.

(6) The amplitude of matter fluctuations σ_8 is a function of the redshift as follows:

$$\sigma_{8,corr}(z) = \frac{\sigma_8(z = 1090)}{\Omega_m + \Omega_\Lambda \cdot (1 + \kappa(z))^2}$$

That function $\sigma_{8,corr}(z)$ is shown in Fig. (7.7). Our result is in precise accordance with observations, and so the model **solves the discrepancy of observed amplitudes of matter fluctuations** σ_8.

Chapter 8

Dimensional Transitions

The GRT is incomplete with respect to the enlargement of the universe (see theorem 20). In this chapter we show how the universe generated the full enlargement ranging from the Planck length to the light horizon by undergoing a sequence of dimensional transitions.

In particular, we analyze the dimensional phase transitions with help of various models, in order to derive essential properties of these transitions (see sections 8.1, 8.2, 8.4).

8.1 Shortcuts in space

In this section we summarize and analyze how the **connectivity in space** changed by the spontaneous formation of shortcuts.

If the density ρ is larger than the critical density $\rho_{cr.\,conn.}$ of the spontaneous formation of shortcuts, then many connections form among measurable regions of space.

For it there are two possibilities in principle:

(1) Either there occurs a formation of **regular connections** so that the connections together with the observable regions form a higher dimensional space. In that case, a relatively **low curvature** of the higher dimensional space is possible. As a consequence, a relatively **low energy** is possible.

(2) Or there occurs a formation of **irregular connections**. In that case, a relatively **high curvature** occurs. As a consequence, a relatively **high energy** is required.

In the following, we analyze the energetically favorable first case.

Theorem 23 Shortcuts can enable a dimensional transition:

If the density in the universe is larger than the critical density for the formation of shortcuts, $\rho_{cr.\,conn.}$, then a dimensional phase transition is enabled in the typical case of relatively low energy.

8.2 Mean field theory

In this section we develop a mean field theory of **objects in space during dimensional phase transitions**.

For it we apply a well established method: van der Waals (1873) analyzed **pairs of objects**, in order to derive the phase transition of condensation. Analogously, we apply the analysis of **pairs of objects**, in order to derive the dimensional phase transitions. Additionally, that method has been successfully applied in many other types of phase transitions (see for instance Carmesin et al. (1986), Carmesin et al. (1989), Carmesin (1993)). More generally, that method is an example for a mean field theory.

Analyzed pairs: In the early universe, the density was very high. As a consequence, there existed a binary fluid constituted by photons and microscopically small black holes (Carmesin (2020b)). So four types of pairs are possible: two photons, a photon in the vicinity of a black hole, a black hole the vicinity of a photon, two black holes. All four possibilities exhibit dimensional phase transitions (Carmesin (2020b)).

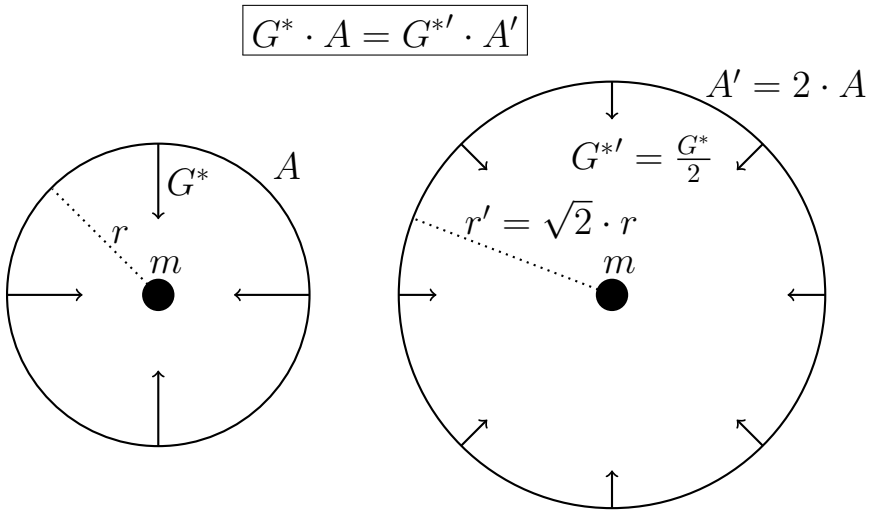

Figure 8.1: Gaussian gravity of a mass m: All balls around m have the same flux $G^*(r) \cdot A(r)$. This means the same product of the gravitational field $G^*(r)$ and area $A(r)$. Consequently, we derive in D dimensions: $G^*(r) \propto \frac{1}{A(r)} \propto \frac{1}{r^{D-1}}$.

In the following, we analyze a black hole as a probing mass in the vicinity of an averaged photon density, as an example[1].

8.2.1 Momentum term for $D \geq 3$

In this section we derive the kinetic energy in higher dimension. The momentum p^2 is the sum $p_x^2 + p_y^2 + p_z^2$ for $D = 3$. Accordingly, we derive in D dimensions:

$$p^2 = \Sigma_{j=i}^{D} p_i^2 \tag{8.1}$$

8.2.2 Gravity term for $D \geq 3$

According to Gaussian gravitation, the gravitational field $G^*(r)$ at a distance r from a mass is proportional to $1/r^{D-1}$ (Fig. 8.1, and Gauss (1840)):

$$G^* \propto \frac{1}{r^{D-1}} \tag{8.2}$$

[1]That example has been intensively analyzed (see for instance Carmesin (2017), Carmesin (2018a), Carmesin (2019b)).

The same proportionality applies to the gravitational force F which a mass M exerts on a mass m at the distance r. Moreover the force is proportional to each of the masses:

$$F \propto \frac{M \cdot m}{r^{D-1}} \tag{8.3}$$

The proportionality factor is a gravitational constant for dimension D, G_D:

$$F = -G_D \cdot \frac{M \cdot m}{r^{D-1}} \tag{8.4}$$

The potential energy or gravitational energy is the integral of the force. It is usual, that the energy is zero in the limit r to infinity:

$$E_G = -G_D \cdot \frac{M \cdot m}{(D-2) \cdot r^{D-2}} \tag{8.5}$$

The gravitational constant can be derived (see e.g. Carmesin (2017), Carmesin (2019b)). The following holds:

$$G_D = G \cdot (D-2) \cdot L_P^{D-3} \tag{8.6}$$

We summarize:

Proposition 14 Gravitation in D dimensions:

(1) Two objects at a distance r, with masses or dynamic masses M and m, exert the gravitational force $F = -G_D \cdot \frac{M \cdot m}{r^{D-1}}$ on each other in $D \geq 3$ dimensions with $G_D = G \cdot (D-2) \cdot L_P^{D-3}$.

(2) The corresponding energy is: $E_G = -G_D \cdot \frac{M \cdot m}{(D-2) \cdot r^{D-2}}$

8.2.3 Special radii at scaled densities $\tilde{\rho}_D$

In this section we analyze the radius b of a black hole and the radius a_M of radiation with dynamic mass M as a function of the density $\tilde{\rho}_D$.

Radius a_M depending on the scaled density: We derive how the radius a_M depends on the scaled density ρ_D. We use natural units (see table 9.3).

According to the redshift, the dynamic mass is proportional to the inverse wavelength $M_{dyn} \propto \frac{1}{a_M}$. For example, for $a_M = L_P$ is $M_{dyn} = \frac{M_P}{2}$ (Fig. 3.1). Both relations result in:

$$\frac{1}{2\tilde{a}_M} = \tilde{M}_{dyn} \tag{8.7}$$

Here we use the term for the density, where V_D denotes the volume of a hyper ball with radius 1:

$$\rho_D = \frac{M_{dyn}}{V_D \cdot a^D} \tag{8.8}$$

Here is:

$$V_D = \frac{\pi^{D/2}}{\Gamma(1+D/2)};\ \Gamma(x+1) = \Gamma(x) \cdot x; \Gamma(1) = 1; \Gamma\left(\frac{1}{2}\right) = \sqrt{\pi} \tag{8.9}$$

We use the Planck density related to a ball $\bar{\rho}_{D,P} = \frac{M_P}{V_D \cdot L_P^D}$ (table 9.3). So we get:

$$\tilde{\rho}_D = \frac{\rho_D}{\bar{\rho}_{D,P}} = \frac{\tilde{M}_{dyn}}{\tilde{a}_M^D} \tag{8.10}$$

In total we get:

$$\frac{1}{2\tilde{a}_M} = \tilde{M}_{dyn} = \tilde{\rho}_D \cdot \tilde{a}_M^D \tag{8.11}$$

Resolved we get:

$$\boxed{\tilde{a}_M = (2\tilde{\rho}_D)^{-1/(D+1)}} \tag{8.12}$$

Schwarzschild radius: We determine the Schwarzschild radius b depending on the density. We proceed like Michell (Michell (1784)). We equate the kinetic energy $\frac{1}{2}M \cdot v^2$ with the potential energy and choose the velocity of light c. So we get:

$$\frac{1}{2} \cdot c^2 = \frac{G_D \cdot m}{(D-2) \cdot b^{D-2}} \tag{8.13}$$

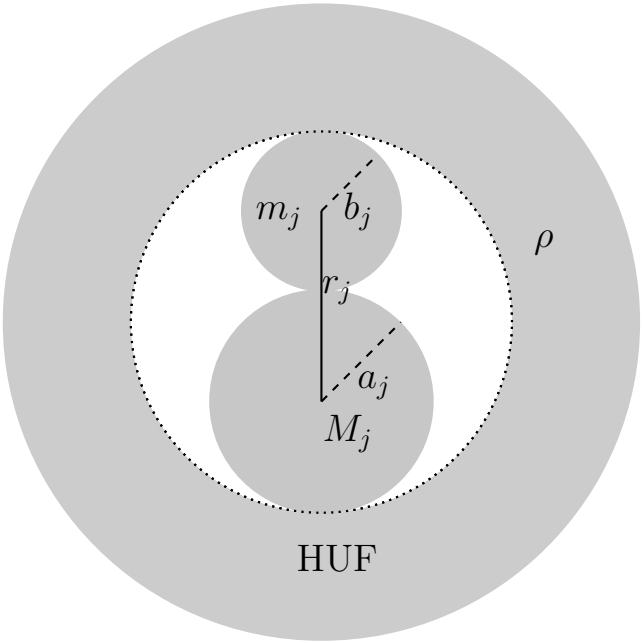

Figure 8.2: Pair j of adjacent objects or particles in a HUF at a density ρ of the universe.

We use $G_D = G \cdot (D-2) \cdot L_P^{D-3}$ and we use natural units. So we get (table 9.3):

$$\boxed{\tilde{b} = (2\tilde{\rho}_D)^{-1/2}} \tag{8.14}$$

8.2.4 Quantized FLE for pairs

In this section we generalize the FLE by deriving the quantized dynamics for the expectation value $\langle \dot{r}_j \rangle$ of the time derivative of the radius r_j of a pair of objects that is located in a HUF. Moreover we form the average over pairs. For it we combine the energy term of the Gaussian gravity (see Eq. 8.5).

Applications of the HUF: Here we investigate the distance r_j and the potential of the mass m_j with respect to the mass M_j.

The gravitational energy of the objects m_j and M_j in the

HUF is as follows:

$$E_G = -G_D \cdot \frac{M_j \cdot m_j}{(D-2) \cdot r_j^{D-2}} \tag{8.15}$$

With the term of the kinetic energy $E_{kin} = \frac{\sum_{i=1}^{D} p_i^2}{2m}$ we get:

$$\frac{\sum_{i=1}^{D} p_{j,i}^2}{2m_j} - G_D \cdot \frac{M_j \cdot m_j}{(D-2) \cdot r_j^{D-2}} = E_j \tag{8.16}$$

The following applies accordingly to quantum objects:

$$\frac{\sum_{i=1}^{D} \hat{p}_{j,i}^2}{2m_j} - \frac{G_D}{D-2} \cdot m_j \cdot M_j \cdot \hat{r}_j^{2-D} = \hat{E}_j \tag{8.17}$$

We derive the expectation value of the energy term (Eq. 8.17) and divide by $m_j \cdot c^2$:

$$\frac{\langle \hat{E}_j \rangle}{m_j \cdot c^2} = \frac{\sum_{i=1}^{D} \langle \hat{p}_{j,i}^2 \rangle}{2m_j^2 \cdot c^2} - \frac{G_D}{(D-2) \cdot c^2} \cdot \left\langle M_j \cdot \hat{r}_j^{2-D} \right\rangle \tag{8.18}$$

We separate the fluctuations from the expectation value by applying the identity

$$\left\langle \hat{p}^2 \right\rangle = \langle \hat{p} \rangle^2 + (\Delta p)^2 \tag{8.19}$$

So we get:

$$\frac{\langle \hat{E}_j \rangle}{m_j \cdot c^2} = \frac{\sum_{i=1}^{D} \langle \hat{p}_{j,i} \rangle^2}{2m_j^2 \cdot c^2} + \frac{\sum_{i=1}^{D} (\Delta p_{j,i})^2}{2m_j^2 \cdot c^2} - \frac{G_D \cdot \left\langle M_j \cdot \hat{r}_j^{2-D} \right\rangle}{(D-2) \cdot c^2} \tag{8.20}$$

We use the identity $\langle \hat{p} \rangle / m = \langle \dot{r} \rangle$. So we get:

$$\frac{\langle \hat{E}_j \rangle}{m_j \cdot c^2} = \frac{\sum_{i=1}^{D} \langle \dot{r}_{j,i} \rangle^2}{2 \cdot c^2} + \frac{\sum_{i=1}^{D} (\Delta p_{j,i})^2}{2m_j^2 \cdot c^2} - \frac{G_D \cdot \left\langle M_j \cdot \hat{r}_j^{2-D} \right\rangle}{(D-2) \cdot c^2} \tag{8.21}$$

In the first summand, we add the components:

$$\sum_{i=1}^{D} \langle \dot{r}_{j,i} \rangle^2 = \langle \dot{r}_j \rangle^2 \tag{8.22}$$

We call the remaining term **reduced normalized energy** $E_{D,j}$:

$$\boxed{E_{D,j} = \frac{\sum_{i=1}^{D}(\Delta p_{j,i})^2}{2m_j^2 \cdot c^2} - \frac{G_D}{(D-2)\cdot c^2} \cdot \left\langle M_j \cdot \hat{r}_j^{2-D} \right\rangle} \tag{8.23}$$

So the following holds (Eq. 8.21):

$$\frac{\langle \hat{E}_j \rangle}{m_j \cdot c^2} = \frac{\langle \dot{r}_j \rangle^2}{2 \cdot c^2} + E_{D,j} \tag{8.24}$$

The left hand side of the above Eq. is identified with half a quantized **curvature parameter** of a pair, $k_j/2$:

$$\frac{-k_j}{2} = \frac{\langle \hat{E}_j \rangle}{m_j \cdot c^2} = \frac{\langle \dot{r}_j \rangle^2}{2 \cdot c^2} + E_{D,j} \tag{8.25}$$

Here we apply the average over the pairs, and we denote it by rectangular brackets:

$$\frac{-[k_j]}{2} = \frac{[\langle \dot{r}_j \rangle^2]}{2 \cdot c^2} + [E_{D,j}] \tag{8.26}$$

In order to obtain a generalized FLE, we multiply by $2c^2/[\langle r_j \rangle^2]$, and we resolve:

$$\boxed{\frac{[\langle \dot{r}_j \rangle^2]}{[\langle r_j \rangle^2]} = -\frac{2[E_{D,j}] \cdot c^2}{[\langle r_j \rangle^2]} - \frac{[k_j] \cdot c^2}{[\langle r_j \rangle^2]}} \tag{8.27}$$

This DEQ is the **quantized FLE for pairs in D dimensions**. We summarize:

Theorem 24 FLE derived from pairs of quantum objects:

The FLE can be derived as an average over pairs of quantum objects. The resulting quantized FLE for pairs in D dimensions is as follows:

$$\frac{[\langle \dot{r}_j \rangle^2]}{[\langle r_j \rangle^2]} = -\frac{2[E_{D,j}] \cdot c^2}{[\langle r_j \rangle^2]} - \frac{[k_j] \cdot c^2}{[\langle r_j \rangle^2]} \tag{8.28}$$

8.2.5 Quantized FLE

In this section we derive the quantized FLE. In the quantized FLE for pairs, the fraction $\frac{[\langle \dot{r}_j \rangle^2]}{[\langle r_j \rangle^2]}$ is an averaged Hubble parameter $[H_j]$. The Hubble parameter $[H_j]$ describes a uniform scaling. This is characterized by a scale factor $dk_{t\to t+dt}$:

$$dk_{t\to t+dt} = \frac{a(t) + \dot{a}(t) \cdot dt}{a(t)} = 1 + H(t) \cdot dt \tag{8.29}$$

Thus a homogeneous scale factor implies a homogeneous Hubble parameter. So the uniform scaling implies that we can replace the averaged Hubble parameter by the global Hubble parameter:

$$\frac{[\langle \dot{r}_j \rangle^2]}{[\langle r_j \rangle^2]} = \frac{\dot{r}^2}{r^2} = H^2 \tag{8.30}$$

We apply this relation to the quantized averaged FLE:

$$\boxed{\frac{\dot{r}^2}{r^2} = -\frac{2[E_{D,j}] \cdot c^2}{[\langle r_j \rangle^2]} - \frac{[k_j] \cdot c^2}{[\langle r_j \rangle^2]}} \tag{8.31}$$

This DEQ is the quantized FLE or **extended FLE, EFLE**. In this DEQ the term with the averaged curvature parameter $[k_j]$ is relatively small (see Collaboration (2020), Carmesin (2020b)). So we get:

$$\boxed{\frac{\dot{r}^2}{r^2} = -\frac{2[E_{D,j}] \cdot c^2}{[\langle r_j \rangle^2]}} \tag{8.32}$$

Theorem 25 Quantized or extended FLE:

(1) The quantized FLE in D dimensions is as follows:

$$\frac{\dot{r}^2}{r^2} = -\frac{2[E_{D,j}] \cdot c^2}{[\langle r_j \rangle^2]} - \frac{[k_j] \cdot c^2}{[\langle r_j \rangle^2]} \tag{8.33}$$

(2) As the averaged curvature parameter $[k_j]$ is nearly zero, the quantized FLE in D dimensions is nearly as follows:

$$\frac{\dot{r}^2}{r^2} = -\frac{2[E_{D,j}] \cdot c^2}{[\langle r_j \rangle^2]} \tag{8.34}$$

8.2.6 Condensation: Ground state

Lohse et al. (2018) and Zilberberg et al. (2018) showed experimentally that quantum systems can use higher dimensional space. Similarly as in the case of the shortcuts (Sect. 8.1), such a possibility may give rise to a dimensional phase transition, that is driven by the attractive gravitational interaction. Thus such a dimensional phase transition is a **condensation**. Hence the corresponding states are **low energy states** (Sect. 8.1). Thus the corresponding states can be modeled by **ground states** in an adequate approximation.

Correspondingly, we analyze the ground state of the mass m_j of a pair j in this section.

Uncertainty relation at dimension D: In this paragraph we show that the uncertainty relation as a function of the dimension D is expressed by Eq. (8.41). In general, the components of the position Δr_i and the momentum Δp_k obey the uncertainty relation:

$$\Delta r_i \cdot \Delta p_k \geq \frac{\hbar}{2} \quad \text{for} \quad i = k \tag{8.35}$$

and

$$\Delta r_i \cdot \Delta p_k \geq 0 \quad \text{for} \quad i \neq k \tag{8.36}$$

This can be expressed with the Kronecker symbol $\delta_{ik} = 1$ for $i = k$ and $\delta_{ik} = 0$ for $i \neq k$:

$$\Delta r_i \cdot \Delta p_k \geq \frac{\hbar}{2} \cdot \delta_{ik} \tag{8.37}$$

We square both sides of the relation and sum both sides:

$$\sum_{i=1}^{D} \sum_{k=1}^{D} (\Delta r_i)^2 \cdot (\Delta p_k)^2 \geq \frac{\hbar^2}{4} \cdot \sum_{i=1}^{D} \sum_{k=1}^{D} \delta_{ik} \tag{8.38}$$

Here we identify:

$$\sum_{i=1}^{D} (\Delta r_i)^2 = (\Delta r)^2 \quad \text{and} \quad \sum_{k=1}^{D} (\Delta p_k)^2 = (\Delta p)^2 \tag{8.39}$$

We apply $\sum_{i=1}^{D}\sum_{k=1}^{D}\delta_{ik}=D$:

$$(\Delta r)^2\cdot(\Delta p)^2\geq\frac{\hbar^2}{4}\cdot D \tag{8.40}$$

We extract the root and show the relation (qed):

$$\boxed{\Delta r\cdot\Delta p\geq\frac{\hbar}{2}\cdot\sqrt{D}} \tag{8.41}$$

Minimal uncertainty at the ground state: In this paragraph we show that the uncertainty takes its minimum at the ground state: We analyze the ground state of the energy operator $\hat{E}_{D,j}$. So the wave function is a Gaussian function at high density (Carmesin (2019b), Carmesin and Carmesin (2020)). Thus the inequality in the uncertainty relation becomes an equality:

$$\Delta p\cdot\Delta r=\frac{\hbar}{2}\sqrt{D} \tag{8.42}$$

So the uncertainty takes its minimum at the ground state.

Energy as a function of spatial uncertainties: In this paragraph we show that the energy $E_{D,j}$ can be expressed as a function of spatial uncertainties $(\hat{\Delta}r_j)^2=\tilde{r}_j^2-\langle\tilde{r}_j\rangle^2$ or $(\Delta r_j)^2=\langle(\hat{\Delta}r_j)^2\rangle$.

For it we apply Eq. (8.39) to Eq. (8.23):

$$E_{D,j}=\frac{(\Delta p_j)^2}{2m_j^2\cdot c^2}-\frac{G_D}{(D-2)\cdot c^2}\cdot\left\langle M_j\cdot\hat{r}_j^{2-D}\right\rangle \tag{8.43}$$

Furthermore, we apply the uncertainty relation in Eq. (8.42). Moreover, we use natural units and mark the corresponding quantities with a tilde:

$$E_{D,j}=\frac{D}{8\tilde{m}_j^2\cdot(\Delta\tilde{r}_j)^2}-\tilde{M}_j\cdot\left\langle\tilde{r}_j^{2-D}\right\rangle \tag{8.44}$$

Here we apply the identity

$$\langle\tilde{r}_j^{2-D}\rangle=\left\langle(\tilde{r}_j^2)^{\frac{2-D}{2}}\right\rangle \tag{8.45}$$

Here we introduce the difference of $\tilde{r}_j^2$ and $\langle \tilde{r}_j \rangle^2$:

$$\tilde{r}_j^2 - \langle \tilde{r}_j \rangle^2 = (\hat{\Delta} \tilde{r}_j)^2 \tag{8.46}$$

The expectation value of $(\hat{\Delta} \tilde{r}_j)^2$ is the square of the standard deviation or uncertainty:

$$\langle (\hat{\Delta} \tilde{r}_j)^2 \rangle = (\Delta \tilde{r}_j)^2 \tag{8.47}$$

As the expectation value of $(\hat{\Delta} \tilde{r}_j)^2$ is the square of the uncertainty, $\hat{\Delta} \tilde{r}_j$ is the corresponding **uncertainty operator**. We apply this uncertainty operator to Eq. (8.45):

$$\langle \tilde{r}_j^{2-D} \rangle = \left\langle \left(\langle \tilde{r}_j \rangle^2 + (\hat{\Delta} \tilde{r}_j)^2 \right)^{\frac{2-D}{2}} \right\rangle \tag{8.48}$$

Here we factorize $\langle \tilde{r}_j \rangle^2$:

$$\langle \tilde{r}_j^{2-D} \rangle = \langle \tilde{r}_j \rangle^{2-D} \cdot \left\langle \left(1 + \frac{(\hat{\Delta} \tilde{r}_j)^2}{\langle \tilde{r}_j \rangle^2} \right)^{\frac{2-D}{2}} \right\rangle \tag{8.49}$$

This Eq. combined with Eq. (8.44) represents the energy $E_{D,j}$ as a function of the uncertainty operator.

Energy as sum of classical term and quantum term: In this paragraph we show that the energy $E_{D,j}$ can be expressed as a sum of classical term and quantum term, in linear order in the fraction $\frac{(\hat{\Delta} \tilde{r}_j)^2}{\langle \tilde{r}_j \rangle^2}$.

For it we expand Eq. (8.49) in linear order:

$$\langle \tilde{r}_j^{2-D} \rangle = \langle \tilde{r}_j \rangle^{2-D} \cdot \left\langle 1 + \frac{2-D}{2} \cdot \frac{(\hat{\Delta} \tilde{r}_j)^2}{\langle \tilde{r}_j \rangle^2} \right\rangle \tag{8.50}$$

Here we evaluate the expectation values:

$$\langle \tilde{r}_j^{2-D} \rangle = \langle \tilde{r}_j \rangle^{2-D} - \frac{D-2}{2} \cdot \frac{(\Delta \tilde{r}_j)^2}{\langle \tilde{r}_j \rangle^D} \tag{8.51}$$

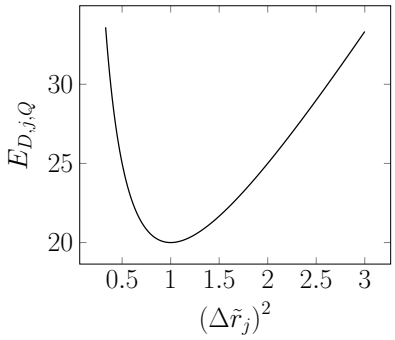

Figure 8.3: Variation of fluctuations (Eq. 8.53): Example: $\frac{D}{8\tilde{m}_j^2} = 10$ and $\frac{(D-2)\tilde{M}_j}{2\langle\tilde{r}_j\rangle^D} = 10$. The quantum term $E_{D,j,Q}$ (Eq. 8.53) is presented as a function of the square of the uncertainty $(\Delta\tilde{r}_j)^2$. The minimum can be determined completely robustly. In the figure: $\Delta\tilde{r}_j \approx 1$ and thus $\Delta\tilde{p}_j \approx \frac{\sqrt{D}}{2}$.

We insert this result in the energy term in Eq. (8.44). So we get:

$$E_{D,j} = \frac{D}{8\tilde{m}_j^2 \cdot (\Delta\tilde{r}_j)^2} - \frac{\tilde{M}_j}{\langle\tilde{r}_j\rangle^{D-2}} + \frac{(D-2)\cdot(\Delta\tilde{r}_j)^2 \cdot \tilde{M}_j}{2\cdot\langle\tilde{r}_j\rangle^D} \quad (8.52)$$

The terms containing the uncertainty $\Delta\tilde{r}_j$ form the quantum term:

$$\boxed{E_{D,j,Q} = \frac{D}{8\tilde{m}_j^2 \cdot (\Delta\tilde{r}_j)^2} + \frac{(D-2)\cdot(\Delta\tilde{r}_j)^2 \cdot \tilde{M}_j}{2\cdot\langle\tilde{r}_j\rangle^D}} \quad (8.53)$$

The rest is the classical gravity term:

$$\boxed{E_{D,j,cl,G} = -\frac{\tilde{M}_j}{\langle\tilde{r}_j\rangle^{D-2}}} \quad (8.54)$$

Hence we get (Fig. 8.3):

$$\boxed{E_{D,j} = E_{D,j,Q} + E_{D,j,cl,G}} \quad (8.55)$$

8.2.7 Minimization of reduced energy via $\Delta\tilde{r}_j$

In this section we show that the energy, minimized with respect to $\Delta\tilde{r}_j$, is presented by Eq. (8.59).

The energy function $E_{D,j,Q}([\Delta\tilde{r}_j]^2)$ shows a clear minimum (Fig. 8.3). The minimum corresponds to the basic state. We determine the minimum: $(\Delta\tilde{r}_j)^2$ is called x:

$$E_{D,j,Q} = \frac{D}{8\tilde{m}_j^2 \cdot x} + \frac{(D-2)\cdot x \cdot \tilde{M}_j}{2 \cdot \langle\tilde{r}_j\rangle^D} \tag{8.56}$$

We determine the derivative

$$E_{D,j,Q}(x)' = -\frac{D}{8\tilde{m}_j^2 \cdot x^2} + \frac{(D-2)\cdot \tilde{M}_j}{2 \cdot \langle\tilde{r}_j\rangle^D} \tag{8.57}$$

The minimum is at the slope zero (Fig. 8.3). Therefore we use $E_{D,j,Q}(x)' = 0$ in the above equation, resolve to x, use $(\Delta\tilde{r}_j)^2$ for x and get:

$$(\Delta\tilde{r}_j)^4 = \frac{D \cdot \langle\tilde{r}_j\rangle^D}{4(D-2)\cdot \tilde{m}_j^2 \cdot \tilde{M}_j} \tag{8.58}$$

We use this result in $E_{D,j,Q}$ and get:

$$\boxed{E_{D,j,Q} = \frac{\sqrt{D\cdot(D-2)\cdot\tilde{M}_j}}{2\tilde{m}\cdot\langle\tilde{r}_j\rangle^{D/2}}} \tag{8.59}$$

Proposition 15 Reduced normalized energy $E_{D,j}$ of a pair j: *The energy $E_{D,j}$ is as follows:*

(1) The expectation value is as follows:

$$E_{D,j} = \frac{\sum_{i=1}^{D}(\Delta p_{j,i})^2}{2m_j^2\cdot c^2} - \frac{G_D}{(D-2)\cdot c^2}\cdot\left\langle M_j \cdot \hat{r}_j^{2-D}\right\rangle \tag{8.60}$$

(2) At the ground state, $E_{D,j}$ is as follows:

$$E_{D,j} = E_{D,j,Q} + E_{D,j,cl,G} \tag{8.61}$$

$$E_{D,j,cl,G} = -\frac{\tilde{M}_j}{\langle \tilde{r}_j \rangle^{D-2}} \tag{8.62}$$

$$E_{D,j,Q} = \frac{\sqrt{D \cdot (D-2) \cdot \tilde{M}_j}}{2\tilde{m} \cdot \langle \tilde{r}_j \rangle^{D/2}} \tag{8.63}$$

8.2.8 Minimization of reduced energy via D

In this section we analyze the energy $[E_{D,j}]$ for the case of a black hole m_j and an averaged photon M_j and as a function of the density.

We apply equation (8.14), and we average:

$$[\tilde{b}_j] = (2\tilde{\rho}_D)^{\frac{-1}{2}} \tag{8.64}$$

Moreover we use equation (8.12), and we average:

$$[\tilde{a}_j] = (2\tilde{\rho}_D)^{\frac{-1}{D+1}} \tag{8.65}$$

With these relations, we plot the graphs of the energy $[E_{D,j}](\rho_D)$ for the dimensions $D = 3$, $D = 7$, $D = 12$ and $D = 301$ (Fig. 8.4). The figure shows: At low density, the energy is minimal at the dimension $D = 3$, however, at high density, minimal energy occurs at high dimension $D >> 3$.

The sequence of the dimensional phase transitions is evaluated for the case of the adequate approximation $\tilde{r}_j \approx \tilde{b}_j$ so that the quantum part of the reduced energy takes the following form (Eq. 8.63):

$$E_{D,j,Q} = \frac{\sqrt{D \cdot (D-2) \cdot \tilde{M}_j}}{2\tilde{m} \cdot \langle \tilde{b}_j \rangle^{D/2}} \tag{8.66}$$

For this case, the reduced energies as a function of the scaled density are shown in Fig. (8.5). That figure illustrates that there is an energetically optimal dimension at each density. Accordingly, the critical densities $\tilde{\rho}_{D,c}$ at which the dimensional transition to a dimension D and from a higher dimension can

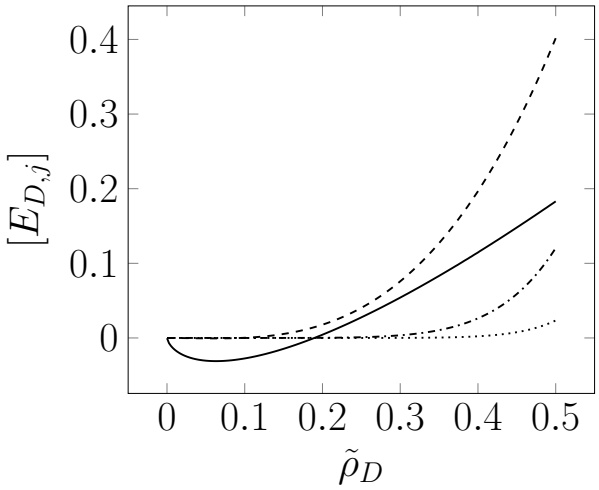

Figure 8.4: Energy $[E_{D,j}]$ for an averaged black hole in the gravitational field of an averaged photon. (Sect. 8.2.8): $[E_{3,j}]$ (solid line), $[E_{6,j}]$ (dashed), $[E_{12,j}]$ (dashdotted), $[E_{18,j}]$ (dotted).

be determined. These critical densities $\tilde{\rho}_{D,c}$ are shown as a function of the dimension D in Fig. (8.6).

A dimension below $D = 3$ does not occur, as the vacuum is represented by corresponding gravitational waves. These can exist in dimensions $D \geq 3$ only, as they have one direction of propagation and at least two transverse directions according to their quadrupolar structure or according to the fact that the elongations in Fig (5.1) cannot become negative.

For D towards infinity, the critical densities $\tilde{\rho}_{D,c}$ tend to $1/2$, see Fig. (8.6).

8.2.9 Distance enlargement factor

In this section we derive a term for the **distance enlargement factor** $Z_{D+s\to D}$, that occurs when the transition from a dimension $D + s$ to D occurs.

To determine the distance enlargement factor $Z_{D+s\to D}$, we model the space with a cube or hypercube from smallest observable regions. A figurative model is shown in the figure (2). Here 216 magnetic balls are arranged in a regular rectangular

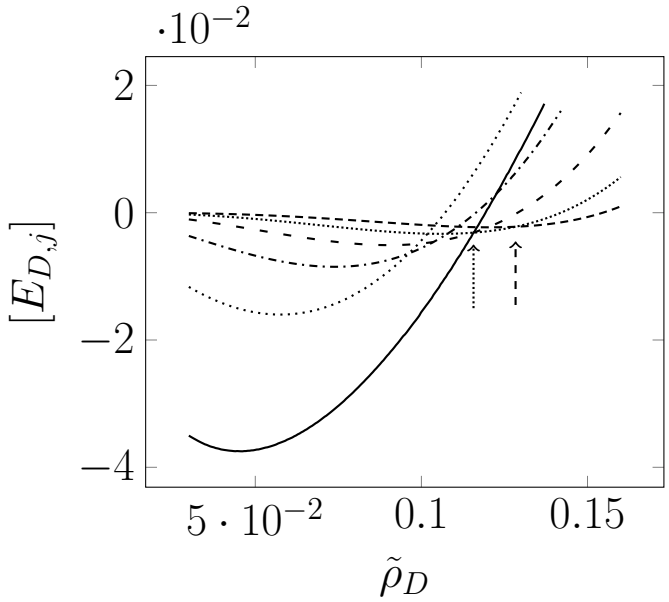

Figure 8.5: Reduced normalized energy $[E_{D,j}]$: $[E_{3,j}]$ (line), $[E_{4,j}]$ (dotted), $[E_{5,j}]$ (dashdotted), $[E_{6,j}]$ (loosely dashed), $[E_{7,j}]$ (dotted closely), $[E_{8,j}]$ (dashed). Dotted arrow marks transition from $D = 7$ to $D = 3$ at critical density $\tilde{\rho}_{D=3,c} = 0.11569$. Dashed arrow marks transition from $D = 8$ to $D = 7$ at critical density $\tilde{\rho}_{D=7,c} = 0.12835$.

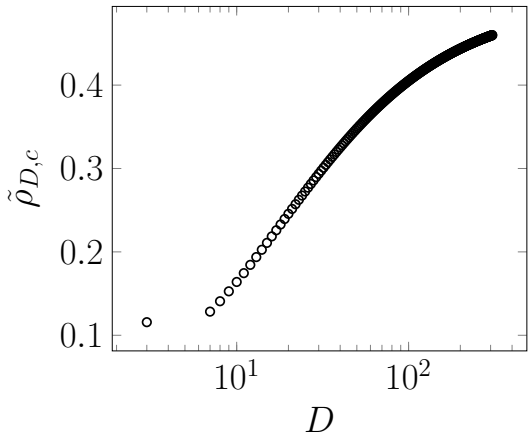

Figure 8.6: Critical densities $\tilde{\rho}_{D,c}$ as a function of dimension D. The dimensional transitions to $D = 3$ start at $D = 7$. So the following dimensions D are established: $D \in \{3, 7, 8, 9, ...\}$

.

grid in three spatial directions (left, $D = 3$) and in two spatial directions (right, $D = 2$). The transition from $D = 3$ to $D = 2$ increases the *edge length*. In the following we determine the factor by which the edge length is increased by a transition from. $D + s$ to D. We call the number of smallest observable regions on an edge in D dimensions n_D. Hence (Fig. 2):

$$Z_{D+s \to D} = \frac{n_D}{n_{D+s}} \tag{8.67}$$

With a dimensional transition, the number of memberless regions remains the same. So we get:

$$n_D^D = n_{D+s}^{D+s} \tag{8.68}$$

We resolve Eq. (8.68):

$$n_D = n_{D+s}^{(D+s)/D} \tag{8.69}$$

We use Eq. (8.69) in Eq. (8.67) and simplify the term. A term for increasing the edge length is obtained:

$$Z_{D+s \to D} = n_{D+s}^{s/D} \tag{8.70}$$

On average, distances in the cube increase in every spatial direction by this factor.

8.2.10 Calculation of the dimensional horizon

In this section we derive the dimensional horizon $D_{horizon}$ or D_{hori}.

For it we start with the distance enlargement factor for all transitions from $D_{horizon}$ to $D = 3$ in Eq. (8.70). Here the edge length n_{D+s} at $D_{horizon} = D + s$ is equal to two. We use this and get:

$$Z_{D+s \to D} = n_{D+s}^{s/D} = Z_{D_{horizon} \to D=3} = 2^{\frac{D_{horizon}-3}{3}} \tag{8.71}$$

$D_{horizon} = 2$

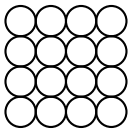

$D_{horizon} = 4$

Figure 8.7: Examples for the dimensional horizon D_{max} or $D_{horizon}$: A row of more than two balls can be put together in two dimensions. In general, the dimension can be increased until the edge length is two balls. With N balls the following applies $N = 2^{D_{horizon}}$.

This distance enlargement factor is the quotient of the factor $q_{D_{horizon}\to t_0}$, by which the light horizon is enlarged, and the corresponding scale factor $k_{D_{horizon}\to t_0}$:

$$Z_{D_{horizon}\to D=3} = \frac{q_{D_{horizon}\to t_0}}{k_{D_{horizon}\to t_0}} \tag{8.72}$$

Here $q_{D_{horizon}\to t_0}$ increases the edge length on the light horizon from approximately L_P (Fig. 2, 8.7) to the light horizon $r_{lh}(t_0)$ (Sect. 9.3.1, table 9.3):

$$q_{D_{horizon}\to t_0} \approx \frac{r_{lh}(t_0)}{L_P} = 2.56 \cdot 10^{61} \tag{8.73}$$

The scale factor leads to a reduction in the radiation density on the dimensional horizon $\tilde{\rho}_{r,D_{horizon}}$ to today's radiation density $\tilde{\rho}_{r,t_0}$. This reduction mainly takes place in space dimension three. Thus the density is proportional to the scale factor to the power minus four. Furthermore $\tilde{\rho}_{r,D_{horizon}}$ is about half the Planck density (Fig. 8.6), thus $\tilde{\rho}_{r,D_{horizon}} \approx \frac{1}{2}$, and $\tilde{\rho}_{r,t_0} = 6.52 \cdot 10^{-127}$ (s. Tab. 9.2). Hence:

$$k_{D_{horizon}\to t_0} \approx \left(\frac{\tilde{\rho}_{r,D_{horizon}}}{\tilde{\rho}_{r,t_0}}\right)^{1/4} = 2.96 \cdot 10^{31} \tag{8.74}$$

We use Eq. (8.73 and Eq. (8.74) in Eq. (8.72)and get:

$$Z_{D_{horizon}\to D=3} = 8.65 \cdot 10^{29} \tag{8.75}$$

To determine the dimensional horizon, we solve Eq. (8.71) after $D_{horizon}$ and use Eq. (8.75):

$$D_{horizon} = \frac{3}{\ln 2} \cdot \ln(Z_{D_{horizon}\to D=3}) + 3 = 301.3 \approx 301 \tag{8.76}$$

Definition 12 Dimensional unfolding:

The **vacuum that is enclosed by the actual light horizon** R_{lh} *was smaller at earlier times according to the* **expansion of space**.

That vacuum changed its dimension at **dimensional phase transitions**, *whereby the* **amount of vacuum** *does not change at the transition, and whereby each transition from a dimension* $D+s$ *to a dimension* D *takes place at a* **critical density** $\tilde{\rho}_{D,c}$, *and whereby the lowest dimension is* $D = 3$.

The largest dimension that the vacuum enclosed by the actual light horizon can take is called **dimensional horizon** $D_{horizon}$.

The process of the dimensional phase transitions starting at the dimensional horizon $D_{horizon}$ *and ending at* $D = 3$ *is called* **dimensional unfolding**.

Theorem 26 Completed time evolution of the universe:

(1a) The Planck length L_P *represents the smallest possible standard deviation of a single observation of space. Correspondingly, space can be modeled in terms of balls or hyperballs.*

(1b) If a cube or hypercube in D *dimensional space consists of a fixed number of balls or hyperballs, and if the length of an edge is established by* n_D *balls or hyperballs, and if a dimensional phase transition from a dimension* $D+s$ *to a dimension* D *occurs, then the edge is enlarged by the following* **distance enlargement factor**:

$$Z_{D+s\to D} = n_{D+s}^{s/D} \tag{8.77}$$

(2) The hypercube in (1) can take a highest possible dimension, the **dimensional horizon** $D_{horizon}$*.*

(3) At $D_{horizon}$*, an edge is constituted by two balls.*

(4) At a dimensional phase transition from $D_{horizon}$ *to a dimension* D*, the distance enlargement factor is as follows:*

$$Z_{D_{horizon}\to D} = 2^{\frac{D_{horizon}-D}{D}} \tag{8.78}$$

(5) The expansion of space ranges from the time of $D_{horizon}$ *until the actual time* t_0*, and is characterized by the scale factor:*

$$k_{D_{horizon}\to t_0} \approx \left(\frac{\tilde{\rho}_{r,D_{horizon}}}{\tilde{\rho}_{r,t_0}}\right)^{1/4} = 2.96 \cdot 10^{31} \tag{8.79}$$

(6) The enlargement of space ranges from the time of $D_{horizon}$ *until the actual time* t_0*, and it ranges from the Planck length* L_P *towards the light horizon* R_{lh}*, and it is characterized by a* **complete distance enlargement factor**

$$q_{D_{horizon}\to t_0} \approx \frac{r_{lh}(t_0)}{L_P} = 2.56 \cdot 10^{61} \tag{8.80}$$

(7) The **distance enlargement factor** *of dimensional phase transitions is the following ratio:*

$$Z_{D_{horizon}\to D=3} = \frac{q_{D_{horizon}\to t_0}}{k_{D_{horizon}\to t_0}} = 8.65 \cdot 10^{29} \tag{8.81}$$

(8) The dimensional horizon is as follows:

$$D_{horizon} = \frac{3}{\ln 2} \cdot \ln(Z_{D_{horizon}\to D=3}) + 3 = 301.3 \approx 301 \tag{8.82}$$

(9) The distance enlargement factor obtained by dimensional phase transitions **repairs the incompleteness of the GRT** *derived in theorem (20).*

(10) The dimensional phase transitions are caused by the fact that the attractive gravitational interaction can decrease the energy per particle in a HUF. Accordingly, that transition can be interpreted as a **condensation**. *In particular, that condensation can be interpreted as a* **gravitational instability of the space under the load of its content**.

(11) The dimensional phase transitions can be modeled for the connections among regions of space in terms of the shortcuts.

(12) The dimensional phase transitions can be modeled for the objects in space by the mean field theory.

8.3 Field variance in a HUF

If there are overdensities in the surroundings of a HUF, then these cause a **field variance** ΔG^{*2} in that HUF. In this section we analyze that variance ΔG^{*2} for the case of a HUF with a radius $\tilde{R}_{HUF}$.

Objects: We consider objects with a mass $\tilde{M}$, a radius $\tilde{a}$ and a volume $V_D \cdot \tilde{a}^D$. As a result of the Heisenberg uncertainty relation and possibly additional stochastic effects, there is a standard deviation of the mass $\Delta\tilde{M}$.

Force: We analyze the force that is exerted upon one particle $\tilde{M}$ in the center of the HUF by all other particles $\tilde{M}_j$ in the surrounding. For it we remind, that the homogeneous part of the masses $\tilde{M}_j$ in the surrounding does not exert any force upon $\tilde{M}$. However, the uncertainties or overdensities or standard deviations $\Delta\tilde{M}_j$ exert a force upon $\tilde{M}$.

Force caused by $\Delta\tilde{M}_j$: An overdensity $\Delta\tilde{M}_j$ at a distance $\tilde{R}_j$ exerts the following force upon $\tilde{M}$:

$$\tilde{F}_j = \frac{\tilde{M} \cdot \Delta\tilde{M}_j}{\tilde{R}_j^{D-1}} \cdot (D-2) \cdot \vec{e}_j \tag{8.83}$$

Hereby $\vec{e}_j$ is the direction vector of the force.

Force caused by the $\Delta\tilde{M}_j$ in a shell: In order to derive the force exerted upon $\tilde{M}$, we apply shells with radii $2\tilde{a}$, $3\tilde{a}$, $4\tilde{a}$ etc. The number $N(\tilde{R}_j)$ of objects in a shell is equal to the volume of that shell with its thickness $\tilde{a}$ divided by the volume of one object:

$$N(\tilde{R}_j) = V_D \cdot D\tilde{R}_j^2 \cdot \tilde{a} \cdot \frac{1}{V_D \tilde{a}^D} = \frac{D\tilde{R}_j^2}{\tilde{a}^{D-1}} \tag{8.84}$$

The direction vectors $\vec{e}_j$ and the forces $\tilde{F}_j$ of the $\Delta\tilde{M}_j$ in the shell are practically random.

Accordingly we derive the expectation value of the force:

$$\langle \tilde{F}_j(\tilde{R}_j) \rangle = \Sigma_j^{N(\tilde{R}_j)} \tilde{F}_j \tag{8.85}$$

We apply that the expectation value of Eq. (8.83):

$$\langle \tilde{F}_j(\tilde{R}_j) \rangle = \frac{\tilde{M} \cdot \Delta\tilde{M}_j}{\tilde{R}_j^{D-1}} \cdot (D-2) \cdot \langle \vec{e}_j \rangle \tag{8.86}$$

Hereby the expectation value of the direction vectors is zero:

$$\langle \vec{e}_j \rangle = 0 \tag{8.87}$$

So we get:

$$\langle \tilde{F}_j(\tilde{R}_j) \rangle = 0 \tag{8.88}$$

Thus the homogeneous surroundings do not exert any dipolar force $\langle \tilde{F}_j(\tilde{R}_j) \rangle$ upon the mass $\tilde{M}$.

However, the overdensities may exert a **force variance** upon $\tilde{M}$. For it we derive the mean of the square:

$$\langle \tilde{F}_j^2(\tilde{R}_j) \rangle = \Sigma_i^{N(\tilde{R}_j)} \tilde{F}_i \cdot \Sigma_k^{N(\tilde{R}_j)} \tilde{F}_k \tag{8.89}$$

We insert the force (Eq. 8.83):

$$\langle \tilde{F}_j^2(\tilde{R}_j)\rangle = \left(\frac{\tilde{M}\cdot(D-2)}{\tilde{R}_j^{D-1}}\right)^2 \cdot \Sigma_i^{N(\tilde{R}_j)}\Sigma_k^{N(\tilde{R}_j)}\Delta\tilde{M}_i\Delta\tilde{M}_k\vec{e}_i\vec{e}_k \tag{8.90}$$

As there are no essential correlations between the overdensities and the direction vectors, we factorize these. Similarly, there are no essential correlations among the overdensities, so we factorize these, and we apply the expectation value $\Sigma_i^N \Delta\tilde{M}_i = N\cdot\Delta\tilde{M}$. Here and in the following, we write $N = N(\tilde{R}_j)$ for short. So we get:

$$\langle \tilde{F}_j^2(\tilde{R}_j)\rangle = \left(\frac{\tilde{M}\cdot(D-2)}{\tilde{R}_j^{D-1}}\right)^2 \cdot N^2\cdot\Delta\tilde{M}^2\cdot\langle\vec{e}_i\vec{e}_k\rangle \tag{8.91}$$

We apply the fact that the average of two random unit vectors is $1/D$:

$$\langle \tilde{F}_j^2(\tilde{R}_j)\rangle = \left(\frac{\tilde{M}\cdot(D-2)}{\tilde{R}_j^{D-1}}\right)^2 \cdot N^2\cdot\Delta\tilde{M}^2\cdot\frac{1}{D} \tag{8.92}$$

If we reverse the direction of a force vector, then the force variance does not change, hence this force variance exhibits quadrupolar symmetry. As the force variance is isotropic, it is characterized by an isotropic quadrupolar tensor.

Integration of the force variance: Next we add up the force variances of all shells. So we get the **complete gravitational variance**:

$$\langle\tilde{F}^2\rangle = \Sigma_{\tilde{R}_j}^{\infty}\langle\tilde{F}_j^2(\tilde{R}_j)\rangle \tag{8.93}$$

We insert Eq. (8.92):

$$\langle\tilde{F}^2\rangle = \Sigma_{\tilde{R}_j}^{\infty}\left(\frac{\tilde{M}\cdot\Delta\tilde{M}(D-2)}{\tilde{R}_j^{D-1}}\right)^2 \cdot N^2(\tilde{R}_j)\cdot\frac{1}{D} \tag{8.94}$$

We insert Eq. (8.84):

$$\langle \tilde{F}^2 \rangle = \Sigma_{\tilde{R}_j}^{\infty} \left(\frac{\tilde{M} \cdot \Delta\tilde{M}(D-2)}{\tilde{R}_j^{D-1}} \right)^2 \cdot \frac{D^2 \tilde{R}_j^4}{\tilde{a}^{2D-2}} \cdot \frac{1}{D} \tag{8.95}$$

We simplify that Eq. and we replace the sum by an integral, ranging from a radius R_{HUF} to infinity:

$$\langle \tilde{F}^2 \rangle = \int_{\tilde{R}_{HUF}}^{\infty} \left(\frac{\tilde{M} \cdot \Delta\tilde{M}(D-2)}{\tilde{a}^{D-1}} \right)^2 \cdot D \cdot \tilde{R}_j^{4-2D} d\tilde{R} \tag{8.96}$$

We integrate:

$$\langle \tilde{F}^2 \rangle = \left(\frac{\tilde{M} \cdot \Delta\tilde{M}(D-2)}{\tilde{a}^{D-1}} \right)^2 \cdot \frac{D}{2D-5} \cdot \tilde{R}_{HUF}^{5-2D} \tag{8.97}$$

Field variance: We derive the corresponding **field variance**:

$$(\Delta\vec{G}^*)^2 = \frac{\langle \tilde{F}^2 \rangle}{\tilde{M}^2} = \left(\frac{\Delta\tilde{M}(D-2)}{\tilde{a}^{D-1}} \right)^2 \cdot \frac{D}{2D-5} \cdot \tilde{R}_{HUF}^{5-2D} \tag{8.98}$$

Here we identify the square of the above bracket with field variance of the overdensity $\tilde{M}$ of a single object with radius $\tilde{a}$ at the surface of that object:

$$(\Delta\vec{G}_1^*)^2 = \left(\frac{\Delta\tilde{M}(D-2)}{\tilde{a}^{D-1}} \right)^2 \tag{8.99}$$

With it we get:

$$(\Delta\vec{G}^*)^2 = (\Delta\vec{G}_1^*)^2 \cdot \frac{D}{2D-5} \cdot \tilde{R}_{HUF}^{5-2D} \tag{8.100}$$

Energy density of the field variance: In order to derive the **energy density of the field variance**, we divide by $8\pi \cdot G \cdot c^2$:

$$u_{f,var} = \frac{(\Delta\vec{G}^*)^2}{8\pi \cdot G \cdot c^2} = \frac{(\Delta\vec{G}_1^*)^2}{8\pi \cdot G \cdot c^2} \cdot \frac{D}{2D-5} \cdot \tilde{R}_{HUF}^{5-2D} \tag{8.101}$$

Here we identify the fraction containing ΔG_1^* by the energy density of the field variance of a single object at its surface:

$$u_{f,var,1} = \frac{(\Delta \vec{G}_1^*)^2}{8\pi \cdot G \cdot c^2} \tag{8.102}$$

With it we get:

$$u_{f,var} = u_{f,var,1} \cdot \frac{D}{2D-5} \cdot \tilde{R}_{HUF}^{5-2D} \tag{8.103}$$

Theorem 27 Variance of the field in a HUF:

(1) In the surroundings of a HUF there are always fluctuations. These can be characterized by the standard deviation or uncertainty $\Delta\tilde{M}$.

(2) If a HUF has a radius $\tilde{R}_{HUF}$*, and if the objects in the surroundings have a radius* $\tilde{a}$*, and fluctuations with standard deviation* $\Delta\tilde{M}$*, then there occurs the following* **field variance** *in the center of the HUF:*

$$(\Delta \vec{G}^*)^2 = (\Delta \vec{G}_1^*)^2 \cdot \frac{D}{2D-5} \cdot \tilde{R}_{HUF}^{5-2D} \tag{8.104}$$

Hereby the **single particle field variance** *is as follows:*

$$(\Delta \vec{G}_1^*)^2 = \left(\frac{\Delta\tilde{M}(D-2)}{\tilde{a}^{D-1}} \right)^2 \tag{8.105}$$

(3) The field variance $(\Delta \vec{G}^*)^2$ *is invariant with respect to a reversal a the field* $\vec{G}_1^*$ *of a single particle. Correspondingly it has a quadrupolar symmetry.*

(4) In the center of the HUF in part (2), there occurs the following energy density of the field variance:

$$u_{f,var} = u_{f,var,1} \cdot \frac{D}{2D-5} \cdot \tilde{R}_{HUF}^{5-2D} \tag{8.106}$$

Hereby the **single particle energy density** *is as follows:*

$$u_{f,var,1} = \frac{(\Delta \vec{G}_1^*)^2}{8\pi \cdot G \cdot c^2} \tag{8.107}$$

(5) In the center of a HUF, the field variance and its energy density tend to zero as the radius $\tilde{R}_{HUF}$ tends to infinity.

(6) In a homogeneous system with fluctuations with a standard deviation $\Delta\tilde{M}$, the dipolar component of the forces $\vec{F}_j$ averages to zero and only a small quadrupolar component remains and tends to zero proportional to the following power law as a function of the distance $\tilde{R}_{HUF}^{5-2D}$. Analogous relations hold for the fields. We call this effect the **self averaging of gravity in homogeneous systems**.

8.4 Bose gas at high density $\tilde{\rho}$

In this section we model and analyze a Bose gas (Bose (1924)) at dimensions $D \geq 3$ and at high density $\tilde{\rho} > 1/4$ in a HUF (Fig. 8.8). As an example, we model photons.

Energy density or pressure: We analyze the gas in terms of the energy density u, which can be interpreted as a pressure of the gas p_{gas}. With it we can analyze two essential phenomena: a possible condensation and the energy density $u_{f,v}$.

Temperature T at a density ρ_D: At a fixed density ρ_D, the temperature T is determined according to the Stefan-Boltzmann law (Carmesin (2020b)):

$$u_D = \bar{a}_D \cdot T^{D+1} \tag{8.108}$$

Hereby the constant a_D is determined in (Carmesin (2020b)). We apply $u_D \cdot c^2 = \rho_D$ and solve for T:

$$T = \sqrt[D+1]{\frac{\rho}{\bar{a}_D \cdot c^2}} \tag{8.109}$$

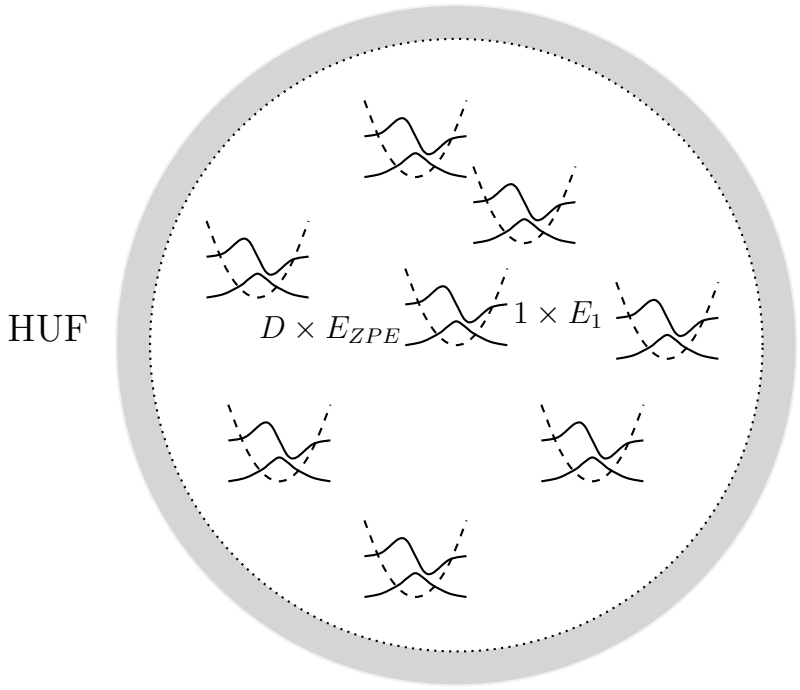

Figure 8.8: Bose gas at high density $\tilde{\rho}_D > 1/4$: local harmonic oscillators (dashed) (Carmesin (2018b),Carmesin and Carmesin (2020)) , D ZPOs (one maximum), one E_1 state (maximum and minimum of Ψ), no other excitation, due to density limit $\tilde{\rho}_D < 1/2$.

This shows that we may analyze the pressure as a function of the density.

8.4.1 Photons at high density

In this section we analyze the physics of a photon at high density.

At high density $\tilde{\rho}_D$, the photon states are represented by the hyperbola in Fig. (3.1), by construction of that hyperbola. Based on the density, the extension or radius or standard deviation of a photon is as follows:

$$\tilde{a} = \tilde{\rho}_D^{\frac{-1}{D+1}} \tag{8.110}$$

Moreover, the energy of that single photon state is as follows:

$$\tilde{E}_1 = \frac{1}{2\tilde{a}} \tag{8.111}$$

We apply these relations to the Bose gas, and we interpret that application as a **mean field approximation**.

Kinetic energy: The kinetic energy E_{kin} of a single photon is equal to h/T. By definition, h/T it is equal to its dynamic mass M:

$$E_{kin} = M = \frac{h}{T} = h \cdot f = \hbar \cdot \omega \tag{8.112}$$

By comparison with Eq. (8.110) we get:

$$\boxed{\tilde{E}_1 = \tilde{E}_{kin} = \tilde{M} = \frac{1}{2\tilde{a}}} \tag{8.113}$$

Overlapping photons: In principle, photons can overlap. However, at densities $\tilde{\rho} > 1/4$ and in the framework of the mean field approximation, it is impossible that two photons are at the same state for the following reason: If two photons, each at a density $\tilde{\rho}$, were in the same state, then the density would be

larger that one half, $\tilde{\rho}_{hypothetical} > 1/2$, but all real densities are smaller than one half, $\tilde{\rho}_{real} < 1/2$. So there is only one excited state at each local harmonic potential (Fig. (8.8).

8.4.2 Harmonic oscillators

In this section we analyze oscillator states that describe the photons.

Oscillations: Photons can be described as states of harmonic oscillators ((Ballentine, 1998, p. 541-554)). At high density, the states of quantum objects are characterized by a very local harmonic potential (Carmesin (2018b),Carmesin (2019b),Carmesin and Carmesin (2020)).

Zero-point energy, ZPE: Harmonic oscillators exhibit zero-point oscillations (Born et al. (1926), Mehra and Rechenberg (1999)), and the corresponding **zero-point energy**. The ZPE of a harmonic oscillator is as follows:

$$E_{ZPE,mode} = \hbar\omega/2 \tag{8.114}$$

According to the usual theory of photons that propagate freely in space ((Ballentine, 1998, p. 526-534)), each oscillator is characterized by $D-1$ directions of polarization.

In our case of high density, the harmonic oscillator is similar to the potential of a particle in a crystal. For that case of crystals, (Fornasini and Grisenti, 2015, p. 1252) show that the empirical results fit to the Einstein model (Einstein (1907)) and there is one mode for each dimension in that model. So there are D modes of the ZPE:

$$\boxed{E_{ZPE} = D \cdot \hbar\omega/2} \tag{8.115}$$

As the single photon states exhibits the energy $\hbar \cdot \omega$, and as the ZPE of a single mode is $\hbar \cdot \omega/2$, the ZPE of a single mode

is one half of $\tilde{E}_1$. So we get:

$$\boxed{\tilde{E}_{ZPE} = \frac{D}{4\tilde{a}}} \tag{8.116}$$

8.4.3 Potential energy term

In this section we analyze the potential energy term.

Radius of the HUF: We choose a HUF the radius $\tilde{r}$ of which is an integer multiple of $\tilde{a}$:

$$\tilde{r} = \bar{\kappa} \cdot \tilde{a} \tag{8.117}$$

Thus the volume of the HUF is $\bar{\kappa}^D$ times the volume of one object. As the density is constant, the number of objects in the HUF is:

$$N = \bar{\kappa}^D \tag{8.118}$$

Potential energy: If a pair of objects with mass M is at a distance R, then their energy of interaction is:

$$E_{pot,pair}(R) = -\frac{G_D \cdot M^2}{(D-2) \cdot R^{D-2}} \tag{8.119}$$

We transform to Planck units:

$$\tilde{E}_{pot,pair}(\tilde{R}) = -\frac{\tilde{M}^2}{\tilde{R}^{D-2}} \tag{8.120}$$

We analyze one of the N objects as a reference object at the center of the HUF with radius r. As we model a Bose gas, the other objects are placed at random positions in the HUF. Thus the averaged potential energy of the reference object with one of the other objects is as follows:

$$\bar{\tilde{E}}_{pot,pair} = \frac{\int_0^{\tilde{r}} \tilde{E}_{pot}(\tilde{R}) \tilde{R}^{D-1} d\tilde{R}}{\int_0^{\tilde{r}} \tilde{R}^{D-1} d\tilde{R}} \tag{8.121}$$

We insert Eq. (8.120):

$$\bar{\tilde{E}}_{pot,pair} = -\tilde{M}^2 \cdot \frac{\int_0^{\tilde{r}} \tilde{R} d\tilde{R}}{\int_0^{\tilde{r}} \tilde{R}^{D-1} d\tilde{R}} \tag{8.122}$$

We evaluate the integrals:

$$\bar{\tilde{E}}_{pot,pair} = -\tilde{M}^2 \cdot \frac{D}{2} \cdot \frac{\tilde{r}^2}{\tilde{r}^D} = -\tilde{M}^2 \cdot \frac{D}{2 \cdot \tilde{r}^{D-2}} \tag{8.123}$$

We attribute one half of the potential energy of the pairs to the considered reference object:

$$\boxed{\bar{\tilde{E}}_{pot} = -\tilde{M}^2 \cdot \frac{D}{4 \cdot \tilde{r}^{D-2}}} \tag{8.124}$$

8.4.4 Energy of one object

In this section we analyze the energy, volume, energy density and pressure corresponding to one object. Thereby the interaction with other objects is included. Altogether that object is representative for the gas.

The averaged energy $\bar{\tilde{E}}$ of the reference object consists of the kinetic energy in Eq. (8.113) plus the ZPE in Eq. (8.116) plus $N-1$ times the potential energy in Eq. (8.124). Additionally we apply Eqs. (8.117, 8.118). So we get:

$$\boxed{\bar{\tilde{E}} = \frac{1}{2\tilde{a}} \cdot \left(1 + \frac{D}{2}\right) - \left(\bar{\kappa}^D - 1\right) \cdot \frac{\tilde{M}^2 \cdot D}{4 \cdot (\bar{\kappa} \cdot \tilde{a})^{D-2}}} \tag{8.125}$$

Pressure of the gas: The pressure is the above energy divided by the volume $\tilde{a}^D$:

$$\boxed{\tilde{p}_{gas} = \left(\frac{1}{2\tilde{a}} \cdot \left(1 + \frac{D}{2}\right) - \frac{\left(\bar{\kappa}^D - 1\right) \cdot \tilde{M}^2 \cdot D}{4 \cdot (\bar{\kappa} \cdot \tilde{a})^{D-2}}\right) \cdot \frac{1}{\tilde{a}^D}} \tag{8.126}$$

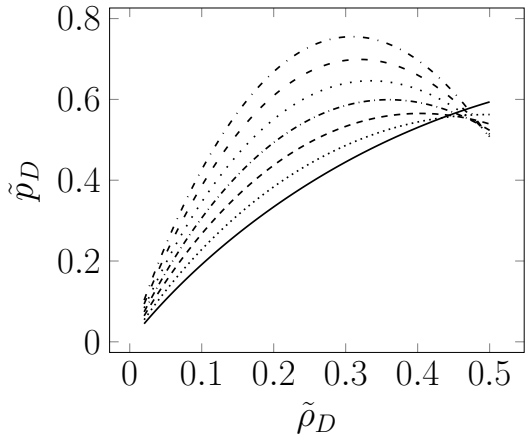

Figure 8.9: $\tilde{p}_D(\tilde{\rho}_D)$:$D = 3$ (solid line), $D = 4$ (dotted), $D = 5$ (dashed), $D = 6$ (dashdotted). $D = 7$ (loosely dotted), $D = 8$ (loosely dashed), $D = 9$ (loosely dashdotted). Dimensional phase transitions occur at the critical densities $\tilde{\rho}_{D=3,c} \approx 0.435$, $\tilde{\rho}_{D=4,c} \approx 0.45$, $\tilde{\rho}_{D=5,c} \approx 0.465$, $\tilde{\rho}_{D=6,c} \approx 0.48$, $\tilde{\rho}_{D=7,c} \approx 0.487$, $\tilde{\rho}_{D=8,c} \approx 0.493$, $\tilde{\rho}_{D=9,c} \approx 0.497$.

Appropriate radius of the HUF: We formulated our Bose gas model for various factors $\bar{\kappa}$ or radii of the HUF $\tilde{r} = \bar{\kappa} \cdot \tilde{a}$. So that Bose gas model can be varied easily. However, if we choose a very large radius $\tilde{r}$, the effect of self averaging occurs (see theorem 27), but it is not automatically compensated in our model. An appropriate values of $\bar{\kappa}$ that causes little self averaging is $\bar{\kappa} = 2$. Larger values of $\bar{\kappa}$ systematically overestimate gravity and give rise to lower bounds for the critical densities $\tilde{\rho}_{D,c}$.

Numerical investigation: For the case of $\bar{\kappa} = 2$, the pressure $\tilde{p}$ of the Bose gas is shown as a function of the density $\tilde{\rho}_D$ for various dimensions D (Fig. 8.9). At low density, the pressure or energy density of the $D = 3$ is minimal and stable. At the density $\tilde{\rho}_{D=3,c} \approx 0.433$, the transition between dimensions three and four takes place. So there occurs a sequence of transitions with critical densities $\tilde{\rho}_{D,c}$

Dimensional transitions at critical densities: At low density, the dimension $D = 3$ minimizes the energy. At the critical density $\tilde{\rho}_{D=3,c} \approx 0.433$, the gas has the same energy for $D = 3$ and $D = 4$, while $D = 3$ does not minimize the energy for higher densities $\tilde{\rho} > \tilde{\rho}_{D=3,c}$. If the density decreases, then there occurs a dimensional transition from $D = 4$ to $D = 3$ at $\tilde{\rho}_{D=3,c}$ (Fig. 8.9). For more numerical results see (Sawitzki and Carmesin (2021)).

Analogously, at the next critical density $\tilde{\rho}_{D=4,c} \approx 0.453$, the energies are equal for $D = 4$ and $D = 5$. Similarly, the critical densities $\tilde{\rho}_{D,c}$ increase monotonously with the dimension D. For instance, the next critical densities are $\tilde{\rho}_{D=5,c} \approx 0.47$, $\tilde{\rho}_{D=6,c} \approx 0.48$, $\tilde{\rho}_{D=7,c} \approx 0.487$, $\tilde{\rho}_{D=8,c} \approx 0.493$, For the transition at $D = 301$ we find the critical density $\tilde{\rho}_{301,c} \approx 0.5$.

Theorem 28 Dimensional phase transitions in the Bose gas:

(1) The present model of a Bose gas with interacting particles is valid for dimensions $D \geq 3$ and for a density $\tilde{\rho}_D$, and it includes the following relations (Fig. 8.8):

(1a) The extension or radius or standard deviation of photon is as follows:

$$\tilde{a} = \tilde{\rho}_D^{\frac{-1}{D+1}} \tag{8.127}$$

(1b) The gas is in a HUF with the following radius $\tilde{r}$, characterized by a parameter $\bar{\kappa}$ that can be chosen freely:

$$\tilde{r} = \bar{\kappa} \cdot \tilde{a} \tag{8.128}$$

Hereby $\bar{\kappa}$ should be chosen so that the self averaging in theorem (27) is appropriate.

(1c) A photon has the following dynamic mass:

$$\tilde{M} = \frac{1}{2 \cdot \tilde{a}} \tag{8.129}$$

(2) As a result, the gas has the following properties:

(2a) The gas is characterized by the following energy function of a single boson:

$$\bar{\tilde{E}} = \frac{1}{2\tilde{a}} \cdot \left(1 + \frac{D}{2}\right) - \left(\bar{\kappa}^D - 1\right) \cdot \frac{\tilde{M}^2 \cdot D}{4 \cdot (\bar{\kappa} \cdot \tilde{a})^{D-2}} \tag{8.130}$$

(2b) The gas exhibits the following **pressure***:*

$$\tilde{p}_{gas} = \left(\frac{1}{2\tilde{a}} \cdot \left(1 + \frac{D}{2}\right) - \frac{\left(\bar{\kappa}^D - 1\right) \cdot \tilde{M}^2 \cdot D}{4 \cdot (\bar{\kappa} \cdot \tilde{a})^{D-2}} \right) \cdot \frac{1}{\tilde{a}^D} \tag{8.131}$$

(3) There occur **dimensional phase transitions** *(Fig. 8.9). that are completely analogous to those in the mean field model (theorem 26):*

(3a) The dimension with the lowest pressure is stable.

(3b) The transition is driven by the attractive force of gravitation, so it is interpreted as a condensation and as a gravitational instability.

(3c) At a critical density $\tilde{\rho}_{D,c}$ the system undergoes a dimensional phase transition from a dimension $D + s$ to D.

(3d) The larger the density $\tilde{\rho}_D$ is, the larger is D.

(3e) The dimension $D_{horizon} = 301$ is achieved at a critical density that is near 0.5.

8.5 Dark energy: theory III: $D \geq 3$

The **dark energy theory I** as well as the **dark energy theory II** provide a description of the dark energy in three dimensional space. In this section we develop and analyze the dark energy in all dimensions ranging from the dimensional horizon $D_{horizon}$ until $D = 3$, from the Big Bang until today[2]. Moreover, in this

[2]That theory has been published since 2018 (Carmesin (2018c), Carmesin (2018b), Carmesin (2019b), Carmesin (2019a))

section we derive the density of the dark energy directly from the universal constants G, c and $\hbar$.

We derive the density of the vacuum $\tilde{\rho}_v$ or the dark energy from the knowledge of the dimensional horizon $D_{horizon} = 301.35 \approx 301$. The dark energy consists of gravitational waves of the space. At the **dimensional horizon** $D_{horizon}$, a quantum object that is causally effective here exhibits an extension or standard deviation $\Delta x = L_P$ and the corresponding energy $E(D_{horizon}) = E_P/2$ and the dynamic mass $M(D_{horizon}) = M_P/2$ and $D = 301$.

During **dimensional unfolding**, the wavelength λ of these quantized waves increases by the **distance enlargement factor** $Z_{D_{horizon} \to D=3}$, as these waves constitute the space. Correspondingly, the energy of a quantized wave decreases by the inverse factor $\frac{1}{Z_{D_{horizon} \to D=3}}$. The gravitational wave has $D-1$ directions of polarization. So 300 directions at $D_{horizon}$ are reduced to two directions at $D = 3$. Hence the energy decreases by another factor 150. So we derive:

$$E(D=3) = \frac{E(D_{horizon})}{150 \cdot Z_{D_{horizon} \to D=3}} \quad \text{or} \tag{8.132}$$

$$M(D=3) = \frac{M(D_{horizon})}{150 \cdot Z_{D_{horizon} \to D=3}} \tag{8.133}$$

Moreover, during the dimensional unfolding, the distances increased by the distance enlargement factor $Z_{D_{horizon} \to D=3}$. Thus the three dimensional volume corresponding to that quantum object is as follows:

$$V = V_{D=3} \cdot (L_P \cdot Z_{D_{horizon} \to D=3})^3 \tag{8.134}$$

Hereby V_D is the volume of the unit hyperball in D dimensions (see appendix). In particular, at $D = 3$ one derives $V_{D=3} = \frac{4\pi}{3}$.

In the process of the **expansion of the space**, the quanta of the space analyzed in this section do not enlarge or increase

their wavelength, instead the number of these quanta increases. The density of these quanta is the dynamical mass divided by the volume:

$$\boxed{\rho_v = \frac{M(D_{horizon})}{V_{D=3} \cdot L_P^3 \cdot 150 \cdot Z^4_{D_{horizon} \to D=3}}} \tag{8.135}$$

Here we apply the fact that the dynamical mass at $D_{horizon}$ is approximately equal to its maximum $M_P/2$:

$$M(D_{horizon}) \approx \frac{M_P}{2} \tag{8.136}$$

Moreover we apply the Planck density related to balls (see appendix):

$$\bar{\rho}_{P,v} = \frac{M_P}{V_{D=3} \cdot L_P^3} = 1.2307 \cdot 10^{96} \, \frac{\text{kg}}{\text{m}^3} \tag{8.137}$$

We insert Eqs. (8.136) and 8.137) into Eq. (8.135) and derive:

$$\boxed{\rho_v = \frac{\bar{\rho}_{P,v}}{300 \cdot Z^4_{D_{horizon} \to D=3}}} \tag{8.138}$$

We insert the distance enlargement factor (Eq. 8.75), including $D_{horizon} = 301.35$,

$$Z_{D_{horizon} \to D=3} = 2^{\frac{D_{horizon}-3}{3}} = 8.65 \cdot 10^{29} \tag{8.139}$$

into the Eq. (8.135) and derive:

$$\rho_v = 5.954 \cdot 10^{-123} \cdot \bar{\rho}_{P,v} \;\; \text{or} \;\; \tilde{\rho}_v = 5.954 \cdot 10^{-123} \tag{8.140}$$

Based on the CMB probe (Collaboration (2020)), the following density can be derived (Sect. 9.2):

$$\tilde{\rho}_{v,CMB} = 4.8181 \cdot 10^{-123} \tag{8.141}$$

The difference amounts to 24 %. That difference is relatively small compared to the factor

$$150 \cdot Z^4_{D_{horizon} \to D=3} = 8.4 \cdot 10^{121} \tag{8.142}$$

by which the density changed from its value at $D_{horizon}$ to its value at $D = 3$, and ρ_v is derived directly from the universal constants G, c and $\hbar$. Hence that relatively small difference and the correct physics provide a clear evidence for the *dark energy theory III*.

Theorem 29 Dark energy theory III, ranging from the dimensional horizon $D_{horizon}$ to $D = 3$:

(1) The dark energy theory III provides a quantum theory of dark energy.

(2) The dark energy theory III provides a description of the dark energy ranging from the dimensional $D_{horizon}$ to the actual and lowest possible dimension $D = 3$.

(3) The dark energy theory III provides a description of the time evolution of the dark energy ranging from its highest three dimensional projected density at $D_{horizon}$

$$\frac{1}{2} \cdot \bar{\rho}_{P,v} = \frac{1}{2} \cdot \frac{M_P}{V_{D=3} \cdot L_P^3} = \frac{1}{2} \cdot 1.2307 \cdot 10^{96} \, \frac{\text{kg}}{\text{m}^3} \tag{8.143}$$

to the actual density:

$$\rho_v = 5.954 \cdot 10^{-123} \cdot \bar{\rho}_{P,v} \quad or \quad \tilde{\rho}_v = 5.954 \cdot 10^{-123} \tag{8.144}$$

(4) The dark energy theory III provides a clear formula for the density:

$$\rho_v = \frac{M(D_{horizon})}{V_{D=3} \cdot L_P^3 \cdot 150 \cdot Z^4_{D_{horizon} \to D=3}} = \frac{\bar{\rho}_{P,v}}{300 \cdot Z^4_{D_{horizon} \to D=3}} \tag{8.145}$$

(5) The difference between the dark energy theory III and the observation amounts to difference of 24 %. That difference is relatively small compared to the factor by which the density varies: $8.4 \cdot 10^{121}$.

(6) That relatively small difference provides a clear evidence for the dark energy theory III.

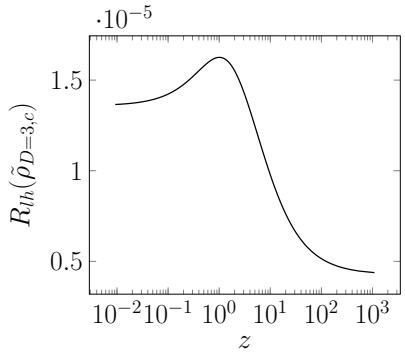

Figure 8.10: Light horizon at $\tilde{\rho}_{D=3,c}$ as a function of the redshift.

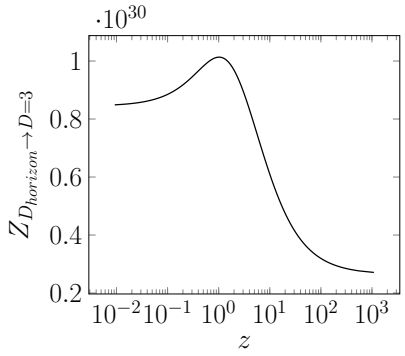

Figure 8.11: Distance enlargement factor $Z_{D_{horizon} \to D=3}$ as a function of the redshift.

8.6 Dark energy: theory IV: polychromatic vacuum

The *dark energy theory III* describes a monochromatic vacuum, whereby the wavelength depends on the light horizon at the critical density $\rho_{D=3,c}$. In this section we describe the time evolution of that horizon, and we analyze the resulting **polychromatic vacuum**.

Light horizon: The calculation of the time evolution of the light horizon has been elaborated in (Carmesin (2018c)) as well as in (Carmesin (2018b)) and in (Carmesin (2019b)). Thereby the

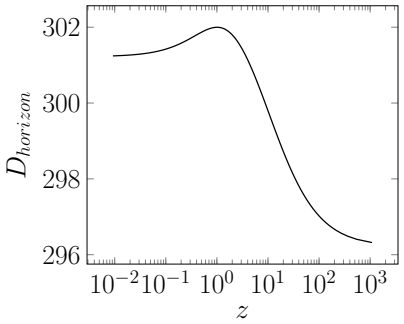

Figure 8.12: Dimensional horizon as a function of the redshift.

density parameter Ω_Λ has been calculated on the basis of the universal constants G, c and h and by application of the *dark energy theory IV* directly ((Carmesin, 2019b, p. 189)):

$$\Omega_\Lambda = 0.6840 \tag{8.146}$$

Hereby the amount of the completely formed vacuum, CFV, is derived on the basis of the FLE. In particular, the LFV and the NFV are not distinguished.

Moreover, the light horizon R_{lh} that could be observed by an observer at a redshift z is derived((Carmesin, 2019b, p. 189)), and it is represented as a function of z in Fig. (8.10).

Distance enlargement factor: Using the light horizon in Fig. (8.10), the distance enlargement factor $Z_{D_{horizon}\to D=3}$ is derived ((Carmesin, 2019b, p. 189)). It is shown in Fig. (8.11).

Dimensional horizon $D_{horizon}$: Using the distance enlargement factor $Z_{D_{horizon}\to D=3}$, we derive the corresponding dimensional horizon:

$$D_{horizon} = \frac{3 \cdot \ln Z_{D_{horizon}\to D=3}}{\ln 2} + 3 \tag{8.147}$$

The dimensional horizon as a function of the redshift is shown in Fig. (8.12).

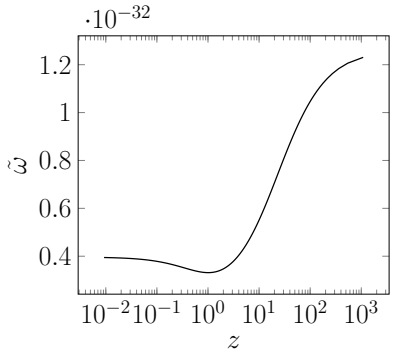

Figure 8.13: Scaled circular frequency $\tilde{\omega}$ of a quantum of dark energy at $D = 3$ as a function of the redshift.

8.6.1 Spectrum

In this section we analyze the spectrum of the quanta of the dark energy. For it we use the distance enlargement factor $Z_{D_{horizon} \to D=3}$ and the primordial energy $\tilde{E}_{D_{horizon}} \approx \frac{1}{2}$ in order to derive the scaled energy or the scaled circular frequency of a quantum of dark energy:

$$\tilde{E} = \tilde{\omega} = \frac{1}{2 \cdot 150 \cdot Z_{D_{horizon} \to D=3}} \tag{8.148}$$

The scaled circular frequency of a quantum of dark energy as a function of the redshift is shown in Fig. (8.13).

8.6.2 Density

In this section we derive the density $\tilde{\rho}_\Lambda$ or $\tilde{\rho}_v$ of the dark energy that forms at a redshift z. For it we divide the scaled energy (Eq. 8.147 and Fig. 8.13) by the scaled volume $Z^3_{D_{horizon} \to D=3}$. Hence we derive:

$$\tilde{\rho}_v = \frac{1}{Z^4_{D_{max} \to D=3} \cdot 2 \cdot 150} \tag{8.149}$$

Note that in ((Carmesin, 2019b, p. 97)), we additionally use the fact that $\tilde{\rho}_{D_{max},c}$ deviates slightly from $\frac{1}{2}$, accordingly we

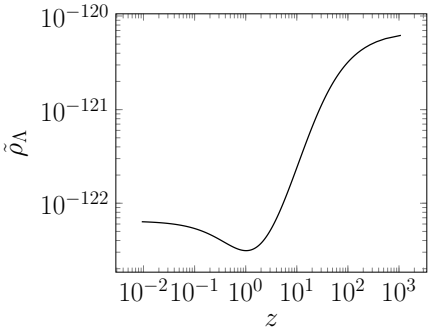

Figure 8.14: Scaled density $\tilde{\rho}_\Lambda$ of dark energy at $D = 3$ as a function of the redshift z at which the quanta formed.

apply the more precise relation:

$$\tilde{\rho}_{v,t_f} = (2\tilde{\rho}_{D_{max},c})^{\frac{4}{D_{max}+1}} \cdot \frac{1}{Z^4_{D_{max}\to D=3} \cdot (D_{max} - 1)} \qquad (8.150)$$

That scaled density of dark energy as a function of the redshift is shown in Fig. (8.14).

8.6.3 Density of the actual polychromatic vacuum

During the evolution of the universe, there formed vacuum consisting of quanta at various circular frequencies (Fig. 8.13). The vacuum that constitutes the present space is the linear combination of these quanta of vacuum. Hence the actual vacuum is a polychromatic vacuum, constituted by a linear combination of various monochromatic quanta of vacuum. In this section we derive the density of that polychromatic vacuum.

For it we integrate along all redshifts ranging from the redshift $z_{D=3,c}$ of the first formation of three dimensional space at the time of the dimensional phase transition at $\tilde{\rho}_{D=3,c}$ until today at $z = 0$. At each redshift z we derive the additional volume $\Delta V(z)$ formed according to the FLE, and we use the density $\tilde{\rho}_\Lambda(z)$ of the monochromatic vacuum forming at that redshift z.

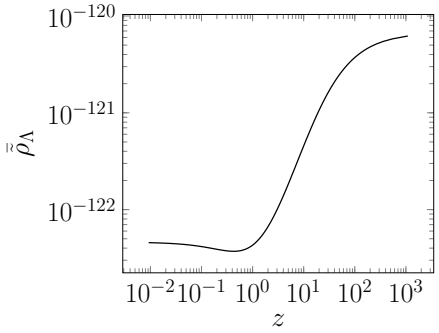

Figure 8.15: Averaged scaled density $\bar{\tilde{\rho}}_\Lambda$ of the polychromatic dark energy or the the polychromatic vacuum at $D = 3$ as a function of the redshift.

Thus we derive the following averaged density:

$$\bar{\tilde{\rho}}_\Lambda(\zeta = z_{D=3,c}, \zeta = z) = \frac{\int_{z_{D=3,c}}^{z} \Delta V(\zeta) \cdot \tilde{\rho}_\Lambda(\zeta) d\zeta}{\int_{z_{D=3,c}}^{z} \Delta V(\zeta) d\zeta} \tag{8.151}$$

8.6.4 Density $\bar{\tilde{\rho}}_\Lambda(\zeta = z, \zeta = 0)$ formed during $\zeta \in [z, 0]$

If a measurement is based on a probe based on radiation emitted at the redshift z, then that radiation experiences redshifts ζ according to the formation of vacuum in the interval $\zeta \in [0, z]$. Thus the density of vacuum generating that redshift is as follows:

$$\bar{\tilde{\rho}}_\Lambda(\zeta = z, \zeta = 0) = \frac{\int_{z}^{0} \Delta V(\zeta) \cdot \tilde{\rho}_\Lambda(\zeta) d\zeta}{\int_{z}^{0} \Delta V(\zeta) d\zeta} \tag{8.152}$$

That scaled averaged density of the formed polychromatic dark energy or of the formed polychromatic vacuum as a function of the redshift is shown in Fig. (8.15).

8.6.5 Time evolution of H_0

In this section we derive the time evolution of the Hubble constant H_0. In particular we derive H_0 as a function of the redshift z.

For it we apply the fraction of H_0 values derived above (Eq. 7.148):

$$\frac{H_0^2(t_0, R_0, z)}{H_0^2(t_0, R_0, z = 1090)} = \Omega_m + \Omega_\Lambda \cdot (1 + \kappa(z))^2 \tag{8.153}$$

In order to apply that Eq., we identify the factor $(1 + \kappa(z))^2$ by a correction factor $\Omega_{\Lambda,corr}(z)$ of the density parameter Ω_Λ:

$$\boxed{\Omega_{\Lambda,corr}(z) = \frac{\bar{\bar{\rho}}_\Lambda(\zeta = z, \zeta = 0)}{\bar{\bar{\rho}}_\Lambda(\zeta = z_{D=3,c}, \zeta = 0)}} \tag{8.154}$$

We use the following approximation that is very close to exactness:

$$\bar{\bar{\rho}}_\Lambda(z = z_{D=3,c}) \hat{=} \bar{\bar{\rho}}_\Lambda(z = 1090) \tag{8.155}$$

With it we derive:

$$\frac{H_0^2(t_0, R_0, z)}{H_0^2(t_0, R_0, z = 1090)} = \Omega_m + \Omega_\Lambda \cdot \Omega_{\Lambda,corr}(z) \tag{8.156}$$

We solve for $H_0(t_0, R_0, z)$:

$$\boxed{H_0(t_0, R_0, z) = H_0(t_0, R_0, z = 1090) \cdot \sqrt{\Omega_m + \Omega_\Lambda \cdot \Omega_{\Lambda,corr}(z)}} \tag{8.157}$$

The resulting evolution is shown in Fig. (8.16). That Fig. clearly shows that the *dark energy theory IV* exhibits a precise accordance with observations ranging from the early ($z = 1090$) to the late ($z = 0.0865$) universe. In particular, the deviation between observation and measurement is very small for three observations: Firstly, there is an accurate accordance for the case of $z = 0.0865$ using observations based on the distance ladder:

$$\Delta H_0 = \frac{\Delta H_{0,\text{ theory IV}} - \Delta H_{0,\text{ observation}}}{H_{0,\text{ observation}}} \tag{8.158}$$

$$\Delta H_{0,\text{ theory IV - distance ladder}} = \frac{73.796 - 74.03}{74.03} = -0.32\% \tag{8.159}$$

Secondly, there is a high accordance for the case of $z = 0.75$ utilizing observations based on weak gravitational lensing:

$$\Delta H_{0,\text{ theory IV - gravitational lens}} = \frac{68.098 - 68.25}{68.25} = -0.22\% \tag{8.160}$$

Thirdly, there is a high accordance for the case of $z = 1090$ applying observations based on the CMB probe:

$$\Delta H_{0,\text{ theory IV - CMB}} = \frac{68.348 - 68.36}{68.36} = 0.018\% \tag{8.161}$$

Furthermore, the *dark energy theory IV* exhibits an even more precise accordance to the observations than the *dark energy theory II*. Moreover, *dark energy theory IV* provides a derivation of the density at $z = 1090$, so that an additional prediction and comparison with observations is enabled. Indeed, the *dark energy theory IV* explains the discrepancy between H_0 probes taken in the early universe and H_0 probes based on the late universe. In fact, this explanation is also provided by the *dark energy theory II*.

8.6.6 Time evolution of σ_8

In this section we derive the time evolution of the amplitude of matter fluctuations σ_8. In particular we derive σ_8 as a function of the redshift z.

We derive the correction factor in Eq. (7.159):

$$\sigma_{8,corrected}(z) = \sigma_8 \cdot \left(\frac{H_0}{H_0(z)}\right)^2 \tag{8.162}$$

We use the reference values of the CMB at $z = 1090$, and we insert Eq. (8.157). So we get:

$$\boxed{\sigma_{8,corrected}(z) = \frac{\sigma_8(z = 1090)}{\Omega_m + \Omega_\Lambda \cdot \Omega_{\Lambda,corr}(z)}} \tag{8.163}$$

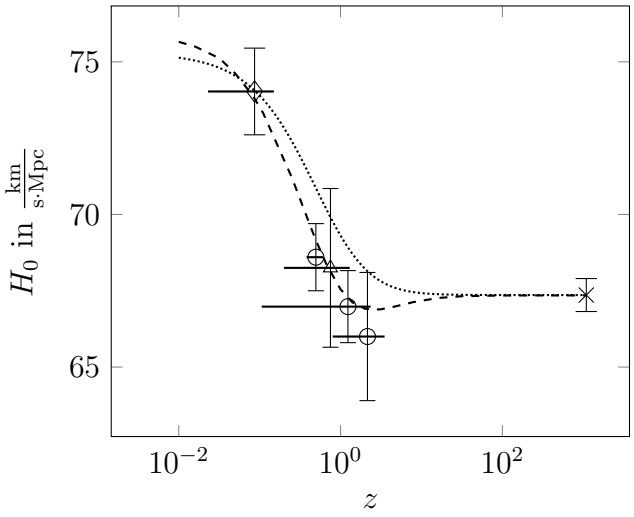

Figure 8.16: H_0 as a function of the redshift z of the probe: distance ladder ($\diamond$, Riess et al. (2019)), baryonic acoustic oscillations (o, Zaldarriaga et al. (2020), Weiland et al. (2018), Blomquist et al. (2019)), weak gravitational lensing (Δ, Lu and Haiman (2020)), CMB ($\times$, Collaboration (2020)). *Dark energy theory II* (dotted). *Dark energy theory IV* (dashed).

The resulting function $\sigma_{8,corrected}(z)$ is evaluated by using the value $\sigma_8(z = 1090) = 0.8111$ (see Sect. 9.2 or Collaboration (2020)). The function $\sigma_{8,corrected}(z)$ is shown in Fig. (8.17).

The Fig. (8.17) illustrates very clearly that the *dark energy theory IV* exhibits a precise accordance with observations. We emphasize that the theoretical values are all within the errors of measurement. We investigate the small differences between theory and measurement in detail: Firstly, there is an accurate accordance for the case of $z = 0.75$ using observations of the **dark energy survey, DES** and based on galaxy clustering and weak lensing:

$$\Delta\sigma_{8,\text{ theory IV - DES}} = \frac{0.7923 - 0.817}{0.817} = -3\% \qquad (8.164)$$

Secondly, there is a high accordance for the case of $z = 0.75$, whereby the observations are based on weak gravitational lens-

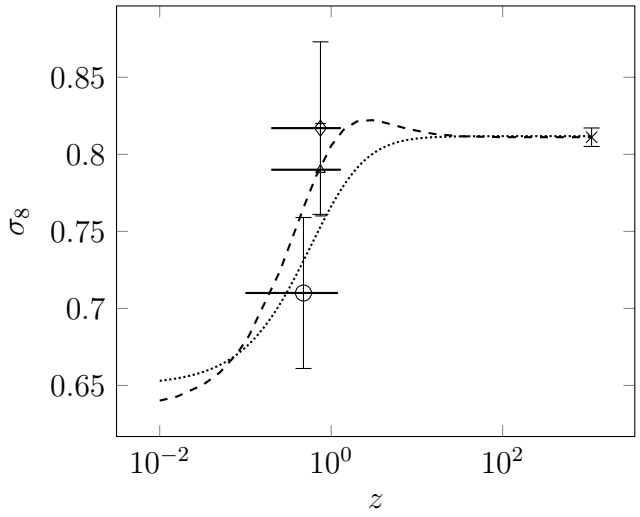

Figure 8.17: σ_8 as a function of the redshift z of the probe: galaxy clustering and lensing ($\diamond$, (Abbott et al., 2019, p. 6, 15)), weak gravitational lenses ((Lu and Haiman, 2020, p. 1, 2)), baryonic acoustic oscillations (o, (Tröster et al., 2020, p. 1, 2)), CMB ($\times$, (Collaboration, 2020, p. 16)). *Dark energy theory II* (dotted). *Dark energy theory IV* (dashed).

ing:

$$\Delta\sigma_{8,\text{ theory IV - gravitational lensing}} = \frac{0.7923 - 0.79}{0.79} = -0.29\% \tag{8.165}$$

Thirdly, there is a precise accordance for the redshift $z = 0.475$ and for observations based on the baryon acoustic oscillations, BAO:

$$\Delta\sigma_{8,\text{ theory IV - BAO}} = \frac{0.7651 - 0.71}{0.71} = 7.8\% \tag{8.166}$$

Furthermore, the *dark energy theory IV* clearly exhibits an even more precise accordance with the observations than the *dark energy theory II* does. Moreover, the *dark energy theory IV* explains the discrepancy between σ_8 probes taken in the early universe and σ_8 probes based on the late universe, see Fig. (8.17). Indeed, this explanation is also provided by the classical *dark energy theory II*[3].

[3]This is enabled by the fact that the time evolution of the Hubble flow is underlying

Theorem 30 Dark energy theory IV provides very precise accordance with observations:

The dark energy theory IV provides a quantum theory of dark energy, including the following properties:

(1) The amount of the produced vacuum is derived on the basis of the FLE, so the distinction between LFV and NFV is not needed.

(2) The polychromatic spectrum of the vacuum is derived, see Fig. (8.13).

(3) The time evolution of the density of vacuum $\tilde{\rho}_v(z)$ formed at a redshift z is derived, see Fig. (8.14).

(4) The time evolution of the light horizon (Fig. 8.10), of the distance enlargement factor (Fig. 8.11) and of the dimensional horizon (Fig. 8.12) are derived.

(5) The density of the vacuum formed in an interval of redshifts $\zeta \in [z_1, z_2]$ is averaged as follows:

$$\bar{\tilde{\rho}}_\Lambda(\zeta = z_1, \zeta = z_2) = \frac{\int_{z_1}^{z_2} \Delta V(\zeta) \cdot \tilde{\rho}_\Lambda(\zeta) d\zeta}{\int_{z_1}^{z_2} \Delta V(\zeta) d\zeta} \tag{8.167}$$

That average $\bar{\tilde{\rho}}_\Lambda(z)$ is shown as a function of z, see Fig. (8.15).

(6) If a measurement is based on a probe constituted by radiation emitted at a redshift z, then this radiation experiences a redshift according to the formation of vacuum in the interval $\zeta \in [0, z]$. Hence the density of vacuum generating that redshift is equal to the averaged density $\bar{\tilde{\rho}}_\Lambda(\zeta = z, \zeta = 0)$.

(6a) In particular, the time evolution of $H_0(z)$ is characterized by the following correction factor:

$$\Omega_{\Lambda,corr}(z) = \frac{\bar{\tilde{\rho}}_\Lambda(\zeta = z, \zeta = 0)}{\bar{\tilde{\rho}}_\Lambda(\zeta = z_{D=3,c}, \zeta = 0)} \tag{8.168}$$

---

the evolution of structure and the evolution of the light horizon.

And a probe at a redshift z causes the following value of $H_0(z)$:

$$H_0(t_0, R_0, z) = H_0(t_0, R_0, z = 1090) \cdot \sqrt{\Omega_m + \Omega_\Lambda \cdot \Omega_{\Lambda,corr}(z)} \tag{8.169}$$

(6b) The resulting $H_0(z)$ values are in very precise accordance with the observations, see Fig (8.16).

(6c) The resulting $H_0(z)$ values explain the discrepancy between $H_0(z)$ values measured by probes of the early universe and $H_0(z)$ values measured by probes of the late universe.

(6d) In particular, the time evolution of $\sigma_8(z)$ is characterized as follows:

$$\sigma_{8,corrected}(z) = \frac{\sigma_8(z = 1090)}{\Omega_m + \Omega_\Lambda \cdot \Omega_{\Lambda,corr}(z)} \tag{8.170}$$

(6e) The resulting $\sigma_8(z)$ values are in very accurate accordance with the observations, see Fig (8.17).

(6f) The resulting $\sigma_8(z)$ values explain the discrepancy between $\sigma_8(z)$ values measured by probes of the early universe and $\sigma_8(z)$ values measured by probes of the late universe.

(6g) The resulting $H_0(z)$ values as well as the derived $\sigma_8(z)$ values of the dark energy theory IV are even more precisely in accordance with the observations then the corresponding $H_0(z)$ values and $\sigma_8(z)$ values of the dark energy theory II.

(6h) The very good accordance of the dark energy theory IV with measurements and its explanatory power provide a clear evidence for that theory.

(6i) It does not present any conflict that the classical dark energy theory II exhibits small differences to the dark energy theory IV that applies quantum physics additionally.

8.7 Time evolution of forms of energy

In this section we analyze the time evolution of those constituents that amount to at least 5 % to the own energy of all objects in the universe at the present time or at some earlier instant of time.

8.7.1 Own energy

In this section we analyze the own energies, as that energy is observed in many experiments or observations.

The own energy of a relativistic object such as a photon or a quantum of vacuum is equal to the Planck constant h divided by its periodic time T:

$$E_{\text{own, relativistic}} = \frac{h}{T} \tag{8.171}$$

The own energy of an object that has a mass in its own system is a characteristic property of that object. For instance, the electron or the elementary particles of dark matter exhibit a specific mass m_{own} (see for instance Tanabashi et al. (2018), Carmesin (2018d), Carmesin (2019b)). The own energy of such an object is determined according to the equivalence of mass and energy:

$$E_{\text{own, mass}} = m_{\text{own}} \cdot c^2 \tag{8.172}$$

8.7.2 Constituents

In this section we analyze the constituents that represent a sufficient amount of the own energy of all objects in the universe.

The constituents of the universe can be sorted in three categories: vacuum, radiation and matter.

Thereby the matter consists of dark matter and visible matter. Hereby the visible matter represents less than 5 % of the all forms of energy, as its density parameter is $\Omega_b = 0.0493$ (see Sect. 9.2). So it is not analyzed in the following. The dark

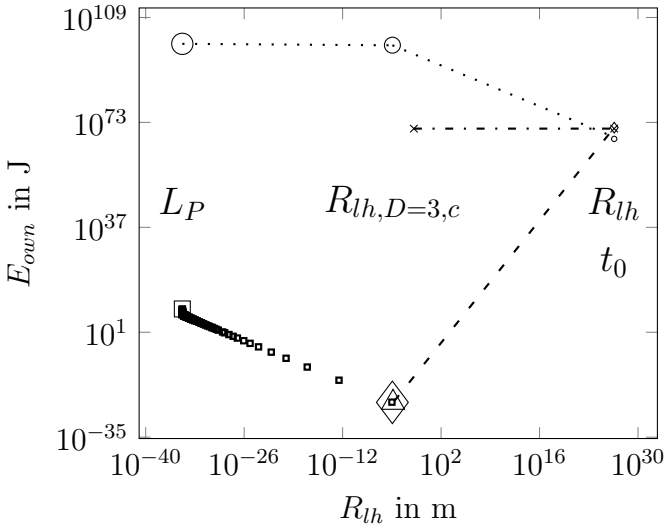

Figure 8.18: Time evolution of **own energies**: Energy of vacuum (squares, $\diamond$, dashed). Energy of radiation ($\circ$, dotted). Energy of dark matter ($\times$, dashdotted). In a HUF or HUF_v, the same amounts of gravitational energy and negative sign occur, so that the corresponding energies are zero: $E_{HUF} = E_{own} + E_{gravity} = 0$.

energy represents 26.45 % of the complete energy, as its density parameter is $\Omega_c = 0.2645$ (see Sect. 9.2).

The radiation represents less that 5 % of energy today, but in the early universe, the radiation represented most of the energy at that time, so we analyze that energy as well.

The vacuum represents 68.47 % of the complete energy, as its density parameter is $\Omega_\Lambda = 0.6847$ (see Sect. 9.2).

8.7.3 Dark energy in the HUF

In this section we analyze the dark energy in a HUF. For it we apply the critical density at which three dimensional space forms for the first time $\tilde{\rho}_{D=3,c} = 0.435$ (Fig. 8.9). We derive the state at that density in two ways: **backward** starting at the actual time t_0 and **forward** starting at $D_{horizon}$. Then we verify that both states are equal.

8.7.3.1 Energy conservation of dark energy

The dark energy is constituted by the energy of the RGWs. In the HUF, that energy is **zero**. In particular, that energy is **conserved**.

8.7.3.2 Own energy at t_0

First we derive the energy density at t_0:

$$u_v(t_0) = \rho_{cr,t_0} \cdot \Omega_\Lambda \cdot c^2 \tag{8.173}$$

We insert (Sect. 9.2):

$$u_v(t_0) = 8.66 \cdot 10^{-27} \frac{\text{kg}}{\text{m}^3} \cdot 0.6847 \cdot c^2 = 5.329 \cdot 10^{-10} \frac{\text{J}}{\text{m}^3} \tag{8.174}$$

We multiply it by the volume $V_{lh}(t_0) = \frac{4\pi}{3} R_{lh}^3(t_0)$. Hereby we use $R_{lh} = 4.142 \cdot 10^{26}\text{m}$. So we get $V_{lh}(t_0) = 2.977 \cdot 10^{80}\text{m}^3$ (Carmesin (2019b), Gott et al. (2005)):

$$\boxed{E_v(t_0) = u_v(t_0) \cdot V_{lh}(t_0) = 1.586 \cdot 10^{71}\text{J}} \tag{8.175}$$

That state is represented by the diamond in Fig. (8.18).

8.7.3.3 Own energy during expansion

During the process of expansion the number of the quanta of dark energy increases proportional to the volume, while the energy per quantum remains invariant. So the energy is proportional to the volume. Hence the energy is proportional to R_{lh}^3:

$$E_v(R_{lh}) \propto R_{lh}^3 \tag{8.176}$$

In particular, for the case $R_{lh} = R_{lh}(t_0)$ we get:

$$E_v(t_0) \propto R_{lh}^3(t_0) \tag{8.177}$$

We form the ratio of both proportional relations:

$$\frac{E_v(R_{lh})}{E_v(t_0)} = \frac{R_{lh}^3}{R_{lh}^3(t_0)} \tag{8.178}$$

We solve for $E_v(R_{lh})$:

$$\boxed{E_v(R_{lh}) = E_v(t_0) \cdot \frac{R_{lh}^3}{R_{lh}^3(t_0)}} \tag{8.179}$$

We present that function by the dashed line in Fig. (8.18).

8.7.3.4 Own energy at $\tilde{\rho}_{D=3,c}$

At the dimensional phase transition to three dimensional space the density is $\tilde{\rho}_{D=3,c} = 0.435$ or $\rho_{D=3,c} = 5.353 \cdot 10^{95} \frac{\text{kg}}{\text{m}^3}$. With it we derive the scale factor from the radius $R_{lh,D=3,c}$ at $\rho_{D=3,c}$ to the radius $R_{lh}(t_0)$. As the density $\rho_{D=3,c}$ represents radiation, we relate it to the density of radiation $\rho_r(t_0) = \rho_{cr,t_0} \cdot \Omega_r = 8.335 \cdot 10^{-31} \frac{\text{kg}}{\text{m}^3}$ as follows:

$$k_{\rho_{D=3,c} \to t_0} = \left(\frac{\rho_{D=3,c}}{\rho_r(t_0)} \right)^{1/4} \tag{8.180}$$

We insert (Sect. 9.2):

$$k_{\rho_{D=3,c} \to t_0} = \left(\frac{5.353 \cdot 10^{95}}{8.335 \cdot 10^{-31}} \right)^{1/4} = 2.831 \cdot 10^{31} \tag{8.181}$$

With it we derive the radius $R_{lh,D=3,c}$:

$$R_{lh,D=3,c} = \frac{R_{lh}(t_0)}{k_{\rho_{D=3,c} \to t_0}} = 1.463 \cdot 10^{-5} \text{m} \tag{8.182}$$

We apply that radius to Eq. (8.179) in order to derive the energy of the vacuum at $R_{lh,D=3,c}$:

$$\boxed{E_v(R_{lh,D=3,c}, backward) = E_v(t_0) \cdot \frac{R_{lh,D=3,c}^3}{R_{lh}^3(t_0)} = 6.992 \cdot 10^{-24} \text{J}} \tag{8.183}$$

That state is presented by the triangle in Fig. (8.18).

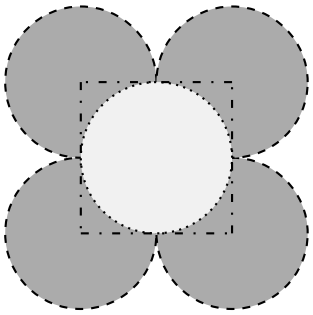

Figure 8.19: Two dimensional sketch at state at $D_{horizon}$: A single quantum of spacetime (dotted, light grey) provides space that is immediately filled by quanta of radiation (dashed, dark grey, in the sketch 'below' the quantum of spacetime). All quanta propagate at the velocity c, so that the sketch represents an averaged scenario that lasts for a short time, as the space expands and exhibits dimensional transitions. Edges of the hypercube (dashdotted).

8.7.3.5 Own energy at the Planck scale

At the dimensional horizon $D_{horizon}$, the states are at the Planck scale. So the quanta that have a causal effect upon us are within the light horizon. So their standard deviation or extension or radius is L_P. Thus their density is $\tilde{\rho}_{D,v} = \frac{1}{2}$. Accordingly, the energy of a quantum of dark energy is $\tilde{E}_{\mathrm{v},\, D_{horizon}} = \frac{1}{2}$ or:

$$\boxed{E_{\mathrm{v},\, D_{horizon}} = 9.781 \cdot 10^8 \mathrm{J}} \tag{8.184}$$

One quantum of spacetime at $D_{horizon}$: At the dimensional horizon, there are $2^{D_{horizon}}$ quanta of radiation that can in principle be arranged in a hypercube. The quanta of vacuum connect these quanta of radiation. One quantum of the vacuum in the center of the hypercube is **sufficient** in order to connect the quanta of radiation. Moreover, at least one quantum of the vacuum is **necessary** in order to connect the quanta of radiation.

Correspondingly, we model exactly one quantum of the vacuum (Fig. 8.19). Below we will confirm this number of one

quantum of the vacuum by the fact that the resulting state at $\tilde{\rho}_{D=3,c} = 0.435$ is equal to the state derived starting from t_0 (see Eqs. 8.182, 8.183 and the triangle in Fig. (8.18).

Radius at $D_{horizon}$: The radius of a quantum is equal to L_P. As there are two objects at an edge at $D_{horizon}$, the diameter at the light horizon corresponds to two L_P, and the light horizon corresponds to one L_P:

$$\boxed{R_{\text{lh, } D_{horizon}} = L_P = 1.616 \cdot 10^{-35}\text{m}} \tag{8.185}$$

8.7.3.6 Own energy during dimensional unfolding

During the process of **dimensional unfolding**, there occurs a sequence of **dimensional phase transitions** at **critical densities** $\tilde{\rho}_{D,c}$. Thereby energy E_v decreases according to the dimensional redshift and to projections of polarization directions, until $D = 3$ is reached at the density $\tilde{\rho}_{D=3,c} = 0.435$. So we get:

$$\boxed{E_{\text{own, vac, D}} = \frac{E_{\text{own, vac, } D_{horizon}}}{(D_{horizon} - D)/2 \cdot Z_{D_{horizon} \to D}}} \tag{8.186}$$

We derive the **distance enlargement factor**:

$$\boxed{Z_{D_{horizon} \to D} = 2^{\frac{D_{horizon} - D}{D}}} \tag{8.187}$$

For instance we get:

$$q_{D_{horizon} \to t_0} = \frac{R_{lh}}{L_P} = 2.563 \cdot 10^{61} \tag{8.188}$$

$$k_{L_P \to t_0} = \left(\frac{\bar{\rho}_P}{\rho_r(t_0)} \right)^{1/4} = 3.486 \cdot 10^{31} \tag{8.189}$$

$$Z_{D_{horizon} \to 3} = \frac{q_{D_{horizon} \to t_0}}{k_{L_P \to t_0}} = 7.352 \cdot 10^{29} \tag{8.190}$$

$$D_{horizon} = 3 + 3 \cdot \frac{\ln(Z_{D_{horizon} \to 3})}{\ln(2)} = 300.64 \tag{8.191}$$

$$E_{\text{own, vac, D=3, cr., forward}} = \frac{E_{\text{own, vac, } D_{horizon}}}{(D_{horizon}-3)/2 \cdot Z_{D_{horizon}\to D=3}} \tag{8.192}$$

$$E_{\text{own, vac, D=3, cr., forward}} = 8.869 \cdot 10^{-24}\text{J} \tag{8.193}$$

The corresponding value of the actual light horizon is evaluated by using the scale factor:

$$\boxed{R_{lh}(\tilde{\rho}_{D,c}) = L_P \cdot Z_{D_{horizon}\to D}} \tag{8.194}$$

These states at the sequence of the dimensional phase transitions are presented by the squares in Fig. (8.18).

At the critical density $\tilde{\rho}_{D=3,c}$ we obtain:

$$R_{lh}(\tilde{\rho}_{D=3,c,forward}) = L_P \cdot Z_{D_{horizon}\to 3} = 1.188 \cdot 10^{-5}\text{m} \tag{8.195}$$

That state is presented by the large diamond in Fig. (8.18). It coincides with the large triangle in that figure. Numerically, the radii of the backward and forward modeling exhibit the following difference (see Eqs. 8.182, 8.195):

$$\Delta R_{lh}(\tilde{\rho}_{D=3,c}) = \frac{1.463 - 1.188}{1.463} = 18.8\% \tag{8.196}$$

Similarly, the energies of the backward and forward modeling exhibit the following difference (see Eqs. 8.183, 8.193):

$$\Delta E_{\text{own, vac, 3}} = \frac{8.869 - 6.992}{8.869} = 21.2\% \tag{8.197}$$

These differences are only relatively small compared to one. That confirms the modeling of only one quantum of vacuum at $D_{horizon}$, the necessary and sufficient quantum.

8.7.4 Energy of radiation in the HUF

In this section we analyze the time evolution of the own energy of the radiation.

Planck scale: At the Planck scale, a quantum of radiation exhibits the same extension and energy density as the quanta of dark energy. So the results of section (8.7.3.5) are applied. As there are $2^{D_{horizon}}$ quanta of radiation (Fig. 8.19), we derive:

$$\boxed{E_{\text{own, rad, } D_{horizon}} = 3.985 \cdot 10^{99}\text{J}} \tag{8.198}$$

That state is presented by the large circle in Fig. (8.18).

8.7.4.1 Own energy at critical densities $\tilde{\rho}_{D,c}$

During the process of **dimensional unfolding**, there occurs a sequence of **dimensional phase transitions** at **critical densities** $\tilde{\rho}_{D,c}$.

Thereby the redshift of the quanta of radiation is proportional to the scale factor. As an appropriate approximation, we apply the exponent $\frac{1}{4}$:

$$\boxed{k_{D_{horizon} \to \tilde{\rho}_D} = \left(\frac{\tilde{\rho}_P}{\tilde{\rho}_D} \right)^{1/4}} \tag{8.199}$$

For the case of the transition to three dimensional space we derive:

$$k_{D_{horizon} \to \tilde{\rho}_{D=3,c}} = \left(\frac{\tilde{\rho}_P}{\tilde{\rho}_{D=3,c}} \right)^{1/4} = 1.231 \tag{8.200}$$

Correspondingly, the energy decreases by that factor:

$$E_{\text{own, rad, } \tilde{\rho}_D} = \frac{E_{\text{own, rad, } D_{horizon}}}{k_{D_{horizon} \to \tilde{\rho}_D}} \tag{8.201}$$

For the case of the transition to three dimensional space we derive by forward calculation:

$$E_{\text{own, rad, } \tilde{\rho}_{D=3,c}\text{, forward}} = \frac{E_{\text{own, rad, } D_{horizon}}}{k_{D_{horizon} \to \tilde{\rho}_{D=3,c}}} = 2.525 \cdot 10^{99}\text{J} \tag{8.202}$$

Transformation of arrangement: At $D_{horizon}$, the volume is arranged by balls at the corners of a hypercube (Fig. 8.19). Accordingly, we present that energy $E_{\text{own, rad, } \tilde{\rho}_{D=3,c}\text{, forward}}$ at the eight edges of the cube in $D = 3$. So the energy flows from outside towards the central ball. Thus the power density times the area πR_{lh}^2 enters the central ball. There is sufficient scattering that that radiation leaves the ball at the whole surface $4\pi R_{lh}^2$. So at a dynamical equilibrium, only one fourth of that radiation is in the central ball. Correspondingly we derive the energy that is within the ball with the radius of the light horizon as follows:

$$E_{\text{own, rad, } \tilde{\rho}_{D=3,c}\text{, forward, ball}} = \frac{E_{\text{own, rad, } \tilde{\rho}_{D=3,c}\text{, forward}}}{4} \tag{8.203}$$

$$E_{\text{own, rad, } \tilde{\rho}_{D=3,c}\text{, forward, ball}} = 0.63126 \cdot 10^{99}\text{J} \tag{8.204}$$

That state is presented by the medium sized circle in Fig. (8.18).

8.7.4.2 Own energy at $t = 0$

We derive the own energy at t_0 by forward calculation. For it we divide the energy $E_{\text{own, rad, } \tilde{\rho}_{D=3,c}\text{, forward, ball}}$ by the redshift:

$$k_{\tilde{\rho}_{D=3,c} \to t_0} = \left(\frac{\tilde{\rho}_{D=3,c}}{\tilde{\rho}_{t_0}} \right)^{1/4} = 2.8309 \cdot 10^{31} \tag{8.205}$$

So we get:

$$E_r(t_0) = \frac{E_{\text{own, rad, } \tilde{\rho}_{D=3,c}\text{, forward, ball}}}{k_{\tilde{\rho}_{D=3,c} \to t_0}} = \frac{0.63126 \cdot 10^{99}\text{J}}{2.8309 \cdot 10^{31}} \tag{8.206}$$

$$E_r(t_0) = 2.2299 \cdot 10^{67} \tag{8.207}$$

As a test we derive that energy directly

$$u_r(t_0) = \rho_{cr,t_0} \cdot \Omega_r \cdot c^2 \tag{8.208}$$

We insert (Sect. 9.2):

$$u_r(t_0) = 8.66 \cdot 10^{-27} \frac{\text{kg}}{\text{m}^3} \cdot 9.265 \cdot 10^{-5} \cdot c^2 = 7.491 \cdot 10^{-14} \frac{\text{J}}{\text{m}^3} \tag{8.209}$$

We multiply it by the volume $V_{lh}(t_0) = 2.977 \cdot 10^{80}\mathrm{m}^3$:

$$\boxed{E_r(t_0) = u_r(t_0) \cdot V_{lh}(t_0) = 2.2299 \cdot 10^{67}\mathrm{J}} \tag{8.210}$$

This coincides with the result in Eq. (8.207) and confirms the derived energies. That state is represented by the small circle in Fig. (8.18).

8.7.5 Energy of dark matter in the HUF

In this section we summarize the energy of the dark matter in a HUF. According to the dimensional phase transitions, elementary particles of dark matter form spontaneously at a small time slot (Carmesin (2018d), Carmesin (2019b)). The corresponding states are represented by two crosses and a dashdotted line in Fig. (8.18).

8.7.6 Energy conservation in the HUF

In this section we summarize and analyze the conservation of energy in a HUF. First we summarize and extend results about the energy conservation in a HUF and described by three factors.

Theorem 31 Law of energy conservation in a HUF:

(1) If a body with own mass m_0 and $m = m_0$ at $r \to \infty$ falls freely in a HUF, and if there is a field generating mass M with $R_S = \frac{2GM}{c^2}$ at a radial coordinate $r = 0$, then the following holds:

(1a) The energy $E(r, v)$ of m as a function of the velocity v and of r is the product of $m_0 \cdot c^2$, the Lorentz factor $\gamma(v) = \frac{1}{\sqrt{1-v^2/c^2}}$ and the position factor $\epsilon(r) = \sqrt{1 - R_S/r}$ (T. 1).

(1b) The product of the Lorentz factor and the position factor is one.

(1c) So the energy of that object is conserved.

(2) If a photon or a dynamical mass with a periodic time T_∞ at $r \to \infty$ falls freely in a HUF, and if there is a field generating mass M with $R_S = \frac{2GM}{c^2}$ at a radial coordinate $r = 0$, then the following holds:

(2a) The energy $E(r, v)$ of that object as a function of the periodic time T and of r is the product of $\frac{h}{T_\infty}$, a **kinetic factor** *$\bar{\gamma}(T) = \frac{T_\infty}{T}$ and the position factor $\epsilon(r) = \sqrt{1 - \frac{R_S}{r}}$ (Sect. 1.8.4).*

(2b) The product of the kinetic factor and the position factor is one.

(2c) So the energy of that mass is conserved.

(3) In particular the position factors of a mass m and of a photon at the same coordinate r are equal. So the position factor of a mass can be determined from the redshift of a photon at the same r (See derivation of g_{ij} T. 1).

Secondly, we summarize and extend results about the conservation of an energy per mass or per dynamic mass or of a **curvature parameter k_j of a pair** j in a HUF and described by three summands.

Theorem 32 Law of curvature conservation in a HUF:

(1) If an object has a rest mass m_0 and a reference energy $E_{ref} = m_0 \cdot c^2$, and with $E_{ref} \to 0$ at $r \to \infty$, and if that object falls freely in a HUF, and if there is a field generating mass M with $R_S = \frac{2GM}{c^2}$ at a radial coordinate $r = 0$, then the following holds:

(1a) The pair $(m; M)$ named by j is described by the following **structured energy function** *$\bar{E}$ (T. 3):*

$$-k_j = \frac{2\bar{E}(r, \dot{r})}{m_0 \cdot c^2} \text{ with } \bar{E}(r, \dot{r}) = \frac{m_0 \dot{r}^2}{2} - \frac{GMm_0}{r} \tag{8.211}$$

Thereby k_j is the **curvature parameter of the pair**.

(1b) The structured energy function is zero.

(1c) More generally, the structured energy function can be defined for general cases of E_{ref} (Carmesin (2020b)).

(1d) For all choices of E_{ref}, the structured energy function is an invariant.

(2) If a photon or a dynamical mass $m = E/c^2$ has a reference energy $E_{ref} = m_{ref} \cdot c^2$, and if $E_{ref} \to 0$ at $r \to \infty$, and if that object falls freely in a HUF, and if there is a field generating mass M with $R_S = \frac{2GM}{c^2}$ at a radial coordinate $r = 0$, and if many such objects propagating isotropically in all directions have an averaged position $r(t) = [r_j(t)]$ (Carmesin (2020b)), then the following holds:

(2a) The pair $(m_{ref}; M)$ named by j is described by the following **structured energy function** *$\bar{E}$ (Eq. 1.62):*

$$-k_j = \frac{2\bar{E}(r,\dot{r})}{E_{ref}} \text{ with } \bar{E}(r,\dot{r}) = \frac{m_{ref}\dot{r}^2}{2} - \frac{GMm_{ref}}{r} \quad (8.212)$$

Thereby k_j is the **curvature parameter of the pair**.

(2b) The structured energy function is zero.

(2c) More generally, the structured energy function can be defined for general cases of E_{ref} (Carmesin (2020b)).

(2d) For all choices of E_{ref}, the curvature parameter k_j of the pair is an invariant.

(3) The masses and dynamic masses can be described in a coherent manner by the structured energy function.

(4) The macroscopic FLE has been derived as an average over pairs of the microscopic structured energy function (see Sect. 1.10.2). So averages over pairs occurring microscopically represent results about the macroscopic evolution of the universe, including the FLE.

(5) If an object starts at the Big Bang, then it starts at the

Planck scale and at the Schwarzschild radius of $M = M_P$, so it is at the escape velocity, hence $E_{ref} \to 0$ at $r \to \infty$, thus $k_j = 0$.

(6) After the Big Bang, there may occur an exchange of energy among such objects, thereby the average $[k_j]$ over pairs remains zero, according to the principle of energy conservation at all local reactions among objects, hence the global curvature parameter k is zero, as $k = [k_j]$. This solves the flatness problem (Guth (1981)). Similarly theorem (3) solves that problem.

(7) The above shows that in a HUF, the energy of matter, the energy of radiation, and the energy of the vacuum are zero. This holds on the microscopic level of pairs, for instance, as well as on the macroscopic level, described by the FLE, for instance.

We summarize our results as follows:

Theorem 33 Time evolution of energy:

The three essential forms of energy, the dark energy, the energy of radiation and the energy of dark matter, exhibit the following properties:

(1) The law of **conservation of energy** *applies in a HUF.*

(2) The complete energy is zero in a HUF. **This solves the flatness problem**.

(3) There is **only one quantum of vacuum** *necessary and sufficient at the dimensional horizon within the light horizon (Fig. 8.19).*

(4) There existed only the one necessary and sufficient quantum of vacuum at the dimensional horizon within the light horizon. This can be derived as a consequence of the evolution of the energy.

(5) The evolution of the three essential forms of energy, ranging from the dimensional horizon until today and beyond, can be **derived completely on the basis of quantum gravity**,

see Fig. (8.18). This shows again how the present theory of quantum gravity including dimensional phase transitions makes complete the incomplete dynamics of the GRT.

(6) The time evolution of energies shows that the space enclosed by the actual light horizon can be traced back to a single quantum of spacetime that was immediately filled by $2^{D_{horizon}}$ *ZPOs of radiation.*

8.8 Relation to the hypothesis of a graviton

In this section we investigate the relation between the **quanta of spacetime** derived, analyzed and successfully applied to observations in this book with the hypothesis of the **graviton** (Blokhintsev and Galperin (1934), Tanabashi et al. (2018)). The hypothetical **graviton** should exhibit the following **three basic properties**:

1. It should be a boson that transfers the gravitational interaction.
2. It should be a quantum object.
3. It should have the spin 2.

The **quanta of spacetime** or **quanta of vacuum** do show these three basic properties of the hypothetical **graviton**:

1. The **quanta of spacetime** are bosons that transfers the gravitational interaction.
2. The **quanta of vacuum** are quantum objects.
3. The **quanta of spacetime** have the spin 2. For it we present three mutually independent reasons: The quanta of vacuum exhibit qadrupolar symmetry, they are represented by spherical harmonic functions $Y_{l=2,m}$, and they are represented by tensors of rank two.

Moreover, the **quanta of spacetime** exhibit **six essential additional properties**:

1. The quanta of vacuum **explain the dark energy** and achieve a very precise accordance with observations, based on first principles only and without using any fit parameter.

2. The quanta of spacetime provide a **detailed mechanism of interaction**: The quanta form additional vacuum, that vacuum generates the curvature of spacetime, that curvature causes the modified propagation of physical objects, and that modified propagation corresponds to the interaction.

3. The quanta of vacuum make **complete the time evolution of the spacetime** of the universe, that was described incompletely by the GRT.

4. The quanta of spacetime include the **time evolution of the dimension of space** ranging from the dimensional horizon until three dimensional space.

5. The energy of the quanta of vacuum forming the space included in the light horizon is **traced back to the energy of a single quantum of the vacuum** at the dimensional horizon.

6. The quanta of vacuum are represented by a Lorentz invariant four-vector including the formed space δV, the present space dV, the time required for the formation of that additional vacuum δt and the gravitational field G^*. So it combines spacetime and gravity in one fully relativistic quantum object.

As the hypothetical graviton has been proposed as a quantum of the gravitational interaction, and as the quanta of vacuum are the derived representations of that interaction, the

graviton is included in the derived quanta of the vacuum.

As the hypothetical graviton has not been proposed as a quantum of the expansion of space or as a quantum of the dark energy or as a quantum that can be traced back to a single quantum at the origin of the space included in the actual light horizon, **the derived quanta of the vacuum extend the concept of the graviton.**

Accordingly we propose that the graviton is included in the quanta of spacetime. In any case, the **quanta of spacetime explain the hypothetical graviton**, as its properties are derived on the basis of quantum physics and GRT.

So far, the hypothesis of the graviton was an interesting problem of physics: While the other bosons of interaction, the photon, the gluon and the W- and Z-bosons have been well understood already (Tanabashi et al. (2018)), the graviton was a hypothetical object. With this book, that situation is reversed: **The graviton now is the best understood boson of interaction.**

Since the fields, waves and quanta are derived as for the other bosons of interaction. But additionally, the quanta of spacetime explain the following: the mechanism of the interaction by the formation of spacetime, the formation of spacetime in the universe, the energy of the single first quantum of vacuum corresponding to the vacuum enclosed by the actual light horizon.

Theorem 34 Explanation of the hypothetical graviton:

(1) The **three basic properties** *of the hypothetical graviton are explained by the quanta of the vacuum.*

(2) The quanta of spacetime provide **six essential additional results***:*

(2a) the explanation of dark energy,

(2b) the detailed mechanism of the gravitational interaction,

(2c) the complete time evolution of spacetime,

(2d) the complete time evolution of the dimension of space,

(2e) the identification of a single primordial quantum of vacuum in the visible universe,

(2f) the structure of the combination of gravity, space and time in terms of a single Lorentz invariant four-vector.

(3) As a result, the quanta of spacetime elaborated here explain the graviton, include the graviton as the boson of the gravitational interaction, explain the microdynamics of gravitational interaction and the macrodynamics of the time evolution of spacetime in a coherent manner, solve the EPR paradox that existed between GRT and quantum physics, and thus essentially extend the concept of the graviton.

8.9 Summary

In this section we summarize our findings.

Questions: In this book we solved essential questions of nature: Is nature **nonlocal** on a microscopic and macroscopic level? What is the **quantum of interaction of gravity, the graviton**? What is the curious **dark energy**, that amounts to ca. 68 % of all energy and matter in the universe? How are the **discrepancies of H_0 and σ_8 values** explained? How did space generate the **extremely rapid distance enlargement** in the early universe? What are the quanta of spacetime?

Novel principles: In order to discover the structures underlying the above questions, we introduced two basic principles:

The **principle of equivalence of curvature and vacuum** is based on the following insight: In general, the space in which

we live exhibits a curvature and consists of vacuum. Hence a possible increase of the volume caused by the curvature is equivalent to additionally formed vacuum.

Using the above principle, we discovered that the amount of vacuum formed according to the microscopic dynamics differs from the vacuum formed according to the macroscopic dynamics. But in contrast, the amounts of formed spacetimes are equal in all investigated cases. Accordingly we introduced the **principle of the equality of spacetimes**.

Nonlocality: Using that principle we derived that the nonlocally formed vacuum is as large as the locally formed vacuum. In particular, the cosmological models derived in GRT describe the increase of the scale radius as a function of the time, and with it they derive the increase of the volume and the decrease of the densities as a function of the time (Einstein (1917), Friedmann (1922), Lemaitre (1927), Straumann (2013)). So the theory of general relativity, GRT, is nonlocal. This finding is indeed surprising, as GRT is based on local assumptions only, but essential resulting structures are nonlocal. In fact Einstein et al. (1935) presumed the locality of GRT, emphasized the nonlocality of quantum theory and posed that situation as a paradox, the EPR paradox. However, that paradox is solved here by the finding that the presumed locality of GRT does not exist. Moreover, our theory describes the formation of space and time in terms of local four-vectors. Our theory includes spontaneously formed shortcuts, these might provide locality in space.

Quanta of spacetime: In order to discover the dynamics of local and nonlocal formation of vacuum, we derived the full **symmetry of quadrupoles or spin 2** of the **rates** of that formation of vacuum. Combining these with **gravitational fields** we obtained the Lorentz invariant **rate gravity four-vector** RGV_i, and a corresponding scalar RGS. Thus we realized that rela-

tivity provides the combined structure of gravity and vacuum formation. Indeed, from that structure we derived the Lorentz invariant **spacetime four-tensor** STT_{ij} and the corresponding spacetime scalar (Chap. 2).

Using these Lorentz invariant quantities, we derived the wave theory, including the DEQs as well as solutions of the homogeneous and inhomogeneous DEQ. So we described the propagation of gravity, vacuum and vacuum formation in spacetime (Chap. 5). We analyzed the modes of these waves, identified generalized coordinates establishing four-vectors, and we quantized these. Hence we derived and analyzed the **quanta of spacetime**.

Dark energy I: Using the quanta of spacetime, we derived the density ρ_Λ of the dark energy in terms of a **basic formula of dark energy**. We obtained very precise accordance to observations: The difference amounts to 0.16 % only.

We discovered that ρ_Λ is constituted by all quanta of spacetime that propagated to Earth, originating from the light horizon to Earth, and including the nonlocally formed vacuum as well (Chap. 6).

Structure formation and dark energy II: We summarized the dynamics of the formation of structures in the universe and derived the essential equations. We combined these with the basic formula of dark energy. Thereby we derived **advanced formulas of dark energy**. These describe the Hubble constant H_0 and the amplitude of matter fluctuations σ_8 as functions of the redshift of the probe that underlies a measurement of these quantities. In fact we obtain precise accordance with observations (Chap. 7).

Dimensional phase transitions: While the above shortcuts provide a dimensional phase transition of the connections of space

at high density, we derived two additional theories for these dimensional phase transitions: a mean field theory and a Bose gas theory.

Moreover we analyzed the geometric structure of the translation invariant space at each dimension. With it we derived the largest possible dimension of the visible universe, the dimensional horizon $D_{horizon}$. With it we obtained the **extremely rapid enlargement of distances** in the early universe. Again we find a precise accordance with observations (Chap. 8).

Dark energy III: Using the dimensional horizon, we derive the time evolution of the quanta of spacetime ranging from the dimensional horizon until today. Thereby we obtain a **quantized dark energy formula** and achieve a good accordance with observation.

Dark energy IV: While the **quantized dark energy formula** describes a monochromatic vacuum, a polychromatic vacuum is realistic. We derived the precise spectrum based on the time evolution according to the FLE. So we obtained the CFV at once, and it is not necessary to add the NFV separately. With it we obtained the the Hubble constant H_0 and the amplitude of matter fluctuations σ_8 as a function of the redshift of the probe that underlies a measurement of these quantities. With it we find a very precise accordance with observations (Chap. 8).

Time evolution of the forms of energy: Based on the full theory of the quanta of spacetime, we showed that **energy is conserved** in the HUF, a frame with an empty ball surrounded by of a homogeneous universe. Moreover we derived the deviations from that HUF and found that these converge to zero, if the radius of the HUF tends to infinity.

Additionally we showed that the energy is zero in the HUF, with it we confirmed the zero energy hypothesis proposed by

(Tryon (1973)). Furthermore we traced back the energy of all quanta of spacetime. We discovered that the energy of a single quantum of spacetime existed at the dimensional horizon, the deviation amounts to 21.1 % only, so that the assumption of two quanta would yield a deviation of 79.9 %, for instance. That primordial quantum of spacetime provided a volume that immediately filled with quanta of radiation. The time evolution of these quanta is in exact accordance with observation.

Graviton: If the quantum of spacetime is transformed to the rate gravity four-vector, RGV_i, then the gravitational field is a component. So the gravitational interaction is presented by a part of that four-vector. In this manner the graviton is included in the quantum of spacetime. So the spin 2 structure, the propagation and the quantization of the graviton are described by the quantum of spacetime.

Moreover, the quantum of spacetime describes precisely the mechanism by which gravity is constituted: At gravitational fields as well as at each density, quanta of spacetime are emitted, these quanta form additional vacuum LFV propagating at the velocity c of light, the heterogeneity of that LFV generates a curvature of spacetime, this curvature influences the propagation of objects through space, and that influence corresponds to the gravitational interaction. As the other bosons of interaction (photon, gluon, W- and Z-boson) do not provide such a detailed insight into the mechanisms of the interaction, the graviton is now the best understood boson of interaction, in this sense.

Evidence based on observations: The present theory provides a precise accordance with observation. This has been achieved without any fit parameter (Carmesin (2020b)). The numerical input is constituted by the universal constants of nature only: the gravitational constant G, the velocity of light c, the Planck constant h and the Boltzmann constant k_B.

Evidence based on solved problems: The present theory provides a coherent solution of many problems or hypotheses in physics:

problem of rapid enlargement of distances (Guth (1981), solved since 2017, Carmesin (2017), Carmesin (2021))

horizon problem (Guth (1981), solved since 2017, Carmesin (2017), Schöneberg and Carmesin (2021))

'inflaton' hypothesis and reheating problem (see Guth (1981) and Nanopoulos et al. (1983), Broy (2016), solved since 2017, Carmesin (2017), Carmesin (2020a))

dark matter problem (Zwicky (1933), Sanders (2010), solved since 2018, Carmesin (2018d))

dark energy problem (Josset et al. (2017), solved since 2018, Carmesin (2018c))

Hubble constant discrepancy (Riess et al. (2019), solved since 2018, Carmesin (2018c))

fine-tuning problem (Landsman (2016), solved for the case of most density parameters since 2019, Carmesin (2019b))

flatness problem (Guth (1981), solved since 2020, Carmesin (2020b))

zero energy hypothesis (Tryon (1973), solved 2020, Carmesin (2020b))

graviton hypothesis (Blokhintsev and Galperin (1934), solved here)

EPR paradox and nonlocality (Einstein et al. (1935), solved here)

σ_8 discrepancy (Tröster et al. (2020), solved here)

Evidence based on invariance: The quanta of spacetime are invariant with respect to Lorentz transformations. Moreover, in the HUF, they are additionally invariant to each linear trans-

formation. The same invariance holds for the quanta and the DEQ of rate gravity waves.

Evidence based on clear foundation: The quanta of spacetime are based on general relativity, quantum physics, the principle of energy conservation in the frame HUF, the principle of the equivalence of curvature and vacuum and the principle of the equality of spacetimes. Based on these principles, the results are derived by usual mathematical operations.

Evidence based on predictions: Here and in the previous books, we derived many results and formulas that enable various predictions: In this book, many very clear and predictive formulas are provided and especially essential results are concisely summarized in 15 propositions and 34 theorems. These can easily be applied according to individual interests, activities, questions or purposes.

Software: Sawitzki and Carmesin (2021), Lieber and Carmesin (2021) and Schöneberg and Carmesin (2021) provide software that can be used in order to generate solutions of DEQs or Eqs. derived here.

Necessity of fundamental theory: In 2020, the Planck Collaboration[4] wrote 'it is important to bear in mind that ... inflation, dark energy and dark matter are not understood at any fundamental level'. Here we derived a fundamental theory. It explains inflation, dark energy, dark matter (Carmesin (2019b)) the graviton, nonlocality and the discrepancy of observed H_0 and σ_8 values. So we provide the requested theory. We invite interested people and experts to discuss our theory[5].

[4]See (Collaboration, 2020, p. 62).

[5]https://www.researchgate.net/profile/Hans_Otto_Carmesin. hans-otto.carmesin.org. Hans-Otto.Carmesin@athenetz.de. h-o.carmesin@studienseminar-stade.net.

Chapter 9

Appendix

Acknowledgement

I thank Matthias Carmesin for helpful discussions. I thank Paul Sawitzki, Philipp Schöneberg, Jörn Kankelfitz, Dennis Feldmann and Jonas Lieber for interesting discussions. I am especially grateful to I. Carmesin for many helpful discussions.

9.1 Constants of nature

In this section we present useful constants of nature.

quantity	observed value
G	$6.674\,30(15)\ \frac{\mathrm{m}^3}{\mathrm{kg}\cdot\mathrm{s}^2}$
c	$299\,792\,458\ \frac{\mathrm{m}}{\mathrm{s}}$, exact
h	$6.626\,070\,150(69)\ \cdot 10^{-34}\ \mathrm{Js}$
k_B	$1.380\,649\,03(51)\ \cdot 10^{-23}\ \frac{\mathrm{J}}{\mathrm{K}}$
ϵ_0	$8.854\,187\,817\ \cdot 10^{-12}\ \frac{\mathrm{F}}{\mathrm{m}}$, exact

Table 9.1: Constants of nature (Newell et al. (2018), Tanabashi et al. (2018)).

9.2 Observed values

In this section we present useful results of observations.

quantity	observed value
H_0 in $\frac{\text{km}}{\text{s·Mpc}}$	67.36 ± 0.54 (0.8 %)
Ω_Λ	0.6847 ± 0.0073 (1.1 %)
Ω_K	$-0.011^{+0.0013}_{-0.0012}$
z_{eq}	3402 ± 26
Ω_m	0.3153 ± 0.0073
Ω_r	$9.265^{+0.288}_{-0.283} \cdot 10^{-5}$ (3.1 %)
σ_8	0.8111 ± 0.006(7.4%)
ρ_{cr,t_0} in $\frac{kg}{m^3}$	$8.660^{+0.137}_{-0.137} \cdot 10^{-27}$ (1.6 %)
$\tilde{\rho}_{cr,t_0}$	$7.037 \cdot 10^{-123}$
$\tilde{\rho}_{v,t_0}$	$4.8181 \cdot 10^{-123}$
Ω_b	0.0493 ± 0.00032
Ω_c	0.2645 ± 0.0048
R_{lh}	$4.1412 \cdot 10^{26}$ m (Carmesin (2019b))

Table 9.2: Data obtained on the basis of the CMB by the Planck satellite ((Collaboration, 2020, p. 15 and 38)) by using the modes TT, TE, EE, the low energy and the lensing results. Quantities with a tilde are presented in natural units alias Planck units (see subsection 9.3). Hereby 1 Mpc = $3.0856776 \cdot 10^{19}$ km.

9.3 Natural units

Planck units or natural units have been introduced by Planck (1899). We mark quantities in natural units by a tilde (s. Tab. 9.3, Carmesin (2019b)).

physical entity	Symbol	Term	in SI-Units
Planck length	L_P	$\sqrt{\frac{\hbar G}{c^3}}$	$1.616 \cdot 10^{-35}\,\mathrm{m}$
Planck time	t_P	$\frac{L_P}{c}$	$5.391 \cdot 10^{-44}\,\mathrm{s}$
Planck energy	E_P	$\sqrt{\frac{\hbar \cdot c^5}{G}}$	$1.956 \cdot 10^{9}\,\mathrm{J}$
Planck mass	M_P	$\sqrt{\frac{\hbar \cdot c}{G}}$	$2.176 \cdot 10^{-8}\,\mathrm{kg}$
Planck volume	$V_{D,P}$	L_P^D	
Planck volume, ball	$\bar{V}_{D,P}$	$V_D \cdot L_P^D$	
Planck density	ρ_P	$\frac{c^5}{G^2\hbar}$	$5.155 \cdot 10^{96}\,\frac{\mathrm{kg}}{\mathrm{m}^3}$
Planck density, ball	$\bar{\rho}_P$	$\frac{3c^5}{4\pi G^2\hbar}$	$1.2307 \cdot 10^{96}\,\frac{\mathrm{kg}}{\mathrm{m}^3}$
Planck density, ball	$\bar{\rho}_{D,P}$	$\frac{M_P}{\bar{V}_{D,P}}$	
Planck temperature	T_P	$T_P = \frac{E_P}{k_B}$	
scaled volume	$\tilde{V}_D$	$\frac{V_D}{\bar{V}_{D,P}}$	
scaled density	$\tilde{\rho}_D$	$\frac{\tilde{M}}{\tilde{r}^D}=\frac{\tilde{E}}{\tilde{r}^D}$	$\rho_D = \tilde{\rho}_D \cdot \bar{\rho}_{D,P}$
scaled length	$\tilde{x}$	L_P	$x = \tilde{x} \cdot L_P$
Planck charge	q_P	$M_P\sqrt{G4\pi\varepsilon_0}$	$11{,}71\,e$

Table 9.3: Planck - units.

9.3.1 Glossary

Words marked bold face can usually be found in the glossary.

Abbreviation: S. (section), C. (chapter), D. (definition), P. (proposition), T. (theorem).

autocorrelation function: $\xi(\vec{x})$ (S. 7.2.3)

Bose gas: quantum gas consisting of quanta with integer spin (S. 8.4)

Big Bang: Start of time evolution of visible space

Big Crunch: The global gravitational instability could cause a global contraction, a Big Crunch.

complex conjugate: We denote a complex conjugate of a number $z = a + i \cdot b$ by a star $z^* = a - i \cdot b$.

CMB, Cosmic Microwave Background Radiation emitted at $z \approx 1090$. (Tab. 9.2)

complete time evolution of spacetime: evolution of the light horizon $R_{lh}(t)$ ranging from the Planck - length L_P to the actual light horizon $R_{lh}(t_0)$ (Fig. 1)

cosmic unfolding: It causes the extremely rapid increase of distance in the early universe (D. 12).

cosmological constant: Λ corresponds to the dark energy with its density ρ_Λ (Tab. 9.2).

curvature parameter: $k = \frac{-2\bar{E}}{m_0 \cdot c^2}$ (Def. 2)

curvature parameter k_j of a pair j: (T. 31)

dark energy: energy of the cosmological density of the vacuum ρ_Λ (Tab. 9.2).

deficit wave function: (T. 14)

density, averaged or homogeneous part: ρ_h (C. 7)

density, critical: ρ_{cr,t_0} or ρ_{cr} (Tab. 9.2)

density, critical, at a dimensional transition: $\tilde{\rho}_{D,c}$ (S. 8.2)

density, critical, shortcuts: $\rho_{cr.conn.}$ (T. 10)

density, fluctuation: $\rho_1(\vec{x}, t) = \rho(\vec{x}, t) - \rho_h$ (C. 7)

density, overdensity: $\delta(\vec{x}, t) = \rho_1(\vec{x}, t)/\rho_h$ (C. 7)

density, overdensity at a sphere with radius R: $\delta_R(\vec{x}, t)$ (C. 7)

density, overdensity, standard deviation at a sphere with radius R: σ_R (C. 7)

density, overdensity, standard deviation at a sphere with radius R_8: $\sigma_8 = \sigma_{R_8}$ It is also called amplitude of matter fluctuations or amplitude of matter fluctuations (C. 7).

density parameter: $\Omega_j = \rho_j/\rho_{cr,t_0}$ 9.2)

density, vacuum: $\rho_\Lambda = \Omega_\Lambda \cdot \rho_{cr,t_0}$ 9.2)

distance enlargement factor: If the dimension decreases, then distances increase by factor Z (T. 26, S. 8.2.9).

dimension of the space: (C. 8)

dimensional horizon D_{max} or $D_{horizon}$: It is the maximal dimension that the space within the actual light horizon can have achieved in the past. Thereby the following transformations of space are essential: the isotropic scale and the enlargement of distance caused by a $\rightarrow$ dimensional transition. (D. 12, T. 26).

dimensional transition or dimensional phase transition: change of spatial dimension D (T. 26).

dimensional unfolding: change of spatial dimension D (D. 12, T. 26).

distance factor: $Z_{t_1 \rightarrow t_2} = Z_{D+s \rightarrow D}$, occurring at a $\rightarrow$ dimensional transition towards a dimension D (T. 26).

dynamical mass: $M = \frac{E}{c^2}$

Energy density of the gravitational field: (P. 5)

Energy skin: (T. 12)

EPR paradox: (C. 4)

excess energy: structured energy function (C. 1)

expansion of space: expansion since the Big Bang at constant dimension D

extended FLE, EFLE: FLE extended by quantum effects (T. 24)

extremely rapid increase of distance in the early universe: conjectured by Alan Guth in 1981 (Guth (1981)), explained by dimensional transitions in this book and since 2017 (Carmesin (2017), Carmesin (2019b)) (Fig. 1)

field variance: Variance of the field in a HUF, characterizing the quality of a HUF (S. 8.3, T. 27)

flat, flatness, flatness problem: Space without curvature is flat (C. 8).

frame: Each observation apparatus is localized in spacetime. That localization establishes a frame. Examples are the HUF and the vacuum HUF, HUF_v (D. 2), LUF (D. 4, FMF (D. 3).

Friedmann - Lemaître equation, FLE: (T. 4)

Fourier transform: $\tilde{f}(k)$ (C. (7)

gravitational field: G^* (C. 1)

gravitational instability: (C. 8)

graviton: (T. 34)

GRT: general relativity theory (C. 1)

horizon: global limit of visibility (C. 1)

Hubble - parameter: $H = \frac{\dot{a}}{a}$ (T. 4)

Hubble - constant: $H_0 = H(t_0)$ Hubble parameter at t_0

Hubble - constant, dimensionless: $h = H_0/100 \cdot \frac{\text{s·Mpc}}{\text{km}}$ (Tab. 9.2)

incomplete: A theory that does not describe the physically known objects or properties is incomplete (T. 20, 26)

inertial frame: frame that is not accelerated

invariant: quantity that remains constant with respect to a transformation. Examples are a Lorentz invariant (D. 9), a HUF zero Lorentz scalar **HZLS** with corresponding a HUF zero Lorentz four-vector **HZFV** (D. 9), a **spacetime scalar STS** (D. 10), a rate gravity scalar **RGS** (T. 7), a rate gravity energy density **RGED** (P. 7), a **rate gravity four-vector** RGV_i (T. 7), a **spacetime tensor** STT_{ij} (C. 1), a **four-momentum of spacetime** (T. 18).

isentropic: States at constant entropy (C. (7)

isotropic formation of vacuum: (C. 2)

Jeans wave number k_J: (Eq. 7.53)

kinetic factor: generalized Lorentz factor, for instance $\bar{\gamma}(T) = \frac{T_\infty}{T}$ (T. 31)

light horizon, actual: $R_{lh} = 4.142 \cdot 10^{26}$ m (Tab. 9.2)

light horizon, actual: At a time t, the volume enclosed by light horizon at the actual time t_0 is or was enclosed by another value $R_{lh}(t)$.

light horizon, at a time t: $R_{lh,t}$ (Carmesin (2019b))

light-travel distance: $d_{licht-travel} = t_{light-travel} \cdot c$

linear growth factor: $D(t)$ (C. 7)

Local observer: (P. 3)

Lorentz factor: energy factor caused by velocity $\gamma = \frac{1}{\sqrt{1-v^2/c^2}}$ (T. 1)

natural units: Planck - units (Tab. 9.3)

nonlocality: (T. 5)

object's own frame: here the object is at rest (C. 1)

operator: observable physical quantities can be represented by operators in QT. Examples are the energy operator, the number operator. Additionally, transformations can be represented by operators, examples are the ladder operators (T. 19, C. 6)

own mass: mass in the object's own frame, also called rest mass (C. 1)

own time: time in the object's own frame, also called proper time (C. 1)

observable physical length: (D. 11, S. 6.4.4)

Planck unit, Planck scale: natural unit (Tab. 9.3)

polychromatic vacuum: it includes several wavelengths of the quanta of space (S. 8.6)

position factor: energy factor caused by position (T. 1)

power density: $P(k) = |\tilde{f}(k)|^2$ (C. 7)

principle in physics: essential and broadly useful concept in physics. Here we utilize the Einstein equivalence principle, principle of energy conservation in a HUF, the principle of linear superposition of the volumes (D. 1), the principle of the equivalence of curvature and vacuum (D. 5) the principle of the equality of spacetimes (D. 8)

probing mass: (T. 3)

quadrupolar symmetry: corresponding to spin 2, tensors of rank 2 and spherical harmonic functions (T. 6, 8)

quantum gravity: combination of gravitation and quantum physics (Carmesin (2019b))

quantum of spacetime or quantum of vacuum: (D. 10), representations are quantized RGWs, quantized spacetime scalar, quantized spacetime tensor (T. 19)

q-classical limit: limit h to zero (Carmesin (2019b))

rapid enlargement of distances: (Fig. 1)

rate gravity wave, RGW: (T. 16)

rate of the formation of relative volume: (T. 7)

redshift: relative increase of the wavelength $z = \frac{\Delta\lambda}{\lambda}$ (C. 1)

reduced normalized energy E_D: (S. 8.2)

scale factor: $k_{t_1 \to t_2}$ (C. 1, 8)

scale radius a: $a(t) = k_{t_{ref} \to t} a(t_{ref}$ (T. 4)

semiclassical theory: theory that uses quantum objects in terms of a classical representation (S. 6.6, 7.5)

self interaction: (P. 12)

shortcut: (C. 3, T. 23)

slope four-vector: (S. 5.2.1)

structured energy term or function: (T. 1)

Schwarzschild radius R_S: at this radius the escape velocity is equal to c (C. 1)

Schwarzschild metric, SSM: (T. 1)

spacetime: combination of space and time (D. 8).

temperature power spectra, TT: (Tab. 9.2)

uncertainty: a standard deviation in QT (C. 1, 6)

unfolding, dimensional: space unfolds when the dimension decreases (D. 12)

uniform scaling: In a uniform scaling enlarges or shrinks a vector $\vec{v}$ by a scale factor $k_{1\to2}$, $\vec{v}' = k_{1\to2}\vec{v}$ (C. 1)

universal constants: (Tab. 9.1)

vacuum: The vacuum has a volume, a density and the velocity c. Essential are locally formed vacuum, LFV, nonlocally formed vacuum, NFV, complete formed vacuum, CFV, locally formed vacuum using shortcuts, LFVUS (C. 1, D. 7, T. 5, D. 10, T. 14)

window function: $W(\vec{x})$ (C. 7)

ZPE: zero-point energy of omnipresent zero-point oscillations (C. 6, 8)

ZPO: zero-point oscillations are omnipresent quantum states corresponding to a ground state (C. 6, 8)

Bibliography

Abbott, B. P. e. a. (2016). Observation of gravitational waves from a binary black hole merger. *Phys. Rev. Lett.*, 116:1–16.

Abbott, T. M. C. et al. (2019). Dark energy survey year 1 results: Cosmological contraints from galaxy clustering and weak lensing. *Phys. Rev. D*, 98:1–31.

Abell, G. O., Corwin, H. J., and P., O. R. (1989). A catalogue of rich clusters of galaxies. *Astrphysical Journal*, 70:1–138.

Alam, S. et al. (2017). The clustering of galaxies in the comleted SDSS-III Baryon Oscillation Spectroscopic Survey: cosmological analysis of the DR12 galaxy sample. *MNRAS*, 470:2617–2652.

Ballentine, L. E. (1998). *Quantum Mechanics*. World Scientific Publishing, London and Singapore.

Bennett, C. L. et al. (2013). Nine-year Wilkinson microwave anisotropy probe (WMAP) Observations: final maps and results. *The Astrophysical Journal Supplement Series*, 208:1–54.

Birkhoff, G. D. (1921). Über die allgemeinen kugelsymmetrischen Lösungen der Einsteinschen Gravitationsgleichungen im Vakuum. *Arkiv f. Mathematik, Astronomi och Fysik*, 15:1–9.

Blokhintsev, D. I. and Galperin, F. M. (1934). Neutrino hypothesis and conservation of energy. *Pod Znamenem Marxisma*, 6:147–157.

Blomquist, M. et al. (2019). Baryon acoustic oscillation from the cross-correlation of the Lyα absorption and quasars in eBOSS DR14. *Astr. and Astrophys.*, 629:A86.

Born, M., Heisenberg, W., and Jordan, P. (1926). Zur Quantenmechanik. II. *Zeitschrift für Physik*, 35:557–615.

Bose, S. (1924). Plancks Gesetz und Lichtquantenhypothese. *Z. f. Physik*, 26:178–181.

Broersen, P. M. T. (2006). *Automatic Autocorrelation and Spectral Analysis*. Springer, London.

Bronstein, I. N. and Semendjajew, K. A. (1980). *Taschenbuch der Mathematik - Neubearbeitung*. Harri Deutsch, Thun and Frankfurt/Main.

Broy, B. J. (2016). *Inflation and effective Shift Symmetries*. PhD thesis, University Hamburg, Hamburg.

Bundesanstalt, P. T. (2007). Optische Atomuhren. *PTB*, pages 1–27.

Carmesin, H.-O. (1987). Mapping of Quadrupolar to Dipolar Many-Particle Systems. *Physics Letters A*, 125:294–298.

Carmesin, H.-O. (1993). Slow dynamics at the liquid-glass transition. *Physica A*, 201:25–29.

Carmesin, H.-O. (1996). *Grundideen der Relativitätstheorie*. Verlag Dr. Köster, Berlin.

Carmesin, H.-O. (2017). *Vom Big Bang bis heute mit Gravitation: Model for the Dynamics of Space*. Verlag Dr. Köster, Berlin.

Carmesin, H.-O. (2018a). A Model for the Dynamics of Space - Expedition to the Early Universe. *PhyDid B, FU Berlin, hal-02077596*, pages 1–9.

Carmesin, H.-O. (2018b). *Entstehung der Raumzeit durch Quantengravitation - Theory for the Emergence of Space, Dark Matter, Dark Energy and Space-Time*. Verlag Dr. Köster, Berlin.

Carmesin, H.-O. (2018c). *Entstehung dunkler Energie durch Quantengravitation - Universal model for the Dynamics of Space, Dark Matter and Dark Energy*. Verlag Dr. Köster, Berlin.

Carmesin, H.-O. (2018d). *Entstehung dunkler Materie durch Gravitation - Model for the Dynamics of Space and the Emergence of Dark Matter*. Verlag Dr. Köster, Berlin.

Carmesin, H.-O. (2019a). A Novel Equivalence Principle for Quantum Gravity. *PhyDid B - Didaktik der Physik - Beiträge zur DPG - Frühjahrstagung - Aachen - Germany - hal-02511998*, pages 1–9.

Carmesin, H.-O. (2019b). Die Grundschwingungen des Universums - The Cosmic Unification - With 8 Fundamental Solutions based on G, c and h. In Carmesin, H.-O., editor, *Universe: Unified from Microcosm to Macrocosm - Volume 1*. Verlag Dr. Köster, Berlin.

Carmesin, H.-O. (2020a). Explanation of the Rapid Enlargement of Distances in the Early Universe. *PhyDid B*, pages 1–9.

Carmesin, H.-O. (2020b). The Universe Developing from Zero-Point Energy: Discovered by Making Photos, Experiments and Calculations. In Carmesin, H.-O., editor, *Universe: Unified from Microcosm to Macrocosm - Volume 3*. Verlag Dr. Köster, Berlin.

Carmesin, H.-O. (2020c). Wir entdecken die Geschichte des Universums mit eigenen Fotos und Experimenten. In Carmesin, H.-O., editor, *Universe: Unified from Microcosm to Macrocosm - Volume 2*. Verlag Dr. Köster, Berlin.

Carmesin, H.-O. (2021). Lernende erkunden die Raumzeit. *Der Mathematik Unterricht*, 2:1–10.

Carmesin, H.-O. and Binder, K. (1987). Isotropic Edwards-Anderson Models for Quadrupolar Glasses: A Monte Carlo Simulation. *Europhysics Letters*, 4:269–274.

Carmesin, H.-O. et al. (2022). *Universum Physik Sekundarstufe II Gesamtband*. Cornelsen Verlag, Berlin.

Carmesin, H.-O., Heermann, D., and Binder, K. (1986). Influence of a Continuous Quenching Procedure on the Initial Stages of Spinodal Decomposition. *Z. Phys. B - Condensed Matter 65, 89-102*, 65:89–102.

Carmesin, H.-O., Percus, J. K., and Frisch, H. L. (1989). Liquid crystals at high dimensionality. *Phys. Rev. B*, 40:9416–9418.

Carmesin, M. and Carmesin, H.-O. (2020). Quantenmechanische Analyse von Massen in ihrem eigenen Gravitationspotenzial. *PhyDid B, FU Berlin*, pages 1–9.

Collaboration, P. (2014). Planck 2013 Results: XVI. Cosmological Parameters. *Astronomy and Astrophysics*, 571:1–66.

Collaboration, P. (2020). Planck 2018 results. VI. Cosmological parameters. *Astronomy and Astrophysics*, pages 1–73.

Coulomb, C.-A. (1785). Construction et usage d'une balance electrique etc. *Histoire de l'Academie des sciences avec les memoires de mathematique et de physique*, 1788:569–577.

Dyson, F. W., Eddington, A. S., and Davidson, C. (1920). A determination of the deflection of light ... *Phil. Tr. of the R. S. of L.*, A220:291–333.

Einstein, A. (1905). Zur Elektrodynamik bewegter Körper. *Annalen der Physik*, 17:891–921.

Einstein, A. (1907). Über die Plancksche Theorie der Strahlung und die Theorie der spezifischen Wärme. *Annalen der Physik*, 22:180–190.

Einstein, A. (1915a). Die Feldgleichungen der Gravitation. *Sitzungsberichte der Königlich Preußischen Akademie der Wissenschaften*, pages 844–847.

Einstein, A. (1915b). Erklärung der Perihelbewegung des Merkur aus der allgemeinen Relativitätstheorie. *Sitzungsberichte der Königlich Preußischen Akademie der Wissenschaften*, pages 831–839.

Einstein, A. (1916). Näherungsweise Integration der Feldgleichungen der Gravitation. *Sitzungsberichte der Königlich Preußischen Akademie der Wissenschaften*, pages 688–696.

Einstein, A. (1917). Kosmologische Betrachtungen zur allgemeinen Relativitätstheorie. *Sitzungsberichte der Königlich Preußischen Akademie der Wissenschaften*, pages 142–152.

Einstein, A., Podolski, B., and Rosen, N. (1935). Can quantum-mechanical description of physical reality be considered complete? *Phys. Rev.*, 47:777–780.

Errani, R. and Penarrubia, J. (2019). Can tides disrupt cold dark matter subhalos? *MNRAS*, pages 1–11.

Euler, L. (1757). Principes generaux du mouvement des fluides. *Memoires de l'academie des sciences de Berlin*, 11:274–315.

Fan, X., Bahcall, N. A., and Renyue, C. (1997). Determining the amplitude of mass fluctuations in the universe. *Astrophys. J.*, 490:L123–L126.

Faraday, M. (1852). On the physical character of the lines of magnetic force. *The London, Edinburgh and Dublin Philosophical Magazine and Journal of Science, Taylor and Francis*, 4(3):401–428.

Fornasini, P. and Grisenti, R. (2015). On EXAFS Debye - Waller factor and recent advances. *Journal of Sychrotron Radiation*, 22:1242–1257.

Fourier, J. (1822). *Theorie Analytique de la Chaleur*. Firmin Didot Pere et Fils, Paris.

Friedmann, A. (1922). Über die Krümmung des Raumes. *Z. f. Physik*, 10:377–386.

Galileo, G. (1638). *Dialogues concerning two new sciences (translated)*. Elfevirii, Leida.

Gauss, C. F. (1840). Recursion der Untersuchungen über die Eigenschaften der positiven ternären quadratischen Formen von Ludwig August Seeber. *J. reine angew. Math.*, 20:312–320.

Gil-Marin, H. et al. (2016). The clustering of the SDSS-14 extended Baryon Oscillation Spectroscopic Survey DR14 quasar sample: structure growth rate measurement from the anisotropic quasar power spectrum in the redshift range $0.8 < 2.2$. *MNRAS*, 477:1604–1638.

Goodstein, D. (1997). The Big Crunch. *EOS, Transactions, American Geophysical Union*, 78:329–334.

Gott, R. J., Juric, M., Schlegel, D., Hoyle, F., Vogeley, M., Tegmark, M., Bahcal, N., and Brinkmann, J. (2005). A map of the universe. *The Astrophysical Journal*, 624:463–484.

Grawert, G. (1977). *Quantenmechanik*. Akademische Verlagsgesellschaft, Wiesbaden.

Guth, A. H. (1981). Inflationary universe: A possible solution to the horizon and flatness problems. *Physical Review D*, 23:347–356.

Hansen, F. K. (2002). *Data Analysis of the Cosmic Microwave Background*. PhD thesis, LMU, München.

Heisenberg, W. (1927). Über den anschaulichen Inhalt der quantentheoretischen Kinematik und Mechanik. *Z. f. Phys.*, 43:172–198.

Howard, S. (2011). Cosmic distance ladder. *Washington Acad. of Sciences*, pages 47–64.

Hubble, E. (1929). A relation between distance and radial velocity among extra-galactic nebulae. *Proc. of National Acad. of Sciences*, 15:168–173.

Joachimi, B. et al. (2020). Kids-1000 methodology: Modelling and inference for joint weak gravitational lensing and spectroscopic galaxy clustering analysis. *Astronomy and Astrophysics*, pages 1–44.

Josset, T., Perez, A., and Sudarsky, D. (2017). Dark energy as the weight of violating energy conservation. *PRL*, 118:021102233–243.

Kant, I. (1755). *Allgemeine Naturgeschichte und Theorie des Himmels*. Petersen, Königsberg.

Kravtsov, A. V. and Borgani, S. (2012). Formation of galaxy clusters. *Annual Review of Astronomy and Astrophysics*, 50:353–409.

Landau, L. and Lifschitz, J. (1979). *Lehrbuch der theoretischen Physik - Statistische Physik*. Akademie-Verlag, Berlin.

Landau, L. and Lifschitz, J. (1981). *Lehrbuch der theoretischen Physik - Klassische Feldtheorie*. Akademie-Verlag, Berlin.

Landsman, K. (2016). The fine-tuning argument: Exploring the improbability of our existence. In Landsman, K. and van Wolde, E., editors, *The Challenge of Chance*. Springer, Berlin.

Lemaitre, G. (1927). Un univers homogene de masse constante et de rayon croissant rendant compte de la vitesse radiale des nebuleuses extra-galactiques. *Annales de la Societe Scientifique de Bruxelles*, A47:49–59.

Lieber, J. and Carmesin, H.-O. (2021). Dynamics in the early universe. *PhyDid B, FU Berlin*, pages 1–10.

Lohse, M. et al. (2018). Exploring 4D Quantum Hall Physics with a 2D Topological Charge Pump. *Nature*, 553:55–58.

Lombardi, M. et al. (2007). NIST Primary Frequency Standards and the Realization of the SI Second. *The J. of Measurement Science*, 2:74–89.

Lu, T. and Haiman, Z. (2020). The matter fluctuation amplitude inferred from weak lensing power spectrum and correlation function in cfht lens data. *MNRAS*, pages 1–11.

Maxwell, J. C. (1865). A dynamical theory of the electromagnetic field. *Philosophical Transactions of the Royal Society of London*, 155:459–512.

Mayer, J. R. (1842). Remarks on the forces of inorganic nature. *Annalen der Chemie und Pharmacie*, 43:233.

Mehra, J. and Rechenberg, H. (1999). Planck's half quanta: A history of the concept of zero-point energy. *Foundations of Physics*, 29:91–132.

Michell, J. (1784). On the means of discovering the distance... *Phil. Trans. R. Soc. Lond.*, 74:35–57.

Michelson, A. A. and Morley, E. (1887). On the relative motion of the earth and the luminiferous ether. *American Journal of Science*, 34:333–345.

Misner, Charles, W., Thorne, Kip, S., and Wheeler, J. A. (1973). *Gravitation*. Freeman, San Francisco.

Moore, T. A. (2013). *A General Relativity Workbook*. University Science Books, Mill Valley, CA.

Morris, M. S., Thorne, K. S., and Yurtsever, U. (1988). Wormholes, time machines, and the weak energy condition. *PRL*, 61:1446–1449.

Nanopoulos, D., Olive, K. A., and Srednicki, M. (1983). After primordial inflation. *Physics Letters B*, 127:30–34.

Navarro, J. F., Frenk, C. S., and White, S. D. M. (1997). A universal density profile from hierarchical clustering. *Astrophysical Journal*, 490:493–508.

Newell, D. B. et al. (2018). The CODATA 2017 values of h, e, k, and N_A for the revision of the SI. *Metrologia*, 55:L13–L16.

Newton, I. (1686). *Newton's Principia - first American Edition - English 1729*. Daniel Adee, New York.

Norman, M. L. (2010). Simulating galaxy clusters. *arxiv*, page 1005p1100v1.

Perlmutter, S. et al. (1998). Discovery of a supernova explosion at half the age of the universe. *Nature*, 391:51–54.

Piatella, O. F., Fabris, J. C., and Bilic, N. (2014). Note on the thermodynamics of the speed of sound of a scalar field. *arxiv*, 1309p4282v2:1–18.

Planck, M. (1899). Über irreversible Strahlungsvorgänge. *Verlag der Königlich Preußischen Akademie der Wissenschaften*, pages 440–480.

Planck, M. (1900). On the theory of the energy distribution law of the normal spectrum. *Verhandl. Dtsch. Phys. G.*, 2:237.

Planck, M. (1911). Eine neue Strahlungshypothese. *Verh. d. DPG*, 13:138–148.

Press, W. and Schechter, P. (1974). Formation of galaxies and clusters of galaxies by selfsimilar gravitational condensation. *Astrophysical Journal*, pages 425–438.

Reblinsky, K. (2000). *Projection effects in clusters of galaxies*. PhD thesis, LMU, München.

Riess, A. G., Casertano, S., Yuan, W., Macri, L., and Scolnic, D. (2019). Large Magellanic Cloud Cepheid Standards Provide a 1the Determination of the Hubble Constant and Stronger Evidence for Physics beyond Lambda-CDM. *The Astrophysical Journal*, 876:1–13.

Riess, A. G. et al. (2000). Tests of the Accelerating Universe with Near-Infrared Observations of a High-Redshift Type Ia Supernova. *The Astrophysical Journal*, 536:62–67.

Riess, A. G. et al. (2016). A 2.4 percent Determination of the Local Value of the Hubble Constant. *The Astrophysical Journal*, 826(1):1–65.

Sanders, Robert, H. (2010). *The Dark Matter Problem*. Cambridge University Press, Cambridge.

Sawitzki, P. and Carmesin, H.-O. (2021). Dimensional transitions in a Bose gas. *PhyDid B, FU Berlin*, pages 1–10.

Schöneberg, P. and Carmesin, H.-O. (2021). Solution of the horizon problem. *PhyDid B, FU Berlin*, pages 1–6.

Schwarzschild, K. (1916). Über das Gravitationsfeld eines Massenpunktes nach der Einstein'schen Theorie. *Sitzungsberichte der Deutschen Akad. d. Wiss.*, pages 186–196.

Slipher, V. (1915). Spectrographic observations of nebulae. *Report of the American Astron. Soc.*, Meeteing 17:21–24.

Smoot, G. F. et al. (1992). Structure in the COBE differential microwave radiometer first-year maps. *Astronomical Journal*, 396:L1–L5.

Sommerfeld, A. (1978). *Mechanik der deformierbaren Medien*. Verlag Harri Deutsch, Frankfurt, 6 edition.

Stephani, H. (1980). *Allgemeine Relativitätstheorie*. VEB Deutscher Verlag der Wissenschaften, Berlin, 2 edition.

Stoica, P. and Moses, R. (2005). *Spectral Analysis of Signals*. Prentice Hall, Upper Saddle River.

Straumann, N. (2013). *General Relativity* . Springer, Dordrecht - Heidelberg - New York - London, 2 edition.

Tanabashi, M., particle data group, et al. (2018). Review of particle physics. *Phys. Rev. D*, 98:1–1898.

Tröster, T. et al. (2020). Cosmology from large-scale structure. *Astronomy and Astrophysics*, 633:1–9.

Tryon, Edward, P. (1973). Is the universe a vacuum fluctuation? *Nature*, 246:396–397.

van der Waals, J. D. (1873). *Over de Continuiteit van den gas- en vloeistoftoestand*. Sijthoff, Leiden.

Weiland, J. L. et al. (2018). Elucidating ΛCDM: Impact of Baryon Acoustic Oscillation Measurements on the Hubble Constant Discrepancy. *ApJ*, 853:119.

Wheeler, J. A. (1962). *Geometrodynamics*. Academic, New York.

Will, C. M. (2006). Was Einstein right? Testing relativity at the centenary. *Living Review Relativity*, 9:1–23.

Wirtz, C. (1922). Radialbewegung der Gasnebel. *Astronomische Nachrichten*, 215:281–286.

Wong, K. C. et al. (2019). H0LiCOW XIII: A 2.4 percent measurement of H_0 of quasars: 5.3σ tension between early and late-Universe probes. *MNRAS*.

Yeche, C. et al. (2019). Baryon acoustic oscillation from the cross-correlation of the Lyα absorption and quasars in eBOSS DR14. *Astr. and Astrophys.*

Zaldarriaga, M. et al. (2020). Combining Full-Shape and BAO Analyses of Galaxy Power Spectra: A 1.6 % CMB-independent constraint on H_0. *JCAP*, 5:32.

Zeldovich, Y. B. (1968). The cosmological constant and the theory of elem. part. *Sov. Astron. A. J.*, 11:381–393.

Zhao, G.-B. et al. (2019). The clustering of galaxies in the comleted SDSS-III Baryon Oscillation Spectroscopic Survey: cosmological analysis of the DR12 galaxy sample. *MNRAS*.

Zilberberg, O. et al. (2018). Photonic topological pumping through the edges of a dynamical four-dimensional quantum Hall system. *Nature*, 553:59–63.

Zwicky, F. (1933). Die Rotverschiebung von extragalaktischen Nebeln. *Helvetica Physica Acta*, 6:110–127.

In order to make Def. (8) more explicit, the word *isotropic* has been added in the present digital book, in addition to the Printed Edition.

Parts of the content of the present book have been presented at the DPG spring conference that started at March 22, 2021.